Andreas Russegger, BSc

Synthesis and Properties of Covalent Dimers and J-Aggregates Based on Porphyrinoid Systems

MASTER'S THESIS

to achieve the university degree of

Master of Science (MSc)

Master's degree programme: Chemistry

submitted to

Graz University of Technology

Supervisor
Assoc.Prof. kand. Sergey Borisov

Institute of Analytical Chemistry and Food Chemistry

Graz, September, 2019

I am a firm believer that without speculation there is no good and original observation.

Charles Darwin

Abstract

In this thesis four palladium(II)-porphyrins and one palladium(II)-tetrabenzoporphyrin with varying amphiphilic character were synthesised and thouroughly characterized and it was attempted to prepare a covalently linked palladium(II)-porphyrin dimer.
Formation of J-aggregates with these Pd(II) complexes and with the corresponding metal-free complexes was investigated in aqueous solutions in presence of different surfactants supporting the aggregation. The two most amphiphilic palladium(II)-porphyrins and the palladium(II)-tetrabenzoporphyrin formed ordered dye aggregates in water with a slipped J-type character. The aggregates were characterized by resonant light scattering, absorption and fluorescence spectroscopy.
The aggegates feature a split Soret band with a red- and a blue-shifted band. Compared to the monomer, the luminescence quantum yields of the aggregates are reduced by at least one order of magnitude. Whereas the metal-free aggregates possess room temperature fluorescence, the palladium(II)-porphyrin aggregates showed phosphorescence only at 77 K.

Kurzfassung

In dieser Arbeit wurden vier Palladium(II)-Porphyrine und ein Palladium(II)-Tetrabenzoporphyrin mit unterschiedlichem amphiphilen Charakter synthetisiert und gründlich charakterisiert und es wurde versucht, ein kovalent gekoppelts Palladium(II)-Porphyrin Dimer herzustellen. Die Bildung von J-Aggregaten mit diesen Pd(II)-Komplexen und mit den entsprechenden metallfreien Komplexen wurde in wässrigen Lösungen in Gegenwart verschiedener Tenside untersucht, die die Aggregation unterstützen. Die beiden amphiphilsten Palladium(II)-Porphyrine und das Palladium(II)-Tetrabenzoporphyrin bildeten geordnete Farbstoffaggregate in Wasser mit einem J-Typ-Charakter. Die Aggregate wurden durch resonante Lichtstreuung, Absorption und Fluoreszenzspektroskopie charakterisiert.
Die Aggegate weisen eine geteilte Soret-Bande mit einer rot- und einer blauverschobenen Bande auf. Gegenüber dem Monomer sind die Lumineszenzquantenausbeuten der Aggregate um mindestens eine Größenordnung reduziert. Während die metallfreien Aggregate bei Raumtemperatur fluoreszieren, zeigten die Palladium(II)-Porphyrin Aggregate erst bei 77 K Phosphoreszenz.

EIDESSTATTLICHE ERKLÄRUNG

Ich erkläre an Eides statt, dass ich die vorliegende Arbeit selbstständig verfasst, andere als die angegebenen Quellen/Hilfsmittel nicht benutzt, und die den benutzten Quellen wörtlich und inhaltlich entnommenen Stellen als solche kenntlich gemacht habe. Das in TUGRAZonline hochgeladene Textdokument ist mit der vorliegenden Masterarbeit identisch.

AFFIDAVIT

I declare that I have authored this thesis independently, that I have not used other than the declared sources/resources, and that I have explicitly indicated all material which has been quoted either literally or by content from the sources used. The text document uploaded to TUGRAZonline is identical to the present master‘s thesis.

29.09.2019	
Datum/Date	Unterschrift/Signature

Danksagung

An dieser Stelle möchte ich mich recht herzlich bei all jenen Personen bedanken, die mich in den letzten Jahren unterstützt und begleitet haben und ohne die ich wahrscheinlich nicht da wäre, wo ich jetzt bin.
Ein ganz großes Dankeschön geht an dich, Sergey, für deine großartige Betreuung. Danke, dass ich jederzeit zu dir kommen konnte und du immer die passende Lösung für meine Probleme hattest.
Ein riesengroßes Dankeschön geht auch an dich, Ingo, dafür, dass du mich in der besten Arbeitsgruppe aufgenommen hast und ich dort sowohl meine Bachelor- als auch meine Masterarbeit machen durfte.
Natürlich geht auch ein großes Dankeschön an das ganze Team der besten Arbeitsgruppe der Welt. Ihr seid die besten Kollegen/Freunde die man sich nur vorstellen kann. Die letzten zwei Jahre bei euch haben mega viel Spaß gemacht, sei es im Labor, beim Feierabendbier, Pausenkaffee, beim gemeinsamen Kochen im Sozialraum oder bei den "Sozial-Events" wie Business-Lauf, Volleyball Turnier oder einen Karpfen in einer Wohnung aussetzen (ein riesengroßes Dankeschön an die Karpfen-Jungs und das Karpfen-Mädel für eine unvergessliche Geschichte).
Ein besonderer Dank geht an Tobi, David, Luki, Tanja, Max und (S)Andy, dafür, dass ich euch jederzeit fragen konnte, wenn ich mal nicht mehr weiterwusste und ihr mir immer geholfen habt.
Danke auch an dich, Eveline. Egal mit welchem Anlegen ich zu dir gekommen bin, du konntest mir immer weiterhelfen, sei es ein fehlender Prüfungstermin oder eine fehlende Prüfungsnote. Es gibt glaub ich nichts, was du nicht organisieren kannst.
Weiters möchte ich mich bei all meinen Studienkollegen und Freunde für die letzten fünf Jahre in Graz mit euch bedanken. Die zahlreichen Partys und Unternehmungen werde ich nie vergessen.
Danke auch an dich, Michi. Ohne dich wäre ich wahrscheinlich nicht nach Graz gegangen. Die Abende mit dir im Tick Tack, “Gü” und Nachtex wahren super, obwohl die Tage danach meist nicht so toll waren.
Danke auch an meine Familie! Ihr habt mich immer bei all meinen Vorhaben unterstützt und an mich geglaubt. Ohne euch wäre das Studium nicht möglich gewesen.
Zu guter Letzt möchte ich mich bei dir, Susi, bedanken. Danke, dass ich mit dir die letzten Jahre gemeinsam bestreiten durfte und du mir auch in anstrengenden Zeiten zur Seite gestanden bist.

Andreas Russegger, BSc Graz, September, 2019

Contents

1 Introduction

J-aggregates are known as highly ordered assembles of dye molecules. They posses properties which strongly differ from those of their dye monomers. For example, they demonstrate very narrow and bathochromically shifted absorption and emission spectra, very small or negligible Stokes shifts, strongly increased molar absorption coefficients, shorter fluorescence lifetimes and a high optical anisotropy.[1, 2]
This type of aggregates was independently discovered in the 1930s by Jelly [3, 4] and Scheiber [5] on the dye 1,1′-diethyl-2,2′cyanine 1,1′-diethyl-2,2′-cyanine chloride (pseudoisocyanine). Since their discovery, J-aggregate formations was also found at many other synthetic and natural chromophores, like perylene bisimides [6, 7], fluorenes [8], BODIPY dyes [9], porphyrins [10–12], chlorins [13] and phthalocyanines [14]. Due to their interesting photophysical properties, J-aggregates can be used as spectral sensitizers of silver halide crystals in photographic films and in the fields of biological sensing, photovoltaics and imaging.[1, 2]

Especially, J-aggregates based on porphyrins are very interesting. Porphyrins are known as one of the most important pigments in nature (e.g. haemoglobin and chlorophyll)[15, 16] and their synthetic representatives are frequently used for artificial applications (e.g. oxygen-sensing [17, 18], OLEDs [16], solar cells [19, 20]). Furthermore, porphyrins can be synthetically modified on their *meso*-positions with various substituents and they easily form metal-complexes. Depending on the substituents and complexed metal they show various photophysical properties, like fluorescence and phosphorescence.

The aim of this work was the synthesis and characterisation of dimers and J-aggregates based on phosphorescent palladium-metallated porphyrins and tetrabenzoporphyrins. J-aggregates made of palladium(II)-porphyrins are particularly interesting since so far there are no literature reports on phosphorescent J-aggregates.
Inspired by the work of Zhijian C. *et al.* on amphiphilic BODIPY J-aggregates, four palladium(II)-porphyrins and one palladium(II)-tetrabenzoporphyrin with different amphiphilic character were synthesised and their behaviour on aggregation was examined. Furthermore, the photophysical properties of the monomeric dye and the aggregates were investigated.

2 Theoretical Background

2.1 Luminescence

This chapter is based on references [21, 22].
Luminescence describes the emission of photons from electronically excited species. Such luminescent compounds or "dyes" can be based on organic (e.g. aromatic hydrocarbons, fluorescein), inorganic (e.g. lanthanide ions, CdS crystals) or organometallic compounds (e.g. $Ru(biPy)_3$). Depending on the mode of excitation various different types of luminescence are known (e.g. photoluminescence, thermoluminescence, chemiluminescence), whereby for this thesis only photoluminescence is important and will be further discussed.
The mode of excitation in photoluminescence is absorption of an photon, which rises an electron from the ground state to an higher electronically excited state. Once in the excited state, it can return to the ground state with emission of fluorescence, phosphorescence or by an other de-excitation pathway. All this de-excitation mechanisms have very characteristic properties which are discussed together with the absorption process on the next pages.

2.1.1 Absorption

Absorption is known as promotion of an electron from an orbital in the ground state to a higher unoccupied orbital by a photon. Thereby, the orbital in the ground state can be a σ, π or a non-bonding n orbital and the excited state either a σ^* or a π^* orbital. Due to the different kinds of orbitals, five transitions between the orbitals are possible ($\pi \rightarrow \pi^*$, $n \rightarrow \sigma^*$, $n \rightarrow \pi^*$, $\sigma \rightarrow \pi^*$ and $\sigma \rightarrow \sigma^*$), whereby, mostly the least energetic transition between the Highest Occupied Molecule Orbital (HOMO) and the Lowest Unoccupied Molecule Orbital (LUMO) is observed. The energy which is needed to promote these transitions have generally the following order:

$$n \rightarrow \pi^* < \pi \rightarrow \pi^* < n \rightarrow \sigma^* < \sigma \rightarrow \pi^* < \sigma \rightarrow \sigma^*$$

For dyes usually the low energetic transitions $n \rightarrow \pi^*$ and $\pi \rightarrow \pi^*$ are the most important ones. Thereby, the energy of the $\pi \rightarrow \pi^*$ transition decreases by increasing the extended π-electron

system. Due to the low energy gap, both transitions can be easily promoted by UV/Vis light which makes UV/Vis spectroscopy suitable for the investigation of dyes. In contrast, the high energetic transitions from σ orbitals as ground state need often far UV light which is rarely used in spectroscopy.

The efficiency of light absorption at a certain wavelength λ is mathematically expressed by the *Lambert-Beer Law* (Equation 2.1), where the absorbance A can be described either by the light intensities before and after the sample (I^0 and I) or by the molar decadic absorption coefficient ϵ, the concentration c of the absorbing species and the absorbing path length l.

$$A(\lambda) = log\frac{I_\lambda^0}{I_\lambda} = \epsilon(\lambda)lc \tag{2.1}$$

2.1.2 Franck-Condon Principle

According to the Born–Oppenheimer approximation, the movements of electrons are much faster than those of nuclei. An electronic transition usually takes 10^{-15} s, whereas molecular vibrations take place in a range between 10^{-10} to 10^{-12} s. Consequently, during an electronic transition no movement of the nuclei is observed. Such a transition is called "vertical transition". Figure 2.1 illustrate that behaviour on a diatomic molecule.

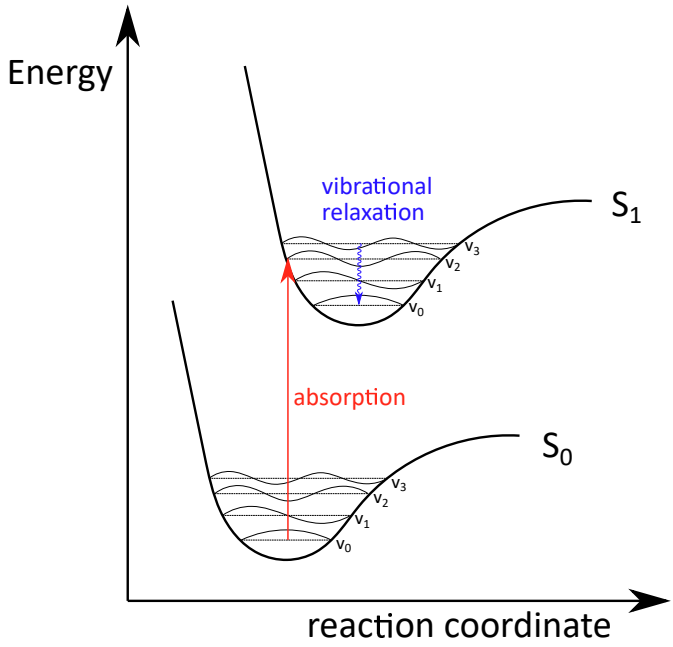

Figure 2.1: Franck-Condon principle illustrated on a diatomic molecule. Thereby, S_0 is the ground state, S_1 is the first excited state and v_n are the vibrational states.

At room temperature, the diatomic molecule is on the lowest vibrational level v_0 of the ground state S_0. By absorbing a photon, the molecule is excited by a vertical transition to a higher electronically and vibrational level. After a while, relaxation occurs and the molecule falls to the lowest vibrational level v_0 of S_1. Thereby, energy is released in form of heat. From that state several de-excitation mechanisms are possible.

2.1.3 De-Excitation Mechanisms

As mentioned above, after absorption of a photon and following vibrational relaxation to the lowest vibrational level of the excited state various de-excitation processes are possible. These processes are internal conversion (IC), fluorescence, intersystem crossing (ISC), delayed fluorescence and phosphorescence which are often visualized by a *Perrin-Jablonski diagram*. In Figure 2.2 such diagram is depicted. Thereby, the abbreviations S_0, S_1, and S_2 stand for the singlet ground state, the first and the second excited singlet state, respectively, and T_1 and T_2 for the first and the second exited triplet state, respectively. Each of these electronic states, vibrational states are associated. The de-excitation mechanisms can be divided in radiative and non-radiative transitions. Radiative-transitions are depicted in Figure 2.2 by straight arrows and non-radiative transitions by wavy arrows.

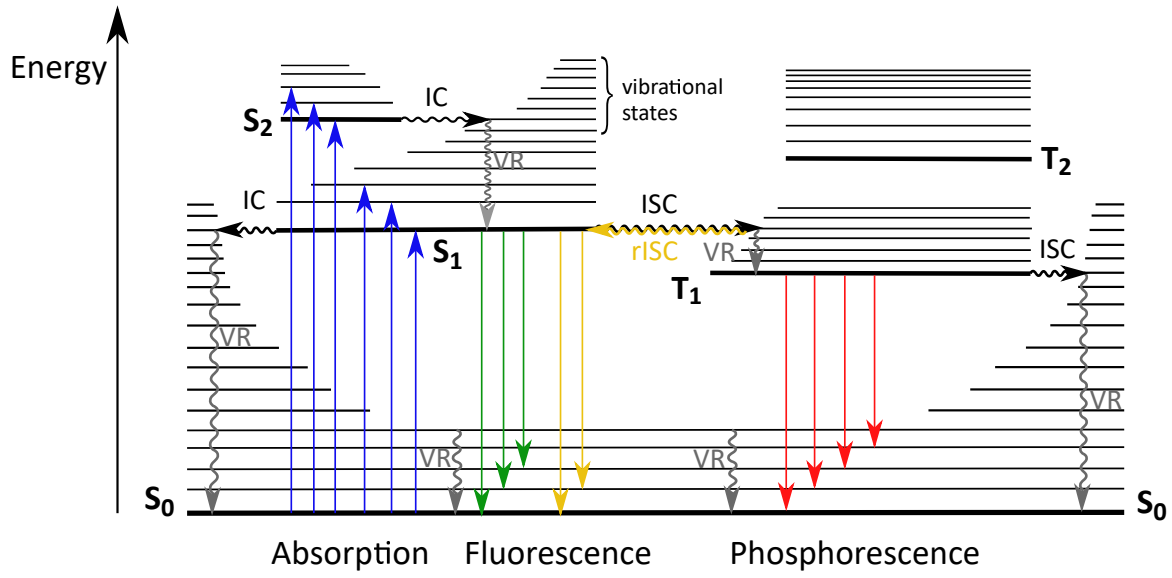

Figure 2.2: Perrin-Jablonski diagram with the electronic singlet (S_0, S_1, and S_2) and triplet states (T_1 and T_2). Non-radiative transitions internal conversion, (reverse) intersystem crossing, and vibrational relaxation are abbreviated by IC, (r)ICS, and VR, respectively. Radiative transitions are illustrated by coloured arrows (absorption: blue, fluorescence: green, delayed fluorescence: orange and phosphorescence: red)

Non-Radiative Transitions

Internal Conversion (IC)

A possible de-excitation pathway of an excited molecule is *internal conversion*. That isoenergetic transition only takes place between two electronic states with the same multiplicity (e.g. S_2 to S_1 and S_1 to S_0) and is generally followed by vibrational relaxation to the lowest vibrational level of the ground or excited state. IC is more likely between electronic states with a small energy gap. Therefore, it is more favoured from S_2 to S_1 than from S_1 to S_0. IC from S_1 to S_0 also competes with other processes, like fluorescence and intersystem crossing.

Intersystem Crossing (ISC)

In contrast to internal conversion, *intersystem crossing* (ISC) is a non-radiative transition between two isoenergetic vibrational levels of two electronic states with different multiplicity. For instance, an excited molecule in the lowest vibrational level of the first excited singlet state S_1 can move to the isoenergetic vibrational level of the triplet state T_n, followed by vibrational relaxation to the lowest vibrational level of T_n. Ordinary, transitions between two states of different multiplicity are forbidden. However, due to strong spin-orbit coupling ISC is possible which is often observed in presence of heavy atoms (e.g. Br, Pd).
In addition to ISC, also the opposite way is possible which is called reverse intersystem crossing (rISC). rISC is more likely if the electronic states S_1 and T_1 are energetically close together and therefore at higher temperatures.

Radiative Transitions

Fluorescence

The transition from S_1 to S_0 by emission of a photon is called *fluorescence*. Apart from a few exceptions, fluorescence is observed from the lowest vibrational level of the first excited singlet state S_1. Due to that, it is independent of the excitation wavelength. In general, the fluorescence band resembles the absorption band ("mirrow image" rule), because of a similar distribution of the vibrational levels of the ground and first excited state. According to Stokes Rule, the fluorescence bands are shifted to longer wavelengths, because of energy loss in the excited state by vibrational relaxation. Typically an overlap between absorption and fluorescence spectrum is observed which is attributed to an absorption from a higher vibrational level of the ground state. That behaviour can be explained by Boltzmann Law. At room temperature molecules are usually on the lowest vibrational level. Nevertheless, a small fraction of molecules can also occupy higher vibrational levels in the ground state which results in a red-shifted absorption

and a blue-shifted fluorescence spectrum. At low temperatures, such shifts should disappear. In addition to section 2.1.2, also the emission of a photon is a very fast process (10^{-15} s). However, before emission or other de-excitation processes occur, the molecule stays for a certain time in the lowest vibrational level of S_1. This span is called "lifetime" and can take much longer (10^{-10}-10^{-7} s). By excitation of a molecule with short pulse of light, an exponential decrease of the fluorescence intensity can be observed. That decay takes a characteristic time which reflects the average lifetime of the molecule in the S_1 state.

Phosphorescence

Emission of a photon from the first excited triplet state T_1 to the ground state S_0 is called *phosphorescence*. Despite transitions between two electronic states with different multiplicity are forbidden, they can be observed in presence of strong spin-orbit coupling. Nevertheless, phosphorescence is a very slow process with a lifetime in the T_1 state of 10^{-6} to 1 s. As a result of the long lifetime and collisions between excited and solvent molecules, intersystem crossing, followed by vibrational relaxation to S_0 is favoured in solution and therefore phosphorescence is seldom observed. However, at low temperature or/and in a rigid medium it can be observed. By now, however, there are also many emitters reported that show strong phosphorescence at room temperature in solution under anoxic conditions. In contrast to fluorescence, phosphorescence spectra are widely shifted to longer wavelengths. The reason for that is the lower energy of T_1 compared to S_0 which is attributed to Hund's Rules.

Delayed Fluorescence

Delayed fluorescence is a radiative transition from S_1 to S_0 which takes place after a rISC from T_1 to S_1. It has the same spectral distribution as regular fluorescence, however, with a longer lifetime. In general, it is observed, if the electronic states T_1 and S_0 are energetically close together and the lifetime of T_1 is long. Depending on the activation type, delayed fluorescence can be divided in thermally activated delayed fluorescence and triplet–triplet annihilation.
As the name says, thermally activated delayed fluorescence is activated by temperature. If the temperature is high enough, the molecule is excited to higher vibrational states of T_1 and rISC is favoured back to the S_1 state.
Especially, in concentrated solutions (high molar concentration) and at high light intensities, triplet–triplet annihilation can be observed. Thereby, many molecules are in the T_1 state and due to a collision between two excited molecules in T_1 state an energy transfer from one molecule to the other can provide. If the transferred energy is high enough, it enables an transition of

one molecule to the S_1 and the other to the S_0 state, followed by de-excitation of the excited molecule (S_1) to the ground state (Equation 2.2).

$$T_1 + T_1 \rightarrow S_0 + S_1 \rightarrow S_0 + S_0 + h\nu \tag{2.2}$$

2.1.4 Lifetime

As mentioned above, after absorption of a photon and a following vibrational relaxation, the molecules stay in the excited S_1 state for a certain time, before de-excitation to the ground state S_0 occurs. This time span is called *lifetime* τ of the excited singlet state. During this lifetime, radiative and non-radiative processes (IC and ISC) can occur. Each of these processes has a specific rate constant which can summed up to the non-radiative rate constant k_{nr} ($k_{nr} = k_{IC} + k_{ISC}$) and the radiative rate constant k_r. Therefore, the rate of disappearance of a excited molecule A with the concentration [A*] can be expressed by Equation 2.3.

$$-\frac{d[A^*]}{dt} = (k_r + k_{nr})[A^*] \tag{2.3}$$

Integration of Equation 2.3 leads to following equation, with the stating concentration of excited states $[A^*]_0$ and the concentration $[A^*]$ at a certain time t.

$$[A^*] = [A^*]_0 \, exp\left(-\frac{t}{\tau}\right) \tag{2.4}$$

Thereby, the lifetime τ_S of excited state S_1 is expressed by

$$\tau = \frac{1}{k_r + k_{nr}} \tag{2.5}$$

2.1.5 Quantum Yields

During the lifetime τ radiative and non-radiative processes with different rate constants are competing with each other. The fraction in which a certain process occurs is called *quantum yield* Φ. It is the ratio of the monitored rate constant (e.g. rate constant of fluorescence k_r^F or phosphorescence k_r^T) to the sum of all competing rate constants. In Equation 2.6, 2.7 and 2.8 the quantum yield for fluorescence Φ_F, intersystem crossing Φ_{ISC} and phosphorescence Φ_P are depicted.

$$\Phi_F = \frac{k_r^F}{k_r^F + k_{nr}} = k_r^F \tau \tag{2.6}$$

$$\Phi_{ISC} = \frac{k_{ISC}}{k_r^F + k_{nr}} = k_{ISC}\tau \tag{2.7}$$

$$\Phi_P = \frac{k_r^T}{k_r^T + k_{nr}} \Phi ISC \tag{2.8}$$

The quantum yields can be influenced by variation of the rate constants. Because of that, parameters like temperature, pH, polarity, viscosity, hydrogen bonding, presence of quenchers, etc. have an impact on the quantum yields. For example, by increasing the temperature non-radiative processes are more likely and the phosphorescence quantum yield is decreased.

2.1.6 Luminescence Quenching

All previously discussed de-excitation processes are intrinsic pathways of an excited molecule A^*. During the lifetime of the excited state, A^* can also interact by photophysical interactions with other molecules or so called *quenchers* Q. Those interactions with quencher molecules can influence the de-excitation processes, like fluorescence and phosphorescence emission, which is called *quenching*. Some of these photophysical interactions being responsible for quenching are collisions with either a heavy atom or a paramagnetic species, electron transfer, excimer or exciplex formation, proton transfer and energy transfer.
In the next sections the two quenching processes static and dynamic quenching are discussed.

Static Quenching

Static quenching is observed either if a luminophore A in the ground state makes an non-fluorescence complex with a quencher molecule Q (Figure 2.3 **(a)**) or if a excited luminophore A^* and Q are very close in space and they cannot change their positions relative to each other during the lifetime of A^* (Figure 2.3 **(b)**). The second type is called the sphere of effective quenching or quenching sphere. Both, types of static quenching are preferred at high quencher concentrations.
Due to the complex formation the amount of effective luminophore is decreased and therefore also the emission intensity. However, the lifetime is unaffected.

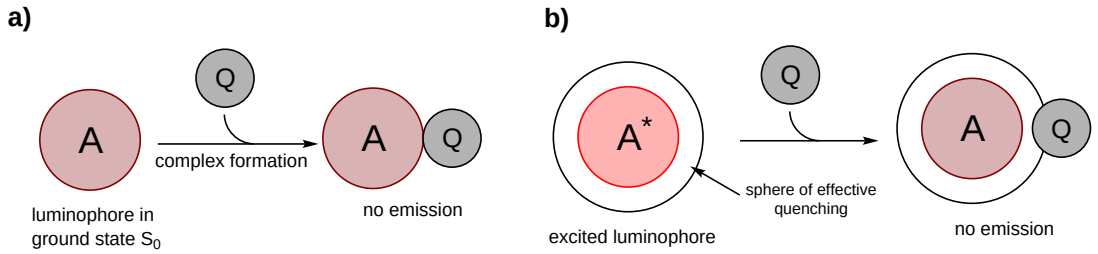

Figure 2.3: Mechanisms of static quenching between a luminophore A and a quencher molecule Q: **(a)** formation of a ground-state non-fluorescent complex and **(b)** sphere of effective quenching.

Static quenching is described by Equation 2.9,

$$\frac{I_0}{I} = 1 + k_a[Q] \tag{2.9}$$

whereby, I and I_0 are the emission intensities with and without the quencher, respectively, K_a represents the association constant and $[Q]$ the concentration of the quencher molecule.

Dynamic Quenching

Dynamic quenching is observed if an excited luminophore A^* interacts with a quencher molecule during the excited state lifetime. Thereby, a non-radiative energy transfer or an electron transfer between A^* and Q takes place and A^* is de-excited to the ground state (Figure 2.4). Because dynamic quenching is a diffusion controlled process, the observed quenching rate constant k_q is time-dependent. In contrast to the time-independent static quenching, hereby, a decrease in emission intensity and lifetime is observed.

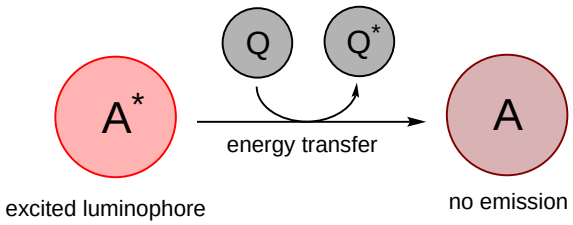

Figure 2.4: Mechanism of dynamic quenching between a luminophore A and a quencher molecule Q.

Dynamic quenching can be described by the Stern-Volmer relation (Equation 2.10),

$$\frac{I_0}{I} = 1 + k_q \tau_0 [Q] = 1 + K_{SV}[Q] \tag{2.10}$$

whereby, I and I_0 are the emission intensities with and without the quencher, respectively, K_{SV} is the Stern-Volmer constant, $[Q]$ the concentration of the quencher molecule and τ_0 the excited state lifetime without quencher.

2.2 Porphyrins

Porphyrins are 18 π aromatic square planar macrocycles consisting of four pyrroles which are linked by four methine carbons. This macrocycle without substituents is also called *porphine*. They have very characteristic photophysical properties (see below at Section 2.2.2) and are known as one of the most important pigments in nature (e.g. chlorophyll, haemoglobin)[15, 16]. Due to the fact that they easily form metal complexes [23] - preferential with divalent metal cations - and can be modified on their *meso*- and β-positions (Figure 2.5), porphyrins are frequently used for man-made applications (e.g. oxygen-sensing [17, 18], solar cells [19, 20], OLEDs [16], cancer imaging and therapeutic applications [24]).
During the last decades, several porphyrin synthesis strategies have been developed, whereby the strategy depends on the substitution pattern and position. Some of these methods are discussed for synthesising *meso*-substituted porphyrins.

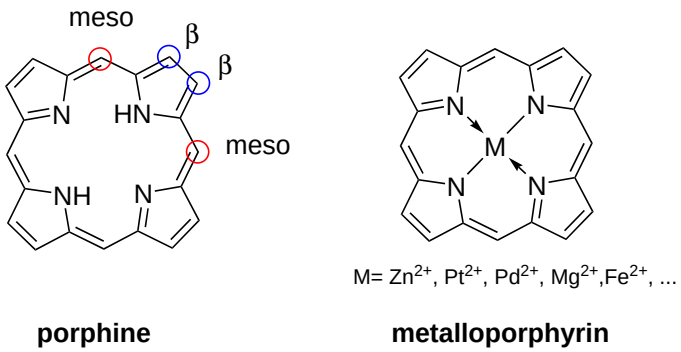

Figure 2.5: Structure of *meso*- and β-unsubstituted porphine and metalloporphyrin.

2.2.1 Synthesis

Porphyrins, bearing one, two, three or four *meso*-substituents - usually phenyl or phenyl derivatives - can be synthesised either by using substituted precursors for the porphyrin synthesis or by introducing further substituents on an already existing porphyrin.[25]

Symmetric *meso*-tetrasubstituted porphyrins (A_4-porphyrins) with phenyl derivative substituents can be synthesised via the so called *Adler-Longo method* [26] or by *Lindsey-Rothemund method* [27, 28] (Figure 2.6). Both methods use pyrrole and benzaldehyde derivatives as reagents and are straightforward.
The Adler-Longo method is a one step synthesis where both reagents are stirred in refluxing propionic acid (141 °C) under air atmosphere.[26] Thereby, pyrrole and aldehydes are condensed at acidic conditions to *porphyrinogen* which is immediately oxidised to the final porphyrin by atmospheric oxygen. Unfortunately, this method has three main drawbacks which are the harsh

reaction conditions, purification problems due to the high level of tar produced and the poor reproducibility.[27]
The Lindsey-Rothemund method overcomes these drawbacks and can be used for synthesising porphyrins with benzaldehydes bearing sensitive functional groups.[27] It is a two-step one-pot synthesis which is carried out at room temperature and inert atmosphere. In a first step, pyrrole and aldehyde are condensed in dry DCM at moderate dilution (10^{-2} M) with traces of an acid catalyst (e.g. TFA, BF_3OEt_2) to the porphyrinogen. In a second step the porphyrinogen is oxidised to the final porphyrin. Instead of oxygen, DDQ or p-chloranil are used here. This method enables a much easier purification and additionally, higher yields at milder conditions. In contrast to the A_4-porphyrins the asymmetric *meso*-tetrasubstituted porphyrins, bearing up to four distinct *meso*-substituents (e.g. ABCD-porphyrins) require much more synthetical effort and the substituted precursor have to be synthesised over several steps.[29]

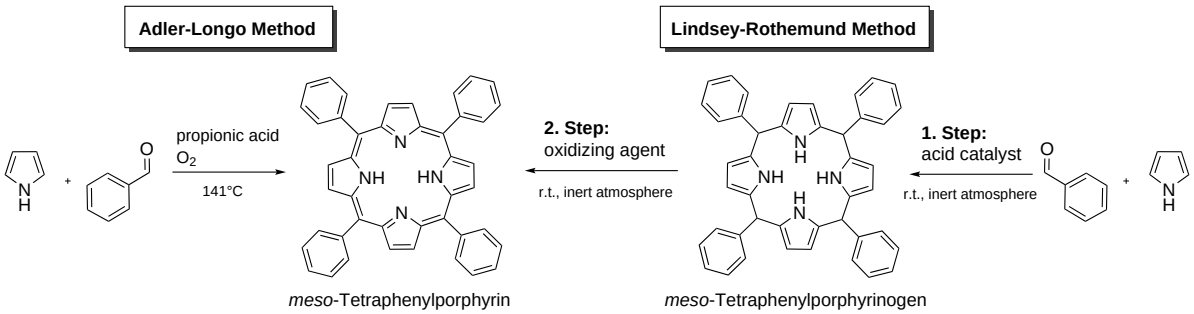

Figure 2.6: Synthesis of *meso*-tetraphenylporphyrin via Adler-Longo and Lindsey-Rothemund method.

Porphyrins, bearing only two *meso*-substituents (i.e. *trans*-A_2-, *trans*-AB-porphyrins) are much easier to synthesize than ABCD-porphyrins. Figure 2.7 gives an overview of six different synthetic routes for *trans*-AB-porphyrins which are divided in *statistical* and *rational methods*. All of these methods are based on the Lindsey-Rothemund method but here either functionalized or non-functionalized dipyrromethanes are used. Statistical methods (Routes 1 and 2) do not require functionalized dipyrromethanes and therefore are realized with less additional synthetic steps. However, the drawback of statistical methods is that they result in a mixture of three porphyrins (*trans*-A_2-,*trans*-B_2- and *trans*-AB-porphyrins) that require chromatographic purification.[25]
On the other hand, rational methods (Routes 3 to 6) require functionalized dipyrromethanes, but they result only in *trans*-AB-porphyrins. Symmetric *trans*-A_2-porphyrins can also be achieved by these six routes. Nevertheless, the most effective approach is Route 1 where dipyrromethane is condensed with corresponding benzaldehyde.[25]

The big advantage of symmetric *trans*-A_2- and asymmetric *trans*-AB-porphyrins are the two free *meso*-positions. These positions can be used for further introduction of new substituents. For

example, they can be substituted with phenyl lithium derivatives and/or brominated with NBS which enables substitution by Pd-catalysed cross-coupling.[30–37] These post modifications are also a possibility to achieve ABCD-porphyrins.[34]

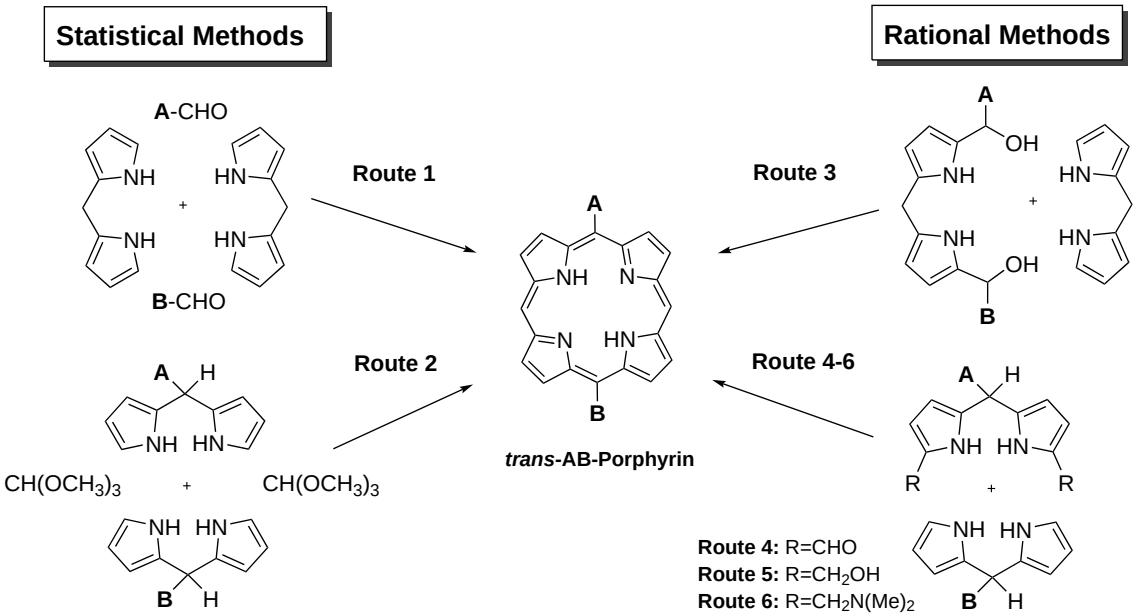

Figure 2.7: Synthesis of *trans*-AB-porphyrins via statistical and rational methods.[25]

Another type of *meso*-substituted porphyrins are A-porphyrins bearing only one *meso*-substituent. These are very rarely investigated and can be prepared by either condensation reactions involving dipyrromethanes or by substitution reaction of unsubstituted porphyine.[38] Figure 2.8 shows a very suitable method of synthesising A-porphyrins. It is again a statistical approach which results in A- and *trans*-A_2-porphyrin. The big advantage is again the free *meso*-positions for additional modifications.[34]

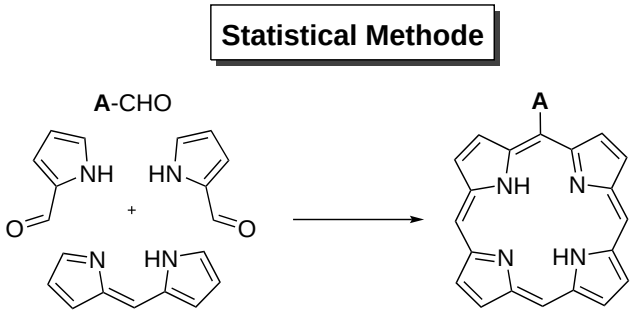

Figure 2.8: Synthesis of A-porphyrins via statistical method.[25]

Metalloporphyrin complexes are obtained by treatment of the porphyrin with metal acetates, oxides, hydroxides or other metal salts.[23] Thereby, the complexation is preferred at higher

temperature and in a basic environment. Presents of strong acids lead to protonation of the porphyrin nitrogen which inhibits the complexation.
The tendency if a metal ion will be complexed or not, usually depends on the metal properties (e.g. ionic radius and oxidation state).[23]

2.2.2 Photophysical Properties

Absorption Spectra

The absorption spectra of porphyrins and metalloporphyrins can be divided in the *Soret* and *Q-band region* (Figure 2.9), which are attributed to $\pi \rightarrow \pi^*$ transitions.[39] The very intense Soret band ($\epsilon = 10^5 M^{-1} cm^{-1}$) - or also known as B-band - appears in the blue part of the UV/Vis spectrum between 380 - 500 nm and belongs to the $S_0 \rightarrow S_2$ transition of the porphyrin. Furthermore, the much less intense Q-bands ($\epsilon = 10^4 M^{-1} cm^{-1}$) at higher wavelengths between 500 - 750 nm result from the $S_0 \rightarrow S_1$ transition.
It can be seen that the visible absorption spectrum changes from a two-banded metalloporphyrin (D_{4h}-type) to a four-banded free-base porphyrin (D_{2h}-type) spectrum (Figure 2.9) which can be explained by the "four-orbital" model of Gouterman.[40, 41].

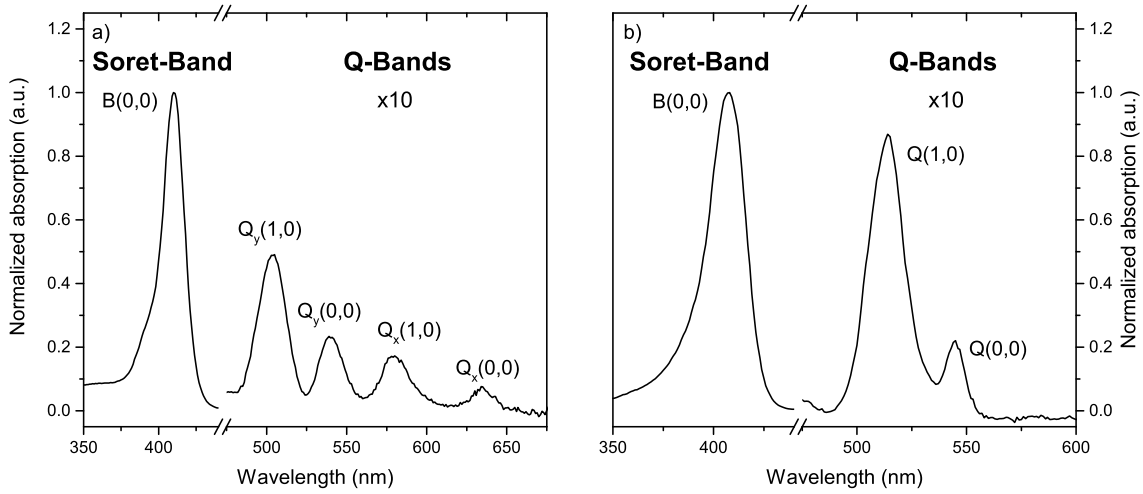

Figure 2.9: Absorption spectra of **(a)** porphyrin **(b)** Pd-porphyrin. The Q-band region is amplified by the factor of ten.

This dramatic effect is attributed to the breaking of the D_{4h} symmetry of the porphyrin ring by the central proton axis. Thus, Q(0,0) splits into Q_x(0,0) and Q_y(0,0) and each band has a vibronic overtone, Q_x(1,0) and Q_y(l,0),respectively (Figure 2.9 **(a)**).
The higher symmetrical metalloporphyrins have D_{4h} symmetry and thus two equivalent dipole transitions in the x and y directions. As a consequence of this only one B- and Q-transition exists. Here, the two Q-bands in the absorption spectra are attributed to two vibrational peaks

Q(0,0) and Q(1,0) (Figure 2.9 **(b)**).
Furthermore, depending on the relative intensities of the Q(0,0) and Q(1,0) bands of the metal complex, a prediction about the complex stability can be done. For example, if the Q-band Q(1,0) has at shorter wavelengths a higher intensity than the Q(0,0) band, the metal forms a stable square-planar complex with the porphyrin and vice versa.[42]
The absorption spectra also depends on the substituents. For example, by increasing the number of phenyl-substituents at the *meso*-positions all bands are shifted to longer wavelengths (Table 2.1). That shift is not as big as would have been expected, because the phenyl-residues are not in the same plane as the porphin core and therefore the π-system only slightly interacts with the porphyine π-system.[43] A much bigger influence on the electronic system is observed by extending the π-system on the porphyine β-positions which leads to π-extended porphyrins.[44] The propably most famous types of π-extanded porphyrins are *tetrabenzoporphyrins* (TBPs) which are discussed later.

Table 2.1: Absorption spectra for *meso*-phenyl-substituted porphyrins in DCM.[38]

		λ (nm)
Compound	Soret band	Q-bands
5-Phenylporphyrin	403	495, 526, 568, 622
5,15-Diphenylporphyrin	406	502, 536, 574, 630
5,10,15-Triphenylporphyrin	412	508, 543, 584, 638
5,10,15,20-Tetraphenylporphyrin	418	515, 549, 590, 645

Emission

The emission properties of metalloporphyrins strongly depend on the type of metal which is coordinated and how their orbitals interact with the porphyrin π-system. Table 2.2 shows the fluorescence and phosphorescence quantum yield (Φ) and lifetime (τ) of *meso*-tetraphenylporphyrin (TPP) and three different metal analogs (M = Mg, Zn, Pd).

Table 2.2: Fluorescence and phosphorescence properties of some metal *meso*-tetraphenylporphyrins (TPP) in methylcyclohexane.

Compound	Φ_f (%)	τ_f (ns)	Φ_p[a] (%)	τ_p[a] (ms)	Ref.
TPP	13	13.6	0.004	6	[45]
MgTPP	15	9.2	1.5	45	[46]
ZnTPP	4	2.7	1.20	26	[45]
PdTPP	0.02	0.02	17	2.8	[46]

[a] Were recorded at 77 K.

Fluorescence and phosphorescence are observed at 77 K for all four porphyrins. However, TPP, MgTPP and ZnTPP show primarily fluorescence and only a very weak phosphorescence at low temperature. The ability of spin orbit coupling is increased with the atomic number of the metal resulting in a stronger phosphorescence and a decreased fluorescence.[46]
In case of metalloporphyrins, the fluorescence spectra consist of two peaks Q(0,0) and Q(0,1) mirror image to the absorption peaks Q(0,0) and Q(1,0) with a Sokes shift of a few nanometres. The phosphorescence bands consists of a strong T(0,0) band and T(0,1) bands of variable intensity with respect to T(0,0).

2.2.3 Tetrabenzoporphyrins

Tetrabenzoporphyrins (TBPs) are π-extended porphyrins and were first synthesised by Helberger *et al.* in 1938 [47] and later in 1940-1950 by Linstead *at al.* [48, 49].
The synthetic strategies which lead to *meso*-substituted TBPs can be divided in the three main groups - *high-temperature template method*, *low-temperature assembling method* by well established Lindsey chemistry and introduction of substituents at the *meso*-positions of the already formed porphyrin system.[50, 51]

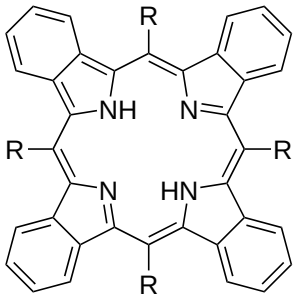

Figure 2.10: Structure of *meso*-substituted tetrabenzoporphyrin.

The advantage of the high-temperature template method is that it usually starts with very cheap reagents, like phthalimide and has less synthetic effort. Unfortunately, it is reported that during the synthesis with phthalimides as starting reagents a couple of side products are produced which are difficult to remove.[52, 53] Furthermore, due to the high temperature (340 - 360 °C) this type of synthesis can be only used for tetrabenzoporphyrins bearing temperature stable substituents.
By substituting the phthalimide starting reagents with dicyanobenzenes, the reaction temperature is lowered to 280 °C and also the purification step is improved due to impurities that are not difficult to remove.[54] However, also this improved method has two drawbacks. First, it requires again high temperatures and second, the number of dicyanobenzene derivatives which

are available is limited.
In contrast to the high-temperature template methods, the low-temperature assembling method by Lindsey chemistry [27, 28] works under much more convenient conditions and is therefore suitable for sensitive substituents. In addition, also TBPs with various substitution-pattern can be synthesised (Section 2.2.1). The approach is based on different types of pyrrole derivatives which are condensed with the respective benzaldehyde to porphyrins.[55] Then, in a second step the porphyrin is oxidised to the final TBP. Figure 2.11 shows four appropriate pyrroles, whereby the *2H*-isoindole (Route 1) cannot be used, because it is an unstable transient molecule.[55] The other three pyrroles are stable enough for this approach and differ in the way how the corresponding porphyrin is oxidized.
Tetrahydroisoindole (Route 2) is easily synthesised by *Barton–Zard reaction* [56–58] and a following decarboxylation reaction.[52, 59] The condensation with a benzaldehyde derivative gives a very stable porphyrin which has to be converted first to the metal porphyrin complex (e.g. Zn, Ni, Cu, Pd) before it is oxidised with DDQ to TBP.[60]
Bicyclooctadiene-fused pyrrole (Route 3) and 4,7-dihydroisoindole (Route 4) are synthesised similarly to tetrahydroisoindole and their porphyrins do not need to be converted in the metal complex. The oxidation of bicyclooctadiene-fused porphyrins is performed by heating the solid over 200 °C under vacuum, whereby the TBP is formed by *retro-Diels-Alder reaction* and the 4,7-dihydroisoindole based porphyrins are oxidized with DDQ in solution.[50, 51, 55, 61, 62]

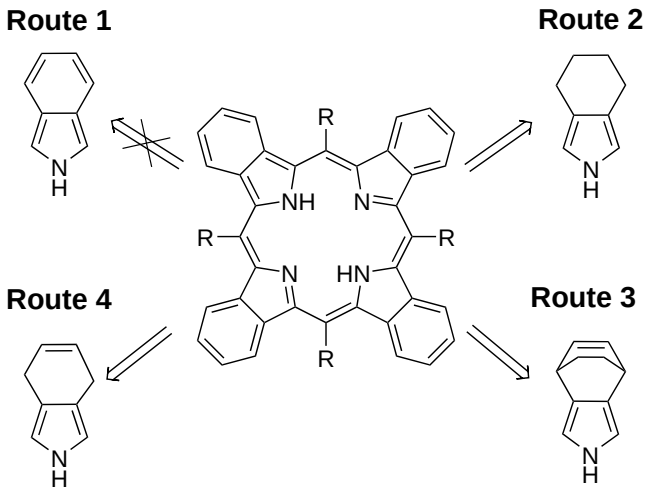

Figure 2.11: Synthesis of tetrabenzoporphyrin by Lindsey-method with different isoindol reagents.[55]

The absorption spectra of TBPs show Soret and Q-bands as do porphyrins, but their Q-bands are far more intense.[41] Due to the lager π-system, the absorption and emission spectra are bathochromically shifted in contrast to porphyrins, which makes TPBs suitable for lots of application, like in OLEDs [63], optical sensors [18], electronic devices [64] and medicine [65]. Figure 2.12 shows die free-base and the Pd-metallated 5,15-diphenyl-TBP and tetraphenyl-TBP,

respectively. Interestingly, the less symmetric free-base 5,15-diphenyl-TBP (Figure 2.12 **(a)**) have both, a split Soret ($B_x(0,0)$ and $B_y(0,0)$) and a split Q-band which is a result of strong mixing of the B and Q states.[66] In contrast, this splitting is not seen in the Pd-metallated TBPs (Figure 2.12 **(c)** and **(d)**) due to the higher symmetry.

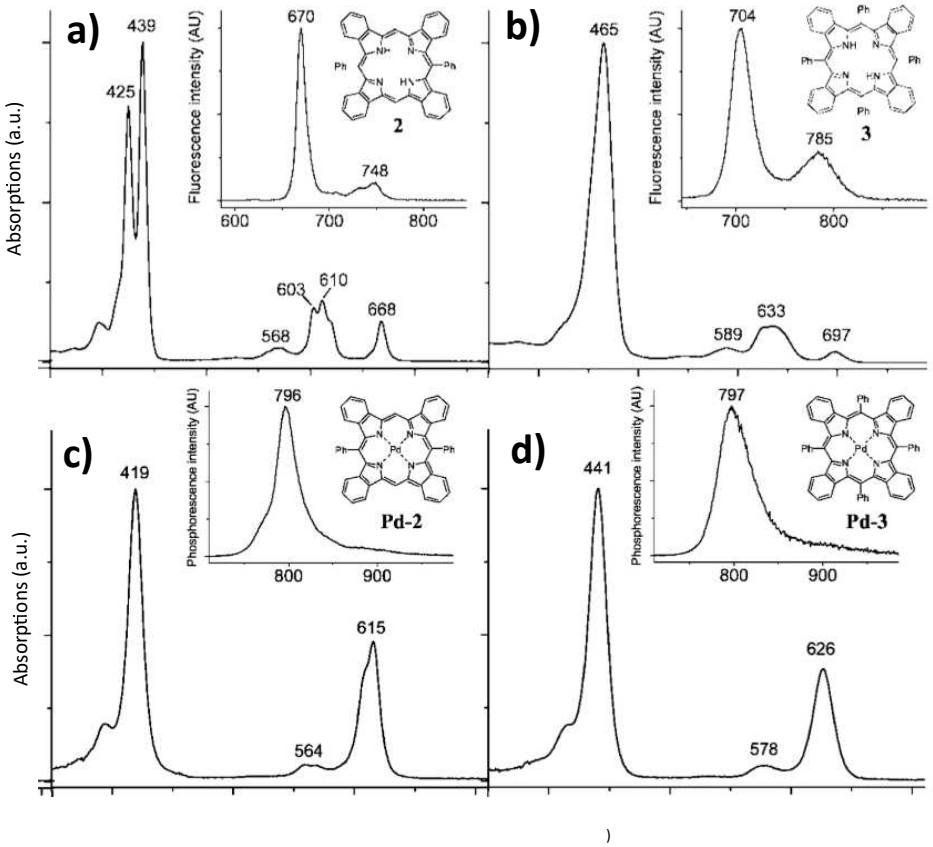

Figure 2.12: Absorption and emission spectra of different kinds of TBPs and PdTBPs.[66] **(a)** 5,15-diphenyl-TBP; **(b)** tetraphenyl-TBP; **(c)** Pd-5,15-diphenyl-TBP; **(d)** Pd-tetraphenyl-TBP

2.3 J-Aggregates

This chapter is based on the reviews [1, 2]. Other references will be cited independently.
J-aggregates are known as highly ordered clusters of dye molecules. They posses properties which strongly differ from those of their non-aggregated monomers. For example, they demonstrate very narrow and bathochromically shifted absorption and fluorescence spectra which have very small or negligible Stokes shifts. Furthermore, they display a strongly increased molar absorption coefficient, shorter fluorescence lifetimes and a high optical anisotropy. Since the discovery in the 1930s by Scheibe and Jelly lots of research has been done on this type of aggregates and such aggregation has been observed for several dye classes. The most famous dye class is pseudoisocyanine (PIC), but J-aggregates are also known for perylene bisimides, merocyanines, BODIPY dyes, fluorene, chlorins and porphyrins. Due to their interesting photophysical properties, they can be used as spectral sensitizers of silver halide crystals in photographic films, in the fields of photovoltaics, biological sensing, imaging and many more. In contrast to J-aggregates, the dye monomer can assemble in quite different *H-aggregates* which have a broad hypsochromically shifted absorption and bathochromically shifted emission spectra.
On the next pages the structure of J- and H-aggregates and their properties are discussed in more detail and after that, more information on the aggregation of porphyrins is given.

2.3.1 Structure of J- and H-Aggregates and Their Properties

J- and H-aggregates are formed by self-organisation, which proceeds by $\pi - \pi$ interactions between highly polarizable groups of atoms together with electrostatic interactions between opposite charges. Furthermore, an amphiphilic character of the molecule also helps by self-organisation. Both types of aggregate can be distinguished by their dye arrangement in the aggregate. Thereby the angle θ between the individual molecules is very important (Figure 2.13).

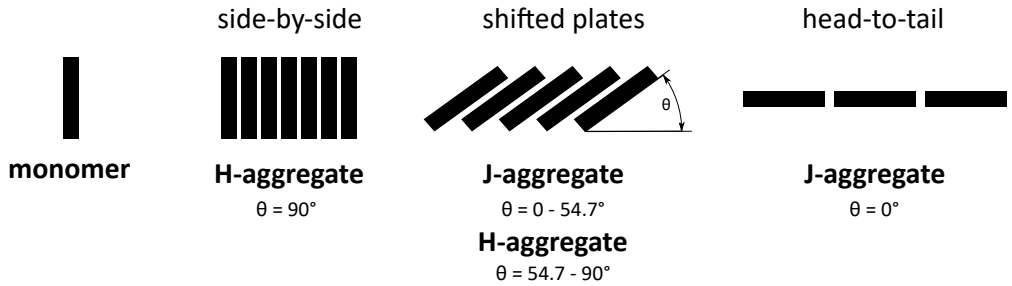

Figure 2.13: Possible orientations of molecules in J- and H-aggregates.[67]

J-aggregates are parallelly aligned and exhibit a shifted “head-to-tail” or “shifted plates”

arrangement with an angle θ between 0 and 54.7°. In contrast, H-aggregates form "side-by-side" or "shifted plates" arrangements with an angle θ between 54.7 and 90°.

Based on the excitation theory of Davydov, Michael Kasha developed a model of excitonic coupled dimers that can describe basic properties of molecular aggregates. In his model the two molecules have transition dipoles which are parallelly aligned along the long axis of the aggregate. In Figure 2.14 such on exciton model is illustrated, whereby for simplicity the ground states of the monomer as well as the dimers have the same energy. By excitation of the dimer, the excited state is split in two excited energy levels because of electronic degeneracy. In the dimer both transition dipoles can have either the same or the opposite orientation. If the transition to the lower or the higher energy level is allowed, depends on the orientation of the dipoles (i.e. same or opposite direction) and the angle θ between them. Basically, transitions to energy levels with equally aligned dipole moments are allowed and those to opposite directions are forbidden. Therefore, for H-dimers the transition to the higher and for J-dimers to the lower excited state is allowed.

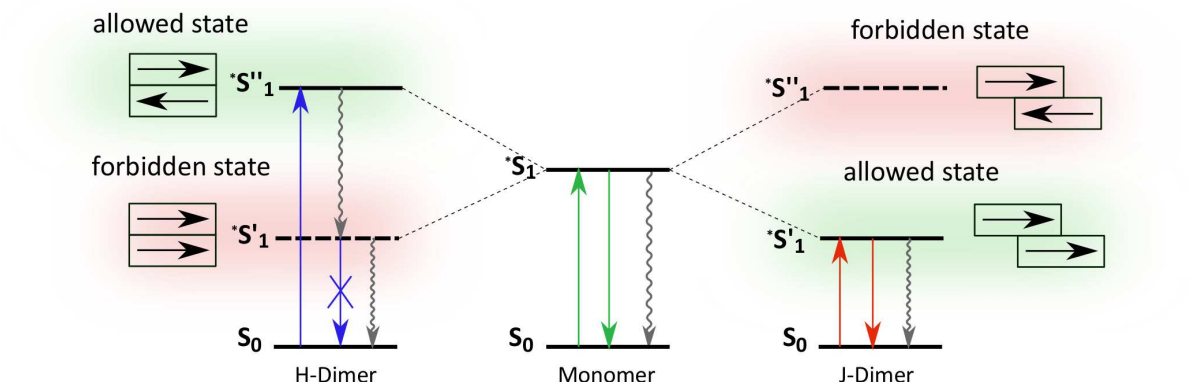

Figure 2.14: Exciton model for J- and H-dimers suggested by Kasha. The "normal" arrows represent absorption and fluorescence, respectively, and the wavy arrows non-radiative de-excitation processes. The arrows next to the excited states illustrate the orientation of the molecule dipole moment.

That behaviour results in a blue-shift of the absorption spectra for H-dimers relative to the monomer and in a red-shift for J-dimers. Additionally, the radiative emission from the lower excited state of H-dimers is symmetry-forbidden while that of J-dimers is allowed. Due to the coupled dipole moments, the emission in J-dimers should be enhanced.
The Kasha model fits often very well with experimental data for J- and H-aggregates, but there are also exceptions. For example, J-aggregates can be poorly emissive, whereas H-aggregates can have fluorescence emission with high quantum yield. This behaviour can be probably explained by distortion of the arrangement and involvements of vibrational modes.
Figure 2.15 shows schematic absorption (blue) and emission (red) spectra from J- and H-aggregates of a cyanine dye. It can be seen that J-aggregate has a very narrow red-shifted

absorption and emission spectra with a negligible Stokes shift which can be explained by a large decoupling of the 0 - 0 transitions from vibrational modes. However, the real reason is still being discussed. The read-shift of the absorption spectra can go up to 100 nm and due to the narrow band the molar absorption coefficient ϵ is strongly increased.

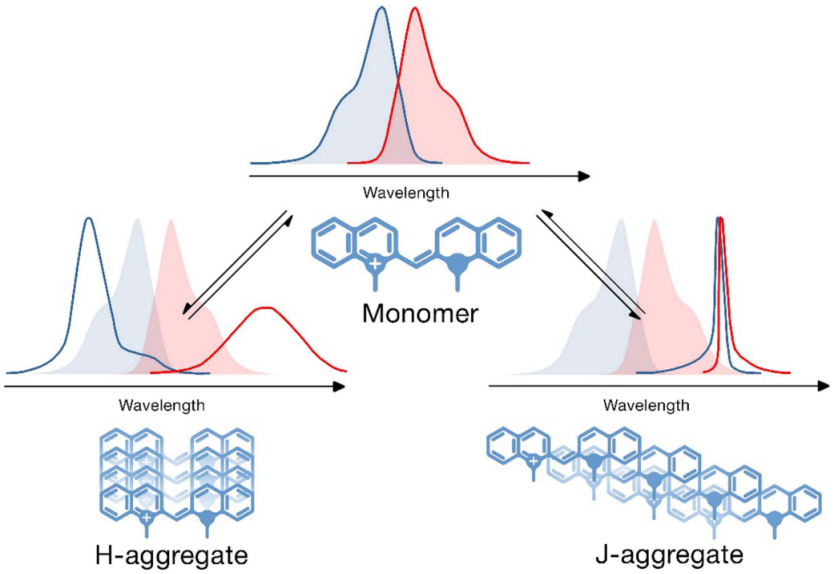

Figure 2.15: Schematic representation of the changes in absorption (blue) and fluorescence (red) spectra on the formation of H- and J-aggregates from cyanine dye monomers.[1]

J-aggregates are also known for very short excitation lifetimes in the picoseconds range which is also called "superradiance". This fast decay is attributed to a strong increase in oscillator strength resulting from the strong coupling between the dipole moments. Furthermore, they demonstrate high optical anisotropy that results in polarized fluorescence emission.

2.3.2 Aggregates Based on Porphyrinic Molecules

Pigments based on porphyrinic molecules play an important role in natural light-harvesting systems (LH) systems. Thereby, chlorophylls and bacteriochlorophylls are the predominant representatives. These porphyrin analogues consists of a chlorin or a bacteriochlorin skeleton which are fused with a five-membered ring with a keto function. Both, chlorophylls and bacteriochlorophylls are complexed with a magnesium ion (Figure 2.16).

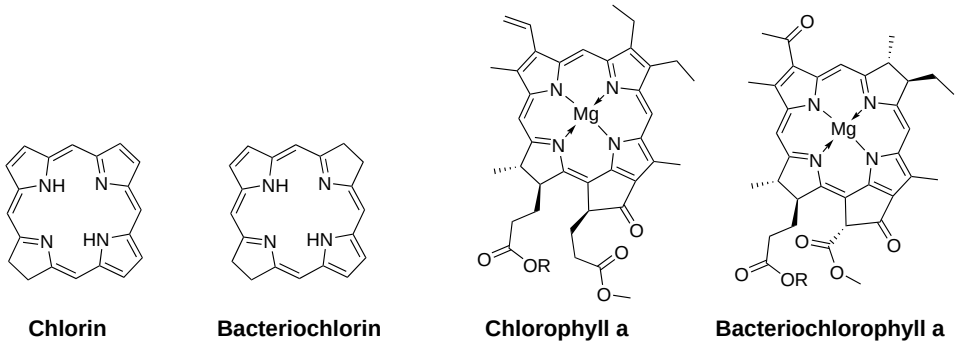

Figure 2.16: Structure of chlorin, bacteriochlorin, chlorophyll a and bacteriochlorophyll a. The substituent R in the chlorophyll a and bacteriochlorophyll a is a phytyl group.

The light-harvesting complexs II (LH II) of purple bacteria *Rhodopseudomonas (Rps.) acidophila* and other bacteria consist of bacteriochlorophyll a (BChl *a*) chromophores which are circularly arranged. In this ring the BChl *a* are aligned in a shifted arrangement with enables J-type coupling.

Inspired from this natural light-harvesting complexes, researchers tried to model such arrays based on artificial chlorin dyes. For example, Würthner and co-workers synthesised Zn chlorins, bearing alkyl-substituents which form J-aggregates in nonpolar solvents (Figure 2.17). Some of this aggregates showed a large bathochromically shifted Q_y-band (approximately 100 nm).

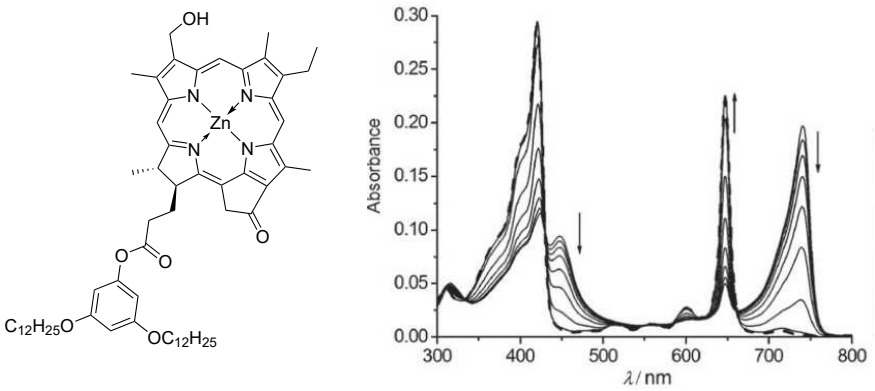

Figure 2.17: J-aggregates based on a semisynthetic zinc chlorin. **left)** Sturcture of the zink chlorin. **right)** Temperature-dependent UV/Vis spectra of the zinc chlorin in a 20:80 mixture of di-n-butyl ether/n-heptane (3×10^{-6} M). The arrows indicate the spectroscopic changes upon increasing the temperature from 15 °C up to 95 °C (bold dashed line: monomer spectrum at 95 °C).[2]

During the decades, it also has been attempted to synthesize J-aggregates based on porphyrins and metalloporphyrins. In the early 1990s Kobuke and co-workers synthesised *meso*-imidazolyl-substituted zinc porphyrins which can form arrays those resemblance dye arrays found in LH

systems of purple bacteria.
Probably, the most intensively studied J-aggregating porphyrin is tetrakis(4-sulfonatophenyl)-porphyrin ($TPPS_4$). In acidic ($pK_a < 4.8$) aqueous solution the pyrrole nitrogen of $TPPS_4$ are protonated, transforming it in its diacidic form (Figure 2.18) which forms J-aggregates.

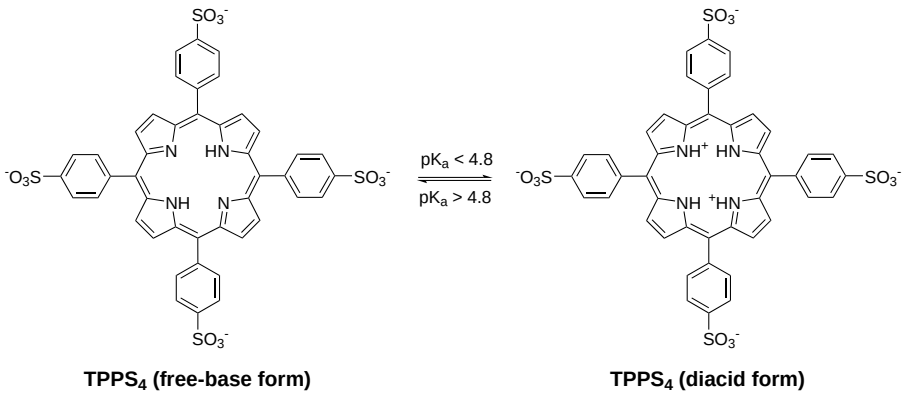

Figure 2.18: Structure of $TPPS_4$ in the free-base and diacid form

The aggregation is mediated by ion pair formation of the cationic porphyrin centres and the anionic sulfonate groups of the diacidic $TPPS_4$. Thereby, it is assumed that the monomers form planar shifted face-to-face J-type assemblies. At very low dye concentrations ($< 10^{-5}$ M), the diacidic $TPPS_4$ is in non-aggregated form. However, it was found that increasing the ionic strength by adding NaCl, KCl or $NaClO_4$ results in aggregation also at this low dye concentrations (Figure 2.19). It is assumed that the counteriouns form a "cloud" around the aggregates, which reduce the electrostatic repulsion between the charged porphyrins.

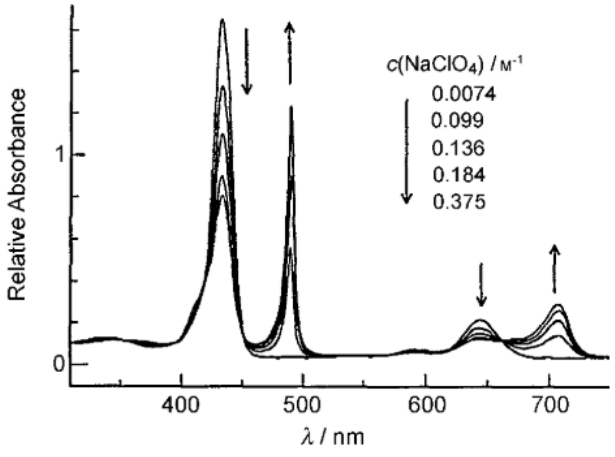

Figure 2.19: UV/Vis absorption spectra of $TPPS_4$ at a constant concentration of 7.2×10^{-6} M in acidic aqueous solution. The arrows indicate, the changes upon addition of $NaClO_4$ which leads to the formation of J-aggregates.[2]

The absorption spectrum of the formed J-aggregates shows two new absorption bands in respect to the monomer. The very narrow band at 491 nm is attributed to the monomeric Soret band and the broader band at 707 nm to the Q-band. Additionally, to the red-shifted absorption bands these aggregates have a decreased quantum yield and lifetime (monomer: 27 %, 4 ns; J-aggregate: 17 %, 3 ns) in presence of NaCl.

3 Materials and Methods

3.1 Chemicals

Table 3.1: List of used chemicals

Chemical	Supplier	CAS-Number
1,3-Cyclohexadiene	Fluorochem	592-57-4
1,8-Diazabicyclo[5.4.0]undeca-7-ene (DBU)	Fluka	6674-22-2
1-Bromododecane	Sigma-Aldrich	143-15-7
1-Nitro-1-cyclohexene	Sigma-Aldrich	2562-37-0
2,3-Dichloro-5,6-dicyano-p-benzochinone (DDQ)	Sigma-Aldrich	84-58-2
2,5,8,11-Tetraoxytridecane-13-ol	Fluorochem	23783-42-8
2-Isopropoxy-4,4,5,5-tetramethyl-1,3,2-dioxyborolane	TCI	61676-62-8
3,4-Dihydroxybenzaldehyde	TCI	139-85-5
4,16-Dibromo[2.2]paracyclophane	Alfa Aesar	96392-77-7
4-Decyloxybenzaldehyde	TCI	24083-16-7
4-Hydroxybenzaldehyde	Sigma-Aldrich	123-08-0
Acetic acid	Roth	64-19-7
Aluminium chloride	Fluka	7446-70-0
Bis(pinacolato)diboron	TCI	73183-34-3
Bis(trimethylsilyl)acetylene	TCI	14630-40-1
Bromobenzene	Acros organics	108-86-1
Dimethoxymethane	TCI	109-87-5
Ethyl isocyanoacetate	Fluorochem	2999-46-4
Ethylene glycol	Roth	107-21-1
Indium(III) chloride	Fluka	10025-82-8
Lithium	Acros organics	7439-93-2
N-Bromosuccinimide	TCI	128-08-5
Paraformaldehyde	Roth	30525-89-4
Phenyl lithium	unknown	591-51-5
Potassium acetate	Merck	127-08-2
Potassium acetate	Merck	127-08-2

continued

Table 3.1 – continued

Chemical	Supplier	CAS-Number
Potassium carbonate	Sigma-Aldrich	584-08-7
Potassium hydroxide	Merck	1310-58-3
Potassium tert-butoxide	Sigma-Aldrich	865-47-4
p-Toluenesulfonic acid monohydrate	Sigma-Aldrich	6192-52-5
p-Toluenesulfonyl chloride	TCI	98-59-9
Pd(amphos)Cl_2	Acros organics	887919-35-9
Pd(dppf)Cl_2	Sigma-Aldrich	72287-26-4
Pyridine	Roth	110-86-1
Pyrrol	ABCR	109-97-7
Pyrrole-2-carboxaldehyde	Sigma-Aldrich	1003-29-8
Sodium fluoride	unknown	7681-49-4
Sodium hydroxide	VWR Chemicals	1310-73-2
Sodium propionate	Sigma-Aldrich	137-40-6
Sodium sulfate	Roth	7757-82-8
tert-Butyl isocyanoacetate	Fluorochem	2769-72-4
tert-Butyllithium solution (1.7M in pentane)	Sigma-Aldrich	594-19-4
Tetrabutylammonium chloride	Sigma-Aldrich	1112-67-0
Trifluoracetic acid	TCI	76-05-1
Trimethoxymethane	TCI	149-73-5

3.2 Solvents

Table 3.2: List of used solvents

Solvent	Supplier	CAS-Number
Benzene	Promochem	71-43-2
Chloroform	VWR Chemicals	67-66-3
Cyclohexane	VWR Chemicals	110-82-7
Dichloromethane	VWR Chemicals	75-09-2
Diethyl ether	VWR Chemicals	60-29-7
Dimethylsulfoxide	TCI	67-68-5
Ethyl acetate	VWR Chemicals	141-78-6
Methanol	VWR Chemicals	67-56-1
N,N-Dimethylformamide	Roth	68-12-2
Novec 7200	3M	163702-06-5
Tetrahydrofuran	VWR Chemicals	109-99-9
Toluene	VWR Chemicals	108-88-3

3.3 Surfactants

Table 3.3: List of used surfactants

NMR-Solvent	Supplier	CAS-Number
Brij® 93	Sigma Aldrich	9004-98-2
Pluronic P123	Sigma Aldrich	9003-11-6
Sodium dodecyl sulfate (SDS)	Fluka	151-21-3
Span 80	TCI	1338-43-8
Triton® X-100	Sigma Aldrich	9002-93-1
Tween 85	TCI	9005-70-3

3.4 NMR-Solvents

Table 3.4: List of NMR-solvents

NMR-Solvent	Supplier	CAS-Number
Acetonitrile D3	Eurisotop	2206-26-0
Chloroform D + 0.03 %TMS	Eurisotop	865-49-6
DMSO D6 + 0.03 %TMS	Eurisotop	2266-27-1

3.5 Chromatography

3.5.1 Thin Layer Chromatography (TLC)

For thin layer chromatography silica gel plates from *Merck* (silica gel 60 F_{254} aluminium sheets 20x20) were used. As detection methods UV–detection (at λ=254 and 366 nm) as well as dinitrophenylhydrazin, vanillin/H_2SO_4 and CAM staining with subsequent developing by hot air stream were used.

3.5.2 Flash Column Chromatography

For preparative flash column chromatography silica gel from *Acros Organics* (silica gel, for chromatography 0.035 – 0.070 mm, 60 Å, nitrogen flushed) was used. The amount of silica used, depending on the specific separation problem, was in general the 100 fold of the amount of crude product. Column diameter was chosen to give a filling level between 15 and 25 cm.

3.6 Structural and Chemical Characterization

3.6.1 Nuclear Magnetic Resonance Spectroscopy (NMR)

^{1}H, COSY, ^{13}C-APT and HSQC spectra were recorded on a *AVANCE III* instrument by *Bruker* (300.36 MHz for ^{1}H-NMR and 75.53 MHz for ^{13}C-APT-NMR) which was coupled to an autosampler. For data analysis *MestReNova* NMR-software (v11.0.4) by *Mestrelab* was used. The residual signal of the deuterated solvent (e.g. $CDCl_3$) was used as an internal standard for the interpretation of the chemical shifts δ. ^{1}H-NMR-data in chapter 4 are depicted in following way: chemical shift δ in ppm (parts per million), multiplicity, coupling constant J in Hz (herz) and the number of protons. For multiplicity, common abbreviations are used: singlet (s), doublet (d), triplet (t), quartet (q), pentet (p), doublet of a doublet (dd), multiplet (m).

3.6.2 High Resolution Mass Spectrometry (HRMS)

High resolution mass spectra were recorded on a *Micromass TofSpec 2E* time-of-flight mass spectrometer by *Bruker*. For external calibration a suitable mixture of polyethylen glycol standards was used. This analysis was done by Prof. Dr. Saf's group at the Institute for Chemistry and Technology of Materials at Graz University of Technology. Data analysis was performed by *MassLynx™* MS-software (v4.1) from *Waters*.

3.6.3 Atmospheric Pressure Chemical Ionization Mass Spectrometer (APCI-MS)

Mass spectra for reaction monitoring was performed on a *expression CMS L* compact mass spectrometer by *Advion*. The spectrometer was equipped with an APCI ionisation source and quadrupol mass analyser (range 10-2000 m/z).
Data analysis was performed with the *Mass Express* software by *Advion*.

3.7 Photophysical Characterization

3.7.1 Absorption Spectra

Absorption spectra were measured on a *VARIAN CARY 50 conc* UV-Vis spectrophotometer by *Varian* and on a *Agilent Cary 60 UV-VIS* UV-Vis spectrophotometer by *Agilent Technologies*. Measurements were performed either at fast or medium scan rate wit baseline correction using the corresponding solvent as blank. For the measurements 10 mm precision cuvettes (type *100-OS* and *104-OS*) by *Hellma Analytics* were used.

3.7.2 Emission and Excitation Spectra

Emission and excitation spectra were recorded on a *FluoroLog®3* spectrofluorometer by *Horiba Scientific* equipped with a *R2658* photomultiplier by *Hamamazu*. For the measurements 10 mm precision cuvettes (type 100-OS) and precision cuvettes with screw-caps (type *100-QS*) by *Hellma Analytics* were used. An OG 590 filter (Schott) was used for recording emission spectra. Data analysis was performed with the *FluorEssence™* software by *Horiba Scientific*.

3.7.3 Temperature Dependency

The temperature for temperature dependency measurements was controlled by a *Cary SPV-1X0 Single Cell Peltier Accessory* peltier element from *Varian* in combination with a *F12-ED* refrigerated/heating circulator by *Julabo*.

3.7.4 Resonance Light Scattering (RLS)

Resonance light scattering measurements were executed on a *FluoroLog®3* spectrofluorometer by *Horiba Scientific* equipped with a *R2658* photomultiplier by *Hamamazu* in synchronous-scan mode and right-angle geometry. Two polarization filters rotated 90° to each other were mounted between light source/sample and sample/detector . All samples were diluted with water to get an absorbance of approximately 0.1.

3.7.5 Lifetime Measurements

Lifetimes were measured using single photon counting recorded on *FluoroLog®3* spectrofluorometer from *Horiba Scientific*. The setup was equipped with a *DeltaHub* module controlling the excitation source a *SpectraLED-390* ($\lambda = 392\,\text{nm}$) and a *NanoLED-450* ($\lambda = 453\,\text{nm}$) from *Horiba Scientific*, respectively. Data analysis was performed on *DAS-6 Analysis* software from *Horiba Scientific*. Thereby, data were fitted by a mono- or bi-exponential decay.

Before measuring the samples were diluted in toluene until the absorption spectrum showed an absorption intensity approximately 0.2.
Solutions of Pd porphyrin dyes were degassed during measurements by bubbling nitrogen (6.0) from *Linde Gas* through.

3.7.6 Relative Quantum Yield

Relative quantum yields (Φ_{rel}) were determined using a solution of H_2OEP in benzene as a standard (Φ= 0.13[68]). Emission and absorption spectra of the synthesised dyes were measured in toluene. All samples were diluted until an absorption intensity below 0.1 was achieved. The solutions of the Pd porphyrin dyes were thoroughly deoxygenated by bubbling nitrogen (6.0) from *Linde Gas* through. Depending on the absorption maximum of the dyes they were excited at 396, 407 and 412nm in the *FluoroLog®3* spectrofluorometer, respectively. An OG 590 filter (Schott) was used for recording emission spectra. Integration of emission spectra was performed with the *FluorEssence™* software by *Horiba Scientific*.

The relative quantum yields were calculated according to equation 3.1.[69]

$$\Phi_C = \Phi_R \frac{E_C}{E_R} \frac{B_R}{B_C} \frac{n_C^2}{n_R^2} \tag{3.1}$$

Φ	quantum yield
E	integrated area of the respective emission
B	absorption related term $(1 - 10^{abs})$
n	refractive index of the solvent
C, R	indices for compound and reference

3.7.7 Measurements at 77 K

Measurements at 77K were performed in a cryostat from *Horiba Scientific* cooled with liquid nitrogen.

4 Experimental

4.1 Synthesis of Pd-5,15-Diarylporphyrins

4.1.1 3,4-Bis(dodecyloxy)benzaldehyde (1b)

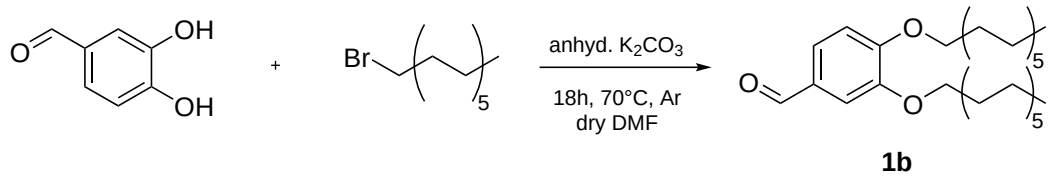

1b

Figure 4.1: Synthesis of compound **1b**

This synthesis was performed analogously to reference [70]. Anhydrous K_2CO_3 (2.77 g, 2.5 eq , 20.04 mmol) was suspended in a stirred solution of 3,4-dihydroxybenzaldehyde (1.04 g, 1 eq , 7.53 mmol) in dry DMF (30 mL) under argon atmosphere. 1-Bromododecane (3.8 mL, 2.1 eq , 15.83 mmol) was added drop wise and the reaction mixture was stirred at 70 °C for 18 h. The reaction progress was controlled via TLC (CH:EE, 10:1) and APCI-MS.
After full conversion the white solution was cooled to room temperature, thereby a white precipitate was formed. The reaction mixture was poured into water (50 mL) and the product was extracted with DCM. The organic layer was dried over anhydrous Na_2SO_4 before removing the solvent under vacuum. The crude product was purified by silica gel column chromatography (eluent: CH/5 % EE) to yield the product as a white powder **1b** (2.95 g, 82.6 %).

^{1}H-NMR (300 MHz, $CDCl_3$): δ 9.83 (s, 1H), 7.41 (d, J = 9.1 Hz, 2H), 6.95 (d, J = 8.0 Hz, 1H), 4.06 (q, J = 7.1 Hz, 4H), 1.85 (h, J = 6.6 Hz, 4H), 1.47 (t, J = 7.6 Hz, 4H), 1.41 – 1.19 (m, 32H), 0.88 (t, J = 6.5 Hz, 6H). ^{13}C-NMR (76 MHz, $CDCl_3$): δ 191.13, 154.85, 149.61, 130.04, 126.71, 111.94, 111.18, 69.32, 69.29, 32.08, 29.85, 29.81, 29.78, 29.76, 29.54, 29.52, 29.24, 29.15, 26.15, 26.11, 22.85, 14.26.

4.1.2 3,6,9,12-Tetraoxatridecyl-4-toluenesulfonate (2)

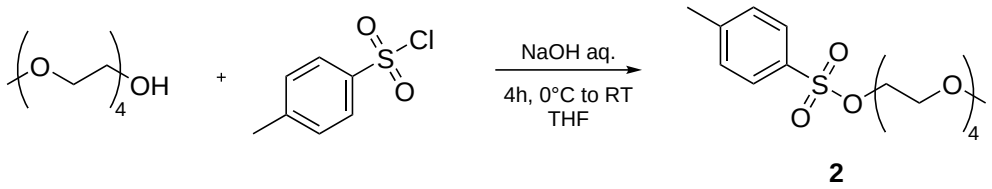

Figure 4.2: Synthesis of compound **2**

This synthesis was performed analogously to reference [71]. 2,5,8,11-Tetraoxytridecane-13-ol (6 mL, 1 eq , 29.96 mmol) was dissolved in THF (15 mL) and cooled down to 0 °C with an ice bath. NaOH (2.50 g, 2 eq , 62.51 mmol) dissolved in water (20 mL) was added and a solution of p-toluenesulfonyl chloride (7.49 g, 1.3 eq , 39.29 mmol) dissolved in THF (15 mL) was added drop wise over 30 min. Then the reaction mixture was allowed to warm up to room temperature. TLC and APCI-MS showed full conversion after stirring the solution for 3.5 h.
The aqueous layer was discarded and the organic layer was collected, washed three times with saturated brine and two times with a 0.1 M HCl solution and dried over anhydrous Na_2SO_4. Removing the solvent under reduced pressure gave a slightly yellowish oil **2** (10.30 g, 94.0 %).

^{1}H-NMR (300 MHz, $CDCl_3$): δ 7.80 (d, J = 8.1 Hz, 2H), 7.34 (d, J = 8.0 Hz, 2H), 4.16 (t, J = 4.9 Hz, 2H), 3.73 – 3.66 (m, 2H), 3.63 (s, 6H), 3.58 (s, 4H), 3.54 (dd, J = 5.7, 3.3 Hz, 2H), 3.37 (s, 3H), 2.45 (s, 3H). ^{13}C-NMR (76 MHz, $CDCl_3$): δ 144.77, 133.07, 129.81, 127.98, 71.94, 70.75, 70.61, 70.53, 69.24, 68.69, 59.02, 21.64.

4.1.3 4-(3,6,9,12-Tetraoxatridec-1-yloxy)benzaldehyde (3a)

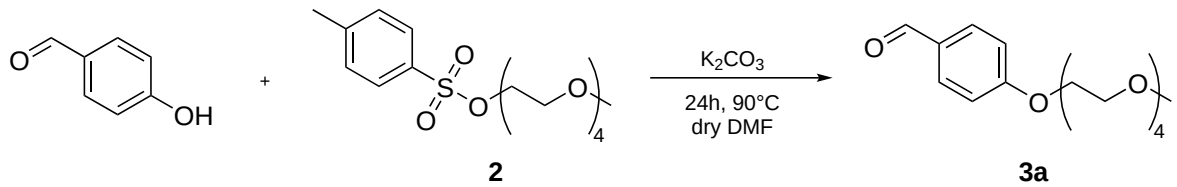

Figure 4.3: Synthesis of compound **3a**

This synthesis was performed analogously to reference [72]. Anhydrous K_2CO_3 (2.3 g, 2 eq , 16.64 mmol) was suspended in a stirred solution of 4-hydroxybenzaldehyde (1.01 g, 1 eq , 8.19 mmol) and **2** (3.26 g, 1.1 eq , 9.01 mmol) dissolved in dry DMF (15 mL). The reaction mixture was heated up to 90 °C and stirred for 24 h. The reaction progress was controlled via TLC (EE, dinitrophenylhydrazin as staining reagent) and APCI-MS.
After full conversion the reaction mixture was diluted with EE and the organic layer was washed

with saturated bicarbonate solution, water and saturated brine. Finally the organic layer was dried over anhydrous Na_2SO_4 and the solvent removed under reduced pressure to receive a yellowish oil **3a** (2.03 g, 79.2 %).

^{1}H-NMR (300 MHz, $CDCl_3$): δ 9.87 (s, 1H), 7.81 (d, J = 8.7 Hz, 2H), 7.01 (d, J = 8.6 Hz, 2H), 4.20 (t, J = 4.8 Hz, 2H), 3.88 (t, J = 4.9 Hz, 2H), 3.79 – 3.58 (m, 10H), 3.53 (dd, J = 5.7, 3.4 Hz, 2H), 3.36 (s, 3H). ^{13}C-NMR (76 MHz, $CDCl_3$): δ 190.87, 163.97, 132.04, 130.18, 115.00, 72.06, 71.03, 70.75, 70.65, 69.59, 67.90, 59.14.

4.1.4 3,4-Bis(3,6,9,12-tetraoxatridec-1-yloxy)benzaldehyde (3b)

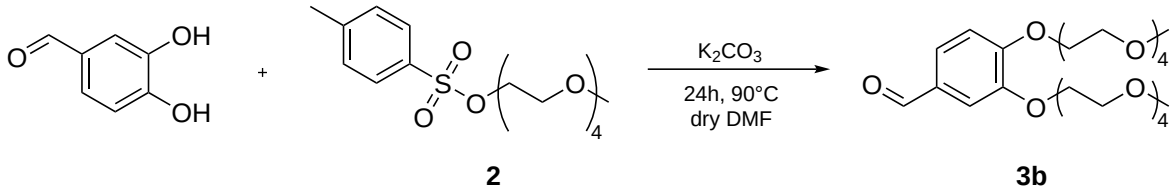

Figure 4.4: Synthesis of compound **3b**

This synthesis was performed analogously to **3a**, however anhydrous K_2CO_3 (2.00 g, 4 eq , 14.47 mmol), 3,4-dihydroxybenzaldehyde (510 mg, 1 eq , 3.69 mmol) and **2** (2.66 g, 2.2 eq , 7.99 mmol) dissolved in dry DMF (15 mL) were used instead. The product was isolated as a brown oil **3b** (1.27 g, 66.3 %).

^{1}H-NMR (300 MHz, $CDCl_3$): δ 9.82 (s, 1H), 7.43 (d, J = 9.0 Hz, 2H), 6.99 (d, J = 8.3 Hz, 1H), 4.22 (dt, J = 9.7, 5.1 Hz, 4H), 3.88 (q, J = 4.9 Hz, 4H), 3.73 (dd, J = 6.3, 3.6 Hz, 4H), 3.64 (d, J = 5.9 Hz, 16H), 3.53 (dd, J = 5.7, 3.4 Hz, 4H), 3.36 (s, 6H). ^{13}C-NMR (76 MHz, $CDCl_3$): δ 190.93, 154.49, 149.33, 130.41, 126.72, 112.74, 112.18, 77.16, 72.05, 71.08, 71.02, 70.79, 70.73, 70.64, 69.68, 69.55, 68.88, 68.80, 59.14.

4.1.5 2,2'-Dipyrromethane (4)

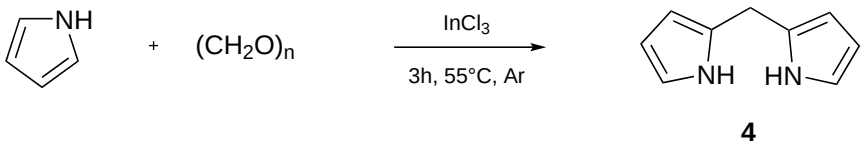

Figure 4.5: Synthesis of compound **4**

This synthesis was performed analogously to reference [73]. Paraformaldehyde (505 mg, 1 eq , 16.82 mmol) was suspended in freshly distilled pyrrole (36 mL) and the reaction mixture was

flushed with a stream of argon for 20 min. Then the suspension was heated up to 55 °C and stirred for 10 min under argon atmosphere. Indium(III) chloride (366 mg, 0.1 eq , 1.65 mmol) was added and the reaction mixture turned from a white suspension into a clear yellow solution. After stirring the solution for 3 h at 55 °C, the heating source was removed, NaOH (2.05 g, 3 eq , 51.25 mmol) was added and the mixture was stirred for a further hour at room temperature. Then the remaining pyrrole was removed under vacuum (70 mbar, 60 °C) to get a white/brownish solid. The solid was extracted with DCM, filtered through a silica frit and the remaining yellowish filtrate was concentrated under vacuum. The crude product was further purified by silica gel column chromatography (gradient from CH to CH+EE (10+2)) to yield the product as a white powder **4** (1.15 g, 46.7 %).

^{1}H-NMR (300 MHz, $CDCl_3$): δ 7.66 (s, 2H), 6.59 (q, J = 2.3 Hz, 2H), 6.14 (q, J = 2.9 Hz, 2H), 6.02 (d, J = 3.4 Hz, 2H), 3.92 (s, 2H). ^{13}C-NMR (76 MHz, $CDCl_3$): δ 129.09, 117.33, 108.38, 106.45, 26.39.

4.1.6 5,15-Diarylporphyrins (5a–c)

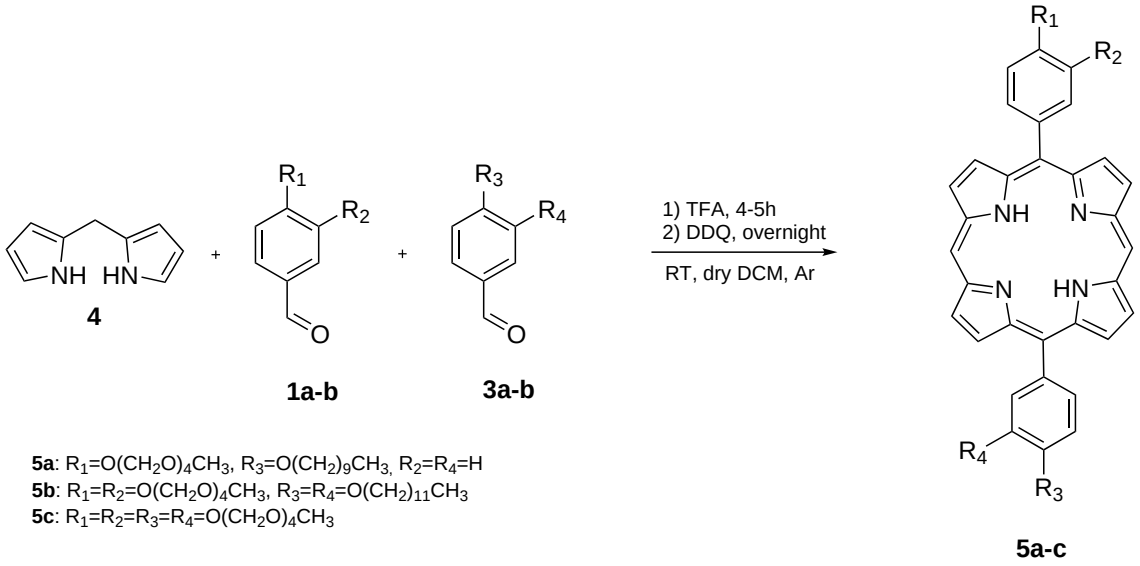

Figure 4.6: Synthesis of compound **5a**–**c**

5-(4-Decyloxyphenyl)-15-(4-(3,6,9,12-tetraoxatridec-1-yloxy)phenyl)-21H,23H-porphyrin (5a)

4-Decyloxybenzaldehyde **1a** (327.5 mg, 1 eq , 1.05 mmol), **3a** (270.7 mg, 1 eq , 1.03 mmol) and **4** (306 mg, 2 eq , 2.09 mmol) were dissolved in dry DCM (200 mL) under argon atmosphere and the mixture was degassed with a stream of argon for 20 min. Trifluoracetic acid (7 drops) was added drop wise and the solution was stirred at room temperature and shielded from light (wrapped in aluminium foil). The reaction was monitored by UV-VIS spectroscopy. After 4.5 h the absorption spectrum of the red, purple fluorescent solution did not change anymore and DDQ (693.0 mg, 3 eq , 3.05 mmol) was added. Afterwards, the solution was stirred overnight, thereby the colour turned to dark red and the solution started to show red fluorescence.
The solvent was removed under reduced pressure and the product was isolated and purified by silica gel column chromatography (DCM/MeOH) to yield a purple powder **5a** (220 mg, 25.5 %). During the purification step, three fractions were collected: the first was 5,15-bis(4-decyloxyphenyl)-21H,23H-porphyrin **24** (eluent: DCM), the second was the desired product (eluent: DCM+MeOH, 100+1) and the third was 5,15-bis(4-(3,6,9,12-tetraoxatridec-1-yloxy)phenyl)-21H,23H-porphyrin (eluent: DCM+MeOH, 100+4).

^{1}H-NMR (300 MHz, $CDCl_3$): δ 10.30 (s, 2H), 9.39 (d, J = 4.7 Hz, 4H), 9.11 (dd, J = 6.7, 4.6 Hz, 4H), 8.17 (d, J = 8.1 Hz, 4H), 7.34 (dd, J = 8.4, 5.3 Hz, 4H), 4.44 (t, J = 4.8 Hz, 2H), 4.27 (t, J = 6.5 Hz, 2H), 4.07 (t, J = 4.8 Hz, 2H), 3.89 (dd, J = 6.1, 3.7 Hz, 2H), 3.76 (dddt, J = 18.3, 15.3, 6.2, 3.4 Hz, 8H), 3.66 – 3.54 (m, 2H), 3.42 (s, 3H), 2.01 (p, J = 6.9 Hz, 2H), 1.64 (q, J = 6.7 Hz, 2H), 1.54 – 1.31 (m, 12H), 0.95 (t, J = 6.5 Hz, 3H), -3.06 (s, 2H). ^{13}C-NMR (76 MHz, $CDCl_3$): δ 159.23, 158.88, 147.68, 147.63, 145.23, 136.01, 135.96, 134.09, 133.66, 131.64, 131.62, 131.19, 131.11, 119.14, 118.90, 113.37, 113.25, 105.28, 72.15, 71.15, 70.93, 70.89, 70.87, 70.75, 70.09, 68.54, 67.94, 59.22, 32.12, 29.85, 29.81, 29.70, 29.56, 26.41, 22.89, 14.32. MALDI TOF: m/z: [M^+] calc. for $C_{51}H_{60}N_4O_6$: 824.4513, found: 824.4526.

5-(3,4-Bis(dodecyloxy)phenyl)-15-(3,4-bis(3,6,9,12-tetraoxatridec-1-yloxy)phenyl)-21H,23H-porphyrin (5b)

1b (269.5 mg, 1 eq , 519.7 µmol), **3b** (254.6 mg, 1 eq , 536.6 µmol) and **4** (150.2 mg, 2 eq , 1.03 mmol) were dissolved in dry DCM (100 mL) under argon atmosphere and the mixture was degassed with a stream of argon for 20 min. Trifluoracetic acid (5 drops) was added drop wise and the solution was stirred at room temperature and shielded from light (wrapped in aluminium foil). The reaction was monitored by UV-VIS spectroscopy. After 5 h the absorption spectrum of the red, purple fluorescent solution did not change anymore and DDQ (693.0 mg, 3 eq , 3.05 mmol) was added. Afterwards, the solution was stirred overnight, thereby the colour turned to dark red and the solution started to fluoresce red.

The solvent was removed under reduced pressure and the product was isolated and purified by silica gel column chromatography (DCM/MeOH) to yield a purple powder **5b** (163.6 mg, 24.7 %).
During the purification step, three fractions were collected: the first was 5,15-bis(3,4-bis(dodecyloxy)phenyl)-21H,23H-porphyrin (eluent: DCM), the second was the desired product (eluent: DCM+MeOH, 100+3) and the third was 5,15-bis(4-(3,6,9,12-tetraoxatridec-1-yloxy)phenyl)-21H,23H-porphyrin **5c** (eluent: DCM+MeOH, 100+8).

^{1}H-NMR (300 MHz, $CDCl_3$): δ 10.30 (s, 2H), 9.39 (d, J = 4.7 Hz, 4H), 9.14 (dd, J = 9.4, 4.6 Hz, 4H), 7.94 – 7.73 (m, 4H), 7.35 (d, J = 8.1 Hz, 1H), 7.30 (d, J = 8.2 Hz, 1H), 4.51 (t, J = 5.0 Hz, 2H), 4.42 – 4.35 (m, 2H), 4.33 (s, 2H), 4.18 (t, J = 6.6 Hz, 2H), 4.11 (t, J = 5.2 Hz, 2H), 3.96 (t, J = 4.9 Hz, 2H), 3.92 (s, 2H), 3.76 (tdd, J = 16.4, 5.3, 2.7 Hz, 10H), 3.60 (ddd, J = 9.1, 6.0, 3.8 Hz, 4H), 3.50 (t, J = 4.9 Hz, 2H), 3.41 (s, 3H), 3.40 – 3.29 (m, 6H), 3.24 (s, 3H), 2.06 (p, J = 7.2 Hz, 2H), 1.93 (p, J = 6.8 Hz, 2H), 1.68 (p, J = 7.3 Hz, 2H), 1.61 – 1.19 (m, 36H), 0.89 (dt, J = 18.1, 6.7 Hz, 6H), -3.07 (s, 2H). ^{13}C-NMR (76 MHz, $CDCl_3$): δ 149.29, 149.08, 147.66, 147.63, 147.55, 147.50, 145.28, 134.83, 134.15, 131.67, 131.61, 131.24, 131.12, 128.53, 128.06, 121.93, 121.20, 119.29, 118.77, 113.19, 112.35, 105.33, 72.13, 71.86, 71.17, 71.02, 70.96, 70.86, 70.76, 70.73, 70.60, 70.53, 70.42, 70.14, 70.05, 69.70, 69.36, 69.32, 59.20, 59.01, 32.12, 32.05, 29.94, 29.91, 29.89, 29.83, 29.77, 29.72, 29.63, 29.59, 29.58, 29.48, 26.42, 26.25, 22.88, 22.81, 14.30, 14.24. MALDI TOF: m/z: [MH^+] calc. for $C_{74}H_{107}N_4O_{12}$: 1243.7886, found: 1243.7855.

5,15-Bis(3,4-bis(3,6,9,12-tetraoxatridec-1-yloxy)phenyl)-21H,23H-porphyrin (5c)

Porphyrin **5c** was obtained as a side product of synthesis **5b**. The product was isolated as a purple solid **5c** (66 mg, 9.6 %).

^{1}H-NMR (300 MHz, $CDCl_3$): δ 10.30 (s, 2H), 9.39 (d, J = 4.7 Hz, 4H), 9.12 (d, J = 4.7 Hz, 4H), 7.88 (d, J = 2.0 Hz, 2H), 7.80 (d, J = 7.9 Hz, 2H), 7.34 (d, J = 8.2 Hz, 2H), 4.50 (t, J = 5.0 Hz, 4H), 4.36 (t, J = 4.9 Hz, 4H), 4.10 (t, J = 5.0 Hz, 4H), 3.95 (t, J = 4.9 Hz, 4H), 3.91 (dd, J = 6.1, 3.5 Hz, 4H), 3.75 (dddd, J = 20.7, 13.0, 5.3, 2.8 Hz, 20H), 3.60 (ddd, J = 9.3, 5.9, 3.2 Hz, 8H), 3.51 (q, J = 4.7 Hz, 4H), 3.45 – 3.30 (m, 18H), 3.24 (d, J = 3.4 Hz, 6H). ^{13}C-NMR (76 MHz, $CDCl_3$): δ 149.04, 147.49, 145.28, 134.77, 131.69, 131.14, 128.51, 121.81, 118.84, 113.10, 105.36, 72.10, 71.85, 71.12, 70.98, 70.92, 70.83, 70.81, 70.72, 70.69, 70.58, 70.50, 70.39, 70.10, 70.01, 69.29, 69.26, 59.17, 58.99. MALDI TOF: m/z: [MH^+] calc. for $C_{68}H_{95}N_4O_{20}$: 1287.6539, found: 1287.6539.

4.1.7 Pd-5,15-Diarylporphyrins (6a–c)

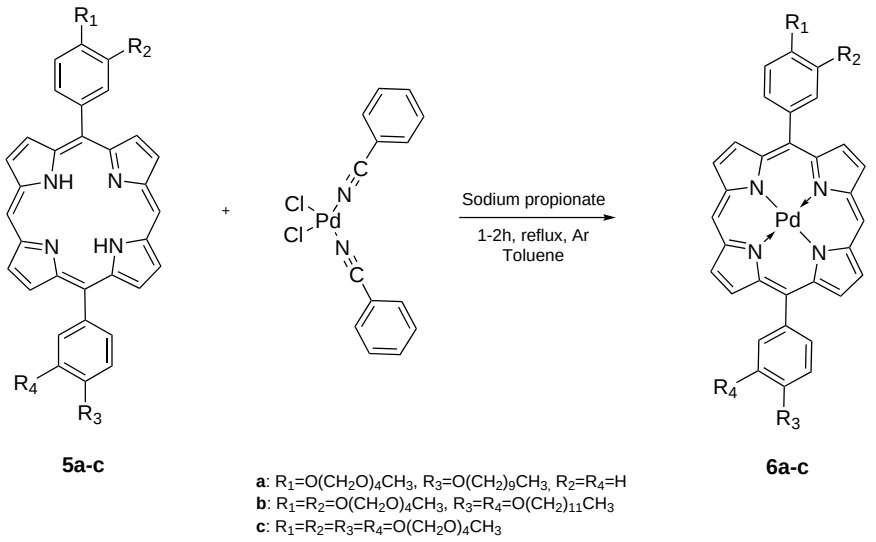

Figure 4.7: Synthesis of compound **6a**–**c**

Pd-5-(4-Decyloxyphenyl)-15-(4-(3,6,9,12-tetraoxatridec-1-yloxy)phenyl)-21H,23H-porphyrin (6a)

Porphyrin **6a** (20.0 mg, 1 eq , 24.2 µmol) was dissolved in toluene (10 mL) in a three neck round bottom flask with additional condenser under argon atmosphere. Sodium propionate (18 mg, 8 eq , 193.9 µmol) was added and the solution was headed to reflux. Then $Pd(BN)_2Cl_2$ (18.8 mg, 1.5 eq , 36.0 µmol) dissolved in toluene (5 mL) was added in three portions over 30 min and the solution was stirred under reflux for 90 min. The reaction was monitored via UV-VIS spectroscopy.
After full conversion, the solvent was evaporated under reduced pressure and the residue was purified by silica gel column chromatography (eluent: DCM+MeOH, 100+1) to yield the product as a red solid **6a** (21.4 mg, 95.4 %).

^{1}H-NMR (300 MHz, $CDCl_3$): δ 10.18 (s, 2H), 9.22 (d, J = 4.8 Hz, 4H), 8.99 (dd, J = 7.5, 4.7 Hz, 4H), 8.05 (d, J = 8.1 Hz, 4H), 7.25 (q, J = 3.8 Hz, 4H), 4.37 (t, J = 4.9 Hz, 2H), 4.20 (t, J = 6.5 Hz, 2H), 4.02 (t, J = 4.8 Hz, 2H), 3.73 (dddd, J = 16.1, 11.3, 5.3, 2.9 Hz, 10H), 3.58 (dd, J = 5.8, 3.5 Hz, 2H), 3.39 (s, 3H), 1.96 (p, J = 6.8 Hz, 2H), 1.62 (d, J = 7.4 Hz, 4H), 1.40 (dd, J = 30.8, 10.4 Hz, 13H), 0.93 (t, J = 6.5 Hz, 3H). ^{13}C-NMR (76 MHz, $CDCl_3$): δ 159.05, 158.69, 141.69, 141.63, 141.00, 135.28, 135.24, 134.10, 133.67, 131.49, 131.42, 130.83, 130.81, 120.57, 120.36, 112.99, 112.87, 106.94, 72.02, 71.00, 70.79, 70.75, 70.73, 70.61, 69.95, 68.38, 67.77, 59.09, 32.00, 29.72, 29.68, 29.57, 29.54, 29.43, 26.28, 22.77, 14.19. MALDI TOF: m/z: [M^+] calc. for $C_{51}H_{58}N_4O_6Pd$: 928.3409, found: 928.3416.

Pd-5-(3,4-Bis(dodecyloxy)phenyl)-15-(3,4-bis(3,6,9,12-tetraoxatridec-1-yloxy)-phenyl)-21H,23H-porphyrin (6b)

This synthesis was performed analogously to **6a**, however porphyrin **6b** (32.0 mg, 1 eq , 24.2 µmol) dissolved in toluene (20 mL), sodium propionate (20.0 mg, 8.7 eq , 208.2 µmol) and $Pd(BN)_2Cl_2$ (13.0 mg, 1.3 eq , 33.9 µmol) dissolved in toluene (8 mL) were used instead. Purification was carried out by silica gel column chromatography (eluent: DCM+MeOH, 100+3). The product was isolated as a red solid **6b** (21.0 mg, 60.7 %).

^{1}H-NMR (300 MHz, $CDCl_3$): δ 10.23 (s, 2H), 9.26 (d, J = 4.9 Hz, 4H), 9.06 (dd, J = 10.3, 4.8 Hz, 4H), 7.92 – 7.75 (m, 2H), 7.72 (t, J = 9.1 Hz, 2H), 7.28 (d, J = 14.3 Hz, 2H), 4.49 (t, J = 5.1 Hz, 2H), 4.31 (q, J = 5.4 Hz, 4H), 4.11 (dt, J = 9.8, 5.9 Hz, 4H), 3.92 (q, J = 4.6 Hz, 4H), 3.76 (dtd, J = 20.4, 10.1, 9.6, 5.1 Hz, 10H), 3.59 (dt, J = 6.6, 3.4 Hz, 4H), 3.51 – 3.45 (m, 2H), 3.40 (s, 3H), 3.39 – 3.27 (m, 6H), 3.23 (s, 3H), 2.05 (p, J = 7.0 Hz, 2H), 1.90 (p, J = 6.9 Hz, 2H), 1.67 (p, J = 7.2 Hz, 2H), 1.53 – 1.44 (m, 4H), 1.43 – 1.19 (m, 32H), 0.92 (t, J = 6.4 Hz, 3H), 0.85 (t, J = 6.6 Hz, 3H). ^{13}C-NMR (76 MHz, $CDCl_3$): δ 149.22, 149.02, 147.45, 147.34, 141.79, 141.66, 141.22, 141.19, 134.97, 134.29, 131.72, 131.58, 131.03, 130.98, 127.91, 127.42, 121.34, 120.88, 120.63, 120.42, 112.96, 112.16, 107.13, 72.13, 71.87, 71.16, 71.01, 70.96, 70.85, 70.73, 70.58, 70.52, 70.42, 70.13, 70.02, 69.72, 69.62, 69.30, 59.19, 59.01, 32.12, 32.04, 29.94, 29.91, 29.88, 29.82, 29.76, 29.61, 29.57, 29.48, 26.42, 26.23, 22.88, 22.80, 14.29, 14.23. MALDI TOF: m/z: [M^+] calc. for $C_{74}H_{104}N_4O_{12}Pd$: 1346.6710, found: 1346.6689.

Pd 5,15-bis(3,4-bis(3,6,9,12-Tetraoxatridec-1-yloxy)phenyl)-21H,23H-porphyrin (6c)

This synthesis was performed analogously to **6a**, however porphyrin **6c** (18.0 mg, 1 eq , 13.5 µmol) dissolved in toluene (10 mL), sodium propionate (19.2 mg, 15 eq , 197.8 µmol) and $Pd(BN)_2Cl_2$ (6.7 mg, 1.3 eq , 17.6 µmol) dissolved in toluene (5 mL) were used instead. Purification was carried out by silica gel column chromatography (DCM+MeOH 100+5). The product was isolated as a red solid **6b** (12.7 mg, 65.4 %).

^{1}H-NMR (300 MHz, CD_3CN): δ 10.19 (s, 2H), 9.22 (dd, J = 4.9, 1.8 Hz, 4H), 8.94 (t, J = 4.4 Hz, 4H), 7.74 (dd, J = 6.2, 2.1 Hz, 2H), 7.60 – 7.48 (m, 2H), 7.20 (t, J = 8.6 Hz, 2H), 4.31 (q, J = 5.4 Hz, 4H), 4.16 (q, J = 4.3 Hz, 4H), 3.99 – 3.89 (m, 4H), 3.77 – 3.42 (m, 40H), 3.35 – 3.13 (m, 24H), 3.08 (d, J = 1.6 Hz, 6H). ^{13}C-NMR (76 MHz, CD_3CN): δ 149.30, 147.50, 142.09, 141.74, 135.09, 132.11, 128.55, 121.35, 121.06, 112.91, 107.93, 72.46, 72.23, 71.07, 70.88, 70.83, 70.73, 70.65, 70.56, 70.48, 70.09, 69.95, 69.43, 69.35, 59.05, 58.87. MALDI TOF: m/z: [M^+] calc. for $C_{68}H_{92}N_4O_{20}Pd$: 1390.5363, found: 1390.5376.

4.2 Synthesis of Pd-5,15-Diaryltetrabenzoporphyrin: Pathway 1

4.2.1 Ethyl 4,5,6,7-tetrahydro-2H-isoindole-l-carboxylate (7)

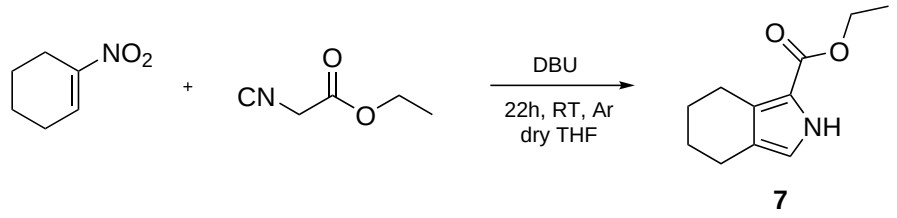

Figure 4.8: Synthesis of compound **7**

This synthesis was performed analogously to reference [74]. Dry THF (30 mL) was degassed by three freeze-pump-thaw cycles in a 50 mL Schlenk tube. 1-Nitro-1-cyclohexene (598.9 mg, 1 eq , 4.71 mmol) and ethyl isocyanoacetate (530.5 mg, 1 eq , 4.69 mmol) were added and DBU (754.8 mg, 1.05 eq , 4.96 mmol) was added drop wise to the brown solution. The mixture was stirred overnight at room temperature. A white/brown precipitate was formed overnight. The reaction was monitored by TLC (DCM) and APCI-MS.
After 22 h all reagents were converted and the solvent was evaporated under reduced pressure. The crude brown product was purified by silica gel column chromatography (eluent: DCM) to yield the product as a white powder **7** (637.0 mg, 70.0 %).

^{1}H-NMR (300 MHz, $CDCl_3$): δ 8.84 (s, 1H), 6.64 (d, J = 3.0 Hz, 1H), 4.30 (q, J = 7.2 Hz, 2H), 2.82 (t, J = 5.8 Hz, 2H), 2.55 (t, J = 5.6 Hz, 2H), 1.74 (tq, J = 12.4, 6.5, 5.0 Hz, 4H), 1.34 (t, J = 7.1 Hz, 3H). ^{13}C-NMR (76 MHz, $CDCl_3$): δ 161.77, 128.26, 122.28, 118.73, 117.89, 77.16, 59.87, 23.56, 23.49, 23.29, 22.06, 14.72.

4.2.2 Bis(3-ethoxycarbonyl-4,5,6,7-tetrahydro-2H-isoindolyl)methane (8)

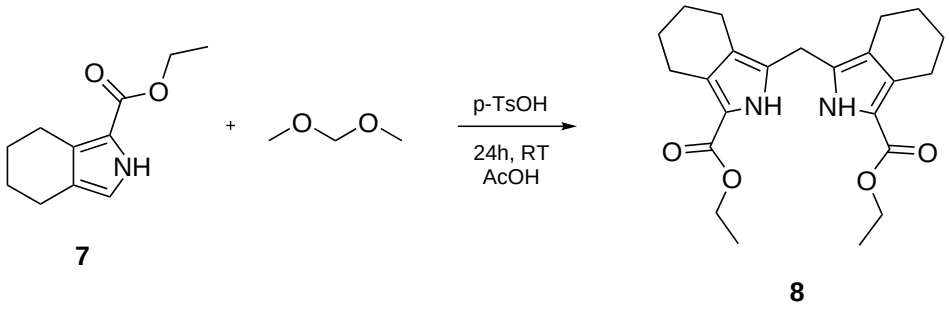

Figure 4.9: Synthesis of compound **8**

This synthesis was performed analogously to reference [60]. **7** (407.0 mg, 2 eq , 2.11 mmol), dimethoxymethane (80.9 mg, 1 eq , 1.06 mmol), p-toluenesulfonic acid monohydrate (40.0 mg, 0.2 eq , 232.3 µmol) were dissolved in AcOH (30 mL). The reaction mixture was stirred 24 h at room temperature, thereby a white precipitate was formed.
After full conversion (detected by TLC (eluent: DCM) and APCI-MS) the mixture was poured onto cold water (50 mL). The precipitate was collected by filtration, washed with water and recrystallised from EtOH to give the product as a white powder **8** (349.0 mg, 83.0 %).

^{1}H-NMR (300 MHz, $CDCl_3$): δ 11.14 (s, 2H), 4.19 (q, J = 7.1 Hz, 4H), 3.69 (s, 2H), 2.75 – 2.57 (m, 4H), 2.39 – 2.24 (m, 4H), 1.71 – 1.50 (m, 8H), 1.25 (t, J = 7.1 Hz, 6H). ^{13}C-NMR (76 MHz, $CDCl_3$): δ 160.83, 129.98, 127.54, 117.53, 115.24, 58.86, 23.02, 22.96, 22.86, 21.68, 20.79, 14.54.

4.2.3 Bis(4,5,6,7-tetrahydro-2H-isoindolyl)methane (9)

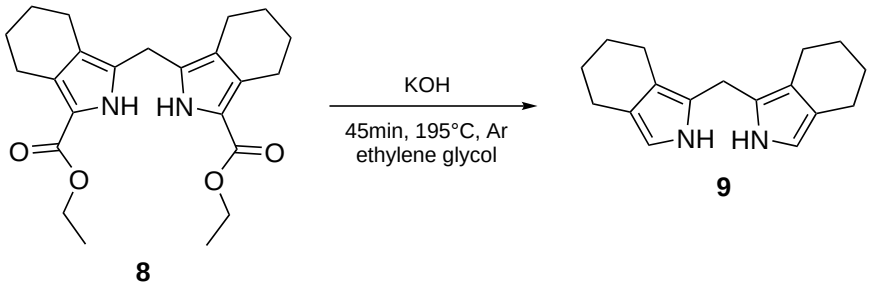

8 **9**

Figure 4.10: Synthesis of compound **9**

This synthesis was performed analogously to reference [60]. **8** (305.5 mg, 1 eq , 766.6 µmol) and KOH (255.9 mg, 6 eq , 4.56 mmol) were suspended in ethylene glycol (20 mL) in a 50 mL Schlenk tube. The suspension was thoroughly degassed by three freeze-pump-thaw cycles and heated up to 195 °C. After 45 min APCI-MS showed full conversion.
The orange reaction mixture was cooled to room temperature by a water bath. Then DCM (25 mL) was added and the organic layer was extracted two times with water (30 mL) and one time by brine. The organic layer was dried with anhydrous Na_2SO_4 and the solvent removed under reduced pressure to give the crude product as a brown oil **9**. The very unstable product was used immediately in the next step (synthesis of compound **10**) without further purification.

4.2.4 5-(4-Decyloxyphenyl)-15-(4-(3,6,9,12-tetraoxatridec-1-yloxy))-tetracyclohexenoporphyrin (10)

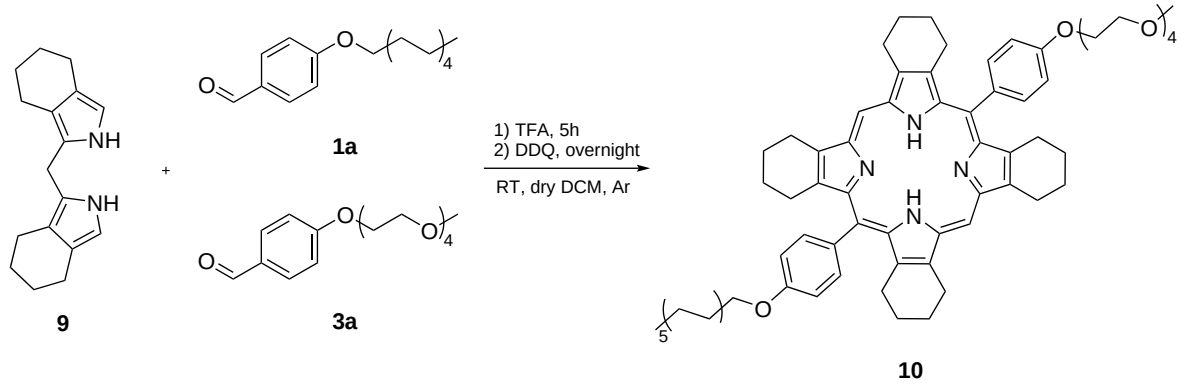

Figure 4.11: Synthesis of compound **10**

Dry DCM (60 mL) was degassed 30 min by a stream of argon. **1a** (105.0 mg, 1 eq , 400.2 µmol), **3a** (136.0 mg, 1 eq , 435.4 µmol) and **9** (207 mg, 2 eq , 813.8 mmol) dissolved in dry DCM (10 mL) were added under argon atmosphere. Trifluoracetic acid (6 drops) was added drop wise and the solution was stirred at room temperature and shielded from light (wrapped in aluminium foil). The reaction was monitored by UV-VIS spectroscopy. After 5 h the absorption spectrum did not change anymore and DDQ (272.0 mg, 3 eq , 1.20 mmol) was added. Afterwards, the solution was stirred overnight.

The solvent was removed under reduced pressure and the product was isolated and purified by silica gel column chromatography (DCM/MeOH) to yield a purple powder **10** (66.3 mg, 15.9 %).

During the purification step, three fractions were collected: the first was 5,15-bis(4-decyloxyphenyl)tetracyclohexenoporphyrin (eluent: DCM+MeOH, 100+1), the second was the desired product (eluent: DCM+MeOH, 100+3) and the third was 5,15-bis(4-(3,6,9,12-tetraoxatridec-1-yloxy)phenyl)tetracyclohexenoporphyrin (eluent: DCM+MeOH, 100+6).

^{1}H-NMR (300 MHz, $CDCl_3$): δ 10.00 (s, 2H), 7.84 (t, J = 7.6 Hz, 4H), 7.18 (t, J = 7.9 Hz, 4H), 4.34 (d, J = 3.8 Hz, 2H), 4.22 (t, J = 6.6 Hz, 2H), 4.18 – 4.08 (m, 8H), 4.05 (t, J = 4.8 Hz, 2H), 3.92 – 3.85 (m, 2H), 3.83 – 3.69 (m, 8H), 3.63 – 3.57 (m, 2H), 3.41 (s, 3H), 2.90 – 2.73 (m, 8H), 2.39 – 2.25 (m, 8H), 2.13 – 1.93 (m, 10H), 1.62 (q, J = 7.4, 6.9 Hz, 2H), 1.50 – 1.32 (m, 12H), 0.94 (t, J = 6.5 Hz, 3H), -2.47 (s, 2H). ^{13}C-NMR (76 MHz, $CDCl_3$): δ 159.42, 159.06, 145.27, 145.21, 141.66, 140.38, 140.36, 139.29, 139.22, 134.39, 134.04, 133.65, 117.48, 117.30, 113.65, 95.89, 72.16, 71.17, 70.90, 70.86, 70.76, 70.20, 68.51, 67.75, 59.23, 32.13, 29.85, 29.82, 29.78, 29.69, 29.56, 26.50, 26.47, 26.40, 24.83, 24.24, 23.34, 22.90, 14.32.

4.2.5 Pd-5-(4-decyloxyphenyl)-15-(4-(3,6,9,12-tetraoxatridec-1-yloxy)-phenyl)tetracyclohexenoporphyrin (11)

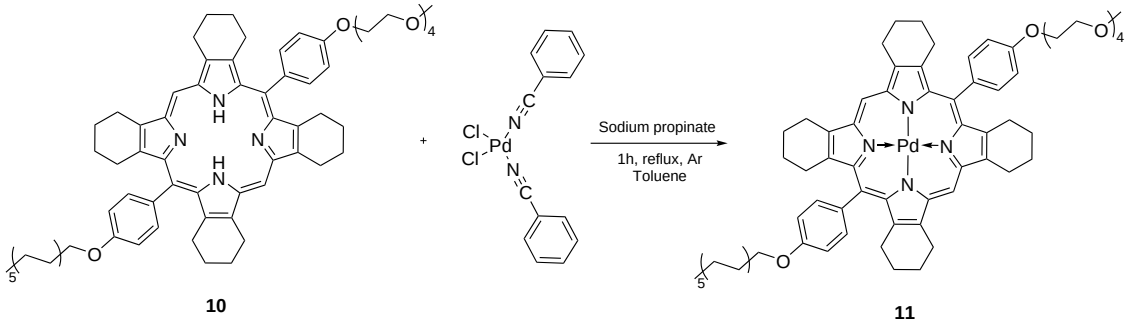

Figure 4.12: Synthesis of compound **11**

Porphyrin **10** (56.3 mg, 1 eq , 54.1 µmol) was dissolved in toluene (30 mL) in a three neck round bottom flask with additional condenser under argon atmosphere. Sodium propionate (18 mg, 8 eq , 193.9 µmol) was added and the solution was headed to reflux. Then $Pd(BN)_2Cl_2$ (26.8 mg, 1.3 eq , 70.3 µmol) dissolved in toluene (7 mL) was added in three portions over 30 min and the solution was stirred under reflux for 120 min. The reaction was monitored via UV-VIS spectroscopy.
After full conversion, the solvent was evaporated under reduced pressure and the residue was purified by silica gel column chromatography (DCM+MeOH 100+1) to yield the product as a red solid **11** (45.2 mg, 73.0 %).

^{1}H-NMR (300 MHz, $CDCl_3$): δ 9.86 (s, 2H), 7.82 (d, J = 8.1 Hz, 4H), 7.19 (d, J = 8.1 Hz, 4H), 4.40 (t, 2H), 4.24 (t, J = 6.7 Hz, 2H), 4.15 – 3.97 (m, 10H), 3.88 (dd, J = 6.1, 3.4 Hz, 2H), 3.76 (dddd, J = 16.9, 14.7, 5.3, 2.9 Hz, 8H), 3.59 (t, J = 5.8, 3.5 Hz, 2H), 3.41 (s, 3H), 2.85 – 2.62 (m, 8H), 2.38 – 2.16 (m, 8H), 2.10 – 1.92 (m, 10H), 1.71 – 1.59 (m, 2H), 1.49 – 1.29 (m, 12H), 0.92 (t, J = 6.2 Hz, 3H).

4.2.6 Pd-5-(4-decyloxyphenyl)-15-(4-(3,6,9,12-tetraoxatridec-1-yloxy)-phenyl)tetrabenzoporphyrin (12)

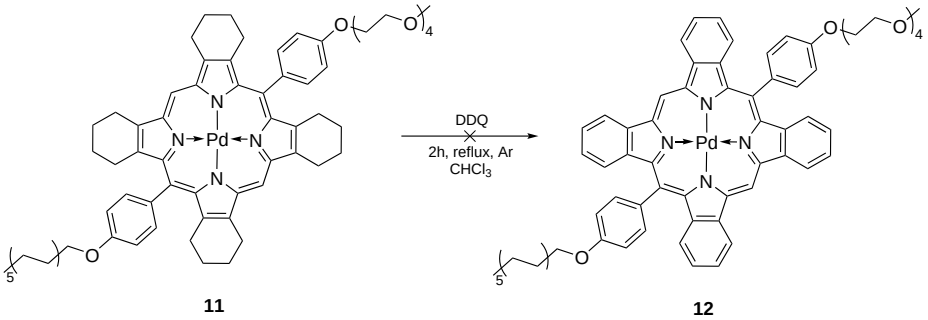

Figure 4.13: Synthesis of compound **12**

Pd-porphyrin **11** (31.0 mg, 1 eq , 27.1 µmol) was dissolved in $CHCl_3$ (5 mL) under argon atmosphere and the solution was flushed 2 min with argon. Then DDQ (61.8 mg, 10 eq , 272.3 µmol) were added. The reaction mixture was heated to 62 °C and stirred for 2 h. The solution turned from red to green. Water was added and the organic layer was washed with water and brine. The $CHCl_3$ layer was dried over anhydrous Na_2SO_4 and the solvent removed under reduced pressure. The green residue was purified by silica gel column chromatography (DCM/MeOH), but no product could be isolated.

4.3 Synthesis of Pd-5,15-Diaryltetrabenzoporphyrin: Pathway 2

4.3.1 2-(Trimethylsilyl)ethynyl p-tolyl sulfone (13)

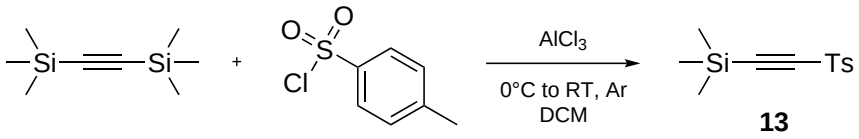

Figure 4.14: Synthesis of compound **13**

This synthesis was performed analogously to reference [44]. In a two-neck round-bottom flask (100 mL) aluminium chloride (4.88 g, 1.22 eq , 36.6 mmol) was dissolved in dry DCM (40 mL) under argon atmosphere and p-toluenesulfonyl chloride (6.86 g, 1.2 eq , 36.0 mmol) was added. The slightly yellow solution was stirred for 30 min at room temperature. In a second two-neck round-bottom flask (100 mL) armed with an addition funnel bis(trimethylsilyl)acetylene

(5.12 g, 1 eq , 30.1 mmol) was dissolved in dry DCM (40 mL) under argon atmosphere and the solution was cooled to 0 °C. The aluminium chloride/p-toluenesulfonyl chloride mixture was transferred via a syringe in the addition funnel and was dropped over a period of 40 min to the bis(trimethylsilyl)acetylene solution. Afterwards, the dark reaction mixture was warmed to RT and stirred overnight under argon atmosphere. The reaction progress was followed by TLC (eluent: CH+EE, 8+1; product **13** $R_f = 0,52$ and deprotected product **14** $R_f = 0,23$) and APCI-MS.
After 22 h the reaction was finished and the reaction mixture was poured in ice water (50 mL). The organic layer was collected and the aqueous layer was extracted three times with DCM (50 mL). Then the organic layers were combined, dried with anhydrous Na_2SO_4 and the solvent removed under reduced pressure. Recrystallisation from CH yielded the product as a grey powder **13** (5.60 g, 73.8 %).

^{1}H-NMR (300 MHz, $CDCl_3$): δ 7.88 (d, J = 8.3 Hz, 2H), 7.37 (d, J = 8.0 Hz, 2H), 2.46 (s, 3H), 0.21 (s, 9H). ^{13}C-NMR (76 MHz, $CDCl_3$): δ 145.54, 138.62, 130.08, 127.71, 101.51, 98.52, 21.88, -1.03.

4.3.2 Ethynyl p-tolyl sulfone (14)

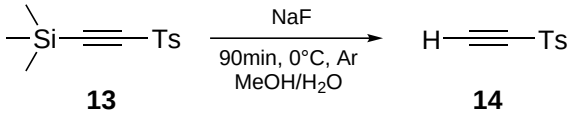

Figure 4.15: Synthesis of compound **14**

This synthesis was performed analogously to reference [44]. In a two-neck round-bottom flask (100 mL) armed with an addition funnel **13** (4.00 g, 1 eq , 15.9 mmol) was dissolved in MeOH (35 mL) and cooled to 0 °C. Then a solution of sodium fluoride (1.04 g, 1.5 eq , 24.8 mmol) dissolved in water (30 mL) was added drop wise over a period of 15 min. After stirring the solution for 90 min at 0 °C, TLC (eluent: CH+EE, 8+1) showed full conversion.
The reaction mixture was warmed to RT, water (20 mL) was added and the mixture was extracted three times with EE (50 mL). The organic layers were combined, washed (two times with water (50 mL), one time with saturated $NaHCO_3$ (50 mL) and one time with brine (50 mL)) and dried with anhydrous Na_2SO_4. The solvent was removed under reduced pressure and the product was isolated as a white powder **14** (2.80 g, 98.0 %).

^{1}H-NMR (300 MHz, $CDCl_3$): δ 7.90 (d, J = 8.4 Hz, 2H), 7.39 (d, J = 8.0 Hz, 2H), 3.45 (s, 1H), 2.47 (s, 3H). ^{13}C-NMR (76 MHz, $CDCl_3$): δ 146.14, 138.01, 130.23, 127.87, 81.18, 21.91.

4.3.3 2-Tosylbicyclo[2.2.2]octa-2,5-diene (15)

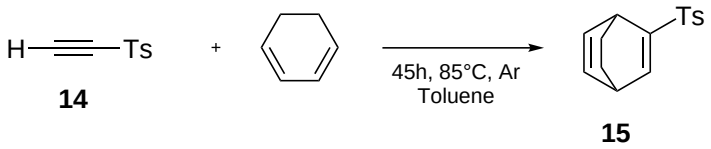

Figure 4.16: Synthesis of compound **15**

This synthesis was performed analogously to reference [62]. In a two-neck round-bottom flask (100 mL) **15** (1.50 g, 1 eq , 8.3 mmol) and 1,3-cyclohexadiene (1.2 mL, 1.5 eq , 12.7 mmol) were dissolved in dry toluene (40 mL) and headed to 70 °C.
After 70 h the yellowish reaction mixture was cooled to room temperature and the solvent was removed under reduced pressure. The crude product was purified by silica gel column chromatography (DCM) to yield a white powder **15** (1.59 g, 73.4 %).

^{1}H-NMR (300 MHz, $CDCl_3$): δ 7.71 (d, J = 8.3 Hz, 2H), 7.30 (d, J = 8.1 Hz, 2H), 7.27 – 7.20 (m, 1H), 6.23 (tt, J = 7.5, 3.8 Hz, 2H), 3.85 (ddq, J = 8.9, 4.6, 2.4 Hz, 2H), 2.42 (s, 3H), 1.43 – 1.13 (m, 4H). ^{13}C-NMR (76 MHz, $CDCl_3$): δ 146.86, 144.32, 144.09, 137.08, 133.70, 133.59, 129.88, 127.91, 38.33, 37.27, 25.30, 24.48, 21.73.

4.3.4 Ethyl 4,7-dihydro-4,7-ethano-2H-isoindole-1-carboxylate (16)

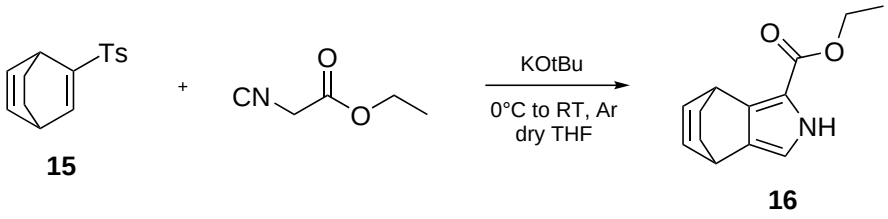

Figure 4.17: Synthesis of compound **16**

This synthesis was performed analogously to reference [62]. In a two-neck round-bottom flask (100 mL) Potassium tert-butoxide (500.0 mg, 2 eq , 4.46 mmol) was dissolved in dry THF (40 mL) and the solution was cooled to 0 °C by an ice bath. Ethyl isocyanoacetate (505.0 mg, 2 eq , 4.46 mmol) was added drop wise and after 30 min a solution of **15** (578.2 mg, 1 eq , 2.22 mmol) dissolved in dry THF (10 mL) was added. The reaction mixture was slowly warmed to room temperature in the ice bath and the solution was stirred over night.
After 22 h TLC (eluent: DCM/MeOH, 100/1; staining reagent: Vanillin/H_2SO_4) (product **16** turns red)) and APCI-MS showed full conversion. Water was added and the reaction mixture was extracted with DCM. The organic layers were combined, dried over anhydrous Na_2SO_4 and

the solvent was removed under reduced pressure. The crude product was purified by silica gel column chromatography (DCM) to yield a white powder **16** (271.3 mg, 56.3 %).

^{1}H-NMR (300 MHz, $CDCl_3$): δ 8.42 (s, 1H), 6.57 (d, J = 2.6 Hz, 1H), 6.50 (t, J = 3.8 Hz, 2H), 4.33 (dt, J = 14.3, 7.5 Hz, 3H), 3.87 (s, 1H), 1.53 (dtdd, J = 31.6, 13.1, 6.2, 3.4 Hz, 4H), 1.37 (t, J = 7.1 Hz, 3H). ^{13}C-NMR (76 MHz, $CDCl_3$): δ 161.81, 136.64, 136.32, 135.54, 131.57, 114.30, 112.92, 77.16, 59.99, 33.78, 33.41, 27.24, 26.56, 14.70.

4.3.5 Bis(3-ethoxycarbonyl-4,7-dihydro-4,7-ethano-2H-isoindol-1-yl)methane (17)

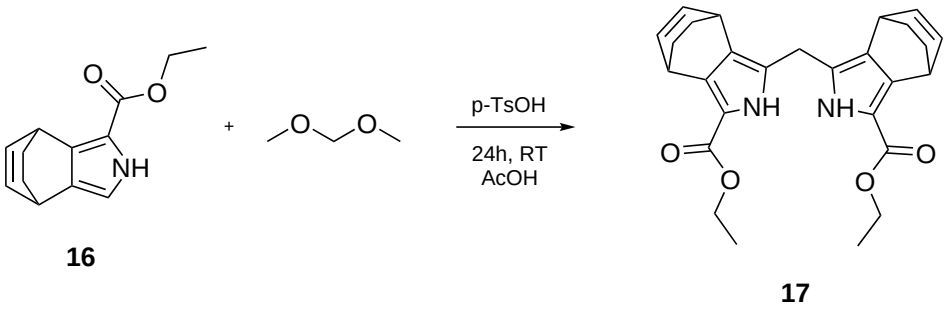

Figure 4.18: Synthesis of compound **17**

This synthesis was performed analogously to reference [61]. **16** (292.7 mg, 2 eq , 1.35 mmol), dimethoxymethane (51.2 mg, 1 eq , 672.8 µmol), p-toluenesulfonic acid monohydrate (20.1 mg, 0.2 eq , 116.7 µmol) were dissolved in AcOH (10 mL). The reaction mixture was stirred 24 h at room temperature.
After full conversion (detected by TLC (DCM) and APCI-MS) the mixture was poured onto cold water (100 mL), thereby a white precipitate was formed. The precipitate was collected by filtration, washed with water and was purified by silica gel column chromatography (gradient: DCM to DCM+MeOH, 100+2) to give the product as a white powder **17** (259.7 mg, 86.3 %).

^{1}H-NMR (300 MHz, $CDCl_3$): δ 9.23 (s, 1H), 9.17 (s, 1H), 6.48 (q, J = 5.0, 3.6 Hz, 4H), 4.30 (dtt, J = 14.2, 7.3, 3.5 Hz, 6H), 4.04 – 3.81 (m, 2H), 3.75 (s, 1H), 3.68 (s, 1H), 1.61 – 1.36 (m, 8H), 1.32 (td, J = 7.2, 2.9 Hz, 6H). ^{13}C-NMR (76 MHz, $CDCl_3$): δ 162.30, 137.72, 136.14, 135.52, 128.54, 128.46, 124.52, 124.40, 112.79, 112.74, 77.16, 60.09, 34.04, 32.56, 32.50, 27.11, 27.08, 26.40, 23.37, 23.29, 14.61.

4.3.6 Bis(4,7-dihydro-4,7-ethano-2H-isoindol-1-yl)methane (18)

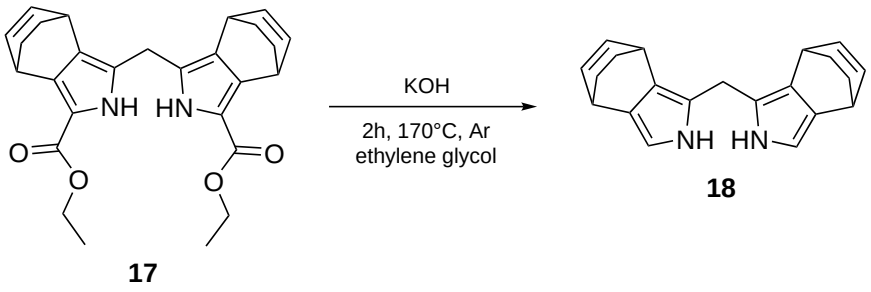

Figure 4.19: Synthesis of compound **18**

This synthesis was performed analogously to reference [61]. **17** (104.6 mg, 1 eq , 234.2 µmol) and KOH (75.8 mg, 6 eq , 1.35 mmol) were suspended in ethylene glycol (11 mL) in a 25 mL Schlenk tube. The suspension was thoroughly degassed by three freeze-pump-thaw cycles and heated up to 175 °C. After 1.5 h APCI-MS showed full conversion.
The black reaction mixture was cooled to room temperature by a water bath. Then DCM was added and the organic layer was extracted two times with water and one time by brine. The organic layer was dried with anhydrous Na_2SO_4 and the solvent removed under reduced pressure to give the crude product as a black oil **18**. The very unstable product was used immediately in the next step (synthesis of compound **19**) without further purification.

4.3.7 5-(3,4-Bis(dodecyloxy)phenyl)-15-(3,4-bis(3,6,9,12-tetraoxatridec-1-yloxy))tetrabicycloporphyrin (19)

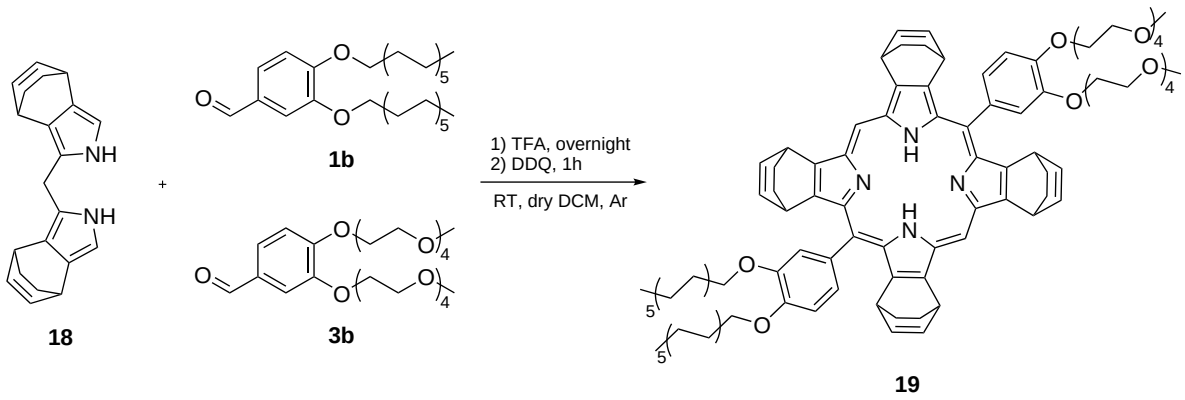

Figure 4.20: Synthesis of compound **19**

1b (34.8 mg, 1 eq , 67.1 µmol), **3b** (31.7 mg, 1 eq , 66.8 µmol) and **18** (40 mg, 2 eq , 132.3 µmol) were dissolved in dry DCM (40 mL) under argon atmosphere and the mixture

was degassed with a stream of argon for 20 min. Trifluoracetic acid (4 drops) was added drop wise and the solution was stirred overnight at room temperature and shielded from light (wrapped in aluminium foil). The reaction was monitored by UV-VIS spectroscopy. After 19 h DDQ (45.3 mg, 3 eq , 199.6 µmol) was added. Afterwards, the solution was stirred for 1 h.
The mixture was filtered through a pad of silica gel and the solvent was removed under reduced pressure. The product was isolated and purified by silica gel column chromatography (DCM/MeOH) to yield a purple powder **19** (12.7 mg, 12.0 %). During the purification step, two fractions were collected: the first was 5,15-bis(3,4-bis(dodecyloxy)phenyl)tetrabicycloporphyrin (eluent: DCM+MeOH, 50+1), the second was the desired product (eluent: DCM+MeOH, 100+2).

MALDI TOF: m/z: $[MH^+]$ calc. for $C_{98}H_{131}N_4O_{12}$: 1555.9763, found: 1555.9713.

4.3.8 5-(3,4-Bis(dodecyloxy)phenyl)-15-(3,4-bis(3,6,9,12-tetraoxatridec-1-yloxy)phenyl)tetrabenzoporphyrin (20)

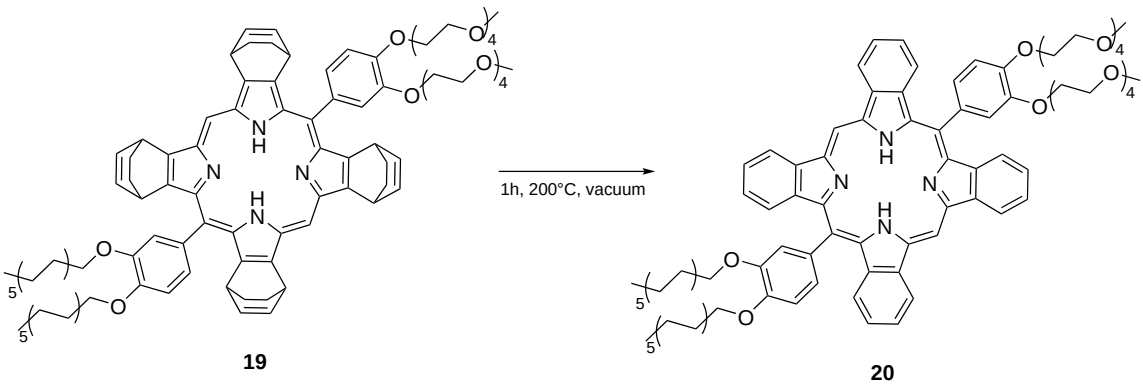

19 **20**

Figure 4.21: Synthesis of compound **20**

19 (12.7 mg, 7.94 µmol) was heated to 200 °C in a glass vial for 1 h under vacuum, thereby the colour changed from purple to dark green. The product was isolated as a green solid **20** (quant.) and was used in the next step (synthesis of **21**) without further purification.

MALDI TOF: m/z: $[M^+]$ calc. for $C_{90}H_{114}N_4O_{12}$: 1442.8434, found: 1442.7067.

4.3.9 Pd-5-(3,4-bis(dodecyloxy)phenyl)-15-(3,4-bis(3,6,9,12-tetraoxatridec-1-yloxy)phenyl)tetrabenzoporphyrin (21)

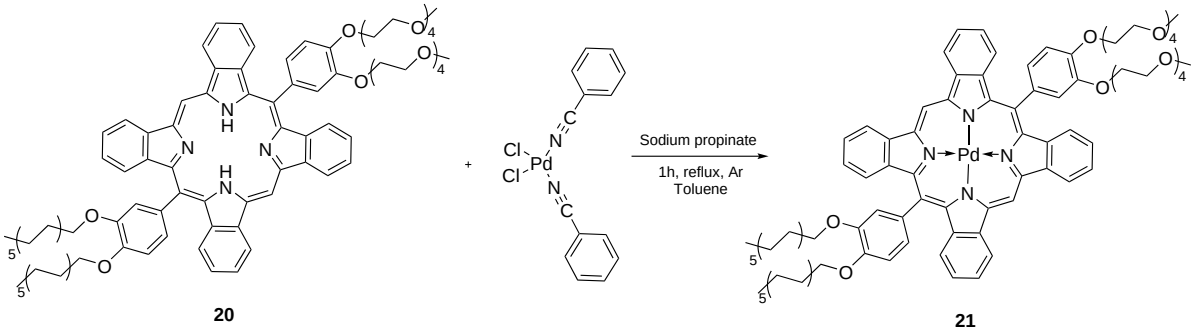

20 21

Figure 4.22: Synthesis of compound **21**

In a three-neck round-bottom flask aimed with a condenser, tetrabenzoporphyrin **20** (11.8 mg, 1 eq , 7.9 µmol) was dissolved in toluene (10 mL) under argon atmosphere. Sodium propionate (8 mg, 10 eq , 83.3 µmol) was added and the solution was headed to reflux. Then $Pd(BN)_2Cl_2$ (4.1 mg, 1.3 eq , 10.7 µmol) dissolved in toluene (5 mL) was added in three portions over 30 min and the solution was stirred under reflux for 2 h. The reaction was monitored via UV-VIS spectroscopy.
After full conversion, the solvent was evaporated under reduced pressure and the residue was purified by silica gel column chromatography (DCM+MeOH 100+2) to yield the product as a green solid **21** (7.0 mg, 55.4 %).

^{1}H-NMR (300 MHz, $CDCl_3$): δ 10.52 (d, J = 64.8 Hz, 2H), 9.26 (d, J = 27.8 Hz, 4H), 7.94 (s, 4H), 7.66 (t, J = 7.0 Hz, 4H), 7.38 (td, J = 24.8, 23.5, 14.2 Hz, 10H), 4.62 (q, J = 5.5 Hz, 2H), 4.44 (q, J = 7.1 Hz, 2H), 4.22 (t, J = 4.8 Hz, 2H), 4.13 – 3.21 (m, 34H), 3.15 (d, J = 10.4 Hz, 3H), 2.25 – 2.08 (m, 2H), 1.89 – 1.70 (m, 4H), 1.61 – 1.07 (m, 38H), 0.99 – 0.89 (m, 3H), 0.82 (dt, J = 7.2, 3.4 Hz, 3H). MALDI TOF: m/z: $[M^+]$ calc. for $C_{90}H_{112}N_4O_{12}Pd$: 1546.7339, found: 1546.7280.

4.4 Synthesis of Pd-5-Arylporphyrins

4.4.1 5-(4-(3,6,9,12-Tetraoxatridec-1-yloxy)phenyl)-21H,23H-porphyrin (22)

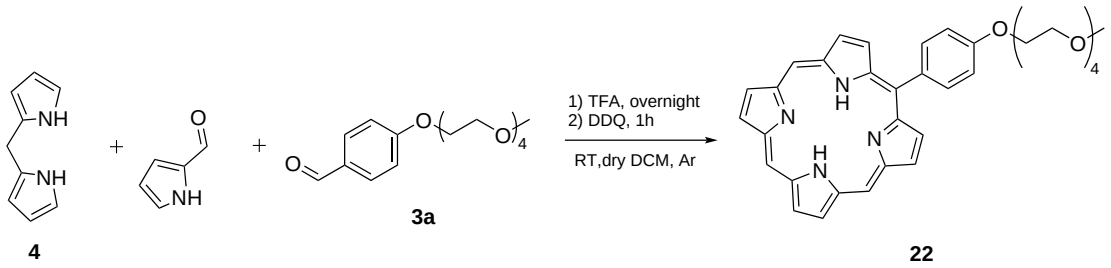

Figure 4.23: Synthesis of compound **22**

In a three-neck round-bottom flask dry DCM (500 mL) was deoxygenated by argon counterflow for about 30 min. Then **4** (201.1 mg, 1 eq , 1.38 mmol), pyrrole-2-carboxaldehyde (263.4 mg, 2 eq , 2.77 mmol) and **3a** (433.7 mg, 1 eq , 1.39 mmol) were dissolved and trifluoracetic acid ((30 µL, 0.02 eq , 392 µmol)) was added under argon atmosphere. The reaction mixture was stirred over night at room temperature and shielded from light (wrapped in aluminium foil). During the first 4 h the clear solution turned from slightly yellow to dark red. The reaction progress was monitored via UV/Vis-spectroscopy. After 24 h DDQ (466.8 mg, 1.5 eq , 2.06 mmol) was added and the solution was stirred for another hour.
The solvent was removed under reduced pressure and the crude product was purified by silica gel column chromatography (DCM/MeOH) to yield a purple powder **22** (30.9 mg, 3.8 %).
During the purification step, two fractions were collected: the first fraction was the desired product (eluent: DCM+MeOH, 100+2) and the second was 5,15-bis(4-(3,6,9,12-tetraoxatridec-1-yloxy)phenyl)-21H,23H-porphyrin (eluent: DCM+MeOH, 100+3).

^{1}H-NMR (300 MHz, $CDCl_3$): δ 10.27 (s, 2H), 10.17 (s, 1H), 9.41 (dt, J = 9.7, 4.7 Hz, 6H), 9.12 (d, J = 4.6 Hz, 2H), 8.15 (d, J = 8.5 Hz, 2H), 7.32 (d, J = 8.3 Hz, 2H), 4.40 (t, J = 4.9 Hz, 2H), 4.04 (t, J = 4.8 Hz, 2H), 3.90 – 3.69 (m, 10H), 3.64 – 3.58 (m, 2H), 3.43 (s, 3H), -3.64 (s, 2H). ^{13}C-NMR (76 MHz, $CDCl_3$): δ 158.86, 146.60, 145.53, 135.88, 134.36, 131.79, 131.45, 131.28, 131.11, 119.50, 113.19, 104.68, 103.43, 72.12, 71.10, 70.89, 70.85, 70.83, 70.71, 70.03, 67.88, 59.19. MALDI TOF: m/z: [M^+] calc. for $C_{35}H_{36}N_4O_5$: 592.2686, found: 592.2679.

4.4.2 Pd-5-(4-(3,6,9,12-tetraoxatridec-1-yloxy)phenyl)-21H,23H-porphyrin (23)

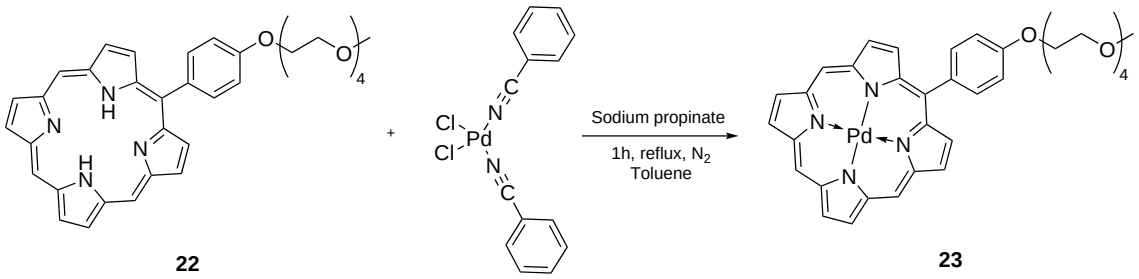

22 23

Figure 4.24: Synthesis of compound **23**

In a three-neck round-bottom flask aimed with a condenser, **23** (21 mg, 1 eq , 35.4 µmol) was dissolved in toluene (10 mL) under argon atmosphere. Sodium propionate (22 mg, 6.5 eq , 229.0 µmol) was added and the solution was headed to reflux. Then $Pd(BN)_2Cl_2$ (18.6 mg, 1.4 eq , 48.5 µmol) dissolved in toluene (5 mL) was added in three portions over 30 min and the solution was stirred under reflux for 2 h. The reaction was monitored via UV-VIS spectroscopy. After full conversion, the solvent was evaporated under reduced pressure and the residue was purified by silica gel column chromatography (DCM+MeOH 100+2) to yield the product as a red solid **23** (15.7 mg, 60.7 %).

^{1}H-NMR (300 MHz, $CDCl_3$): δ 9.93 (s, 2H), 9.75 (s, 1H), 9.14 (d, J = 4.7 Hz, 2H), 9.10 – 8.99 (m, 4H), 8.94 (d, J = 4.7 Hz, 2H), 8.05 (d, J = 8.3 Hz, 2H), 7.29 (d, 2H), 4.36 (t, J = 4.8 Hz, 2H), 4.02 (d, J = 4.1 Hz, 2H), 3.89 – 3.68 (m, 10H), 3.63 – 3.56 (m, 2H), 3.41 (s, 3H). ^{13}C-NMR (76 MHz, $CDCl_3$): δ 158.78, 141.08, 140.72, 140.43, 135.36, 134.33, 131.27, 130.98, 130.96, 130.72, 120.64, 113.05, 106.13, 105.01, 72.14, 71.10, 70.90, 70.86, 70.84, 70.72, 70.05, 67.87, 59.21. MALDI TOF: m/z: [M^+] calc. for $C_{35}H_{34}N_4O_5Pd$: 696.1577, found: 696.1552.

4.5 Attempted Synthesis of a Covalently Linked Pd-Porphyrin Dimer

4.5.1 5,15-Bis(4-decyloxyphenyl)-21H,23H-porphyrin (24)

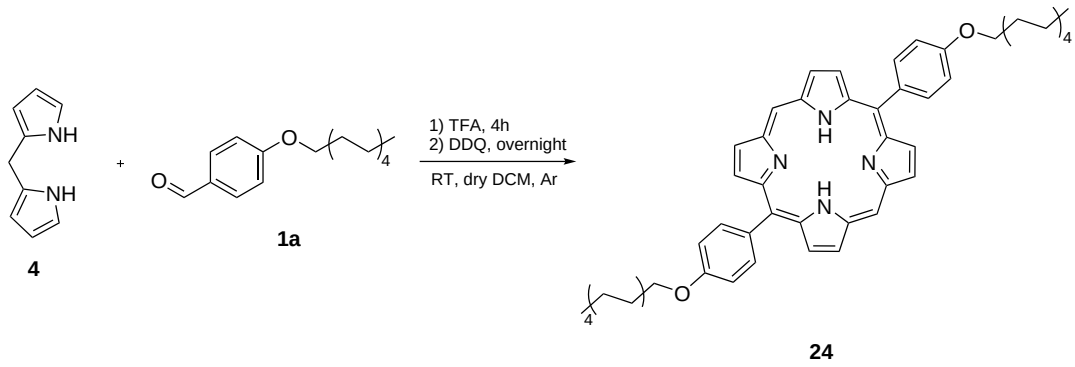

Figure 4.25: Synthesis of compound **24**

1a (219 mg, 1 eq , 1.50 mmol) and **4** (370 mg, 1 eq , 1.41 mmol) were dissolved in dry DCM 200 mL under argon atmosphere and the mixture was degassed with a stream of argon for 20 min. Trifluoracetic acid (6 drops) was added drop wise and the solution was stirred at room temperature and shielded from light (wrapped in aluminium foil). The reaction was monitored by UV-VIS spectroscopy. After 4 h the absorption spectrum of the red, purple fluorescent solution did not change anymore and DDQ (463.0 mg, 1.5 eq , 2.04 mmol) was added. Afterwards, the solution was stirred overnight, thereby the colour turned to dark red and the solution started to fluoresced red.
The solvent was removed under reduced pressure and the product was isolated and purified by silica gel column chromatography (CH to CH+EE, 100+10) to yield a purple powder **24** (159 mg, 27.5 %).

^{1}H-NMR (300 MHz, $CDCl_3$): δ 10.30 (s, 2H), 9.39 (d, J = 4.7 Hz, 4H), 9.12 (d, J = 4.6 Hz, 4H), 8.18 (d, J = 8.3 Hz, 4H), 7.34 (d, J = 8.2 Hz, 4H), 4.29 (t, J = 6.6 Hz, 4H), 2.09 – 1.94 (m, 4H), 1.71 – 1.59 (m, 4H), 1.49 – 1.30 (m, 24H), 0.92 (t, J = 7.0 Hz, 6H), -3.07 (s, 2H).

4.5.2 5,15-Bis(4-decyloxyphenyl)-10-phenyl-21H,23H-porphyrin (25)

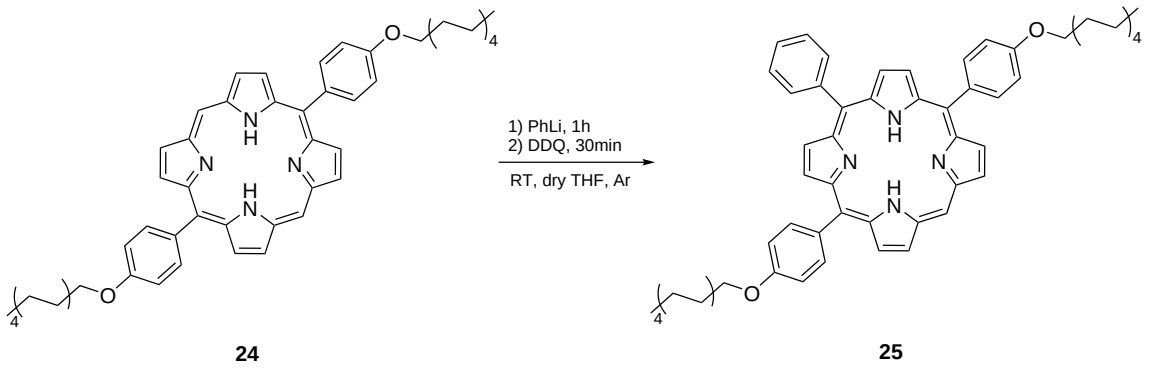

24 **25**

Figure 4.26: Synthesis of compound **25**

In a Schlenk tube (10 mL) **24** (20.1 mg, 1 eq , 25.8 µmol) was dissolved in dry THF (5 mL) under argon atmosphere and the solution was degassed by argon counterflow over 15 min. Phenyl lithium (800 µL of a 0.24 M solution in diethyl ether, 7.4 eq , 192.0 µmol) was added via a syringe. The non-fluorescing mixture was stirred for 1 h at room temperature, then a solution of THF/H_2O (3 mL, 4/1 (v/v)) was added. Thereby the dark yellow reaction mixture turned to dark green. DDQ (23.0 mg, 4 eq , 101.3 µmol) was added and the solution turned back to a red colour and started to fluoresce again.
The solvent was removed under reduced pressure and the crude product was purified by silica gel column chromatography (eluent: DCM) and recrystallisation from $CHCl_3$/MeOH to yield the product as a purple powder **25** (11.0 mg, 50.1 %).

^{1}H-NMR (300 MHz, $CDCl_3$): δ 10.19 (s, 1H), 9.32 (d, J = 4.7 Hz, 2H), 9.06 (d, J = 4.6 Hz, 2H), 8.95 (d, J = 4.7 Hz, 2H), 8.88 (d, J = 4.9 Hz, 2H), 8.23 (d, J = 6.9 Hz, 2H), 8.14 (d, J = 8.2 Hz, 4H), 7.76 (q, J = 6.7, 6.0 Hz, 3H), 7.30 (d, J = 8.4 Hz, 4H), 4.25 (t, J = 6.5 Hz, 4H), 2.00 (p, J = 7.1 Hz, 4H), 1.64 (p, J = 7.3 Hz, 4H), 1.54 – 1.32 (m, 24H), 0.95 (t, J = 6.4 Hz, 6H), -2.94 (s, 2H). ^{13}C-NMR (76 MHz, $CDCl_3$): δ 159.19, 142.86, 135.87, 134.64, 134.07, 131.49, 131.27, 130.85, 127.80, 126.67, 120.54, 119.64, 113.06, 104.80, 77.16, 68.51, 32.13, 29.85, 29.81, 29.71, 29.68, 29.56, 26.41, 22.90, 14.32.

4.5.3 5-Bromo-10,20-bis(4-decyloxyphenyl)-15-phenyl-21H,23H-porphyrin (26)

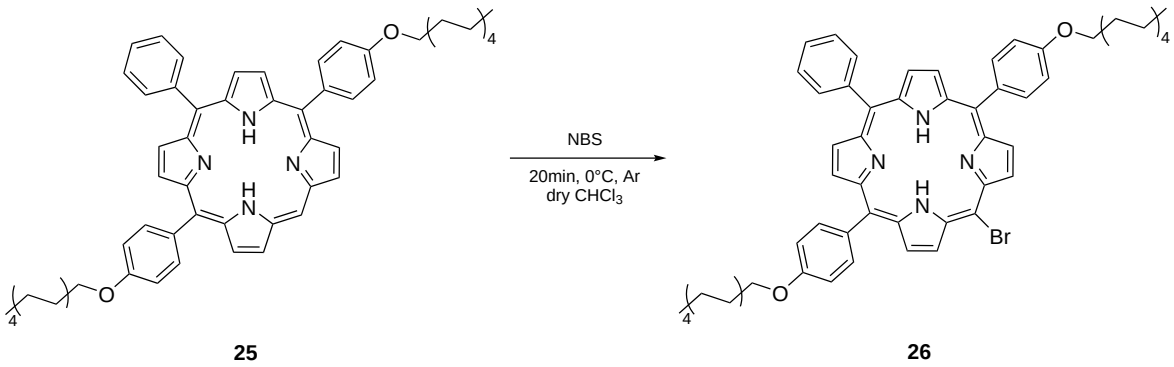

25 26

Figure 4.27: Synthesis of compound **26**

In a two-neck round-bottom flask (25 mL) **25** (11 mg, 1 eq , 12.9 µmol) was dissolved in dry $CHCl_3$ (4 mL) and pyridine (14 µL, 13 eq , 173.5 µmol) was added. The reaction mixture was cooled to 0 °C and NBS (3.44 mg, 1.5 eq , 19.3 µmol) dissolved in dry $CHCl_3$ (3 mL) was added. The reaction progress was observed by UV/Vis-spectroscopy.
After 20 min the reaction was terminated and acetone (1 mL) was added. The mixture was washed two times with water and one time with brine, then the organic layer was dried over anhydrous Na_2SO_4 and the solvent was removed under reduced pressure. The crude product was purified by recrystallisation from $CHCl_3$/MeOH to yield the product as a purple powder **26** (quant.).

^{1}H-NMR (300 MHz, $CDCl_3$): δ 9.66 (d, J = 4.9 Hz, 2H), 8.94 (d, J = 4.8 Hz, 2H), 8.89 – 8.73 (m, 4H), 8.19 (d, J = 6.7 Hz, 2H), 8.07 (d, J = 8.2 Hz, 4H), 7.83 – 7.67 (m, 3H), 7.26 (d, J = 20.9 Hz, 4H), 4.23 (t, J = 6.5 Hz, 4H), 1.98 (p, J = 6.9 Hz, 4H), 1.63 (p, J = 7.3 Hz, 4H), 1.50 – 1.27 (m, 24H), 0.94 (d, J = 3.7 Hz, 6H), -2.71 (s, 2H). ^{13}C-NMR (76 MHz, $CDCl_3$): δ 159.27, 142.13, 135.75, 134.58, 134.05, 127.94, 126.87, 120.98, 120.83, 112.96, 102.90, 68.51, 32.12, 29.84, 29.81, 29.70, 29.66, 29.56, 26.40, 22.89, 14.32.

4.5.4 Pd-5-bromo-10,20-bis(4-decyloxyphenyl)-15-phenyl-21H,23H-porphyrin (27)

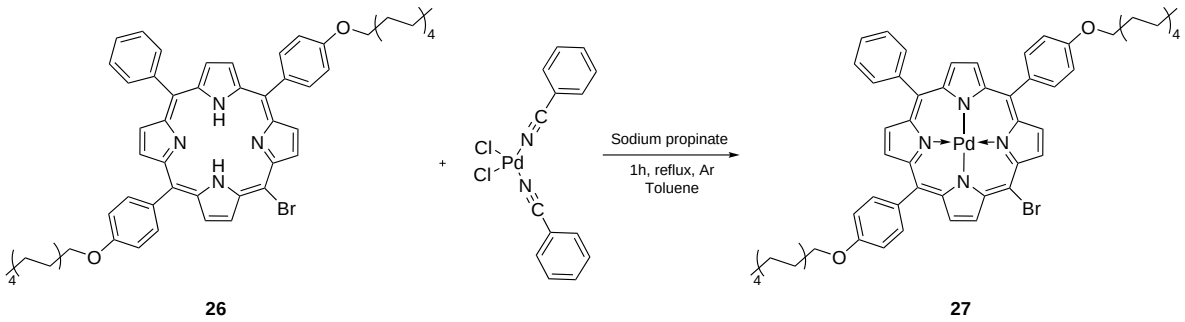

26 **27**

Figure 4.28: Synthesis of compound **27**

Porphyrin **26** (12.0 mg, 1 eq , 12.9 µmol) was dissolved in toluene (10 mL) in a three neck round bottom flask with additional condenser under argon atmosphere. Sodium propionate (18 mg, 14.5 eq , 187.4 µmol) was added and the solution was headed to reflux. Then $Pd(BN)_2Cl_2$ (9.0 mg, 1.8 eq , 23.5 µmol) dissolved in toluene (5 mL) was added in three portions over 30 min and the solution was stirred under reflux for 2 h. The reaction was monitored via UV-VIS spectroscopy.
After full conversion, the solvent was evaporated under reduced pressure and the residue was purified by silica gel column chromatography (CH+EE, 100+1) to yield the product as a red solid **27** (11.2 mg, 83.9 %).

^{1}H-NMR (300 MHz, $CDCl_3$): δ 9.60 (d, J = 5.1 Hz, 2H), 8.88 (d, J = 5.2 Hz, 2H), 8.83 – 8.69 (m, 4H), 8.12 (d, J = 6.9 Hz, 2H), 7.99 (d, J = 8.2 Hz, 4H), 7.74 (t, J = 7.5 Hz, 3H), 7.22 (d, J = 8.0 Hz, 4H), 4.19 (t, J = 6.5 Hz, 4H), 1.96 (p, J = 6.5 Hz, 4H), 1.61 (t, J = 7.8 Hz, 4H), 1.48 – 1.32 (m, 24H), 0.93 (t, J = 6.3 Hz, 6H). ^{13}C-NMR (76 MHz, $CDCl_3$): δ 159.25, 142.67, 142.37, 142.05, 141.72, 141.51, 135.27, 134.14, 133.63, 132.39, 132.02, 131.54, 131.34, 127.98, 126.90, 122.35, 112.95, 105.04, 68.49, 32.12, 29.85, 29.81, 29.70, 29.65, 29.56, 26.40, 22.90, 14.32.

4.5.5 4,16-Bis(4,4,5,5-tetramethyl-1,3,2-dioxborolan)-[2.2]-paracylcophane (28)

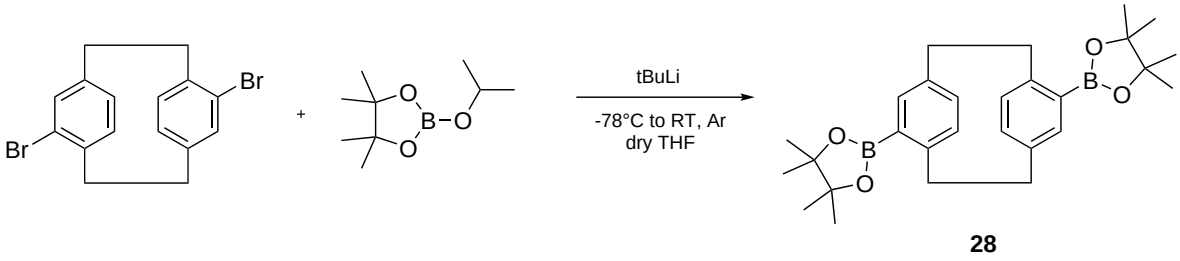

Figure 4.29: Synthesis of compound **28**

This synthesis was performed analogously to reference [75]. In a Schlenk tube (25 mL) dry THF (5 mL) was cooled to −78 °C by an EtOH/N_2 bath and tert-butyllithium (800 µL of a 1.7 M solution in pentane, 5 eq , 1.36 mmol) was added and stirred for 10 min. To the yellow solution a mixture of 4,16-dibromo[2.2]paracyclophane (104 mg, 1 eq , 284.08 µmol) dissolved in dry THF (5 mL) was added via a syringe, thereby the solution turned slightly yellow. The reaction mixture was stirred for 1 h at −78 °C, then a solution of 2-isopropoxy-4,4,5,5-tetramethyl-1,3,2-dioxyborolane (164.2 mg, 3 eq , 882.31 µmol) in dry THF (2 mL) was added. The mixture was slowly warmed to −20 °C in the cooling bath and then the bath was removed. APCI-MS showed full conversion of the 4,16-dibromo[2.2]paracyclophane.
Water (5 mL) was added to quench the remaining tert-butyllithium and the solution was extracted two times with EE (20 mL). The organic layers were combined, dried over anhydrous Na_2SO_4 and the solvent was removed under reduced pressure. The crude product was purified by silica gel column chromatography (gradient: CH to CH+EE, 100+5) and recrystallisation from hexane to yield the product as a white powder **28** (18.0 mg, 13.8 %).

^{1}H-NMR (300 MHz, $CDCl_3$): δ 7.06 (s, 2H), 6.47 (dd, J = 7.7 Hz, 4H), 3.92 (ddd, J = 12.4, 9.6, 3.0 Hz, 2H), 3.05 (dddd, J = 34.6, 16.4, 13.2, 9.2 Hz, 6H), 1.39 (d, J = 2.6 Hz, 24H). ^{13}C-NMR (76 MHz, $CDCl_3$): δ 147.49, 140.18, 138.82, 135.60, 133.45, 83.28, 35.50, 35.39, 25.23, 24.97

4.5.6 Dimer (29)

In a Schlenk tube (10 mL) **27** (4.00 mg, 2 eq , 4.30 µmol) and **28** (0.99 mg, 1 eq , 2.15 µmol) were dissolved in toluene (2 mL) under argon atmosphere. $PdCl_2$(Amphos)$_2$ (mg, 0.2 eq , µmol) dissolved in toluene (1 mL) and a aqueous solution of Na_2CO_3 (4.00 mg of a 0.5 M solution, 2 eq , 4.30 µmol) were added and the reaction mixture was degassed by argon counterflow for 15 min. The red solution was headed to 100 °C and stirred for five days. However, even after 5 days, no product was observed.

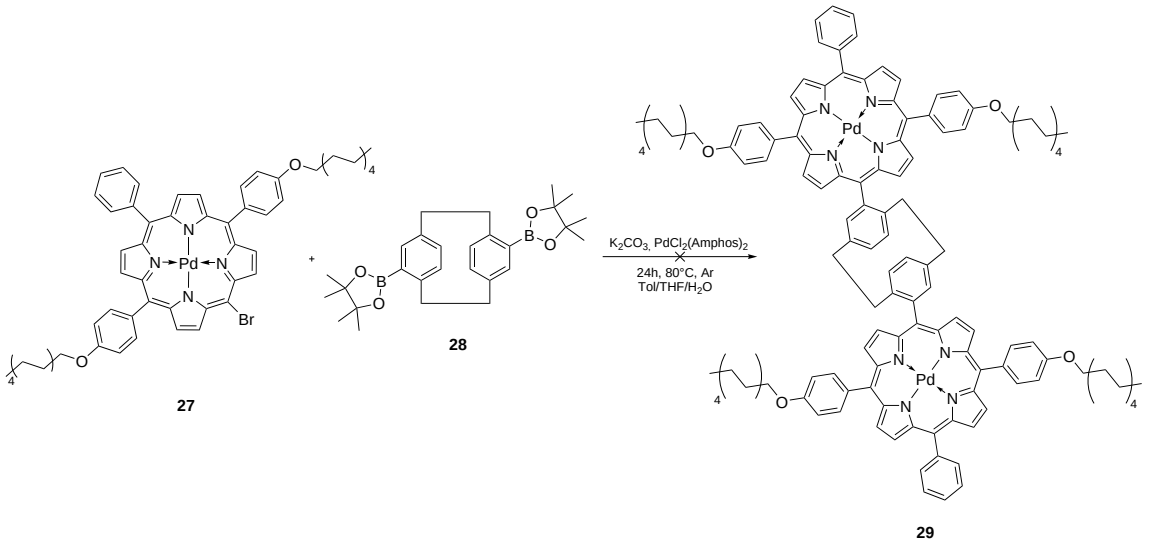

Figure 4.30: Synthesis of compound **29**

4.6 Formation of Dye Aggregates

Stock solutions of each dye (approximately 0.33 g/L) in THF and surfactant stock solutions (20 g/L and 10 g/L) in THF (except for SDS - stock solution in water) were prepared. In a typical procedure a defined amount of surfactant stock solutions was transferred in a glass vial and the solvent was evaporated by a stream of nitrogen. 80 μL dye stock, 120 μL THF and a stirring bar were added. Then 2 mL water were quickly added under heavy stirring. Finally, the residual THF was removed by heavy stirring and by blowing it of with a stream of nitrogen for about 10 min.
The concentration of dye molecules in the final aggregate solution is given in table 4.1.

Table 4.1: Concentration of dye molecules in the final aqueous aggregate solution

Dye	Concentration mg/L	μmol/L
MTMDP	13.5	16.3
PdMTMDP	13.9	14.9
DTDDP	13.5	10.8
PdDTDDP	13.9	10.3
PdTTP	14.7	10.5
PdMTP	14.8	21.3
PdDTDDTBP	15.7	10.2

5 Results and Discussion

J-aggregates were discovered in the 1930s by Jelly [3, 4] and Scheiber [5]. This type of aggregates was observed for the first time on the dye 1,1′-diethyl-2,2′cyanine 1,1′-diethyl-2,2′-cyanine chloride (pseudoisocyanine).
In recent decades J-aggregate formation could also be observed for many other synthetic and natural chromophores, like perylene bisimides [6, 7], fluorenes [8] and BODIPY dyes [9]. Aggregates from porphyrinoid molecules, such as porphyrins [10–12], chlorins [13] and phthalocyanines [14] have been obtained, as well. However, for J-aggregates based on porphyrins only free-base porphyrins [10–12] (e.g. $TPPS_4$) and some metallated porphyrins [76–78] have been investigated so far.
The aim of this work was the investigation of dimers and J-aggregates based on phosphorescent palladium-metallated porphyrins. It should also be found out, whether phosphorescence can be observed and how it restrains. The first part of this work discusses the synthesis of such dimers and J-aggregates and the second part is dedicated to their characterisation.
For better readability, the porphyrin names are abbreviated in both parts. MTMDP is compound **5a**, DTDDP is **5b**, PdMTMDP is **6a**, PdDTDDP is **6b**, PdTTP is **6c**, PdMTP is **23** and PdDTDDTBP is **21**.

5.1 Synthetic Considerations

In order to allow self-organization of dye molecules, the monomers require two important structural properties. On the one hand the monomers need a polarizable chromophore as the functional part and on the other hand substituents, which are responsible for self-organization and solubility.[79]
Inspired by the work of Zhijian C. *et al.* on amphiphilic aza-BODIPY dye J-aggregates [9], a similar surfactant-like design for the Pd-porphyrins was chosen (Figure 5.1).
The first synthesised Pd-porphyrin dye PdMTMDP consists of a palladium-metallated porphin core as chromophore and two substituents - a hydrophilic 4-TEGoxyphenyl and a hydrophobic 4-decyloxyphenyl group - which are substituted face-to-face in meso position at the porphin core. Both, the amphiphilic character and the $\pi - \pi$ interaction between the porphyrin centre should enable the formation of aggregates in water.

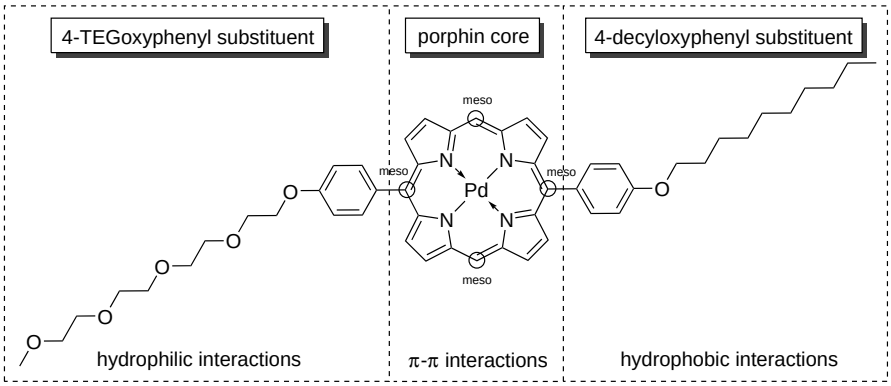

Figure 5.1: Surfactant-like PdMTMDP **6a**

To study the impact of amphiphily on aggregation, three further Pd-porphyrins (PdDTDDP, PdTTP and PdMTP) with different amphiphilic character were synthesised. Moreover, the Pd-tetrabenzoporphyrin PdDTDDTBP was synthesised to investigate the impact of a lager π-system on aggregation. All structures are depicted in Figure 5.2 and their synthesis is discussed in next section.
During this work it was also tried to synthesise a covalently linked Pd-porphyrin dimer. Unfortunately, no dimer could be synthesised during this work which is discussed later.

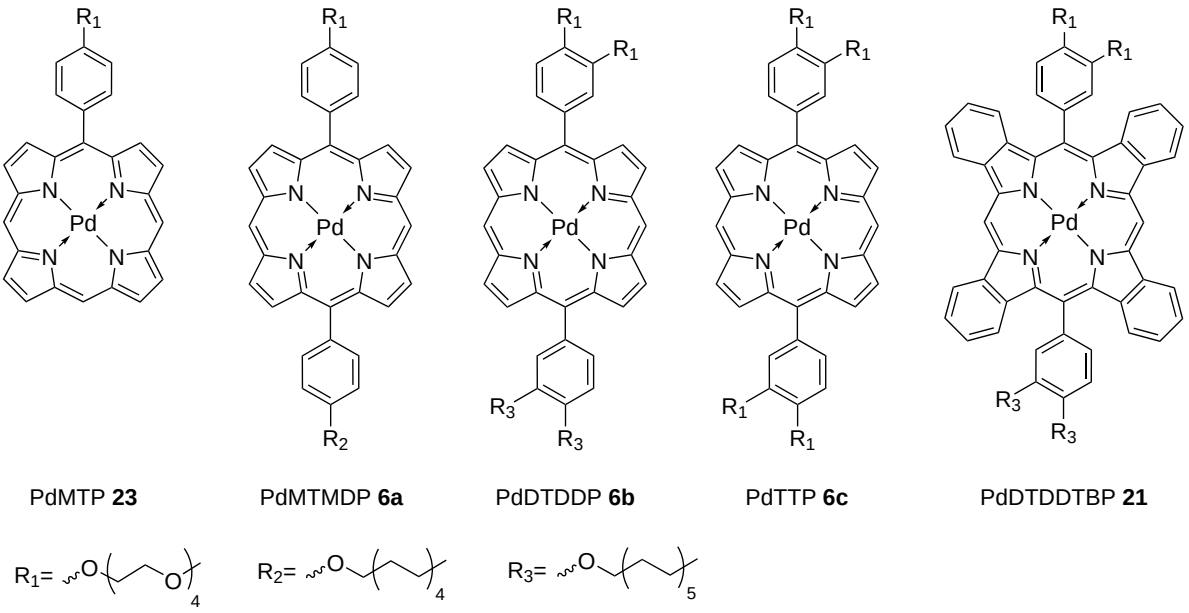

Figure 5.2: Synthesised Pd-porphyrins

This chapter also describes the approach of aggregate formation. Thereby, aggregation of the five synthesised Pd-porphyrins (PdMTP, PdMTMDP, PdDTDDP, PdTTP and PdDTDDTBP) and two metal-free porphyrins (MTMDP and DTDDP) was further investigated.

5.1.1 Dye and Dimer Synthesis

Synthesis of Benzaldehydes with Hydrophilic and Hydrophobic Substituents

For the following porphyrin and dimer synthesis two hydrophilic TEGoxybenzaldehydes and two hydrophobic alkyloxybenzaldehydes were needed.

The commercially available 4-decyloxybenzaldehyde **1a** was bought from TCI and 3,4-didodecyloxybenzaldehyde **1b** was synthesised according to literature [70] by nucleophilic substitution of 3,4-dihydroxybenzaldehyde with 1-bromodecane in good yield (Figure 5.3 **(a)**).
In a similar way, both, 4-TEGoxybenzaldehyde **3a** and 3,4-bis(TEGoxy)benzaldehyde **3b** were synthesised in two steps. In a first reaction TEG-4-toluenesulfonate **2** was synthesised by nucleophilic substitution of 2,5,8,11-tetraoxytridecane-13-ol with p-toluenesulfonyl chloride in excellent yields.[71] In a second step **2** was coupled with 4-hydroxybenzaldehyde and 3,4-dihydroxybenzaldehyde, respectively (Figure 5.3 **(b)**).[72]
All benzaldehydes could be obtained without any problems and in good yields.

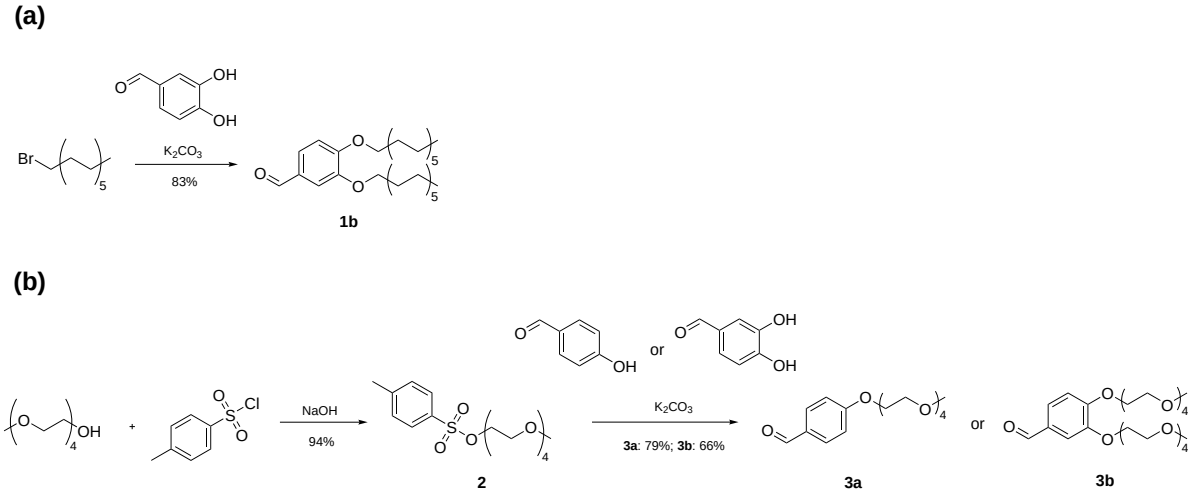

Figure 5.3: Overview of benzaldehyde synthesis: **(a)** Synthesis of 3,4-didodecyloxybenzaldehyde **1b**. **(b)** Synthesis of two different TEGoxybenzaldehyds **3a** and **3b**

Synthesis of 5,15-AB-Type Pd-Porphyrins

As described in chapter 2.2 there are six common synthesis strategies for 5,15-AB-type porphyrins. In this work the statistical version of the "classical" acid-catalysed condensation of 2,2'-dipyrromethane **4** with two different benzaldehydes (**1a** and **3a** or **1b** and **3b**) was used. This synthesis gives three different products - the A_2, AB and B_2-porphyrin. Due to the large difference in the hydrophilic character between the porphyrins, an easy separation by silica gel column chromatography was possible.

The whole synthesis procedure of 5,15-AB-type Pd-porphyrins is shown in Figure 5.4.
In a first step 2,2'-dipyrromethane **4** was synthesised according to literature [73]. Thereby, formaldehyde was generated by decomposition of paraformaldehyde in hot pyrrole (pyrrole:paraformaldehyde ratio, 25:1). Assisted by the weak Lewis acid $InCl_3$, the pyrrole was condensed with the formaldehyde. This synthesis was straightforward and gave the desired product in moderate yields.
In a next step **4** was condensed with two different benzaldehydes (**1a** and **3a** or **1b** and **3b**) in a similar way to literature [80–82]. As acid-catalyst TFA was used. After oxidation of the formed porphyrinogen with DDQ, three different porphyrins could be isolated by silica gel column chromatography. For example, in the case of used benzaldehydes **1b** and **3b**, the porphyrins 5,15-bis(3,4-bis(dodecyloxy)phenyl)-21H,23H-porphyrin, 5-(3,4-bis(dodecyloxy)phenyl)-15-(3,4-bis(3,6,9,12-tetraoxatridec-1-yloxy)phenyl)-21H,23H-porphyrin **5b** and 5,15-bis(4-(3,6,9,12-tetraoxatridec-1-yloxy)phenyl)-21H,23H-porphyrin **5c** could be isolated.
In a last step the porphyrins were metallated by refluxing them with $(C_6H_5CN)_2PdCl_2$ and sodium propionate in toluene for a few hours to give the desired Pd-porphyrins in good yields. This method is already known with $PdCl_2$/sodium acetate [83] or with $Pd(OAc)_2$/sodium acetate [84], but it also worked very well with $(C_6H_5CN)_2PdCl_2$/sodium propionate.

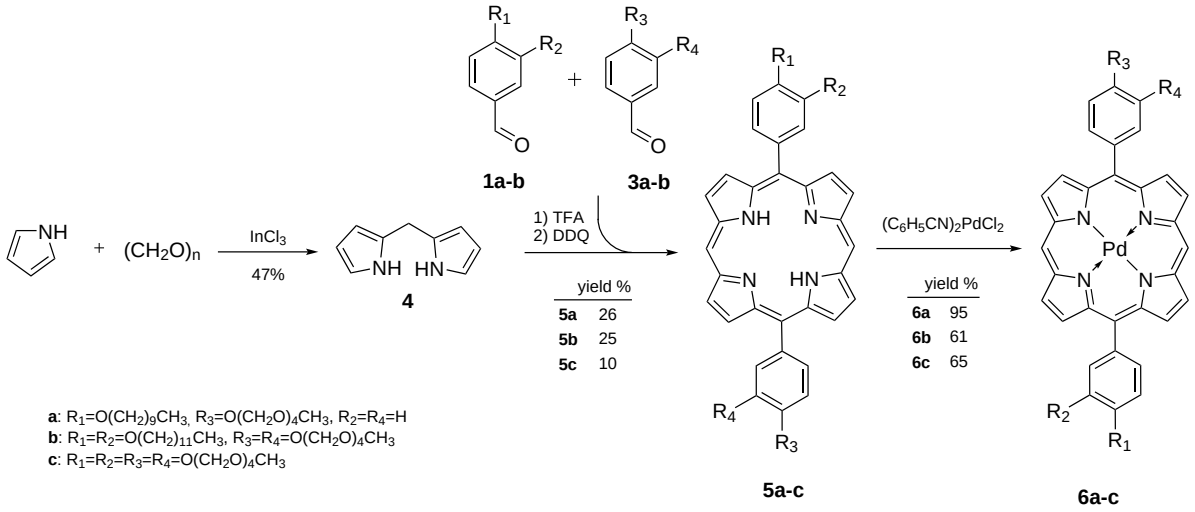

Figure 5.4: Overview of Pd-porphyrin synthesis

Synthesis of 5,15-AB-Type Pd Tetrabenzoporphyrins

For the synthesis of 5,15-AB-type Pd-tetrabenzoporphyrins, two different approaches have been tried.

Approach 1 An overview is given in Figure 5.5. For the first approach commercially available 1-nitro-1-cyclohexene and ethyl isocyanoacetate were used as starting reagents. Both chemicals

formed isoindole **7** in good yield in a Barton–Zard reaction[56–58] with the week base DBU. In a following step **7** was condensed with dimethoxymethane in acetic acid, according to literature[74, 85], to obtain the desired dipyrromethane **8** also in good yield.
Dipyrromethane **8** was decarboxylated with KOH in ethylene glycol at 195 °C. This reaction required lots of attention and absolutely oxygen-free conditions.[85] Already traces of oxygen led to the destruction of the product.
After 45 min **8** was completely decarboxylated to dipyrromethan **9** and after a short workup **9** was condensed with the benzaldehydes (**1a** and **3a**) and oxidized with DDQ to tetracychlohexaneporphyrin **10** in the same way like the 5,15-AB porphyrins.
Tetracychlohexaneporphyrins TCHP (Ar_4TCHP as well as Ar_2TCHP) are very unreactive compounds and cannot further be oxidized with DDQ to the desired tetrabenzoporphyrins.[60] However, metallated tetracychlohexaneporphyrins (Ar_4TCHP) can be oxidized. Therefore, **10** was metallated to PdTCHP **11** by the same procedure described above at 5,15-AB porphyrins.

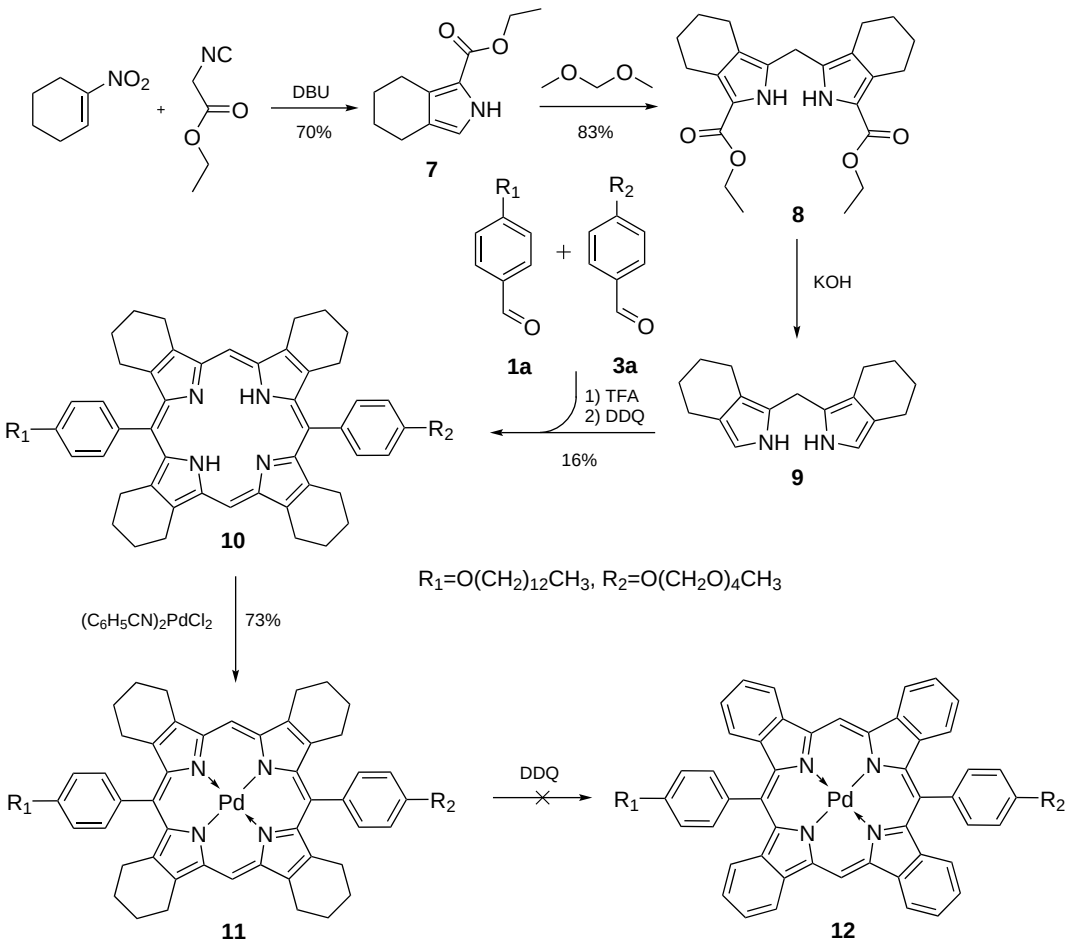

Figure 5.5: Overview of Pd tetrabenzoporphyrin synthesis (approach 1)

In the last step it was tried to aromatize $PdAr_2TCHP$ **11** to $PdAr_2TBP$ **12** with DDQ in refluxing $CHCl_3$ like in literature [18, 59, 86]. Unfortunately, the oxidation step failed. MALDI MS analysis showed only a mixture of undefined byproducts. Filatov *et al.* also described in their work that aromatization of MAr_2TCHPs with DDQ is not possible in contrast to MAr_4TCHP and results in chlorinated MAr_2TCHPs and higher oligomers.[60]

Approach 2 All synthetic steps are depicted in Figure 5.7. The first two steps were conducted according to literature [44]. In the first step commercially available bis(trimethylsilyl)acetylene was converted with p-toluenesulfonyl chloride and $AlCl_3$ in a Friedel-Crafts like reaction to **13**. In the next step **13** was deprotected with NaF to get compound **14**. Both steps had excellent yields.
Subsequently, compound **14** was reacted with 1,3-cyclohexadiene in a Diels-Alder reaction.[62] This reaction was done at 70 and 85 °C, respectively. At 85 °C the reaction was complete after 24 h, but APCI-MS analysis showed big amount of a byproduct. The byproduct could be identified as 1-methyl-4-(phenylsulfonyl)benzene (Figure 5.6). The same reaction carried out at 70 °C took three days, but resulted in less byproduct. It is possible that the optimal temperature for this reaction resulting in less byproduct and higher reaction speed is between 70 and 85 °C, but this has not been tried so far.

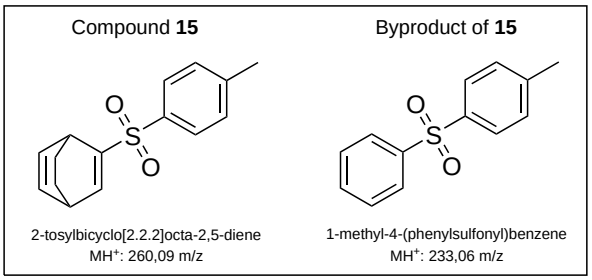

Figure 5.6: Structures of compound **15** and byproduct of **15**

In step four **15** and ethyl isocyanoacetate was converted in a Barton–Zard reaction according to literature [62] to isoindol **16**. In contrast to approach 1, the stronger base KOtBu was necessary. The next three steps were identical to approach 1. Isoindol **16** was condensed to **17**, **17** was decarboxylated with KOH to dipyrromethane **18** in ethylene glycol at 170 °C. Dipyrromethane **18** was condensed with the benzaldehydes (**1b** and **3b**) to obtain the metal-free tetrabicycloporphrin DTDDTBCP **19**.
DTDDTBCP **19** could be easily aromatized to tetrabenzoporphyrin $H_2DTDDTBP$ **20** by heating the solid compound to 200 °C under vacuum.[50, 51, 61, 62] In a last step the final $PdAr_2TBP$ **21** could be received again by metallation of **20** with $(C_6H_5CN)PdCl_2$ and sodium propionate in refluxing toluene.

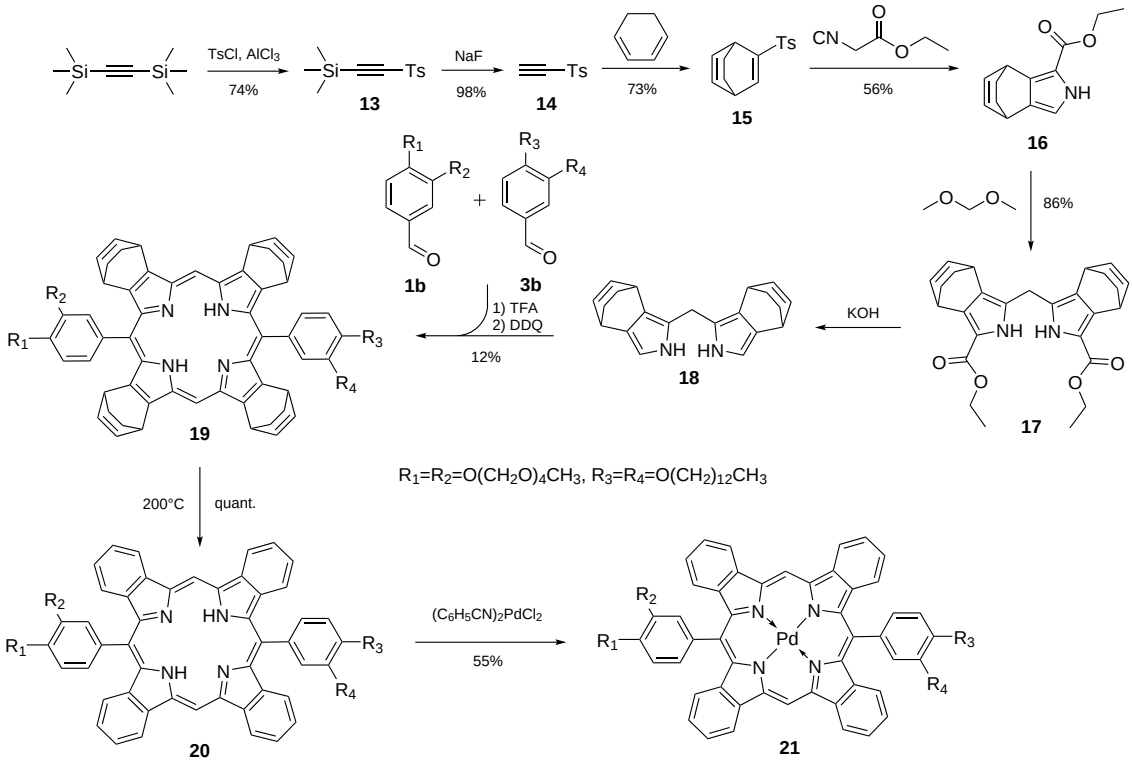

Figure 5.7: Overview of Pd tetrabenzoporphyrin synthesis (approach 2)

Synthesis of A-Type Pd-Porphyrin

The synthesis was done in two steps, starting with dipyrromethane **4**. An overview of the steps is given in Figure 5.8.

MTP **22** was synthesised similar to literature.[38] Therefore, dipyrromethane **4**, pyrrole-2-carboxaldehyde and benzaldehyde **3a** were condensed with TFA as acid-catalyst. This reaction resulted in disubstituted 5,15-bis(TEGoxyphenyl)porphyrin as main product and 5-TEGoxyphenylporphyrin **22** as side product. After isolating **22** by silica gel column chromatography, it was metallated with $(C_6H_5CN)PdCl_2$ to obtain the desired PdMTP **23**.

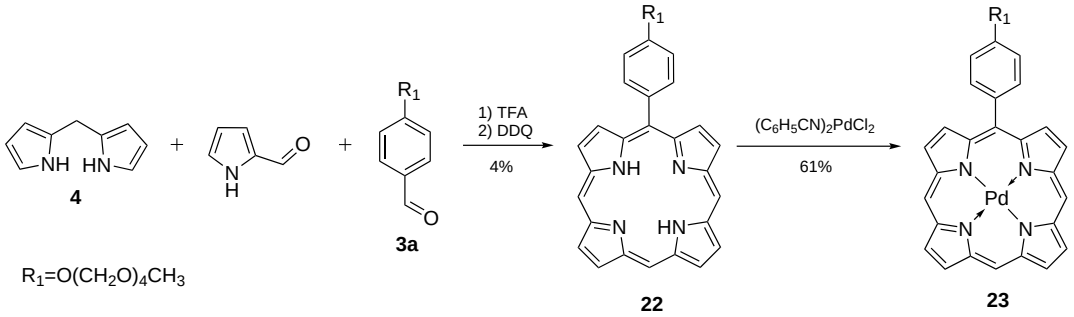

Figure 5.8: Overview of PdMTP synthesis

Attempted Synthesis of a Covalently Linked Pd-Porphyrin Dimer

An overview of the synthesis is given in Figure 5.9. In a first step porphyrin **24** was synthesised by condensation of dipyrromethane **4** with benzaldehyde **1b**. It could also be isolated as side product by synthesising porphyrin **5a**.
Bromation of **24** would have lead to a mixture of mono and disubstituded porphyrins, which can not be separated by silica gel column chromatography.[37] Consequently, **5a** was converted into **25** with PhLi. **25** has only one free *meso*-position which was bromated with NBS in a next step to yield bromated porphyrin **26**. Then **26** was metallated to Pd-porphyrin **27** like the other porphyrins.
In parallel, 4,16-dibromo[2.2]paracyclophane was borylated with 2-isopropoxy-4,4,5,5-tetramethyl-1,3,2-dioxyborolane according to literature [75]. In a last step it was tried to link two Pd-porphyrins **27** with the borylated paracyclophane **28** via Suzuki coupling. Unfortunately, this reaction failed, maybe due to sterically hindrance. During the reaction time of 5 days only a second, more hydrophobic, spot could be detected via TLC. This spot may have belonged to the mono substituted linker, but it was not further investigated.

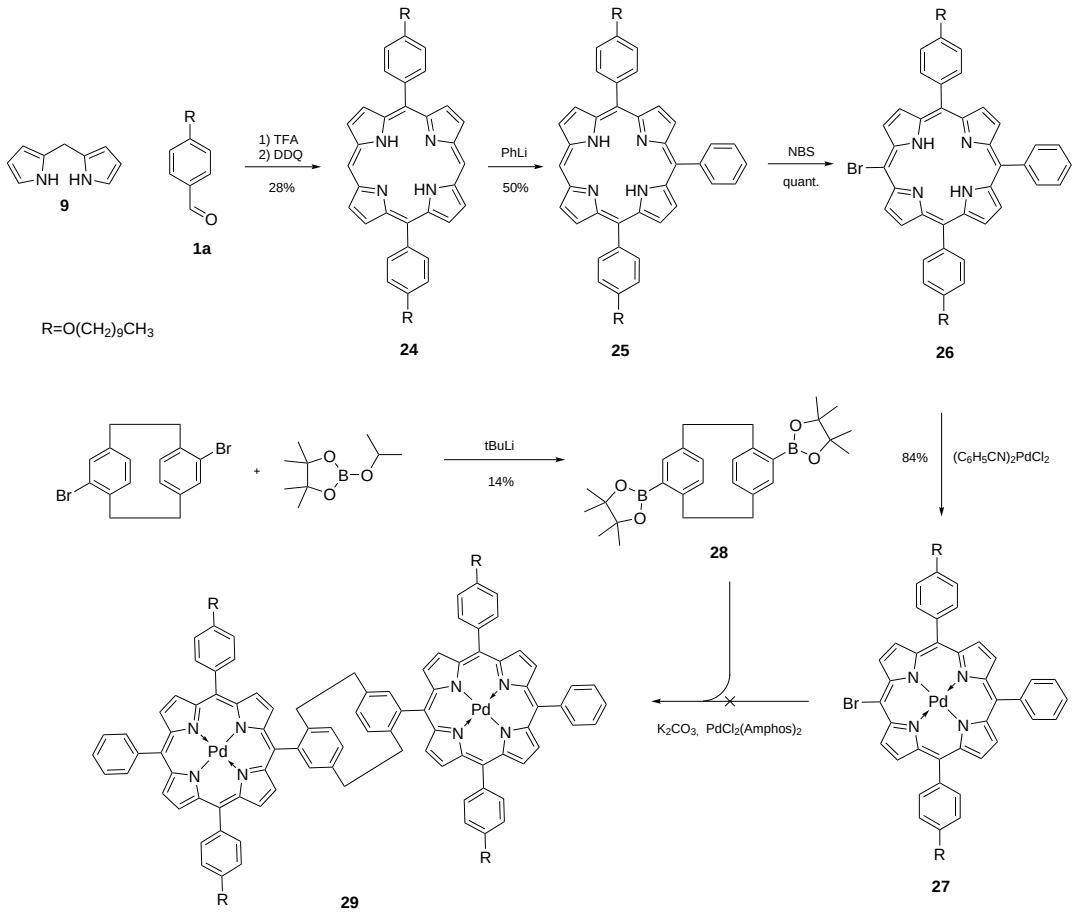

Figure 5.9: Overview of Pd-porphyrin dimer synthesis

5.1.2 Formation of Dye-Surfactant Aggregates

Next it was tried to convert the synthesised dyes to aggregates. The idea was to form dye-surfactant aggregates, which should be more stable in water than only the dye alone. Additionally, in case of some dye classes (cyanine dyes), dye-surfactant aggregates have a higher structural order, resulting in better photophysical properties (e.g. enhanced quantum yields).[87] Due to these benefits, this work was focused on dye-surfactant aggregates.

Dependency on Surfactant Concentration

In a first measurement series the dye aggregation dependency on surfactant concentration was investigated. Therefore, aqueous solutions of PdMTMDP (1.49×10^{-5} M) with surfactant concentrations of 0, 5, 50, 500, and 5000 mg/L Pluronic P123 were prepared. Afterwards, absorption spectra were directly measured between 350 and 1000 nm.
The absorption spectra between 350 and 650 nm are shown in Figure 5.10. None of the spectra show the red-shifted narrow band characteristic for J-aggregates. Nevertheless, for solutions with a low surfactant concentration a larger red-shift of the Soret and Q-bands is observed which can be interpreted as a dye-dye interaction.

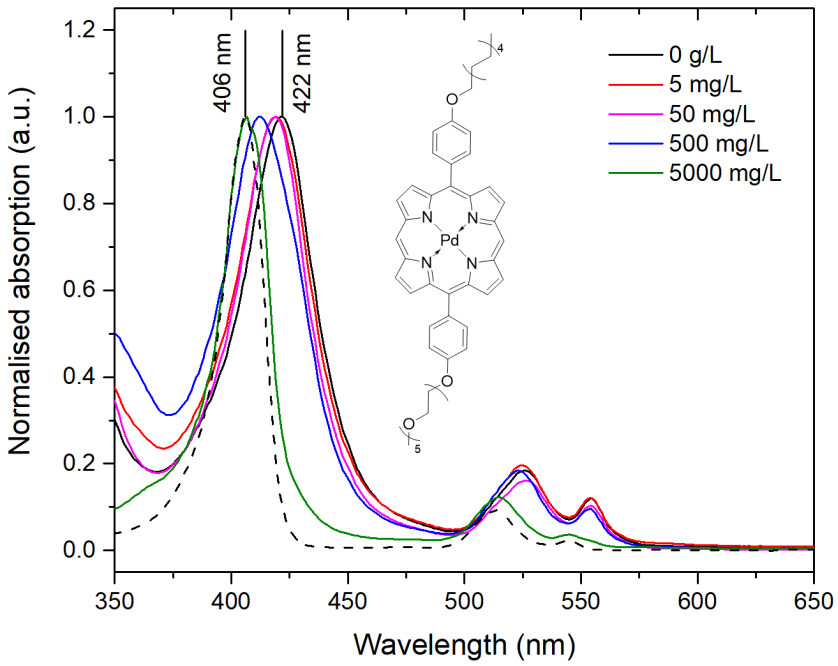

Figure 5.10: Absorption spectra of PdMTMDP (1.49×10^{-5} M) with different Pluronic P123 concentrations in water. The dashed line represent the monomeric absorption spectrum of PdMTMDP in THF.

The largest red-shift (16 nm) can be recognized for the solution without any surfactant. By

increasing the amount of surfactant, the spectra are shifted to shorter wavelengths and get closer to the monomeric absorption spectrum of PdMTMDP. At a concentration of 5 g/L Pluronic P123 dye-surfactant and monomer spectrum are nearly identical.
This effect could be also observed by the solution colour. Solutions with a low Pluronic P123 concentration had a yellow and those with a high concentration a reddish colour.
It can be said that a high surfactant concentration leads to dye monomers and dye-dye interactions are preferred at low surfactant concentrations. Due to that all further measurements were carried out with a concentration of 50 mg/L of the respective surfactant.

Dependency on Used Surfactant

In a second series of measurements the dependency between surfactant type and aggregation was studied. Therefore, a series of seven dye-surfactant solutions for all Pd-porphyrins (PdMTMDP, PdDTDDP, PdTTP, PdMTP and PdDTDDTBP) and two metal-free porphyrins (MTMDP and DTDDP) was produced - six with different surfactants and one without any surfactant. The surfactant concentration was 50 mg/L and the dye concentrations were between 1.02×10^{-5} and 2.13×10^{-5} M. As surfactants, five neutral (Brij 93 (BR), Span 80 (SP), Pluronic P123 (PLU), Triton X100 (TRI) and Tween 85 (TW)) and one negatively charged surfactant (SDS) were used (Figure 5.11).

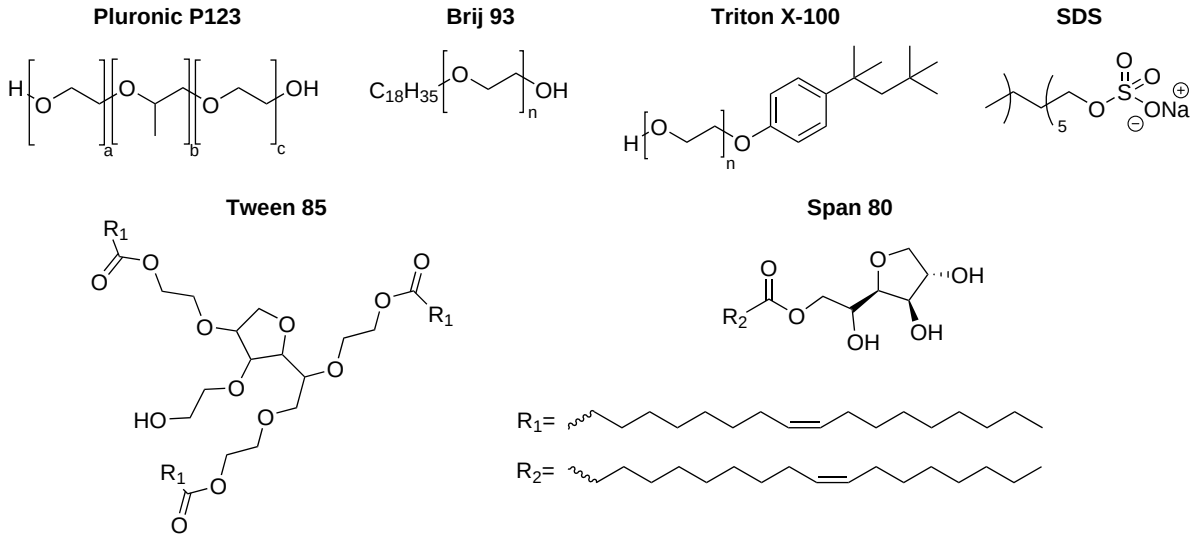

Figure 5.11: Structures of the used surfactants

Absorption spectra of all solutions were recorded between 350 and 1000 nm directly after their preparation. All spectra are shown in Figure 5.13 and 5.14. By doing this measurement series some interesting observations could be done. First, DTDDP, PdDTDDP and PdTTP show a split Soret band - except for PdTTP-TW, -TRI and -PLU. This splitting is attributed to

a strong exciton coupling between the transition dipoles, B_x and B_y, and a fixed orientation of neighbouring porphyrins (Figure 5.12). Thereby, the coupling between the B_x transition dipoles leads to a red shifted J-type absorption band and the B_y transition dipoles to a blue shifted H-type band in contrast to the monomer. The observed absorption spectrum is the sum of the absorption bands.[88] This effect is already known in literature.[88–92]

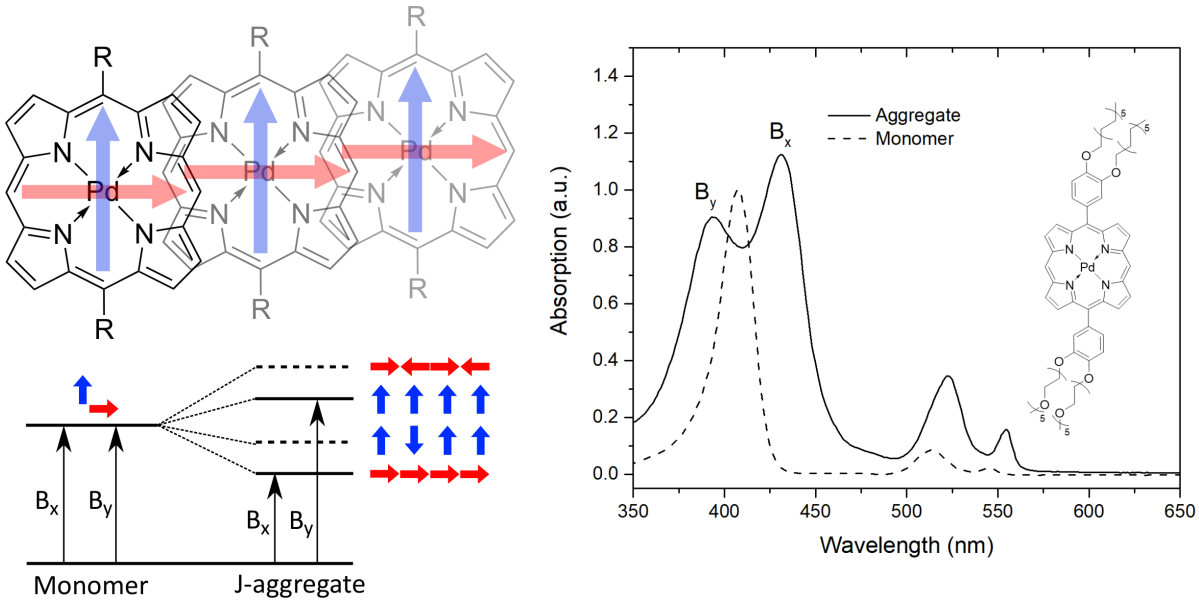

Figure 5.12: left) Schematic exciton model for Soret band of Pd-porphyrin J-aggregates. The arrows indicate the transition dipoles along x-axis (B_x-band, red) and y-axis (B_y-band, blue).[90] **right)** Absorption spectra of PdDTDDP-Span 80 aggregates (solid line) with split Soret band (B_x and B_y) and monomeric PdDTDDP (dashed line) in THF.

Second, the absorption spectra of the PdDTDDTBP has a doubly split Soret band, which indicates two types of aggregates with different orientations between their monomers. In literature such splittings have not been described.
Third, aggregation is favoured by increasing the amphiphilic character of the dyes. PdMTP with one TEG-group shows only a broadening of the Soret band which indicates an unfixed orientation of the assembly.[88] The more amphiphilic MTMDP and PdMTMDP have a red shifted and DTDDP, PdDTDDP and PdTTP have a split Soret band. By increasing the π-system of the porphyrin core, π-extended PdDTDDTBP shows a larger red-shift and a second splitting of the Soret band in comparison to PdDTDDP.
For all dye-surfactant solutions a bathochromic shift of their Q-bands can be observed.

Consequently, dye assemblies with a H- and J-type character could be formed by DTDDP, PdDTDDP, PdTTP and PdDTDDTBP, but they do not show the “classical” strongly bathochromically shifted and narrow absorption bands. That behaviour can be explained by only slightly shifted porphyrins in the J-aggregate structure.

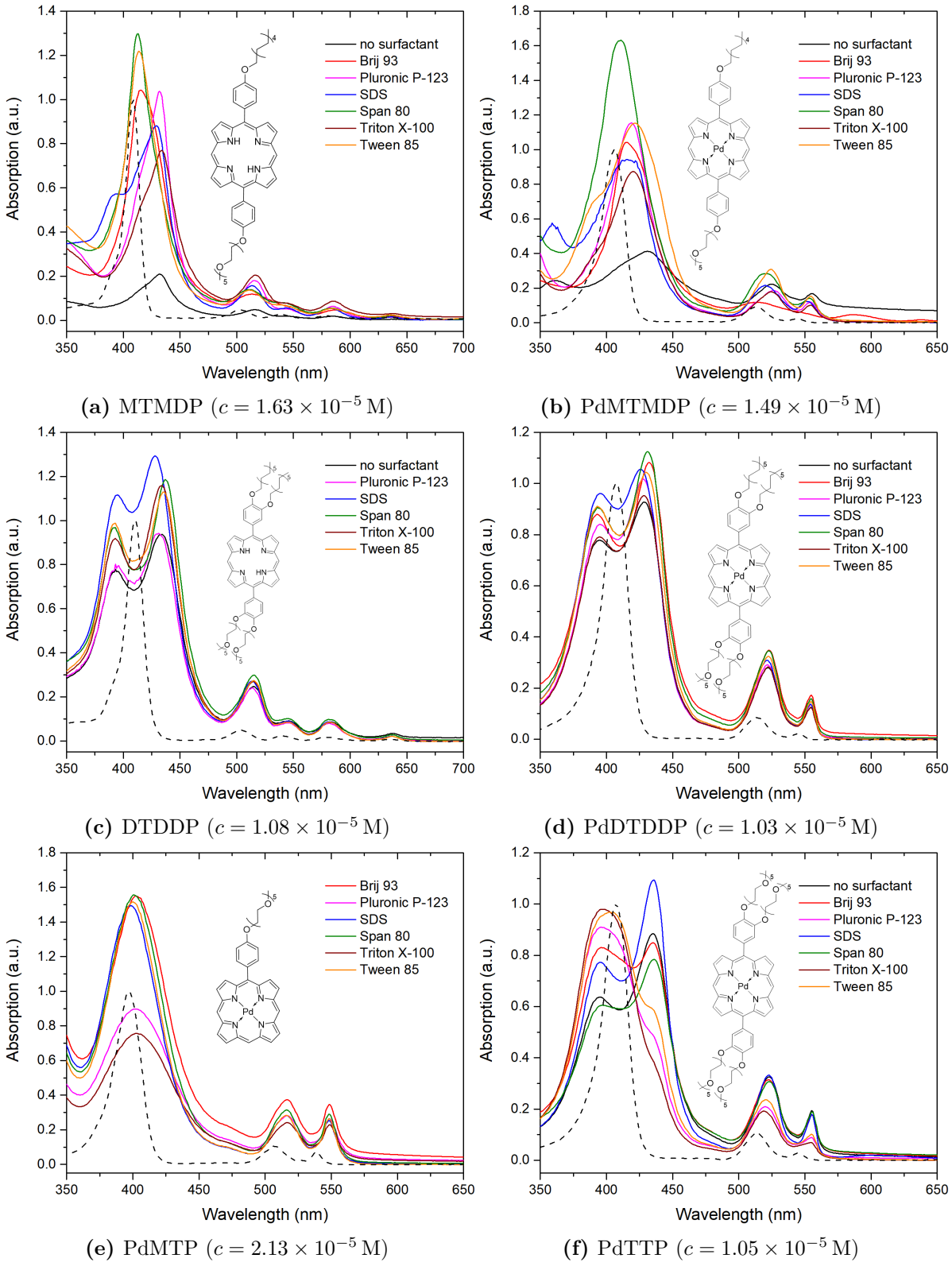

(a) MTMDP ($c = 1.63 \times 10^{-5}\,\mathrm{M}$)

(b) PdMTMDP ($c = 1.49 \times 10^{-5}\,\mathrm{M}$)

(c) DTDDP ($c = 1.08 \times 10^{-5}\,\mathrm{M}$)

(d) PdDTDDP ($c = 1.03 \times 10^{-5}\,\mathrm{M}$)

(e) PdMTP ($c = 2.13 \times 10^{-5}\,\mathrm{M}$)

(f) PdTTP ($c = 1.05 \times 10^{-5}\,\mathrm{M}$)

Figure 5.13: Absorption spectra of dye aggregate solutions with different types of surfactants ($c = 50\,\mathrm{mg/L}$) in water. The dashed lines represent the absorption spectrum of the monomeric species in THF.

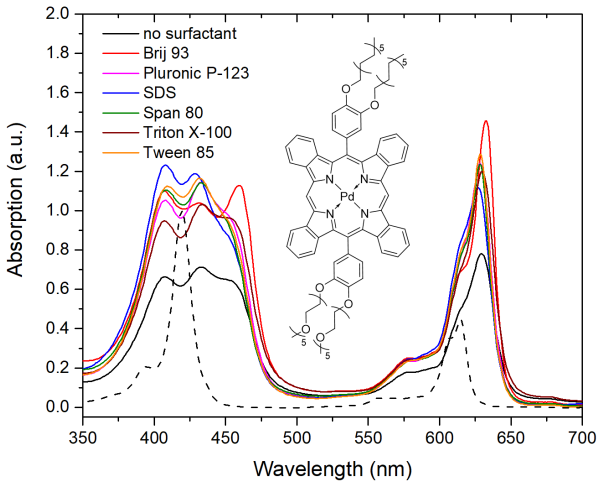

Figure 5.14: Absorption spectra of PdDTDDTBP ($c = 1.57 \times 10^{-5}$ M) aggregate solutions with different types of surfactants ($c = 50$ mg/L) in water. The dashed line represents the the absorption spectrum of the monomeric species in THF.

Stability of Dye-Surfactant Solutions

Directly after preparation, all dye-surfactant solutions, except for PdMTP and DTDDP-BR, are clear and had no precipitation. PdMTP alone is not soluble in water and directly precipitates. Second, DTDDP forms a turbid solution with Brij 93.
The stability of the solutions was further observed and after one week many solutions formed precipitates. Table 5.1 shows which solutions are stable over time.

Table 5.1: Stability of the dye-surfactant solutions. ✓means "stable" and ×means "formed a precipitate after one week"

	Surfactant						
	without	PLU	BR	TRI	SP	TW	SDS
PdMTP	×	×	×	×	×	×	✓
MTMDP	×	×	✓	×	✓	×	✓
PdMTMDP	✓	✓	✓	✓	✓	✓	✓
DTDDP	×	×	×	✓	✓	✓	✓
PdDTDDP	✓	✓	✓	✓	✓	✓	✓
PdTTP	×	×	×	×	✓	✓	✓
PdDTDDTBP	×	×	✓	×	✓	✓	✓

5.2 Monomer and Aggregate Characterisation

In this chapter the characterisation of the dyes (MTMDP, DTDDP, PdMTMDP, PdDTDDP, PdTTP, PdMTP and PdDTDDTBP) and the dye-surfactant solutions is discussed. For each dye only one dye-surfactant solution was characterised. These solutions are MTMDP-SP, DTDDP-SP, PdMTMDP-SP, PdDTDDP-SP, PdTTP-SDS, PdMTP-SDS and PdDTDDTBP-BR.

5.2.1 Dye Characterisation

Photophysical Properties

All measurements were carried out in THF. The photophysical properties for the metal-free porphyrins MTMDP and DTDDP are given in Table 5.2 and their absorption/emission spectra in Figure 5.15. Both porphyrins have similar properties and correlates very well with literature data for 5,15-diphenylporphyrin [93] and other metal-free porphyrins [94, 95]. It can be said that additional two oxy-substituents on the phenyl-rings of DTDDP have no influence on the photophysical properties, compared to MTMDP.

Table 5.2: Spectral properties of two metal-free porphyrins in THF at room temperature.

Dye	λ_{max} abs (nm)	λ_{max} em (nm)	Q.Y.$_{\text{rel}}$[a] (%)	τ_f (ns)	τ_f (77 K) (ns)
MTMDP	409, 503, 540, 579, 634	639, 700	8.2	9.6	11.9
DTDDP	410, 505, 539, 579, 634	639, 703	8.2	9.8	12.7

[a] The relative quantum yields were obtained using H_2OEP in benzene (Φ= 13 % [68]) as a reference.

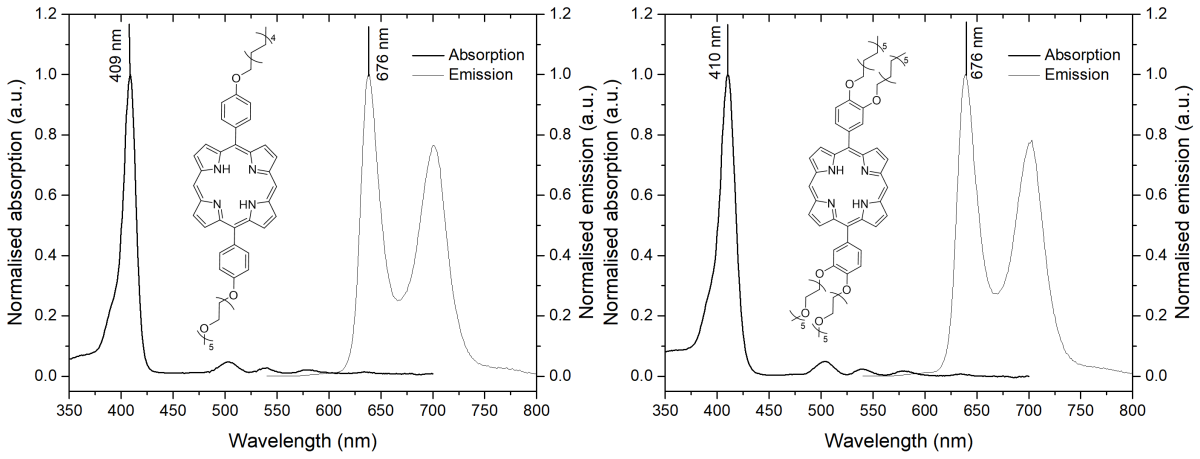

(a) MTMDP (λ_{ex} = 409 nm) **(b)** DTDDP (λ_{ex} = 410 nm)

Figure 5.15: Normalised absorption and emission spectra of metal-free porphyrins in THF at room temperature.

Excitation and emission spectra were also measured at 77 K, which are illustrated in Figure 5.16. At 77 K their lifetimes are slightly increased and the emission spectra are sharper than at room temperature. Furthermore, the emission bands are slightly shifted to shorter wavelengths, whereas the excitation spectra are shifted to longer wavelengths.

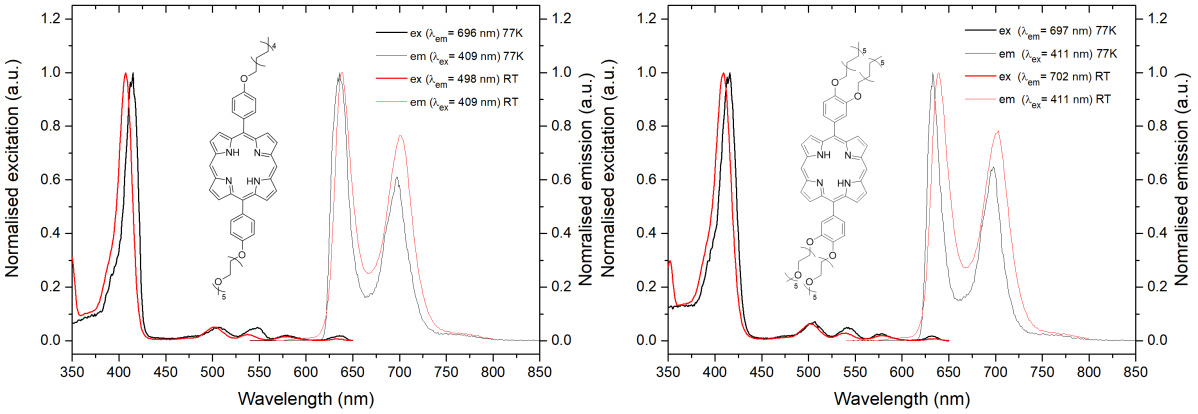

(a) MTMDP **(b)** DTDDP

Figure 5.16: Normalised excitation and emission spectra of metal-free porphyrins in THF at 77 K and room temperature.

Spectral properties of the Pd-porphyrins are shown in Table 5.3. Their absorption and emission spectra are depicted in Figure 5.17. The emission spectra, quantum yields and lifetimes were recorded under anoxic conditions.
PdMTMDP, PdDTDDP and PdTTP have similar absorption and emission spectra which are typical for Pd 5,15-diphenylporphyrins.[96, 97] Also their quantum yields are nearly identical. However, their lifetimes τ_p at room temperature are three times lower then PdMTP and 2.5 times lower then PdDTDDP. Additionally, they are also lower than other 5,15-diphenylporphyrins derivates in literature.[97] It seems that the lifetimes decrease by increasing the numbers of oxy-phenyl *meso*-substituents and oxy-groups on the phenyl rings. At 77 K their lifetimes are much longer and show a similar behaviour to compounds in literature.[97]

Table 5.3: Spectral properties of the synthesised Pd-porphyrins in THF at room temperature. Emission, quantum yield and lifetime were measured under anoxic conditions by bubbling argon and nitrogen through, respectively.

Dye	λ_{max} abs (nm)	λ_{max} em (nm)	Q.Y.$_{rel}$[a] (%)	τ_p (μs)	τ_p (77 K) (ms)
PdMTP	397, 507, 539	657, 726 (sh)	10.8	492	-
PdMTMDP	406, 514, 544	678, 734 (sh)	12.0	184	1.35
PdDTDDP	408, 514, 545	677, 739 (sh)	12.8	148	1.40
PdTTP	407, 514, 545	676, 731 (sh)	11.5	140	1.42
PdDTDDTBP	419, 614	793	10.7	408	0.67

[a] The relative quantum yields were obtained using H_2OEP in benzene (Φ= 13 % [68]) as a reference.
sh: shoulder

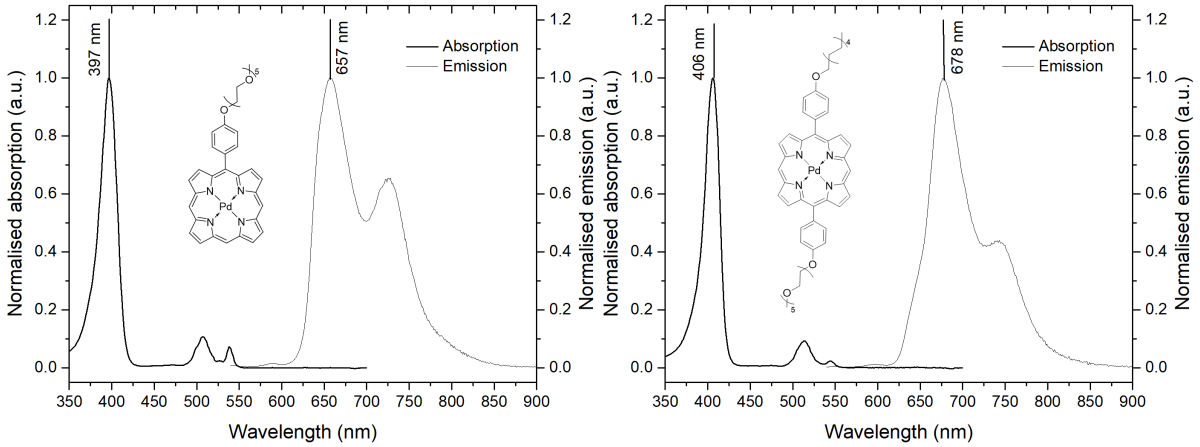

(a) PdMTP ($\lambda_{ex} = 397\,\text{nm}$)

(b) PdMTMDP ($\lambda_{ex} = 406\,\text{nm}$)

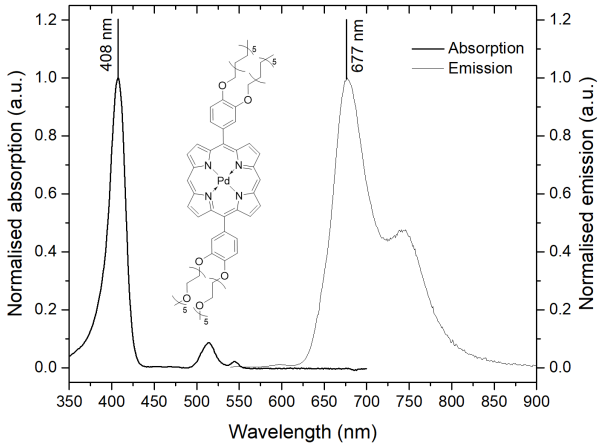

(c) PdDTDDP ($\lambda_{ex} = 408\,\text{nm}$)

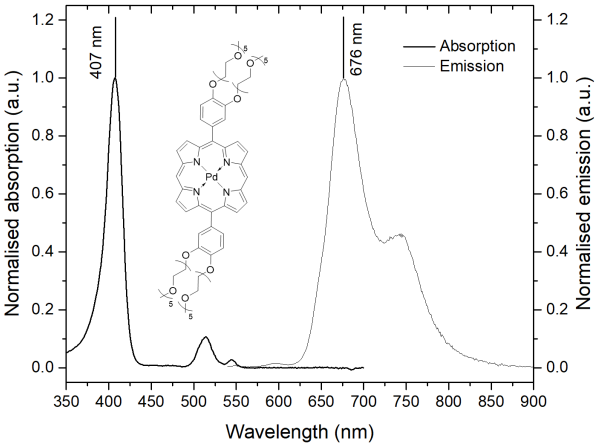

(d) PdTTP ($\lambda_{ex} = 407\,\text{nm}$)

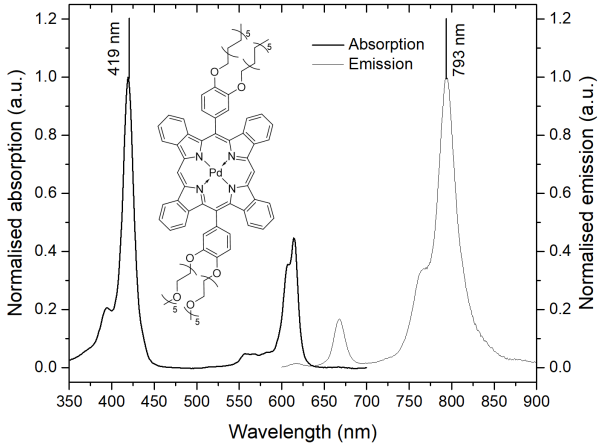

(e) PdDTDDTBP ($\lambda_{ex} = 419\,\text{nm}$)

Figure 5.17: Normalised absorption and emission spectra of Pd-porphyrin monomers in THF. Before recording the emission spectra, the solutions were degassed 15 min by a stream a argon.

PdMTP has a hypsochromically shifted absorption and emission spectrum, due to the absence of one phenyl substituent in contrast to the other Pd-porphyrins. Furthermore, the quantum yield is reduced and the lifetime is increased.
Due to the larger π-system of the porphyrin core, PdDTDDTBP has a bathochromically shifted absorption and emission spectrum in contrast to the other Pd-porphyrins. The photophysical properties match very well with values in literature for Pd-5,15-diphenyltetrabenzoporphyrin (PdDPTBP).[60] The only deviation to literature is a shorter lifetime (490 μs for PdDPTBP at room temperature) and a lower quantum yield (19 % for PdDPTBP). However, in 2016 Vinogradov and co-workers wrote that the phosphorescence quantum yields of metalloporphyrins can vary by as much as three to four times for the same compound, even when measurements are reported to have been performed under nearly identical conditions.[98]
Excitation and emission spectra measured at 77 K are shown in Figure 5.18. Like the metal-free porphyrins, all Pd-porphyrins show a similar behaviour of their excitation and emission spectra at 77 K.

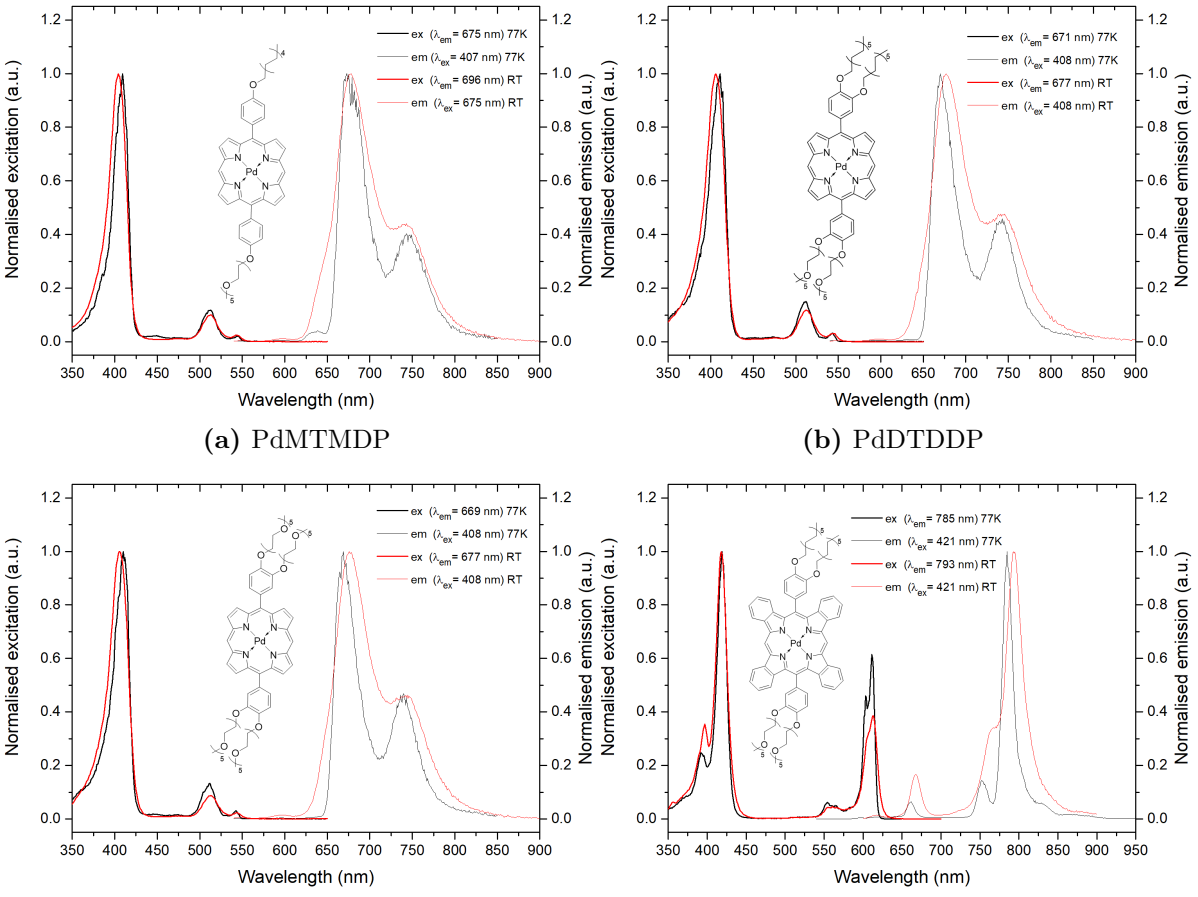

(a) PdMTMDP **(b)** PdDTDDP

(c) PdTTP **(d)** PdDTDDTBP

Figure 5.18: Normalised excitation and emission spectra of Pd-porphyrins in THF at 77 K and room temperature.

For all Pd-porphyrins emission spectra were measured under anoxic and air-saturated conditions. Thereby, some impurities in PdMTMDP and PdDTDDTBP could be found.

Figure 5.19 **(a)** shows that some amount of free-base porphyrin MTMDP is present which is manifested by fluorescence at air saturated conditions ($\lambda_{max} = 639\,\text{nm}$) and is also visible in the excitation spectra. Also MALDI-MS analysis confirmed that impurity (Appendix 10.3, Figure 10.30).

In PdDTDDTBP two remaining impurities could be found (Figure 5.19 **(a)**). One of them is the metal-free tetrabenzoporphyrin DTDDTBP. It shows strong fluorescence at 668 nm and the characteristic split Soret band in the excitation spectrum.[60] The other impurity could not be identified. The phosphorescent compound is responsible for the shoulder at 776 nm and has a similar excitation spectrum to PdDTDDTBP. Both impurities cannot be seen in the MALDI-MS spectrum (Appendix 10.3, Figure 10.38).

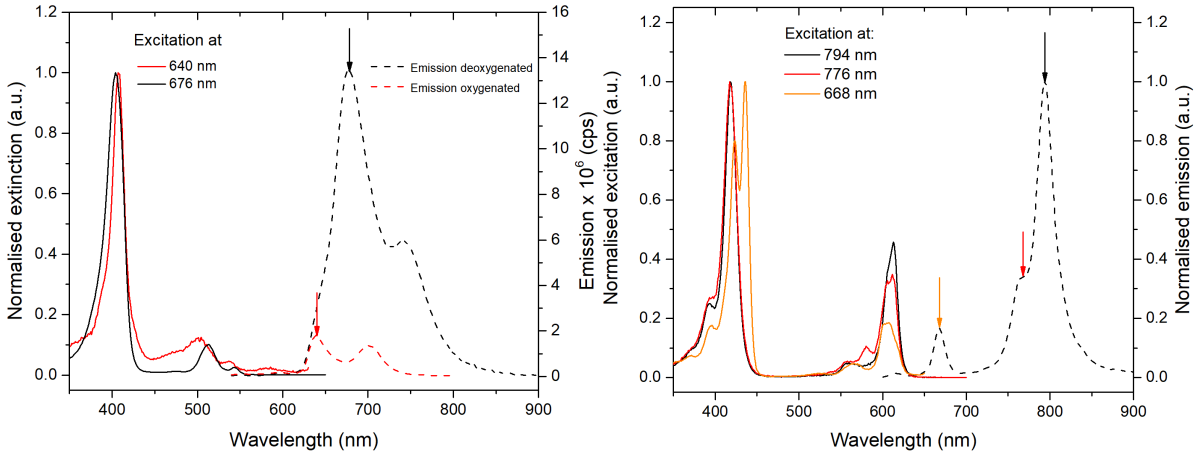

(a) **(b)**

Figure 5.19: (a) Remaining impurities of PdMTMDP. Emission spectrum ($\lambda_{ex} = 406\,\text{nm}$) of the contaminated PdMTMDP under deoxygenated condition (black dashed line) and under air-saturated conditions (dashed red line). Solid black line: excitation spectrum of PdMTMDP - measured under deoxygenated conditions. Solid red line: excitation spectrum of MTMDP - measured under air atmosphere. **(b)** Remaining impurities of PdDTDDTBP. Dashed black line: emission spectrum ($\lambda_{ex} = 419\,\text{nm}$) of the contaminated PdDTDDTBP at deoxygenated conditions. Solid black line: excitation spectrum of PdDTDDTBP. Solid red line: excitation spectrum of a unidentified by-product. Solid orange line: excitation spectrum of DTDDTBP.

5.2.2 Characterisation of Dye-Surfactant Aggregates

Resonance Light Scattering (RLS)

Up to this point, only the absorption spectrum gave an indication of formed J-aggregates. To confirm that, RLS measurements were performed. RLS is a very sensitive and selective technique for investigating solutions of aggregates and is only observed for extended aggregates of chromophores.[99–101] This technique is performed in synchronous-scan mode and right-angle geometry of the spectrofluorometer. When light from a excitation source passes through a solution of chromophore aggregates, the light is scattered and detected at the excitation wavelength. This effect is greatest near the absorption maximum and is enhanced when the chromophores are strongly electronically coupled in the aggregate.[101] Therefore, RLS spectra look very similar to absorption spectra.
By doing RLS measurements at the palladium and metal-free porphyrin-surfactant solutions two additional polarisation filters - rotated 90° to each other - were used to reduce the background scattering of the solvent. All measured solutions show an increase in scattering in contrast to water (Figure 5.20). Thereby, DTDDP-SP, PdDTDDP-SP, PdTTP-SDS and PdDTDDTBP-BR have a very large increase in scattering, which indicates aggregates with strongly electronically coupled porphyrins.

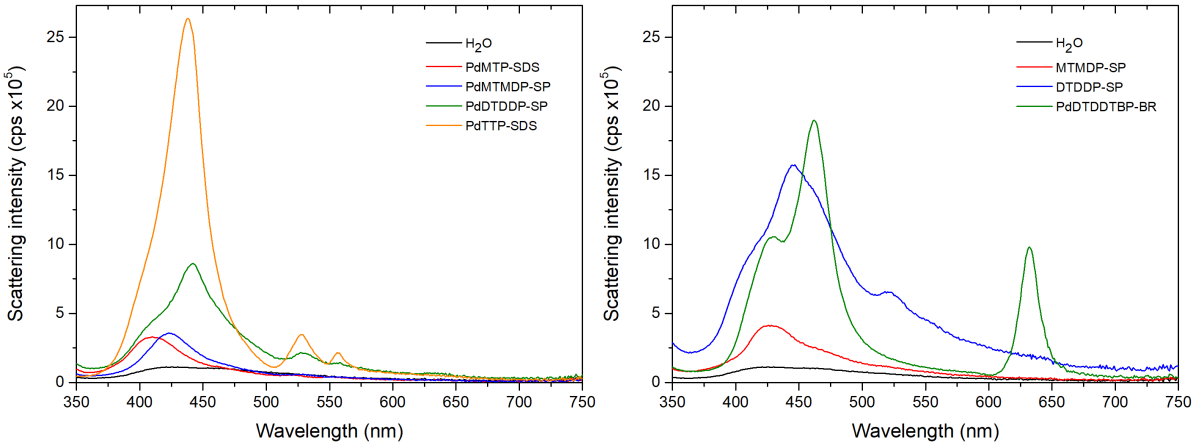

Figure 5.20: RLS profiles of water, five palladium and two metal-free porphyrin aggregate solutions. Before measuring, all samples were diluted with water to get an absorbance of approximately 0.1.

Comparing absorption and RLS spectra of these porphyrin-surfactant solutions (Figure 5.21), it can be shown that the enhanced scattering only belongs to the strongly coupled red-shifted B_x band. This behaviour can be explained by the fact that only the B_x transition dipoles along the

aggregate axes (J-type arrangement) have a large oscillator strength and therefore an enhanced scattering.

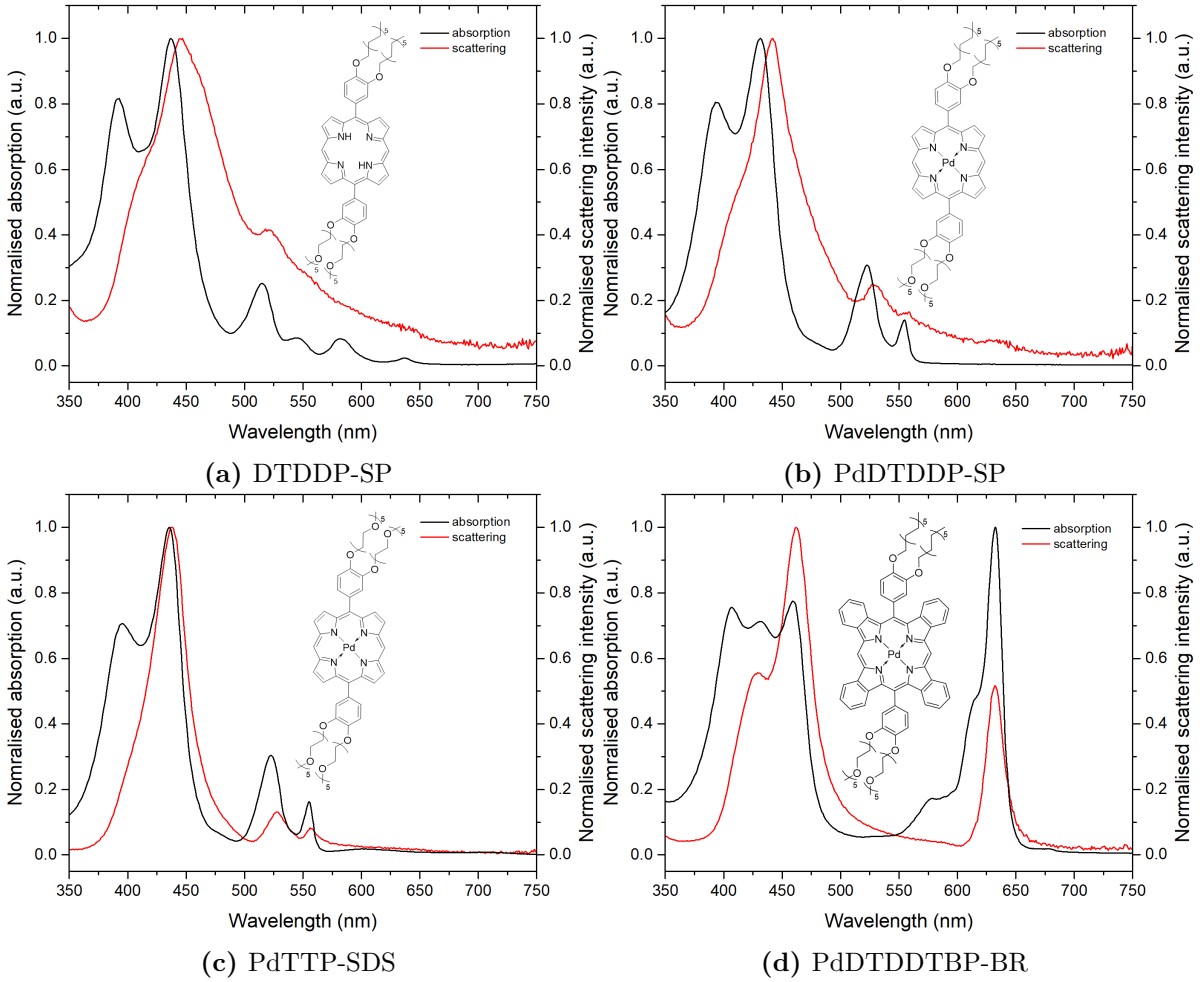

(a) DTDDP-SP

(b) PdDTDDP-SP

(c) PdTTP-SDS

(d) PdDTDDTBP-BR

Figure 5.21: RLS and absorption spectra of four solutions of aggregate.

The following statements can be made by the RLS measurements:

- All synthesised Pd-porphyrins and both metal-free porphyrins make kinds of aggregates in water.
- Porphyrin-surfactant solutions with less amphiphilic porphyrins (PdMTP-SDS, MTMDP-SP and PdMTMDP-SP) show lower tendency to form ordered aggregates and have a week electronic coupling between the porphyrins.
- Porphyrin-surfactant solutions with highly amphiphilic porphyrins (DTDDP-SP, PdDTDDP-SP, PdTTP-SDS) and with a extended π-system (PdDTDDTBP-BR) prefer aggregate formation with a strong electronic coupling. Thereby, only the B_x band of the aggregates show an enhanced scattering.

Temperature Dependent Equilibria in the Aggregates

Temperature dependence was measured for aggregate solutions DTDDP-SP, PdDTDDP-SP, PdTTP-SDS and PdDTDDTBP-BR. The spectra are shown in Figure 5.22. By heating the aggregate solutions, DTDDP-SP and PdDTDDTBP-BR show a huge change in there absorption spectra, whereas PdDTDDP-SP and PdTTP-SDS have only small changes. The shift in absorption spectra for DTDDP-SP and PdDTDDTBP-BR can be attributed to a decrease on aggregates and an increase in the concentration of the monomer molecules.
The aggregates of PdDTDDP-SP and PdTTP-SDS are much more stable at higher temperature and therefore no monomer formation is observed.

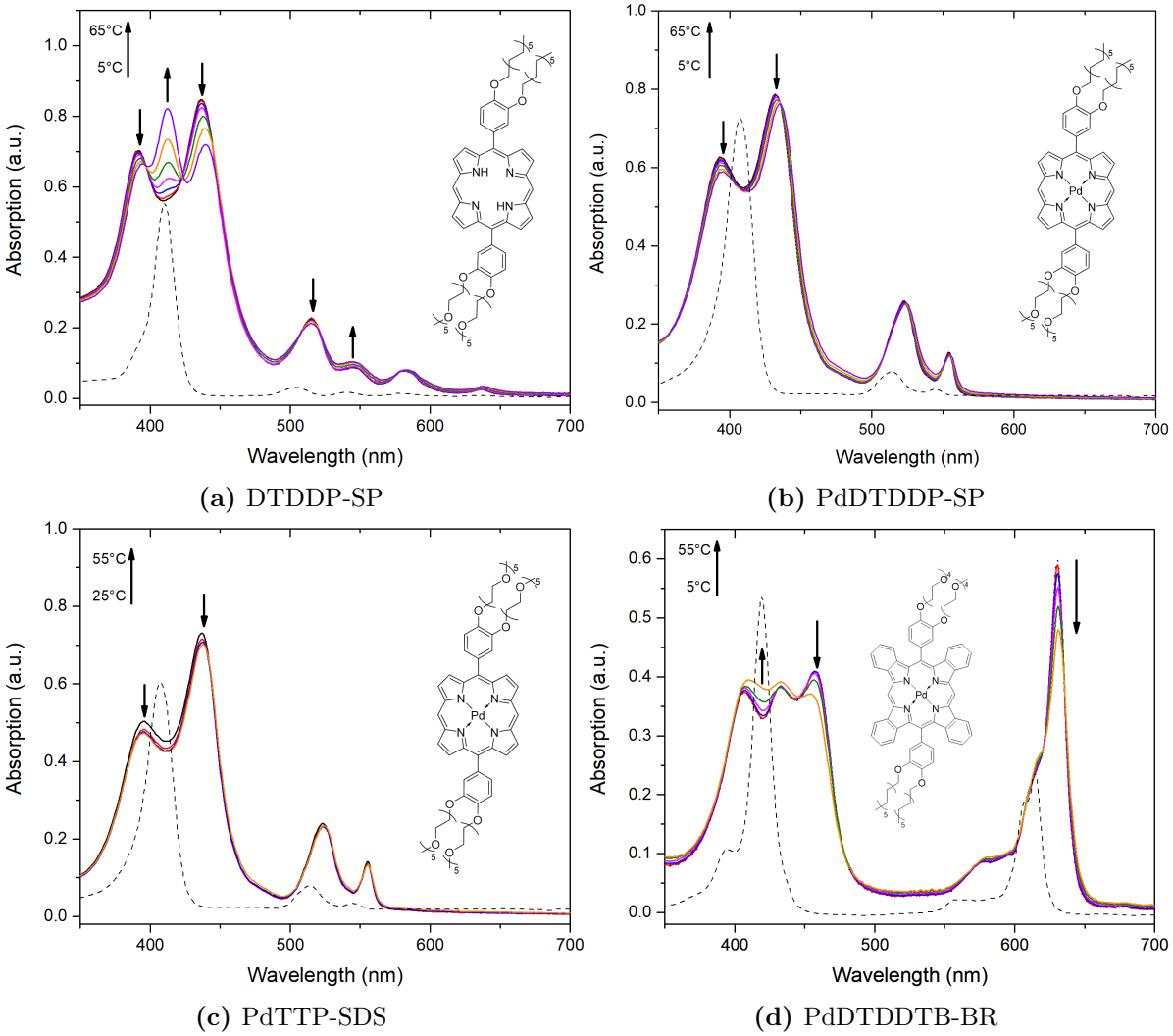

(a) DTDDP-SP **(b)** PdDTDDP-SP

(c) PdTTP-SDS **(d)** PdDTDDTB-BR

Figure 5.22: Temperature dependence of four aggregate solutions. The dashed line represents the absorption spectra of the dye monomer in THF.

Photophysical Properties

Photophysical properties of the metal-free porphyrin aggregate solutions are listed in Table 5.4. MTMDP-SP shows very similar spectral properties to the monomer in THF (Figure 5.23) and the lifetime has a bi-exponential decay with a longer and a shorter component. It appears that the longer component belongs to the monomer or low-ordered assemblies (monomer: 9.6 ns at RT and 11.9 ns at 77 K) and the shorter one to higher ordered aggregates. This assumption is affirmed by Villari *et al.*. They also reported a strongly decreased lifetime in porphyrin aggregates due to the strong electronic coupling between the chromophores.[92] Furthermore, the quantum yield shows a ten times lower value which is also reported for some porphyrin dimers (free-base and Zn-complexes), whereby the fluorescence intensity decreases by lowering the interplanar distance between two porphyrins.[88] This effect is attributed to a strong π-system overlap in face-to-face (H-type) dimers which produces non-fluorescence decay processes. However, due to the very similar spectra and the long lifetime component it is confirmed that MTMDP-SP only makes faint-fluorescent low-ordered assemblies.

Table 5.4: Photophysical properties of the metal-free porphyrin aggregates in water.

Dye	λ_{max} abs (nm)	λ_{max} em[b] (nm)	Q.Y.$_{rel}$[a] (%)	τ_f (ns)[c]	τ_f[b, c] (77 K) (ns)
MTMDP-SP	411, 506, 542, 582, 634	639, 702	0,3	10.3/2.9	9.8/1.7
DTDDP-SP	393, 437, 515, 545, 583, 637	640, 704	0,9	9.9/3.3	7.2/1.8

[a] The relative quantum yields were obtained using H_2OEP in benzene (Φ= 13 % [68]) as a reference.

[b] Measured at 77 K.

[c] Bi-exponential signal with a longer and a shorter component. Lifetimes were measured at 633 nm.

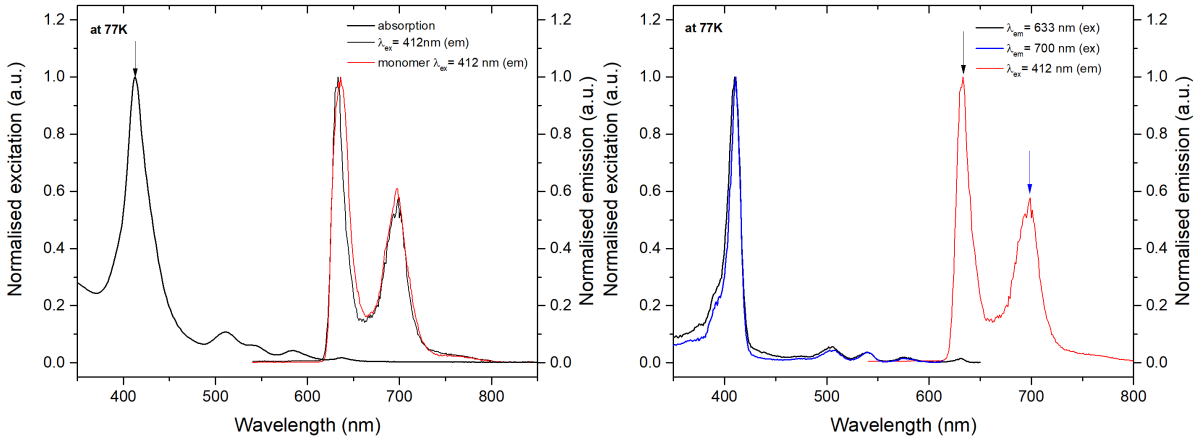

Figure 5.23: Absorption (at RT) emission and excitation (at 77 K) spectra of MTMDP-SP solutions: **(a)** Absorption and emission spectra. **(b)** Excitation spectra measured at two different emission wavelengths.

The spectral properties of DTDDP-SP differs more from its monomer, compared to MTMDP-SP. In addition to an absorption spectrum with a split Soret band, it also has an emission spectrum with an enhanced emission band at 704 nm (Figure 5.24 **(a)**). The excitation spectra in Figure 5.24 **(b)**, obtained by collecting emissions at 641 and 704 nm, indicate that both, monomers (or low orientated assemblies) and aggregates contribute to the emission. It seems that the monomers are present in much lower concentration than the aggregates, because of the higher quantum yield of the monomer (ten times) leading to a higher relative contribution in the excitation spectrum.

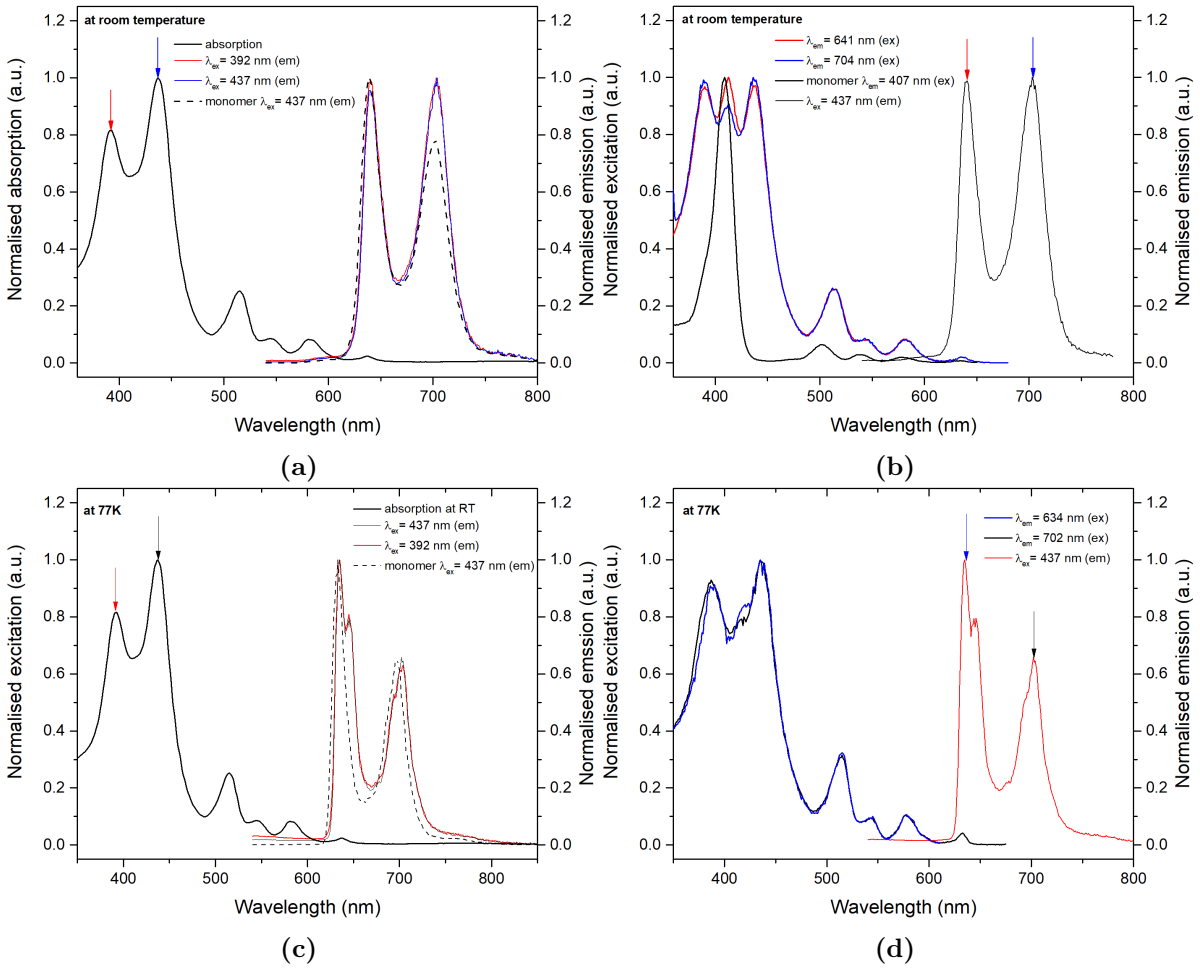

Figure 5.24: Absorption, emission and excitation spectra of DTDDP-SP aggregates: **(a)** Emission spectra measured at two different wavelengths at room temperature. **(b)** Excitation spectra collected at two different emission wavelengths at room temperature. **(c)** Emission spectra measured at two different wavelengths at 77 K. **(d)** Excitation spectra measured on two different emission wavelengths at 77 K.

Like MTMDP-SP, also DTDDP-SP has a bi-exponential decay with two components. Again, the longer component can be attributed to the monomer and the shorter one to the aggregates.

Furthermore, the quantum yield is ten times lower in comparison to the monomer, but higher than that of MTMDP-SP. This is indicative for more aggregates with a shifted orientation. The emission spectrum of DTDDP-SP generally looks different at 77 K. Also, some splitting in the first band at 644 nm can be seen (Figure 5.24 **(c)**). It may be that the smaller peak actually belongs to the monomer and the absolute position is different since the environment of the dye is different for monomer and aggregates. Furthermore, at 77 K both emission bands are attributed to the aggregate excitation spectrum (Figure 5.24 **(d)**). In summary, it can be said that DTDDP-SP prefers formation of J-aggregates in water.

In Table 5.5 the photophysical properties of the Pd-porphyrin-surfactant solutions are listed. The emission of dye-surfactant solutions under deoxygenated conditions is very weak at room temperature. Accordingly, the quantum yields are below 0.1 %. Since the strong decrease in the phosphorescence intensity may be due to a highly efficient quenching by molecular oxygen, the emission spectra were also acquired at 77K.

Table 5.5: Photophysical properties of Pd-porphyrin-surfactant solutions in water.

Dye	λ_{max} abs (nm)	λ_{max} em[b] (nm)	Q.Y.$_{rel}$[a] (%)	τ_p[b,c] (77 K) (ms)
PdMTMDP-SP	411, 520, 554	679, 745	<0,1	-
PdDTDDP-SP	393, 431, 523, 555	727	<0,1	1.4/0.86
PdTTP-SDS	396, 436, 523, 555	669, 740	<0,1	1.7/0.87[d]
PdDTDDTBP-BR	407, 431, 459, 633	-	<0,1	-

[a] The relative quantum yields were obtained using H_2OEP in benzene (Φ= 13 % [68]) as a reference.

[b] Measured at 77 K.

[c] Bi-exponential signal with a longer and a shorter component.

[d] Lifetimes were measured at 733 nm.

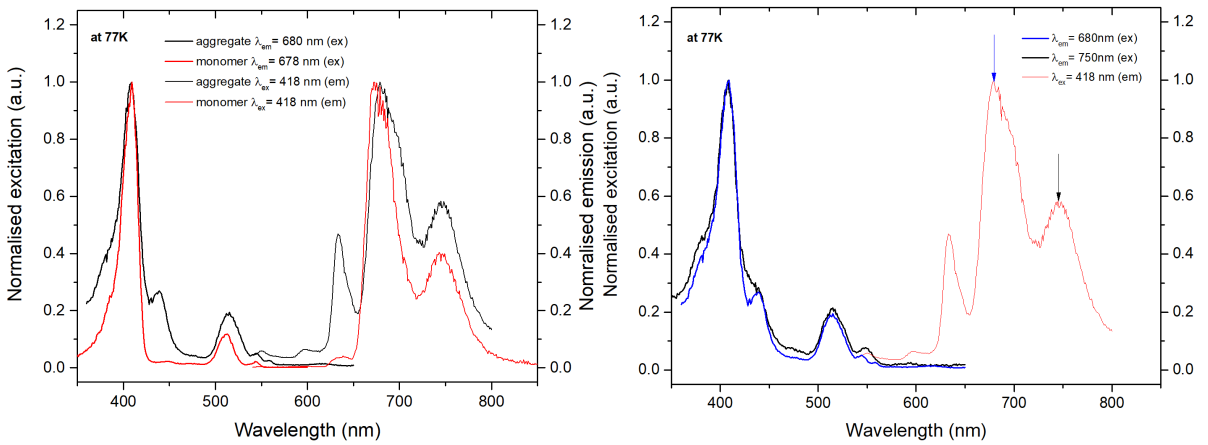

Figure 5.25: Emission and excitation spectra of PdMTMDP-SP solutions at 77 K: **(a)** Comparison of emission and excitation spectra between dye-surfactant solution and monomer (THF). **(b)** Comparison of excitation spectra, measured at two different emission wavelengths.

The emission spectrum of the PdMTMDP-SP solution is very similar to the monomer emission at 77 K (Figure 5.25 **(a)**). In the excitation spectrum a small shoulder at 440 nm is observed by collecting the emission at 750 nm, which may belong to aggregates (Figure 5.25 **(b)**). Unfortunately, the aggregate emission is also overlapped by the monomer emission. In other words, since the emission is so weak compared to that of the monomer, even traces of the monomer strongly contribute to the emission and excitation spectra and a further investigation cannot be done. Considering all photophysical data and the results from RLS measurements, it can be said that also PdMTMDP-SP forms only a few J-aggregates in water.

The PdDTDDP-SP solution also shows only weak emission at room temperature (Figure 5.26 **(a)**).

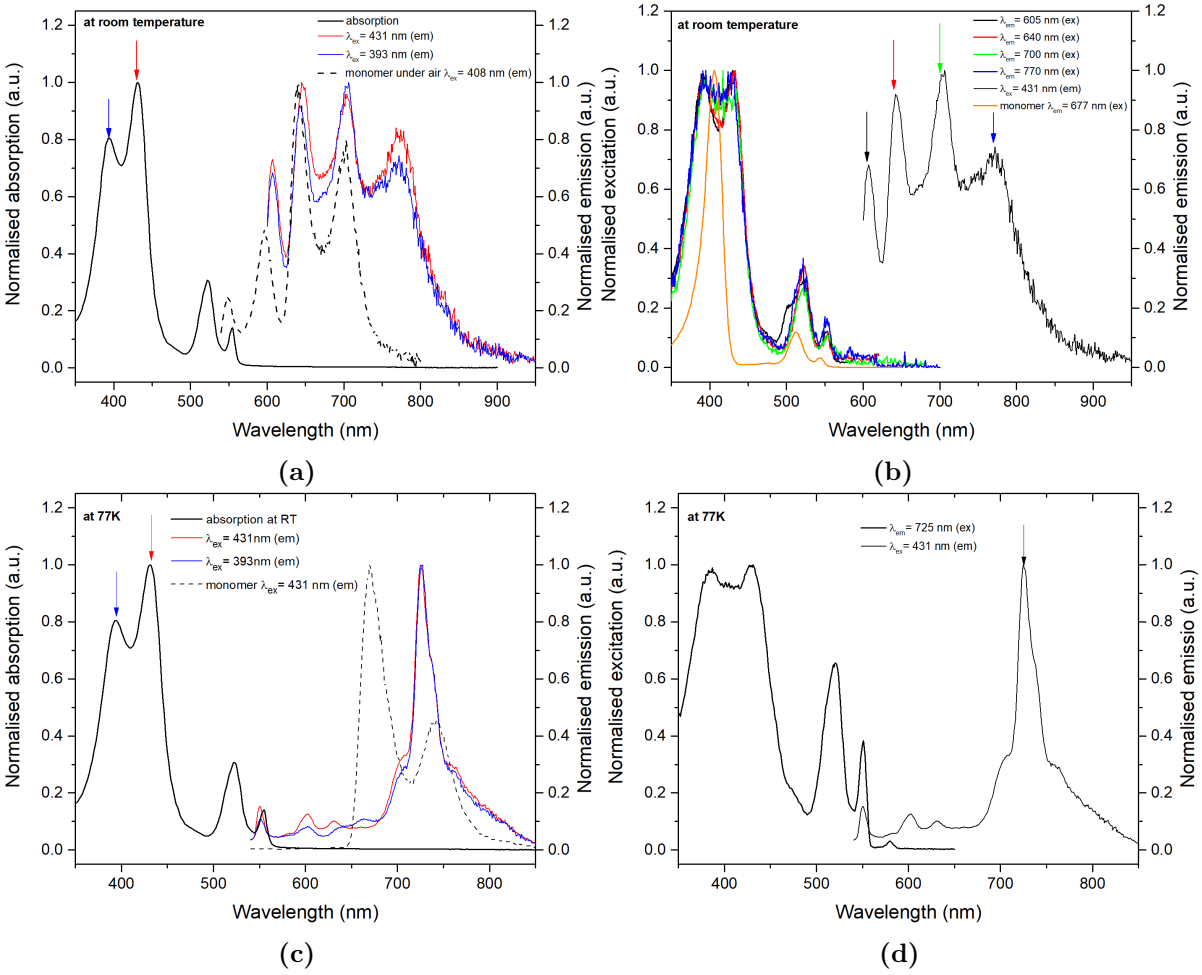

Figure 5.26: Absorption, emission and excitation spectra of PdDTDDP-SP aggregates: **(a)** Emission spectra measured at two different wavelengths at room temperature. **(b)** Excitation spectra measured on four different emission wavelengths at room temperature. **(c)** Emission spectra measured on two different emission wavelengths at 77 K. **(d)** Emission and excitation spectra from the aggregate at 77 K.

The bands at 605, 640 and 700 nm belong to impurities, which are also found in the monomer emission spectrum. A fourth band is observed at 770 nm, that belongs to the aggregates. However, excitation spectra, collected at 605, 640, 700 and 770 nm, all have the same shape - also the bands form impurities (Figure 5.26 **(b)**). This behaviour can maybe be explained by an energy transfer from the impurities to the aggregate, which leads to the identical excitation spectra.
By decreasing the temperature to 77 K another remarkable effect is observed. The emission increases and a phosphorescent band at 725 nm appears which is 55 nm bathochromically shifted in contrast to the monomer emission maximum (Figure 5.26 **(c)**). A possible explanation for this behaviour can be very efficient quenching or "super-quenching" at room temperature which is known for J-aggregates.[1] Thereby, traces of oxygen are enough to quench the whole emission. At 77 K the oxygen diffusion is hindered in the frozen solution and the emission can be observed.
Further aspects which speak for J-aggregates is the bi-exponential decay of the lifetime with a longer and a shorter component and again the excitation spectrum with the characteristic split Soret band at 77 K (Figure 5.26 **(d)**). Here, again the longer component is identical to the monomer (1.4 ms) and the shorter one can be attributed to the aggregates.
Consequently, by considering all results, it was found that PdDTDDP-SP forms J-aggregates and shows a weak phosphorescence at 725 nm.

A similar behaviour also could be seen for PdTTP-SDS. Depending on the excitation wavelength, two different emission spectra are observed at 77 K (Figure 5.27 **(a)**). Excitation at 395 nm gives an emission spectrum which is similar to the monomer, but has an enhanced emission at 728 nm in contrast to that. By exciting PdTTP-SDS at 435 nm, the emission at 728 nm becomes stronger and the band at 675 nm decreases.

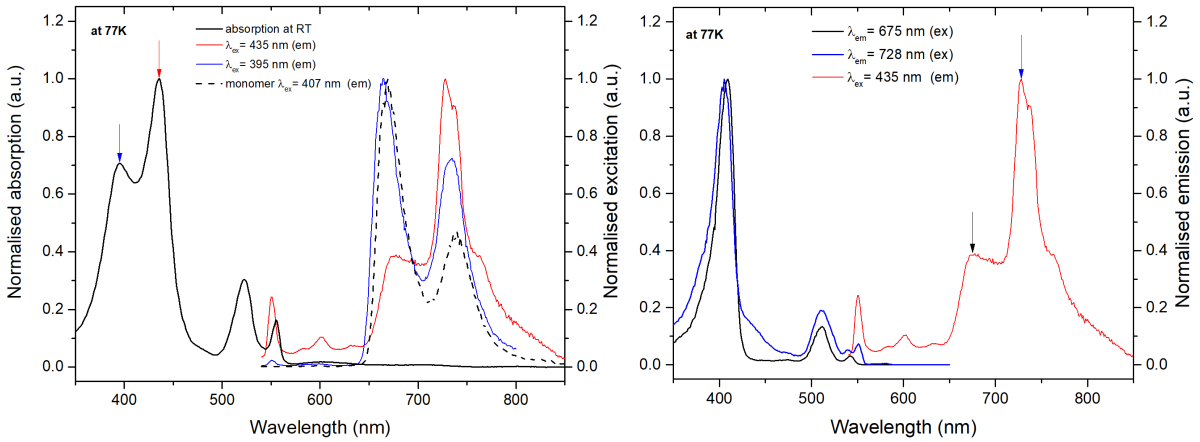

Figure 5.27: Absorption, emission and excitation spectra of PdTTP-SDS aggregates at 77 K: **(a)** Emission spectra measured at two different wavelengths. **(b)** Excitation spectra, measured at two different emission wavelengths.

Recording the excitation spectra, by collecting the emission at 675 and 728 nm, results in two spectra which are very similar to the monomer spectrum. Interesting is the excitation spectrum at $\lambda_{em} = 728$ nm (Figure 5.27 **(b)**) which has an increased absorbance between 425 and 460 nm. It appears that this belongs to the aggregates. Lifetime measurements show that the band at 665 nm has a similar lifetime to the monomer (PdTTP-SDS: 1.6 ms and PdTTP: 1.4 ms at 77 K) and the band at 728 nm has a bi-exponential decay with a monomer and aggregate component.

In contrast to PdDTDDP-SP and PdTTP-SDS, PdDTDDTBP-BR does not show phosphorescence above 700 nm at 77 K and room temperature (Figure 5.28 **(a)** and **(c)**).

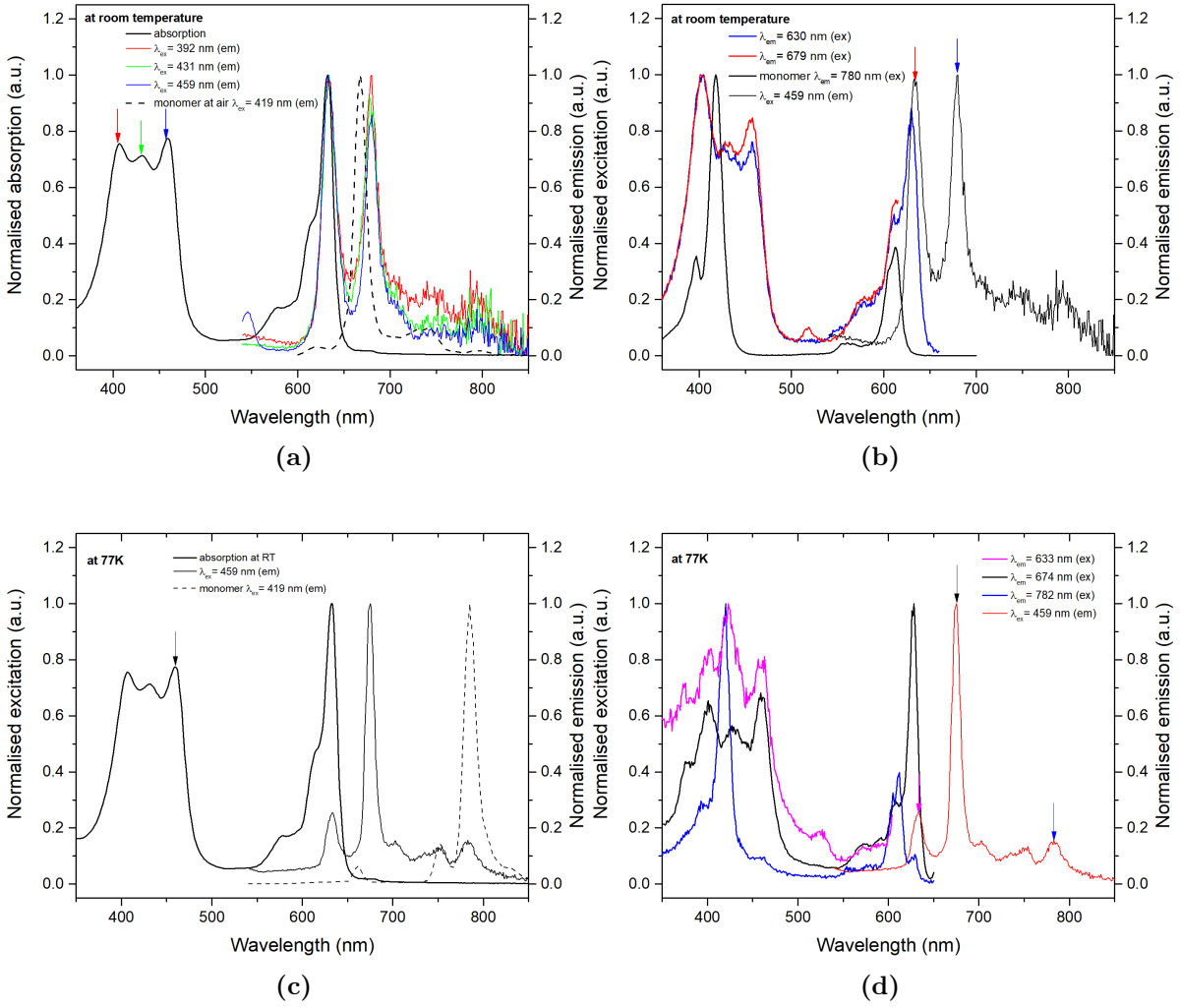

Figure 5.28: Absorption, emission and excitation spectra of PdDTDDTBP-BR solutions: **(a)** Emission spectra measured at three different wavelengths at room temperature. **(b)** Excitation spectra measured on two different emission wavelengths at room temperature. **(c)** Comparison between the emission of dye-surfactant solutions and monomer at 77 K. **(d)** Excitation spectra, measured on three different emission wavelengths at 77 K.

Only the fluorescence at 674 nm from the free-base tetrabenzoporphyrin impurity is visible (Figure 5.28 **(a)** and **(c)**). Again, recording the excitation spectra by collecting the emission at 630 and 674 nm (emission bands of impurities) gives the aggregate excitation spectra (Figure 5.28 **(c)** and **(d)**) which is attributed to an energy transfer from the impurities to the aggregates. The weak emission at 782 nm belongs to PdDTDDTBP monomer (Figure 5.28 **(d)**; blue excitation spectrum).
Consequently, PdDTDDTBP-BR makes aggregates, but they have no radiative emission.

6 Conclusion

In this thesis four new palladium(II)-porphyrins and a π-extended palladium(II)-tetrabenzoporphyrin with a varying amphiphilic character were synthesised by Lindsey-method and it was attempted to form J-aggregates in water with them. Thereby, the aggregation was supported by different types of surfactants.

Two palladium(II)-porphyrins **6c** and **6b** as well as its corresponding metal-free analogue **5b** formed highly ordered dye-surfactant assemblies in a J-type arrangement. The structure of Pd-porphyrin **6c** features two 3,4-bis(TEGoxy)phenyl groups and that of **6b** and **5b** one 3,4-bis(dodecyloxy)phenyl and one 3,4-bis(TEGoxy)phenyl group substituted on the 5,15-*meso*-position of the porphine core.

The absorption spectra of these aggregates feature a split Soret band with a red- and a blue-shifted band due to the strongly electronically coupled transition moments. Because of the strong coupling the red-shifted transition shows an enhanced scattering in RLS measurements. Furthermore, the aggregates posses shorter lifetimes than their monomers. While the metal-free porphyrin shows fluorescence at room temperature, the palladium(II)-porphyrins have only an extremely weak emission, but phosphorescence is observed at 77 K. This effect can be attributed to "superquenching" by traces of oxygen. Both, the strong quenching and the shorter lifetimes are already known for other types of J-aggregates.

The π-extended palladium(II)-tetrabenzoporphyrin **21** also forms ordered aggregates which have a doubly split Soret band. This effect can be attributed two different types of aggregates. In contrast to the non-π-extended palladium(II)-porphyrins, the tetrabenzoporphyrin shows no emission, also at 77 K.

7 References

1. Bricks, J. L., Slominskii, Y. L., Panas, I. D. & Demchenko, A. P. Fluorescent J-aggregates of cyanine dyes: basic research and applications review. *Methods and applications in fluorescence* **6,** 1–31 (2017).
2. Würthner, F., Kaiser, T. E. & Saha-Möller, C. R. J-aggregates: From serendipitous discovery to supramolecular engineering of functional dye materials. *Angewandte Chemie (International ed. in English)* **50,** 3376–3410 (2011).
3. JELLEY, E. E. Spectral Absorption and Fluorescence of Dyes in the Molecular State. *Nature* **138,** 1009–1010 (1936).
4. JELLEY, E. E. Molecular, Nematic and Crystal States of I: I-Diethyl–Cyanine Chloride. *Nature* **139,** 631 (1937).
5. Scheibe, G. Variability of the absorption spectra of some sensitizing dyes and its cause. *Angew. Chem.* **49,** 563–564 (1936).
6. Wang, H., Kaiser, T. E., Uemura, S. & Würthner, F. Perylene bisimide J-aggregates with absorption maxima in the NIR. *Chemical communications (Cambridge, England),* 1181–1183 (2008).
7. Kaiser, T. E., Stepanenko, V. & Würthner, F. Fluorescent J-aggregates of core-substituted perylene bisimides: Studies on structure-property relationship, nucleation-elongation mechanism, and sergeants-and-soldiers principle. *Journal of the American Chemical Society* **131,** 6719–6732 (2009).
8. Deng, Y., Yuan, W., Jia, Z. & Liu, G. H- and J-aggregation of fluorene-based chromophores. *The journal of physical chemistry. B* **118,** 14536–14545 (2014).
9. Chen, Z. *et al.* Near-IR Absorbing J-Aggregate of an Amphiphilic BF2 -Azadipyrromethene Dye by Kinetic Cooperative Self-Assembly. *Angewandte Chemie (International ed. in English)* **56,** 5729–5733 (2017).
10. Okada, S. & Segawa, H. Substituent-control exciton in J-aggregates of protonated water-insoluble porphyrins. *Journal of the American Chemical Society* **125,** 2792–2796 (2003).
11. Ohno, O., Kaizu, Y. & Kobayashi, H. J –aggregate formation of a water–soluble porphyrin in acidic aqueous media. *The Journal of Chemical Physics* **99,** 4128–4139 (1993).

12. Maiti, N. C., Mazumdar, S. & Periasamy, N. J- and H-Aggregates of Porphyrin−Surfactant Complexes: Time-Resolved Fluorescence and Other Spectroscopic Studies. *The Journal of Physical Chemistry B* **102,** 1528–1538 (1998).

13. Huber, V., Katterle, M., Lysetska, M. & Würthner, F. Reversible self-organization of semisynthetic zinc chlorins into well-defined rod antennae. *Angewandte Chemie (International ed. in English)* **44,** 3147–3151 (2005).

14. Cong, F. *et al.* Tuning J-type dimers of non-peripherally substituted zinc tetra-4-tert-butylphenophthalocyanine. *Spectrochimica acta. Part A, Molecular and biomolecular spectroscopy* **71,** 1397–1401 (2008).

15. Tanaka, T. & Osuka, A. Conjugated porphyrin arrays: synthesis, properties and applications for functional materials. *Chemical Society reviews* **44,** 943–969 (2015).

16. Tuffy, B. *Porphyrin Materials for Organic Light Emitting Diodes* (Brian Tuffy, 2011).

17. Quaranta, M., Borisov, S. M. & Klimant, I. Indicators for optical oxygen sensors. *Bioanalytical reviews* **4,** 115–157 (2012).

18. Zach, P. W., Freunberger, S. A., Klimant, I. & Borisov, S. M. Electron-Deficient Near-Infrared Pt(II) and Pd(II) Benzoporphyrins with Dual Phosphorescence and Unusually Efficient Thermally Activated Delayed Fluorescence: First Demonstration of Simultaneous Oxygen and Temperature Sensing with a Single Emitter. *ACS applied materials & interfaces* **9,** 38008–38023 (2017).

19. Campbell, W. M. *et al.* Highly Efficient Porphyrin Sensitizers for Dye-Sensitized Solar Cells. *The Journal of Physical Chemistry C* **111,** 11760–11762 (2007).

20. Walter, M. G., Rudine, A. B. & Wamser, C. C. Porphyrins and phthalocyanines in solar photovoltaic cells. *Journal of Porphyrins and Phthalocyanines* **14,** 759–792 (2010).

21. Lakowicz, J. R. *Principles of fluorescence spectroscopy* 3rd ed. (Springer, New York, 2006).

22. Valeur, B. *Molecular Fluorescence* 1st ed. (Wiley-VCH, Weinheim, 2002).

23. Treibs, A. Metallkomplexe von Porphyrinen. *Justus Liebigs Annalen der Chemie* **728,** 115–143 (1969).

24. Berg, K. *et al.* Porphyrin-related photosensitizers for cancer imaging and therapeutic applications. *Journal of microscopy* **218,** 133–147 (2005).

25. Taniguchi, M., Balakumar, A., Fan, D., McDowell, B. E. & Lindsey, J. S. Imine-substituted dipyrromethanes in the synthesis of porphyrins bearing one or two meso substituents. *Journal of Porphyrins and Phthalocyanines* **09,** 554–574 (2005).

26. Adler, A. D. *et al.* A simplified synthesis for meso-tetraphenylporphine. *The Journal of organic chemistry* **32,** 476 (1967).

27. Lindsey, J. S., Schreiman, I. C., Hsu, H. C., Kearney, P. C. & Marguerettaz, A. M. Rothemund and Adler-Longo reactions revisited: synthesis of tetraphenylporphyrins under equilibrium conditions. *The Journal of organic chemistry* **52,** 827–836 (1987).

28. Lindsey, J. S. & Wagner, R. W. Investigation of the synthesis of ortho-substituted tetraphenylporphyrins. *The Journal of Organic Chemistry* **54,** 828–836 (1989).

29. Lindsey, J. S. Synthetic routes to meso-patterned porphyrins. *Accounts of chemical research* **43,** 300–311 (2010).

30. Abada, Z., Ferrié, L., Akagah, B., Lormier, A. T. & Figadère, B. Synthesis and characterization of original N-meso chiral substituted diarylporphyrins. *Tetrahedron Letters* **53,** 6961–6964 (2012).

31. Enakieva, Y. Y. *et al.* General and Scalable Approach to A 2 B- and A 2 BC-Type Porphyrin Phosphonate Diesters. *European Journal of Organic Chemistry* **2016,** 4881–4892 (2016).

32. Hartnell, R. D., Edwards, A. J. & Arnold, D. P. Peripherally-metallated porphyrins: meso-η^1-porphyrinyl-platinum(II) complexes of 5,15-diaryl- and 5,10,15-triarylporphyrins. *Journal of Porphyrins and Phthalocyanines* **06,** 695–707 (2002).

33. Khandagale, S. B., Pilania, M., Arun, V. & Kumar, D. Metal-catalyzed direct heteroarylation of C-H (meso) bonds in porphyrins: facile synthesis and photophysical properties of novel meso-heteroaromatic appended porphyrins. *Organic & biomolecular chemistry* **16,** 2097–2104 (2018).

34. Senge, M. O. *et al.* Synthesis of meso -Substituted ABCD-Type Porphyrins by Functionalization Reactions. *European Journal of Organic Chemistry* **2010,** 237–258 (2010).

35. Yagi, S., Yamada, R., Tsuji, N., Murakami, S. & Takagishi, T. Conformational Control of a Polyether-Linked Porphyrin Dimer Induced by Complexation with a Sodium Cation. *Supramolecular Chemistry* **12,** 293–297 (2000).

36. Yamada, Y., Kubota, T., Nishio, M. & Tanaka, K. Sequential and spatial organization of metal complexes inside a peptide duplex. *Journal of the American Chemical Society* **136,** 6505–6509 (2014).

37. Enakieva, Y. Y. *et al.* General and Scalable Approach to A2B- and A2BC-Type Porphyrin Phosphonate Diesters. *European Journal of Organic Chemistry* **2016,** 4881–4892 (2016).

38. Ryppa, C. *et al.* Synthesis of mono- and disubstituted porphyrins: A- and 5,10-A2-type systems. *Chemistry (Weinheim an der Bergstrasse, Germany)* **11,** 3427–3442 (2005).

39. Giovannetti, R. The use of spectrophotometry UV-Vis for the study of porphyrins. *Macro to nano spectroscopy* **1,** 87–108 (2012).

40. Gouterman, M. Spectra of porphyrins. *Journal of Molecular Spectroscopy* **6,** 138–163 (1961).

41. Dolphin, D. *The Porphyrins V3: Physical Chemistry, Part A* (Elsevier Science, Oxford, 1978).

42. Milgrom, L. R. *The colours of life: An introduction to the chemistry of porphyrins and related compounds* (Oxford Univ. Press, Oxford, 1997).

43. Zhang, Y.-H., Ruan, W.-J., Li, Z.-Y., Wu, Y. & Zheng, J.-Y. DFT study on the influence of meso-phenyl substitution on the geometric, electronic structure and vibrational spectra of free base porphyrin. *Chemical Physics* **315,** 201–213 (2005).

44. Sommer, J. R. *et al.* Photophysical Properties of Near-Infrared Phosphorescent π-Extended Platinum Porphyrins. *Chemistry of Materials* **23,** 5296–5304 (2011).

45. Harriman, A. Luminescence of Porphyrins and Metalloporphyrins: Part 1 .–Zinc(II), Nickel(II) and Manganese(II) Porphyrins. *Journal of the Chemical Society, Faraday Transactions 1: Physical Chemistry in Condensed Phases* **76,** 1978–1985 (1980).

46. Harriman, A. Luminescence of Porphyrins and Metalloporphyrins: Part 3.-Heavy-atom Effects. *Journal of the Chemical Society, Faraday Transactions 2: Molecular and Chemical Physics* **77,** 1281–1291 (1981).

47. Helberger, J. H., von Rebay, A. & Hevér, D. B. Über die Einwirkung von Metallen auf o–Cyanacetophenon sowie auf 3–Methylphtalimidin: Synthese des Tetrabenzoporphins: III. Mitteilung zur Kenntnis der Benzoporphine. *Justus Liebigs Annalen der Chemie* **533,** 197–215 (1938).

48. Barrett, P. A., Linstead, R. P., Rundall, F. G. & Tuey, G. A. P. Phthalocyanines and related compounds: Part XIX. Tetrabenzporphin, tetrabenzmonazaporphin and their metallic derivatives. *Journal of the Chemical Society (Resumed),* 1079–1092 (1940).

49. Linstead, R. P. & Weiss, F. T. Phthalocyanines and related compounds: Part XX. Further investigations on tetrabenzporphin and allied substances. *Journal of the Chemical Society (Resumed),* 2975–2981 (1950).

50. Galanin, N. E., Shaposhnikov, G. P. & Koifman, O. I. Methods for synthesis of meso-substituted tetrabenzoporphyrins. *Russian Chemical Reviews* **82,** 412–428 (2013).

51. Carvalho, C. M. B., Brocksom, T. J. & de Oliveira, K. T. Tetrabenzoporphyrins: synthetic developments and applications. *Chemical Society Reviews* **42,** 3302 (2013).

52. Borisov, S. M. & Klimant, I. Efficient metallation in diphenylether – A convenient route to luminescent platinum(II) complexes. *Dyes and Pigments* **83,** 312–316 (2009).

53. Ichimura, K. *et al.* Formation of tetrabenzoporphine skeleton by the reactions of phthalimide with zinc carbonates. *Inorganica chimica acta* **186,** 95–101 (1991).

54. Hutter, L. H., Müller, B. J., Koren, K., Borisov, S. M. & Klimant, I. Robust optical oxygen sensors based on polymer-bound NIR-emitting platinum(II)–benzoporphyrins. *J. Mater. Chem. C* **2,** 7589–7598 (2014).

55. Filatov, M. A., Cheprakov, A. V. & Beletskaya, I. P. A Facile and Reliable Method for the Synthesis of Tetrabenzoporphyrin from 4,7-Dihydroisoindole. *European Journal of Organic Chemistry* **2007,** 3468–3475 (2007).

56. Barton, D. H. R., Jocelyne, K. & Zard, S. Z. A useful synthesis of pyrroles from nitroolefins. *Tetrahedron* **46,** 7587–7598 (1990).

57. Barton, D. H. R. & Zard, S. Z. New Synthesis of Pyrrols from Nitroalkenes. *Journal of the Chemical Society, Chemical Communications,* 1098–1100 (1985).

58. May Jr., D. A. & Lash, T. D. *The Journal of organic chemistry* **57,** 4820–4828 (1992).

59. Borisov, S. M. *et al.* New NIR-emitting complexes of platinum(II) and palladium(II) with fluorinated benzoporphyrins. *Journal of Photochemistry and Photobiology A: Chemistry* **201,** 128–135 (2009).

60. Filatov, M. A., Lebedev, A. Y., Vinogradov, S. A. & Cheprakov, A. V. Synthesis of 5,15-diaryltetrabenzoporphyrins. *The Journal of organic chemistry* **73,** 4175–4185 (2008).

61. Giraud-Roux Maryline, Proni Gloria, Nakanishi Koji & Berova Nina. Syntheses and spectroscopic properties of methylbenzoate derivatives of tetrabenzoporphyrin, application to circular dichroism studies. *Heterocycles* **61,** 417–432 (2003).

62. Okujima, T. *et al.* Synthesis of 4,7-dihydro-2H-isoindole derivatives via Diels-Alder reaction of tosylacetylene. *Heterocycles* **70,** 619–626 (2006).

63. Borek, C. *et al.* Highly efficient, near-infrared electrophosphorescence from a Pt-metalloporphyrin complex. *Angewandte Chemie (International ed. in English)* **46,** 1109–1112 (2007).

64. Senge, M. O. *et al.* Nonlinear Optical Properties of Porphyrins. *Advanced Materials* **19,** 2737–2774 (2007).

65. Kadish, K. M., Smith, K. M. & Guilard, R. *Applications: past, present and future* (Academic Press, San Diego, Calif., 2000).

66. Lebedev, A. Y., Filatov, M. A., Cheprakov, A. V. & Vinogradov, S. A. Effects of structural deformations on optical properties of tetrabenzoporphyrins: free-bases and Pd complexes. *The journal of physical chemistry. A* **112,** 7723–7733 (2008).

67. Fluorescent and triplet state photoactive J-type phthalocyanine nano assemblies: controlled formation and photosensitizing properties. *Journal of Materials Chemistry* **20,** 6726 (2010).

68. Ohno, O., Kaizu, Y. & Kobayashi, H. Luminescence of some metalloporphins including the complexes of the IIIb metal group. *The Journal of Chemical Physics* **82,** 1779–1787 (1985).

69. Crosby, G. A. & Demas, J. N. Measurement of photoluminescence quantum yields. Review. *The Journal of Physical Chemistry* **75,** 991–1024 (1971).

70. Sandeep, A., Praveen, V. K., Shankar Rao, D. S., Krishna Prasad, S. & Ajayaghosh, A. Transforming a C3 -Symmetrical Liquid Crystal to a π-Gelator by Alkoxy Chain Variation. *ACS Omega* **3,** 4392–4399 (2018).

71. Ding, Z. *et al.* Detection of Picric Acid by Terpy-Based Metallo-Supramolecular Fluorescent Coordination Polymers in Aqueous Media. *Chinese Journal of Chemistry* **35,** 447–456 (2017).

72. Poolman, J. M. *et al.* A toolbox for controlling the properties and functionalisation of hydrazone-based supramolecular hydrogels. *Journal of Materials Chemistry B* **4,** 852–858 (2016).

73. Laha, J. K., Dhanalekshmi, S., Taniguchi, M., Ambroise, A. & Lindsey, J. S. A Scalable Synthesis of Meso-Substituted Dipyrromethanes. *Organic Process Research & Development* **7,** 799–812 (2003).

74. Rausaria, S. *et al.* Retooling manganese(III) porphyrin-based peroxynitrite decomposition catalysts for selectivity and oral activity: A potential new strategy for treating chronic pain. *Journal of medicinal chemistry* **54,** 8658–8669 (2011).

75. Meyer-Eppler, G. *et al.* Synthesis, chiral resolution, and absolute configuration of dissymmetric 4,15-difunctionalized [2.2]paracyclophanes. *The Journal of Organic Chemistry* **79,** 6679–6687 (2014).

76. Kobuke, Y. & Miyaji, H. Supramolecular Organization of Imidazolyl-Porphyrin to a Slipped Cofacial Dimer. *Journal of the American Chemical Society* **116,** 4111–4112 (1994).

77. Yamaguchi, T., Kimura, T., Matsuda, H. & Aida, T. Macroscopic spinning chirality memorized in spin-coated films of spatially designed dendritic zinc porphyrin J-aggregates. *Angewandte Chemie (International ed. in English)* **43,** 6350–6355 (2004).

78. Wang, Z., Medforth, C. J. & Shelnutt, J. A. Porphyrin nanotubes by ionic self-assembly. *Journal of the American Chemical Society* **126,** 15954–15955 (2004).

79. Balaban, T. S., Goddard, R., Linke-Schaetzel, M. & Lehn, J.-M. 2-Aminopyrimidine directed self-assembly of zinc porphyrins containing bulky 3,5-di-tert-butylphenyl groups. *Journal of the American Chemical Society* **125,** 4233–4239 (2003).

80. Lecas-Nawrocka, A., BOITREL, B. & ROSE, E. Condensation of of 3,3'-Diethyl-4,4'-Dimethyl-2,2'-Dipyrrylmethane with Substituted Benzaldehydes. *Tetrahedron Letters* **33,** 481–484 (1992).

81. Lee, C.-H. & S. Lindsey, J. One-flask synthesis of meso-substituted dipyrromethanes and their application in the synthesis of trans-substituted porphyrin building. *Tetrahedron* **50,** 11427–11440 (1994).

82. Manka, J. S. & LAWRENCE, D. S. High yield synthesis of 5, 15-diarylporphyrins. *Tetrahedron Letters* **30,** 6989–6992 (1989).

83. E, W. *et al.* Control of the orbital delocalization and implications for molecular rectification in the radical anions of porphyrins with coplanar 90 degrees and 180 degrees beta,beta'-fused extensions. *The journal of physical chemistry. A* **112,** 556–570 (2008).

84. Golf, H. R. A., Reissig, H.-U. & Wiehe, A. Synthesis of SF5-Substituted Tetrapyrroles, Metalloporphyrins, BODIPYs, and Their Dipyrrane Precursors. *The Journal of organic chemistry* **80,** 5133–5143 (2015).

85. Novak, B. H. & Lash, T. D. Porphyrins with Exocyclic Rings. 11.1 Synthesis and Characterization of Phenanthroporphyrins, a New Class of Modified Porphyrin Chromophores. *The Journal of organic chemistry* **63,** 3998–4010 (1998).

86. Finikova, O. S., Cheprakov, A. V., Beletskaya, I. P., Carroll, P. J. & Vinogradov, S. A. Novel versatile synthesis of substituted tetrabenzoporphyrins. *The Journal of organic chemistry* **69,** 522–535 (2004).

87. Guralchuk, G. Y. *et al.* Anomalous Surfactant-Induced Enhancement of Luminescence Quantum Yield of Cyanine Dye J-Aggregates. *The Journal of Physical Chemistry C* **112,** 14762–14768 (2008).

88. Satake, A. & Kobuke, Y. Artificial photosynthetic systems: assemblies of slipped cofacial porphyrins and phthalocyanines showing strong electronic coupling. *Organic & biomolecular chemistry* **5,** 1679–1691 (2007).

89. Kobuke, Y. Porphyrin supramolecules by complementary coordination for units constructing photosynthetic systems. *Journal of Porphyrins and Phthalocyanines* **8,** 156–174 (2004).

90. Morisue, M. *et al.* Perfluorophenyl–Directed Giant Porphyrin J–Aggregates. *Chemistry–A European Journal* **30,** 7322–7329 (2019).

91. van Esch, J. H., Feiters, M. C., Peters, A. M. & Nolte, R. J. M. UV-Vis, Fluorescence, and EPR Studies of Porphyrins in Bilayers of Dioctadecyldimethylammonium Surfactants. *The Journal of Physical Chemistry* **98,** 5541–5551 (1994).

92. Villari, V., Mineo, P., Scamporrino, E. & Micali, N. Role of the hydrogen-bond in porphyrin J-aggregates. *RSC Advances* **2,** 12989 (2012).

93. Monteiro, C. J., Pereira, M. M., Vicente, M. G. H. & Arnaut, L. G. Photophysical properties of unsymmetric meso-substituted porphyrins synthesized via the Suzuki coupling reaction. *Tetrahedron* **68,** 8783–8788 (2012).

94. Bonnett, R. *et al.* Photophysical properties of meso–tetraphenylporphyrin and some meso–tetra (hydroxyphenyl) porphyrins. *Photochemistry and Photobiology* **48,** 271–276 (1988).

95. Fonda, H. N. *et al.* Spectroscopic, photophysical, and redox properties of some meso-substituted free-base porphyrins. *The Journal of Physical Chemistry* **97,** 7024–7033 (1993).

96. Şen, P. *et al.* Photophysical properties and study of the singlet oxygen generation of tetraphenylporphyrinato palladium(II) complexes. *Journal of Porphyrins and Phthalocyanines* **17,** 964–971 (2013).

97. Volostnykh, M. V. *et al.* Platinum(ii) and palladium(ii) complexes with electron-deficient meso-diethoxyphosphorylporphyrins: synthesis, structure and tuning of photophysical properties by varying peripheral substituents. *Dalton transactions (Cambridge, England : 2003)* **48,** 8882–8898 (2019).

98. Esipova, T. V., Rivera-Jacquez, H. J., Weber, B., Masunov, A. E. & Vinogradov, S. A. Two-Photon Absorbing Phosphorescent Metalloporphyrins: Effects of π-Extension and Peripheral Substitution. *Journal of the American Chemical Society* **138,** 15648–15662 (2016).

99. Pasternack, R. F., Schaefer, K. F. & Hambright, P. Resonance light-scattering studies of porphyrin diacid aggregates. *Inorganic chemistry* **33,** 2062–2065 (1994).

100. Pasternack, R. F., Bustamante, C., Collings, P. J., Giannetto, A. & Gibbs, E. J. Porphyrin assemblies on DNA as studied by a resonance light-scattering technique. *Journal of the American Chemical Society* **115,** 5393–5399 (1993).

101. Pasternack, R. F. & Collings, P. J. Resonance light scattering: a new technique for studying chromophore aggregation. *Science* **269,** 935–939 (1995).

8 List of Figures

9 List of Tables

10 Appendix

10.1 Abbreviations

Table 10.1: List of abbreviations

Abbreviations	Explanation
AcOH	Acetic acid
Ar	Argon
CAS	Chemical Abstracts Service
CH	Cyclohexane
DCM	Dichloromethane
DDQ	2,3-dichloro-5,6-dicyano-1,4-benzoquinone
DMF	Dimethylformamide
DMSO	Dimethyl sulfoxide
EE	Ethyl acetate
eq.	Equivalent
HRMS	High Resolution Mass Spectrometry
KOtBu	Potassium tert-butoxide
MALDI	Matrix-assisted laser disorption/ionization
MeOH	Methanol
NBS	N-Bromosuccinimide
$Pd(dppf)Cl_2$	[1,1′-Bis(diphenylphosphino)ferrocene]dichloropalladium(II)
$PdCl_2(Amphos)_2$	Bis[di-tert-butyl(4-dimethylaminophenyl)phosphine]dichloropalladium(II)
RLS	Resonant Light Scattering
RT	Room temperature
TFA	Trifluoroacetic acid
THF	Tetrahydrofuran
TLC	Thin layer chromatography
TOF	Time-of-Flight
Tol	Toluene
UV	Ultraviolet
Vis	Visible

10.2 NMR Data

Compound 1b

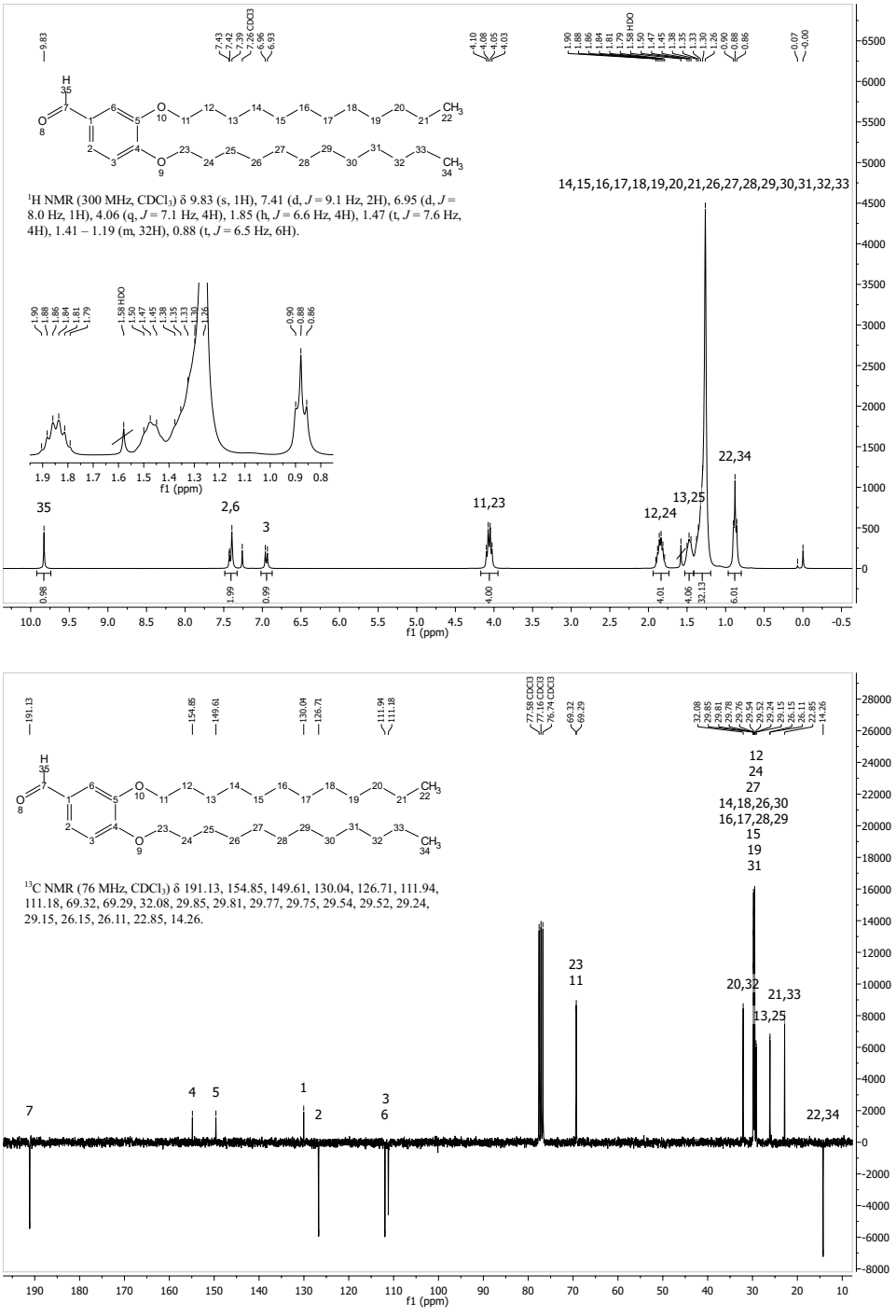

Figure 10.1: ^{1}H-NMR and ^{13}C-APT-NMR spectra of compound **1b**

Compound 2

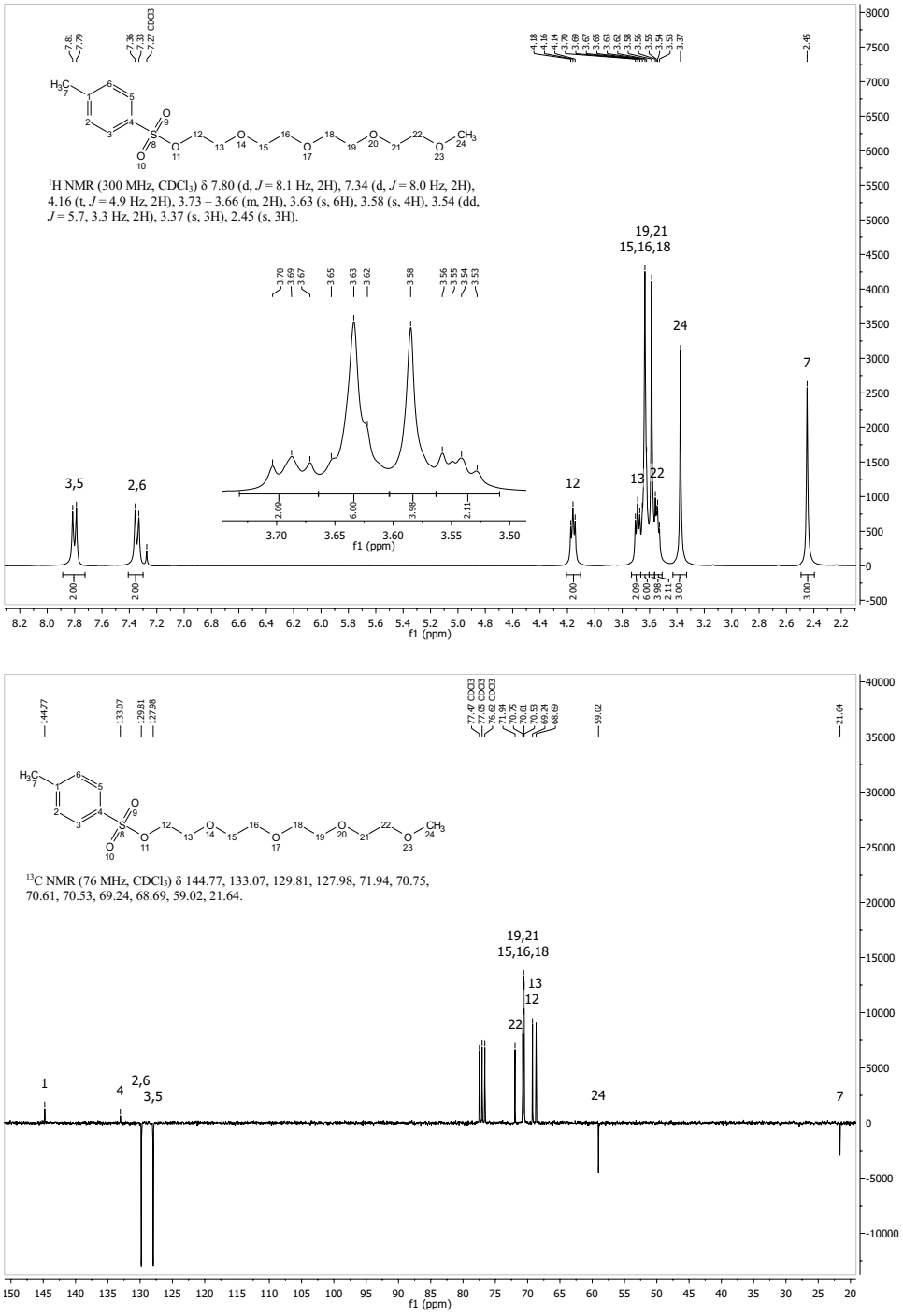

Figure 10.2: ^{1}H-NMR and ^{13}C-APT-NMR spectra of compound **2**

Compound 3a

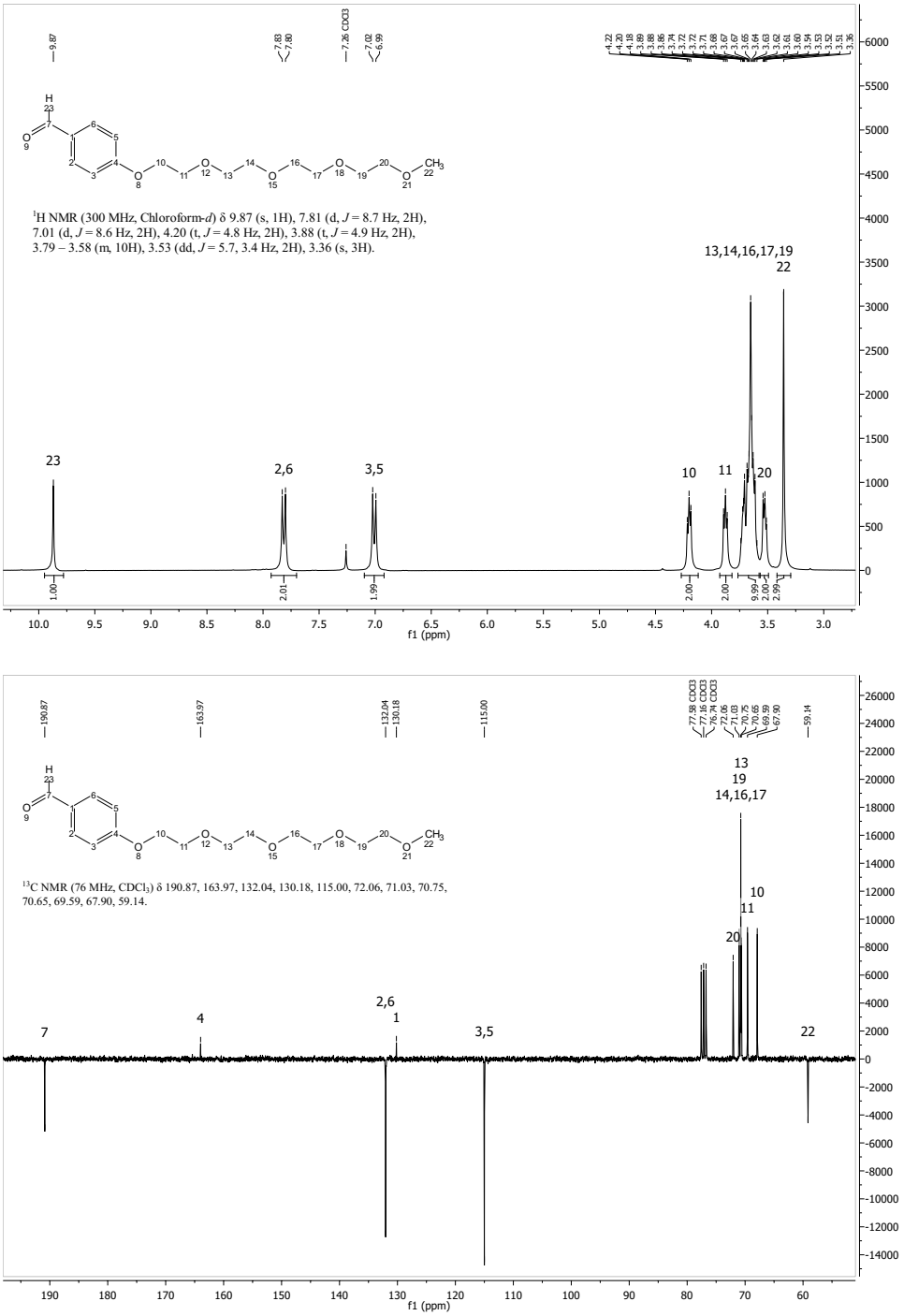

Figure 10.3: ^{1}H-NMR and ^{13}C-APT-NMR spectra of compound **3a**

Compound 3b

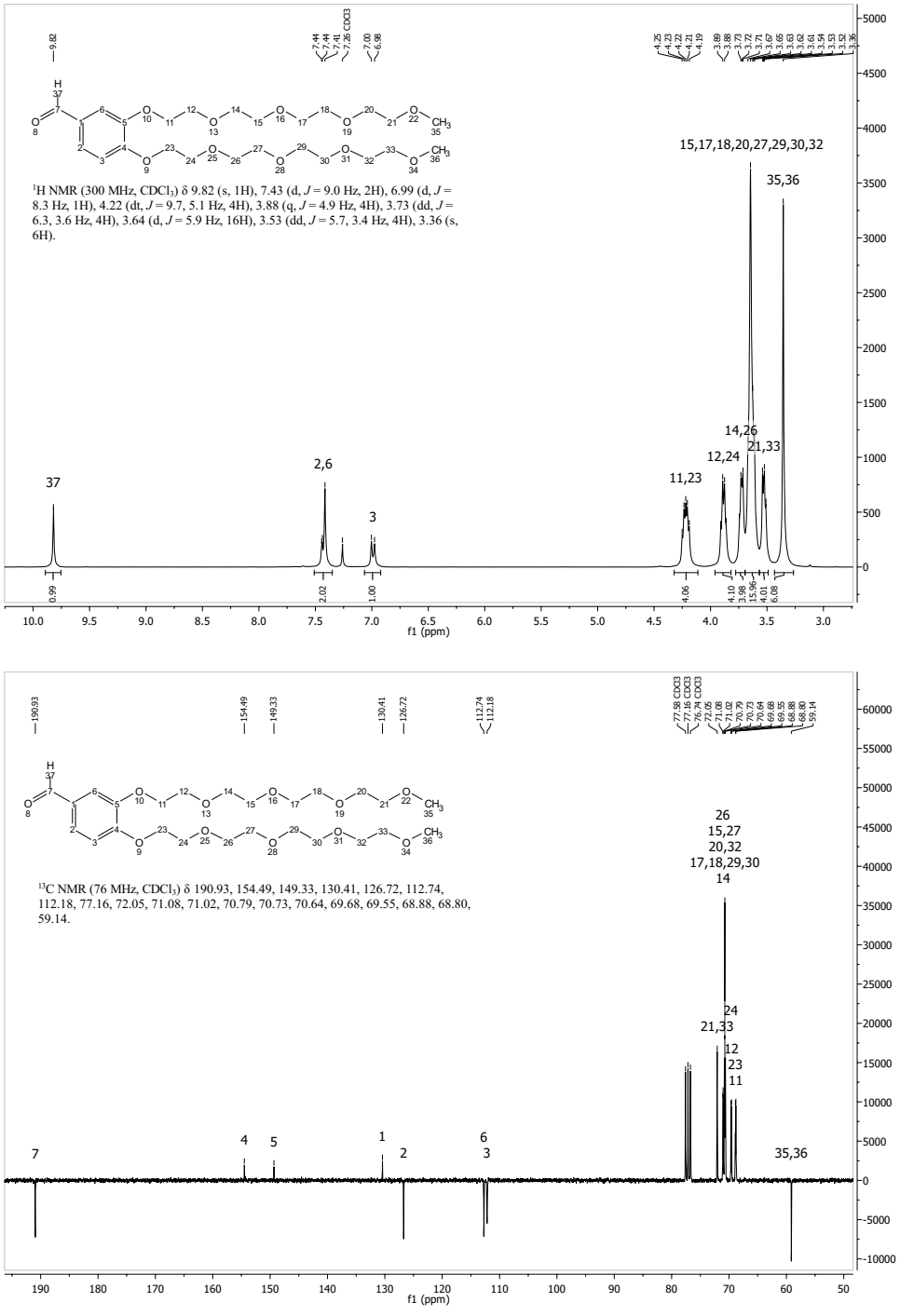

Figure 10.4: ^{1}H-NMR and ^{13}C-APT-NMR spectra of compound **3b**

Compound 4

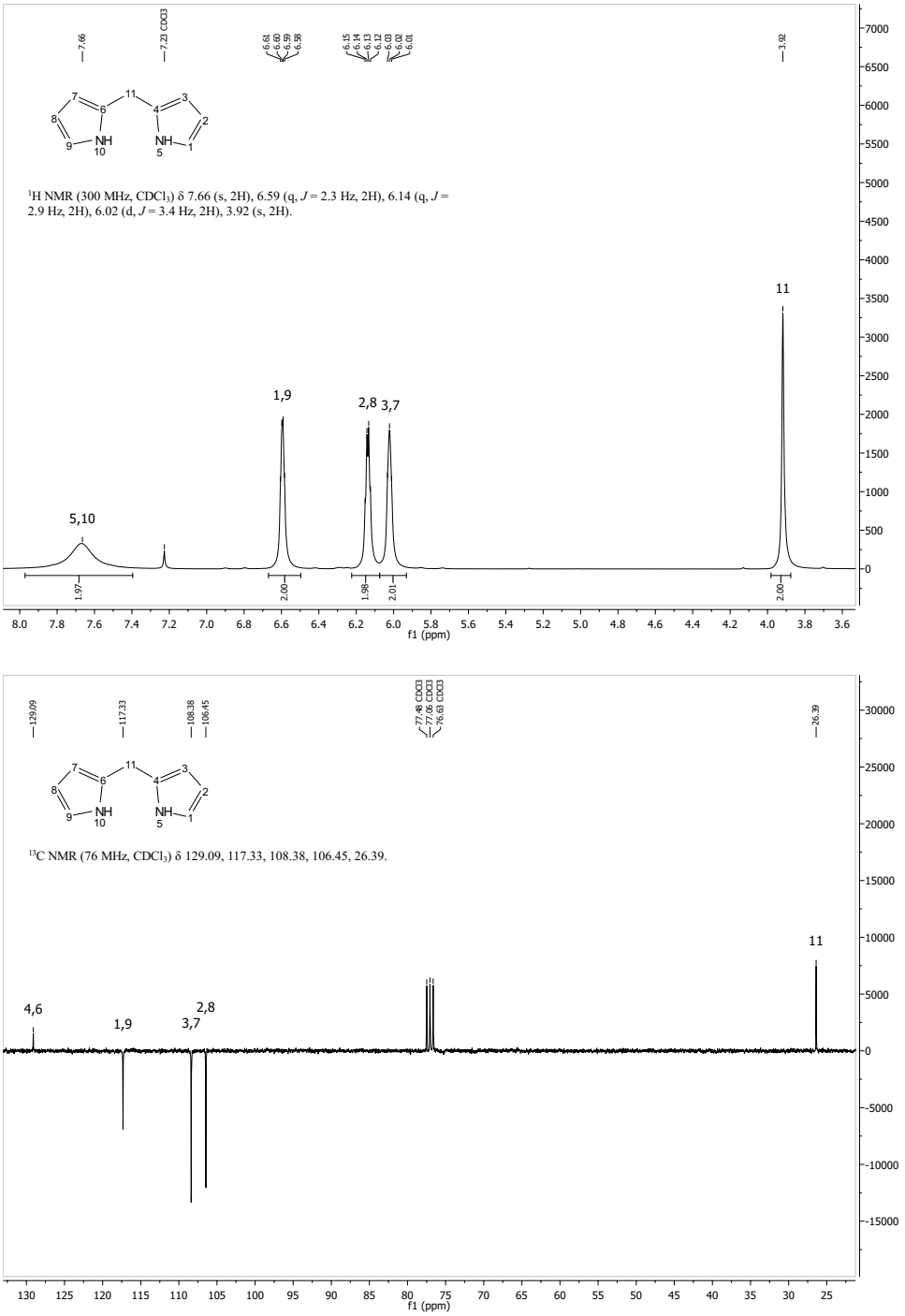

Figure 10.5: ^{1}H-NMR and ^{13}C-APT-NMR spectra of compound **4**

Compound 5a

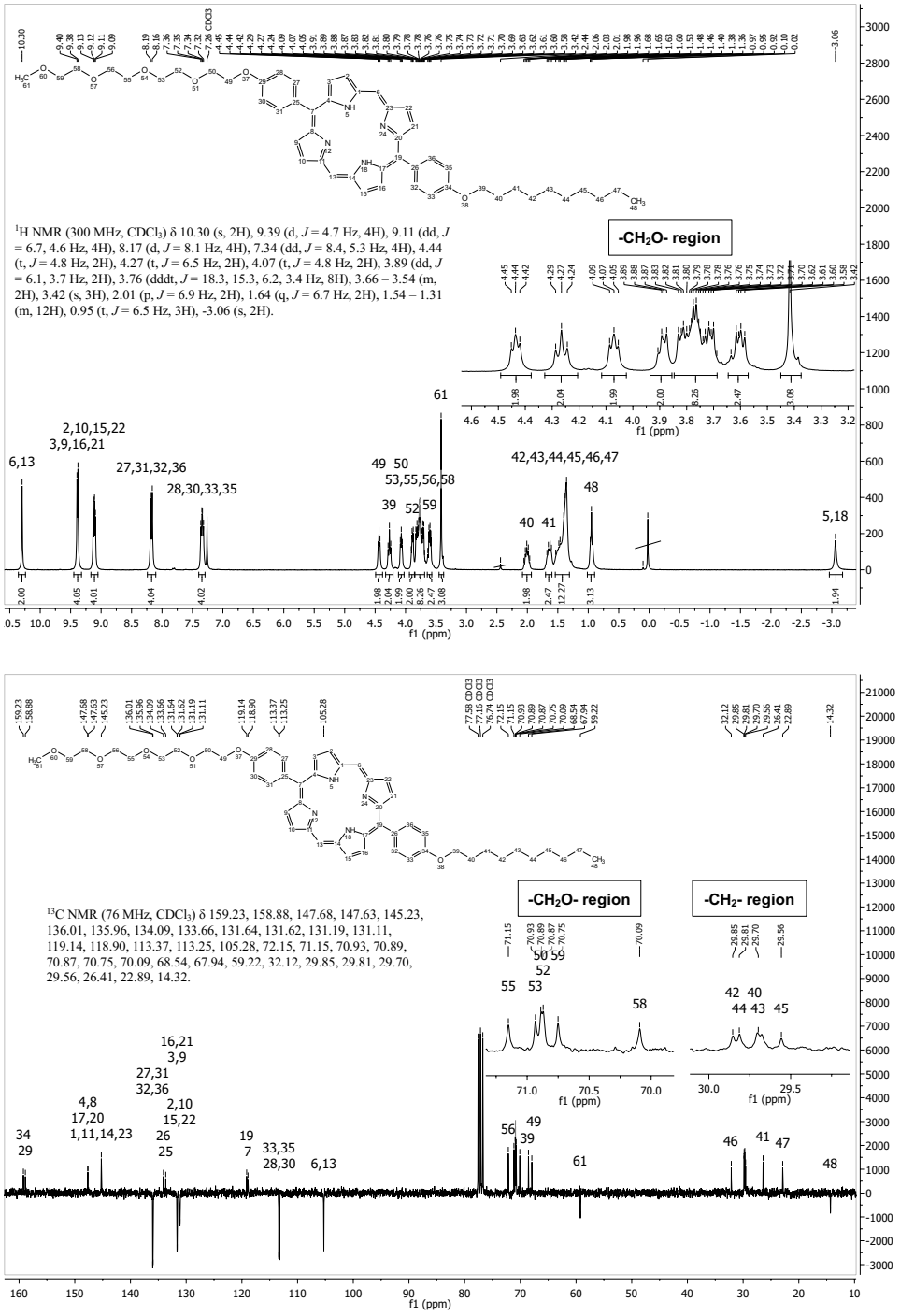

Figure 10.6: ^{1}H-NMR and ^{13}C-APT-NMR spectra of compound **5a**

Compound 5b

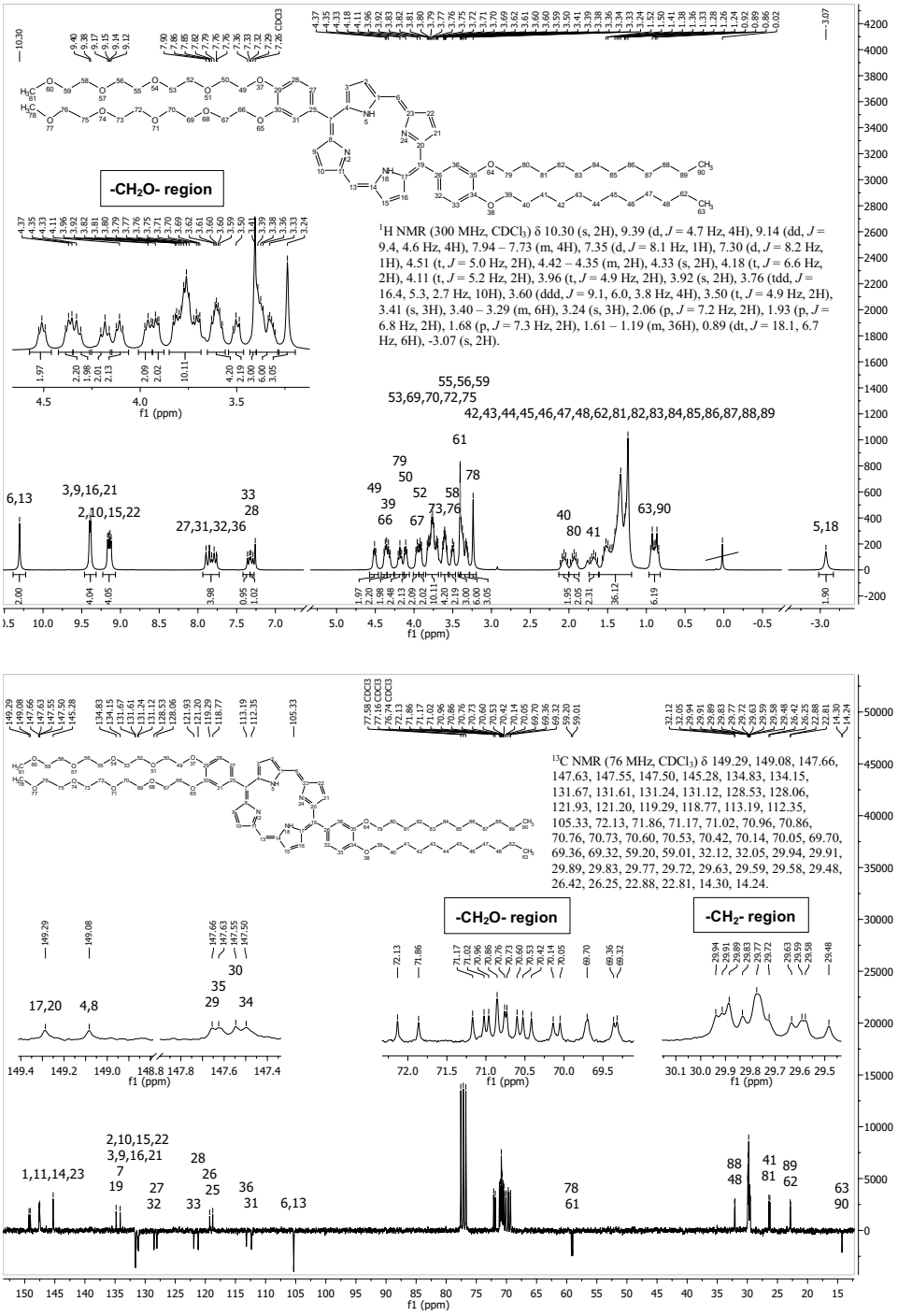

Figure 10.7: ^{1}H-NMR and ^{13}C-APT-NMR spectra of compound **5b**

Compound 5c

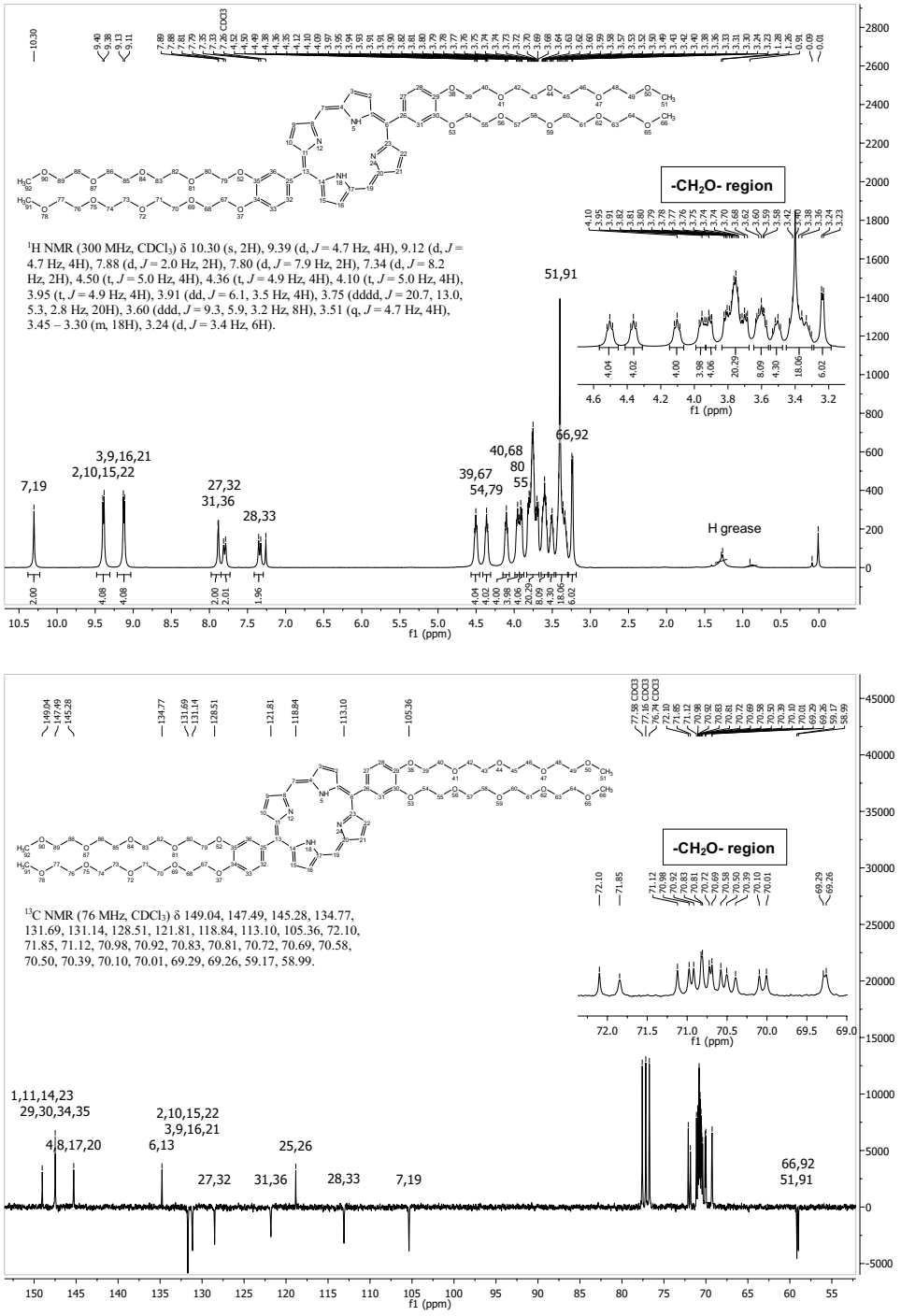

Figure 10.8: ^{1}H-NMR and ^{13}C-APT-NMR spectra of compound **5c**

Compound 6a

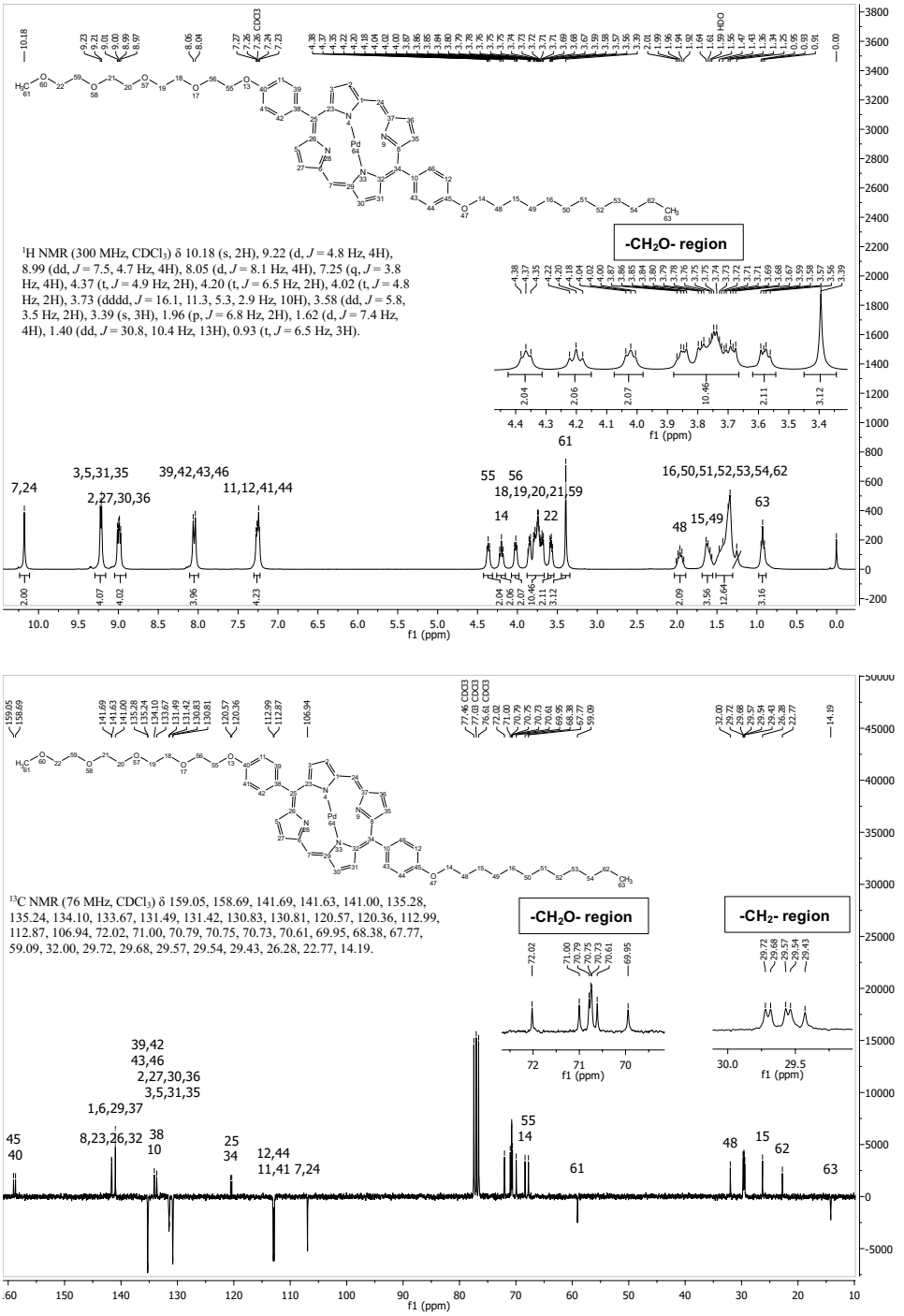

Figure 10.9: ^{1}H-NMR and ^{13}C-APT-NMR spectra of compound **6a**

Compound 6b

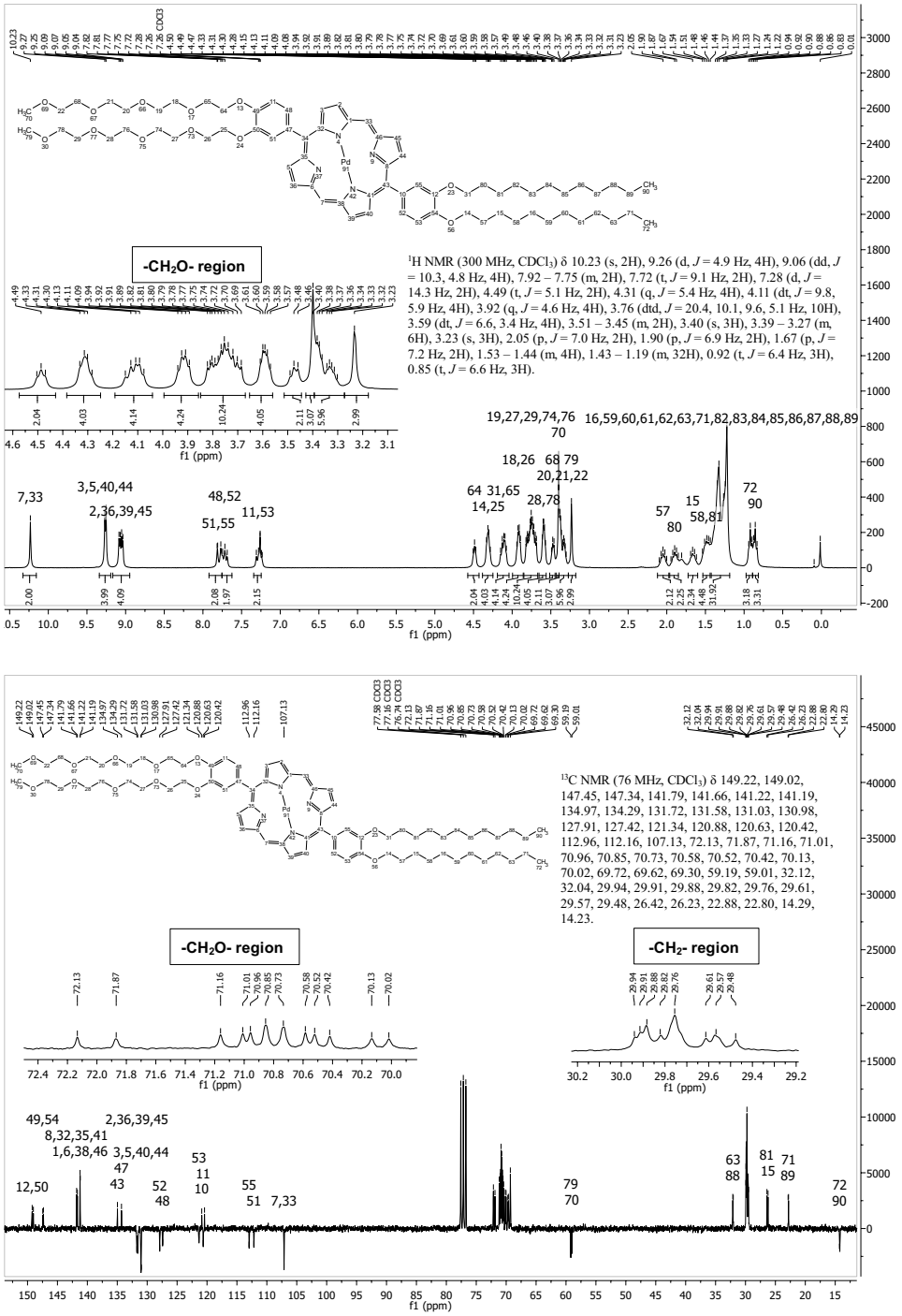

Figure 10.10: ^{1}H-NMR and ^{13}C-APT-NMR spectra of compound **6b**

Compound 6c

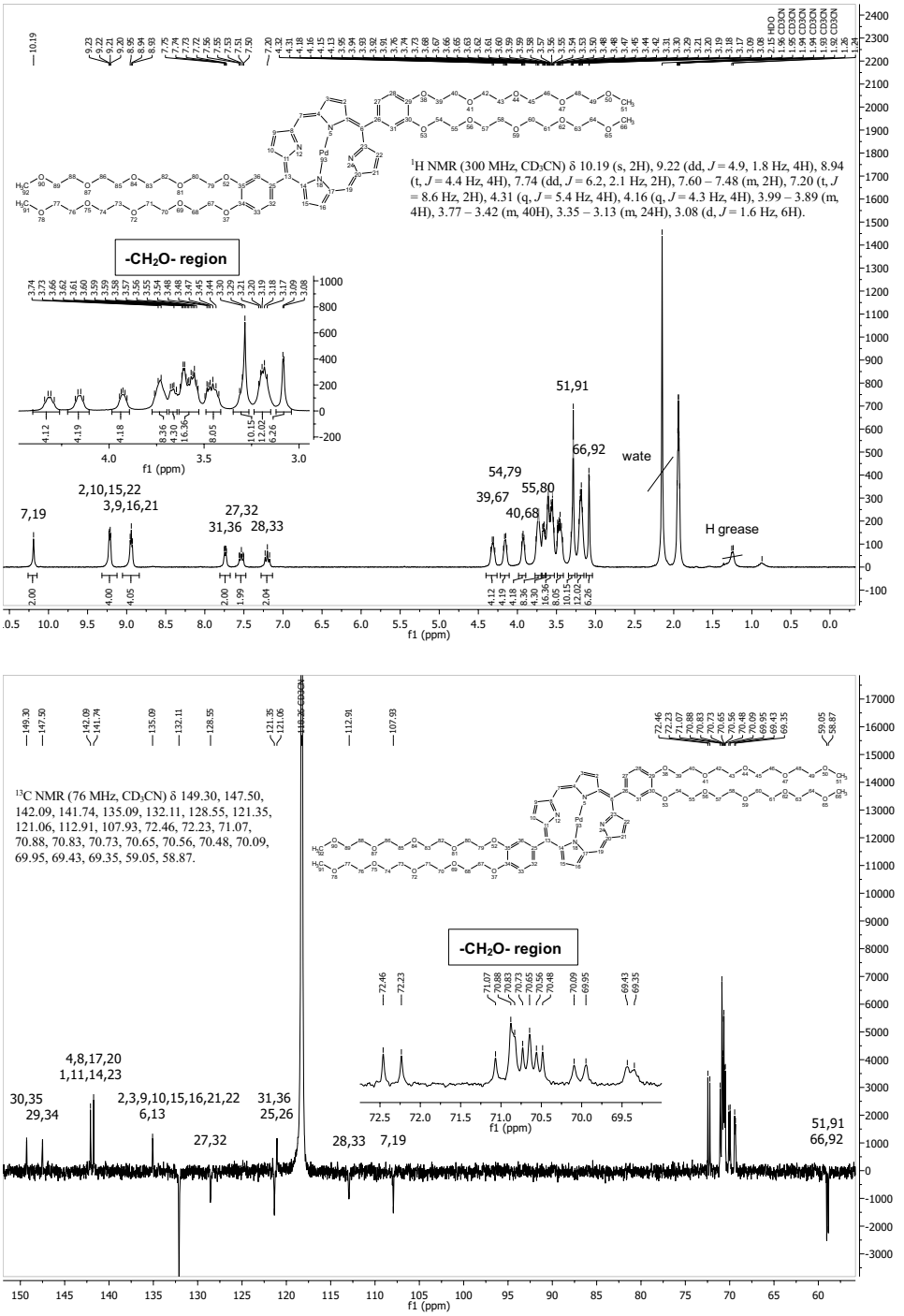

Figure 10.11: ^{1}H-NMR and ^{13}C-APT-NMR spectra of compound **6c**

Compound 7

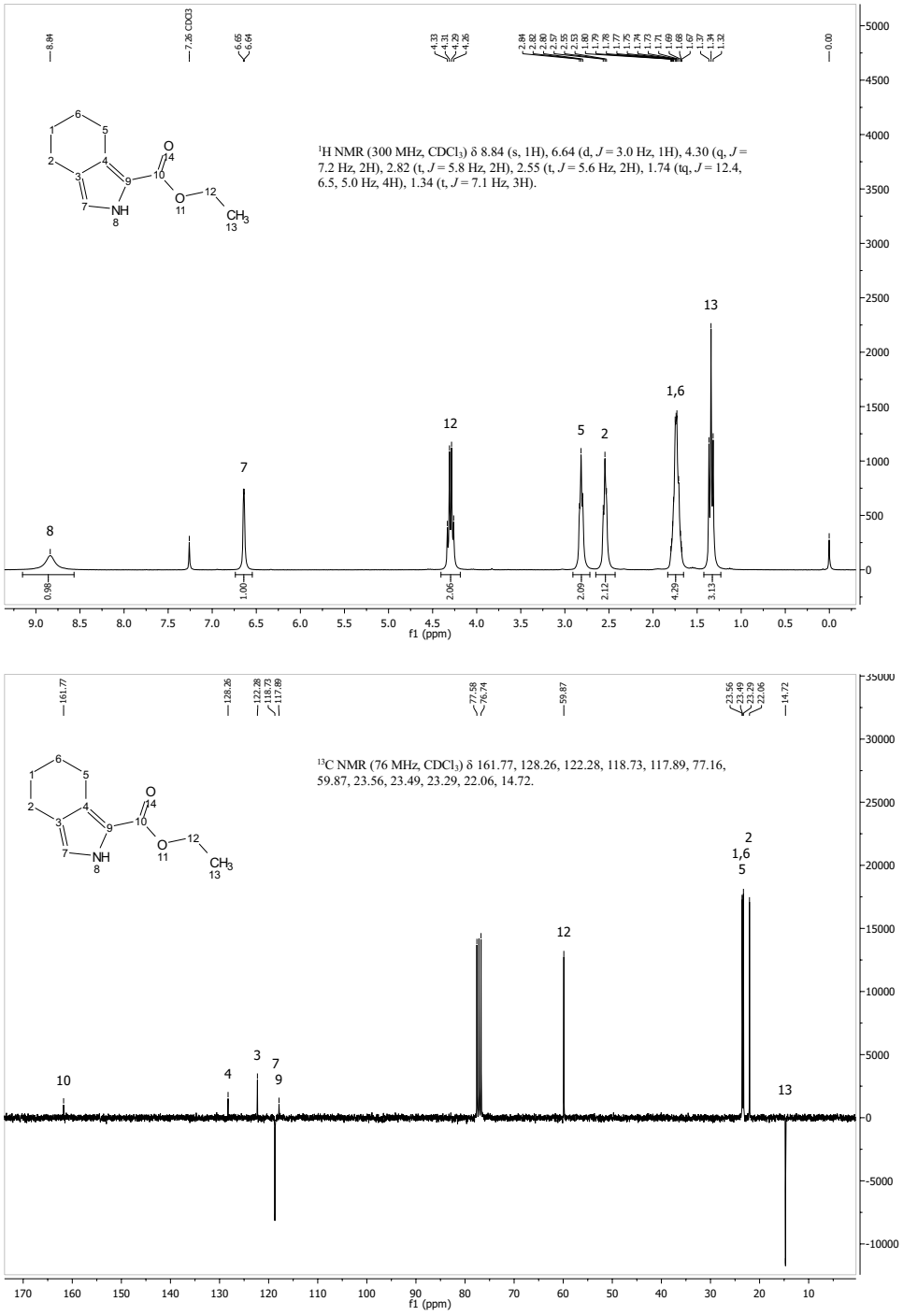

Figure 10.12: ^{1}H-NMR and ^{13}C-APT-NMR spectra of compound **7**

Compound 8

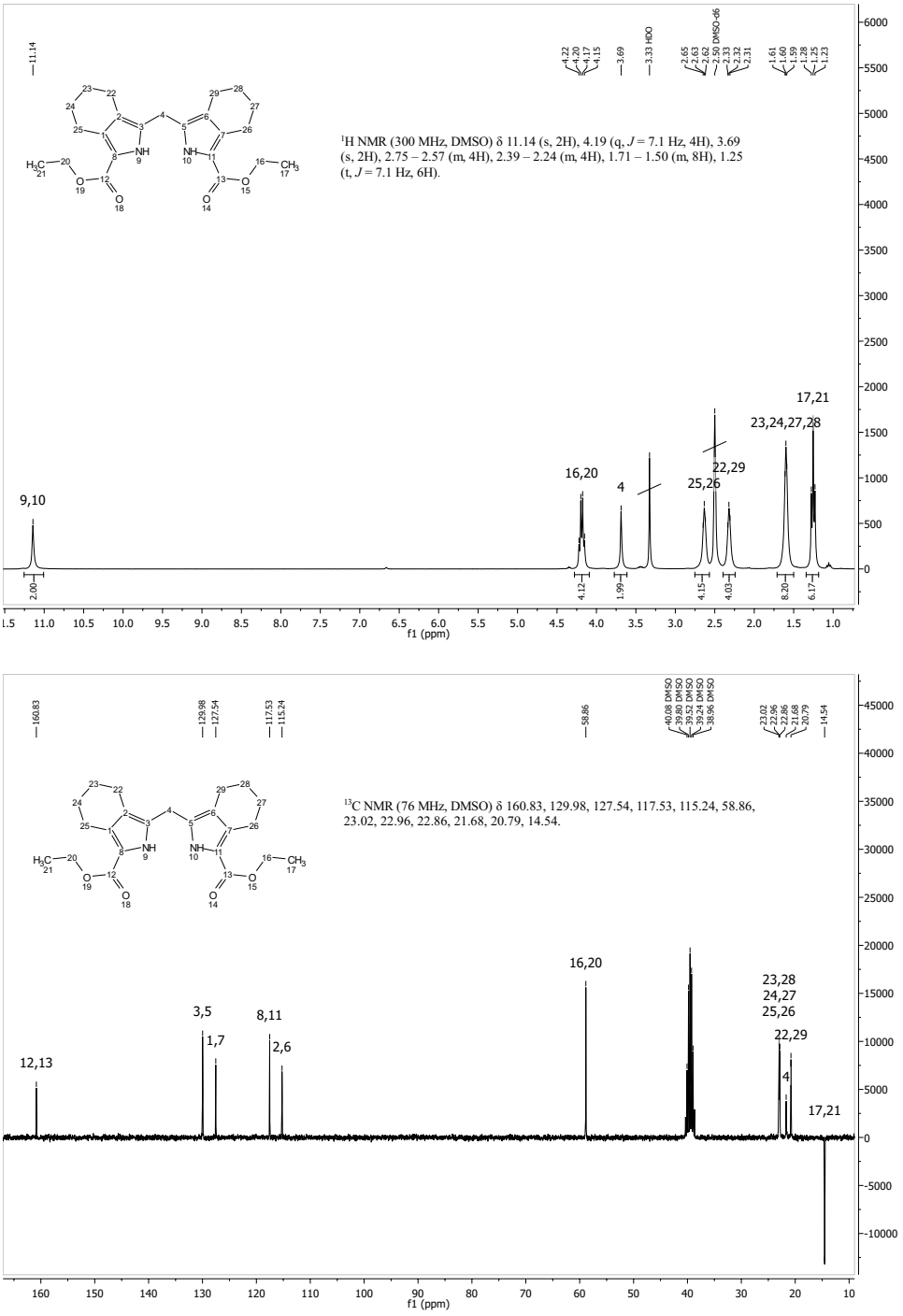

Figure 10.13: ^{1}H-NMR and ^{13}C-APT-NMR spectra of compound **8**

Compound 10

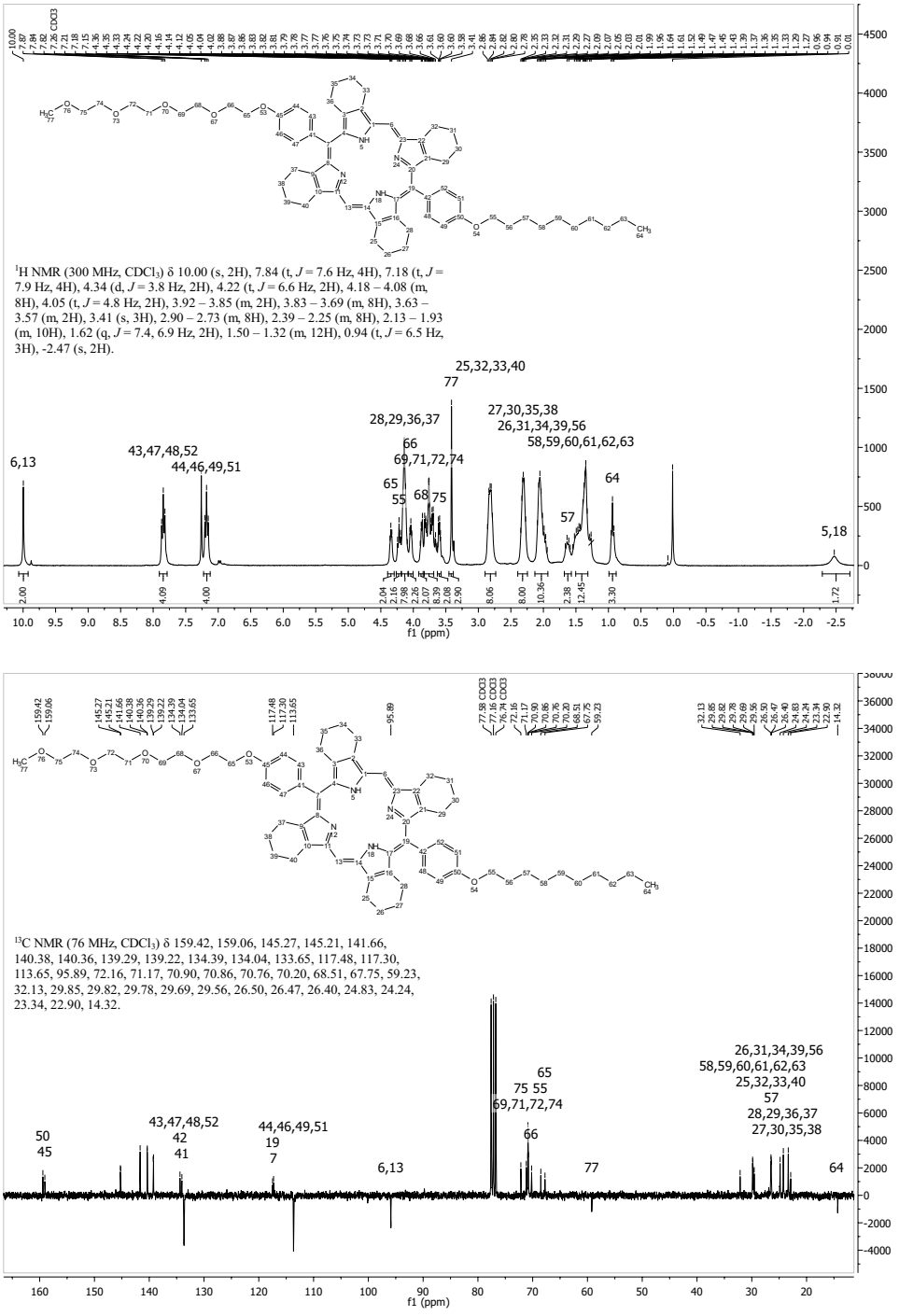

Figure 10.14: ^{1}H-NMR and ^{13}C-APT-NMR spectra of compound **10**

Compound 11

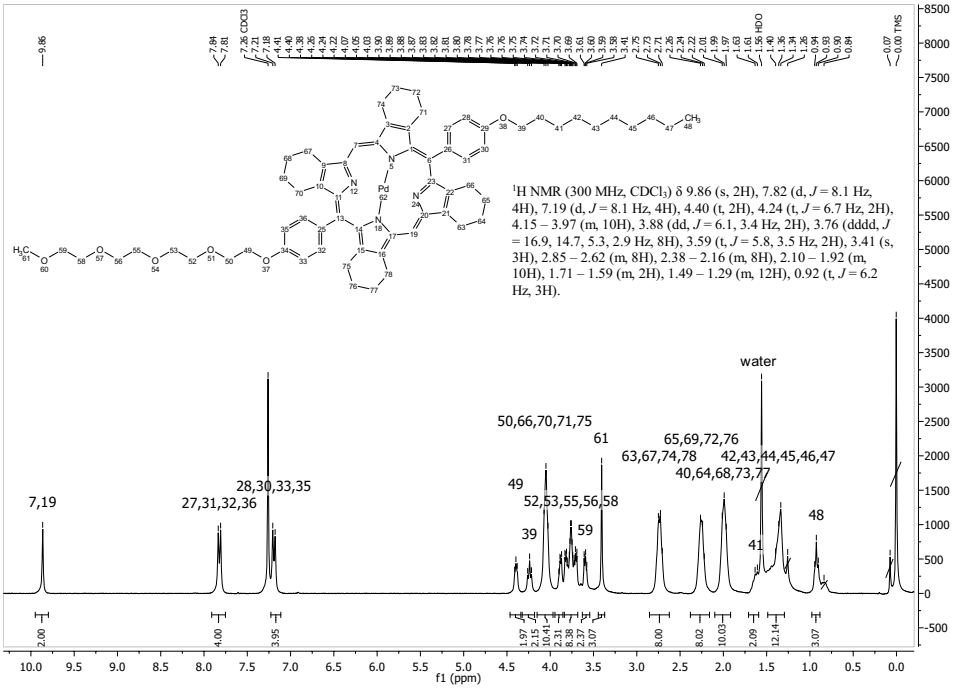

Figure 10.15: ^{1}H-NMR spectra of compound **11**

Compound 13

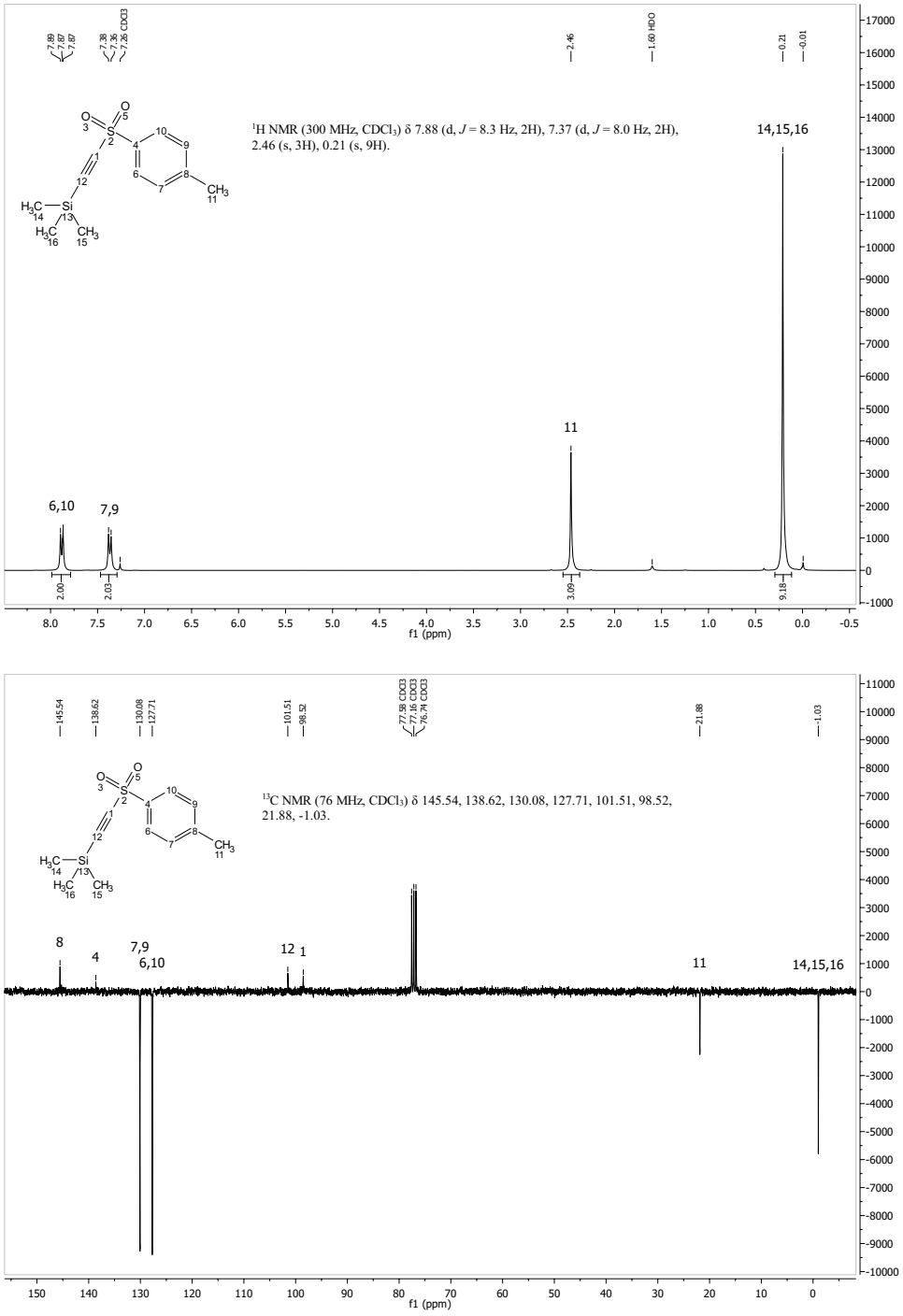

Figure 10.16: ^{1}H-NMR and ^{13}C-APT-NMR spectra of compound **13**

Compound 14

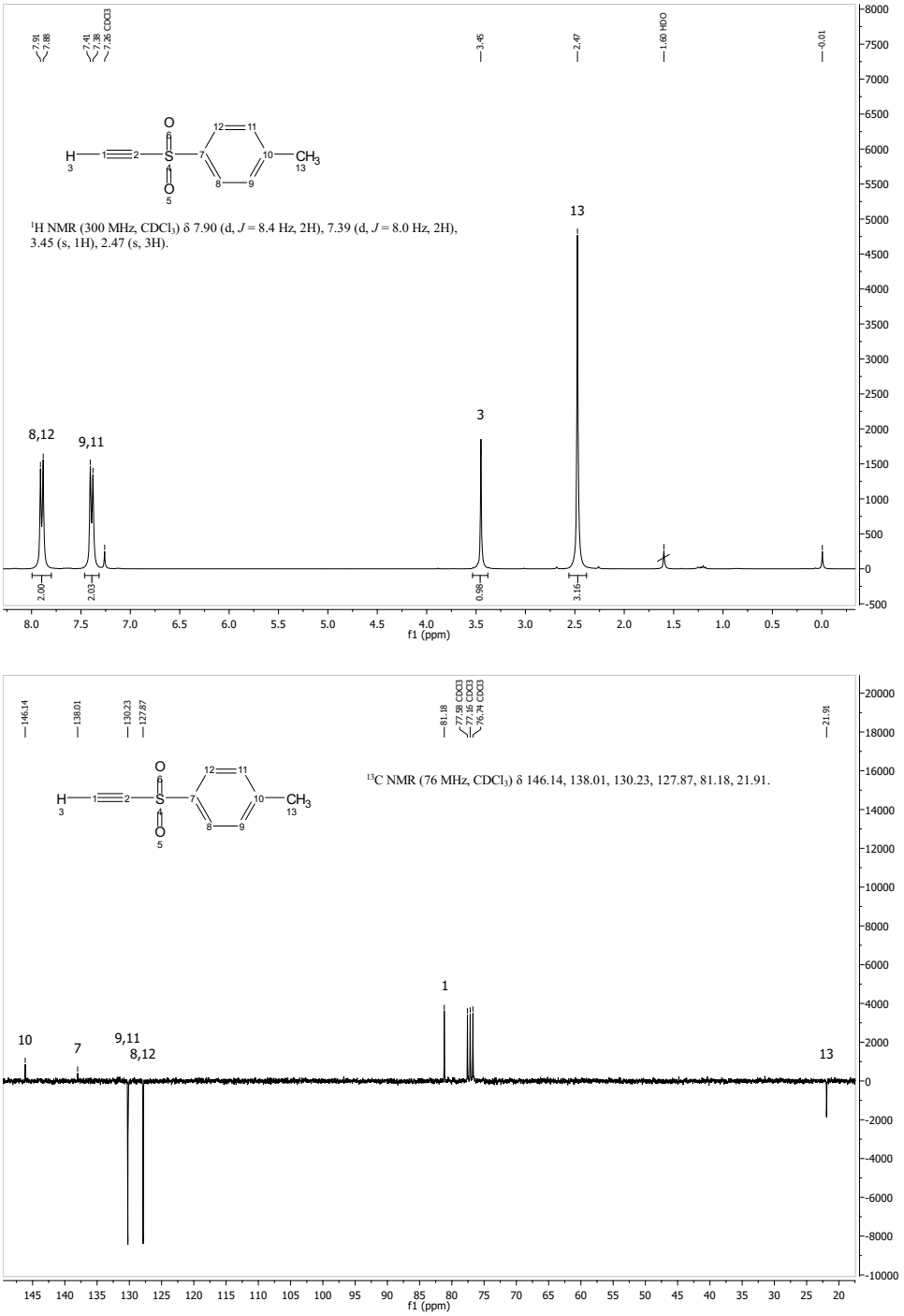

Figure 10.17: ^{1}H-NMR and ^{13}C-APT-NMR spectra of compound **14**

Compound 15

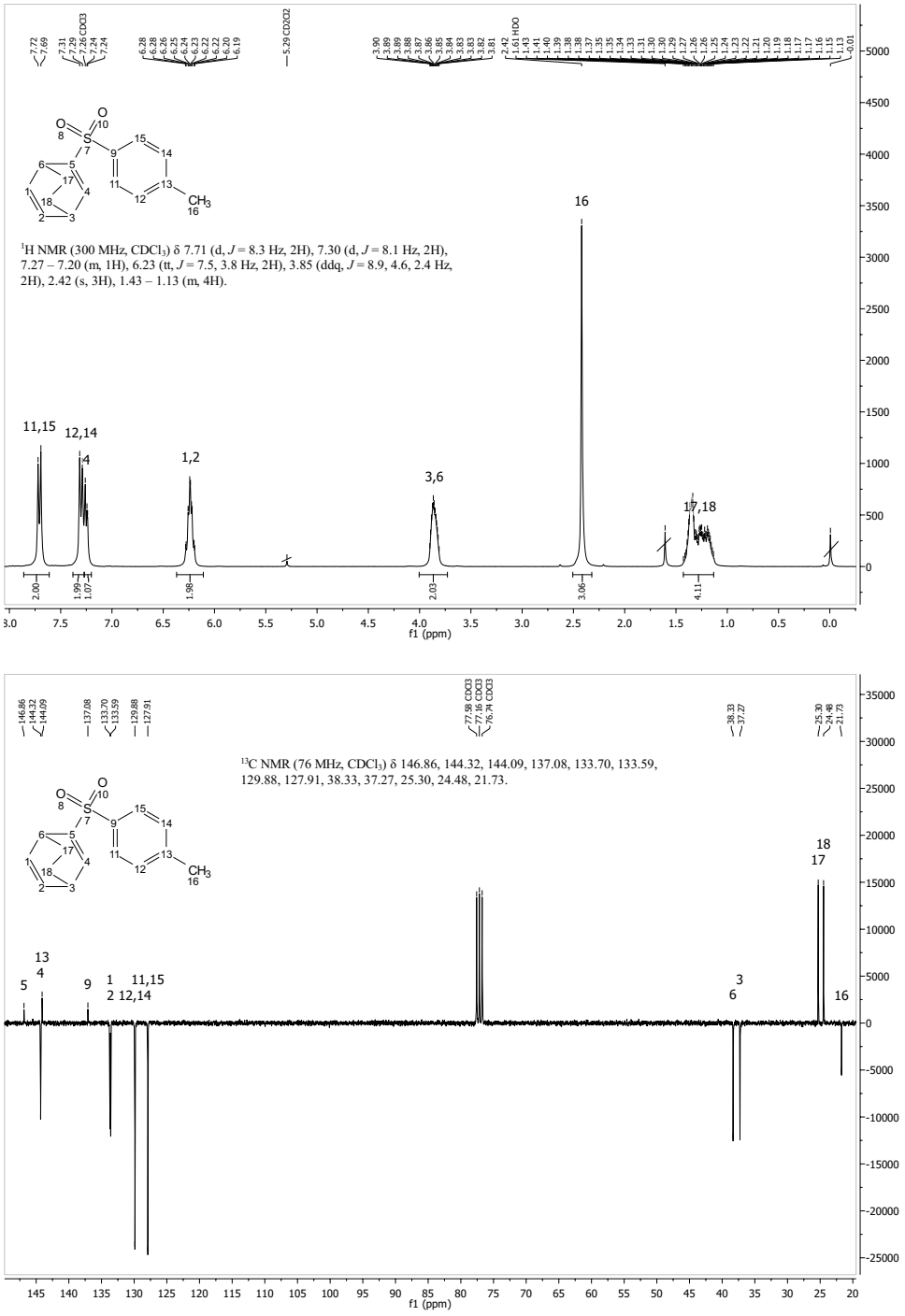

Figure 10.18: ^{1}H-NMR and ^{13}C-APT-NMR spectra of compound **15**

Compound 16

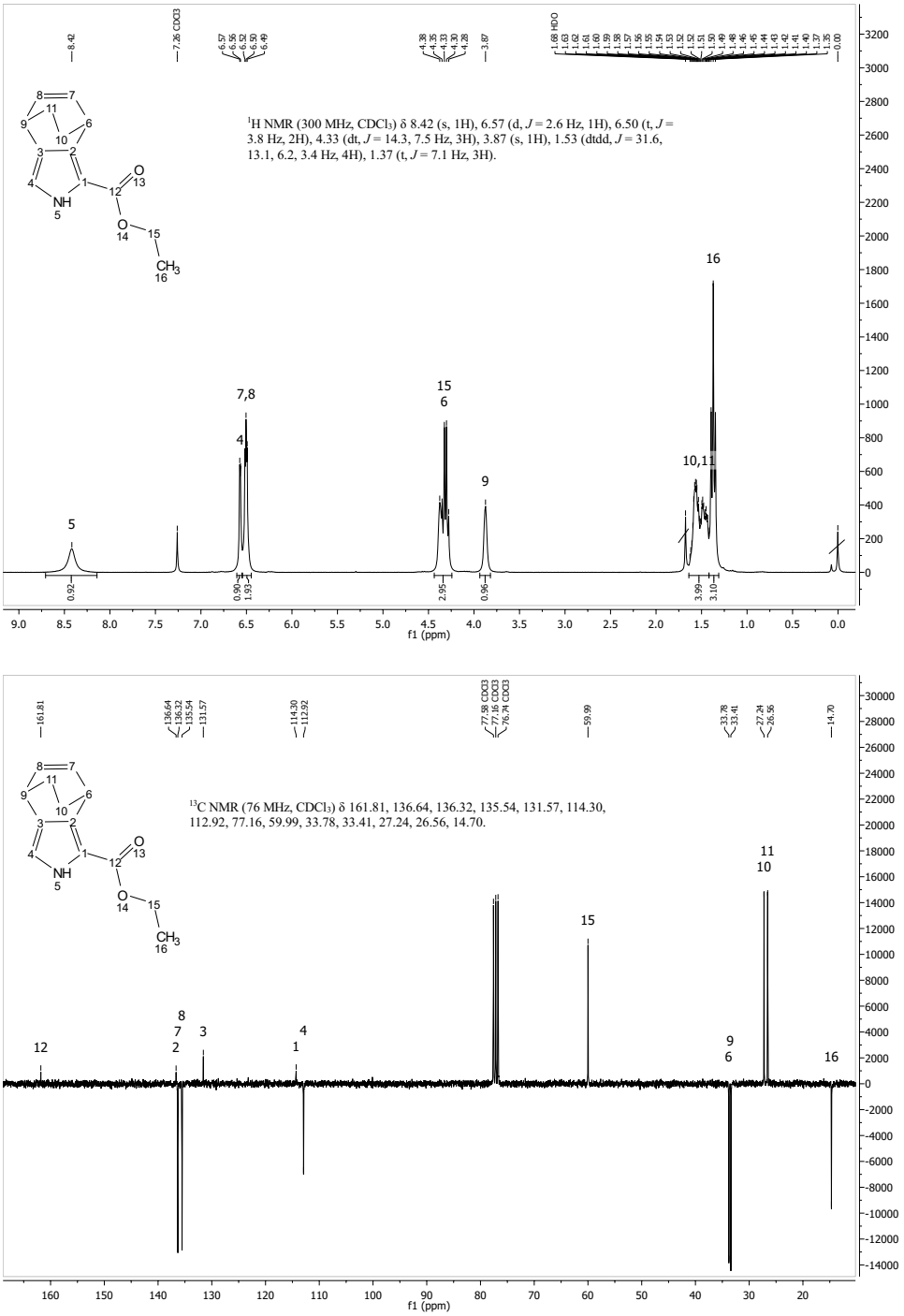

Figure 10.19: ^{1}H-NMR and ^{13}C-APT-NMR spectra of compound **16**

Compound 17

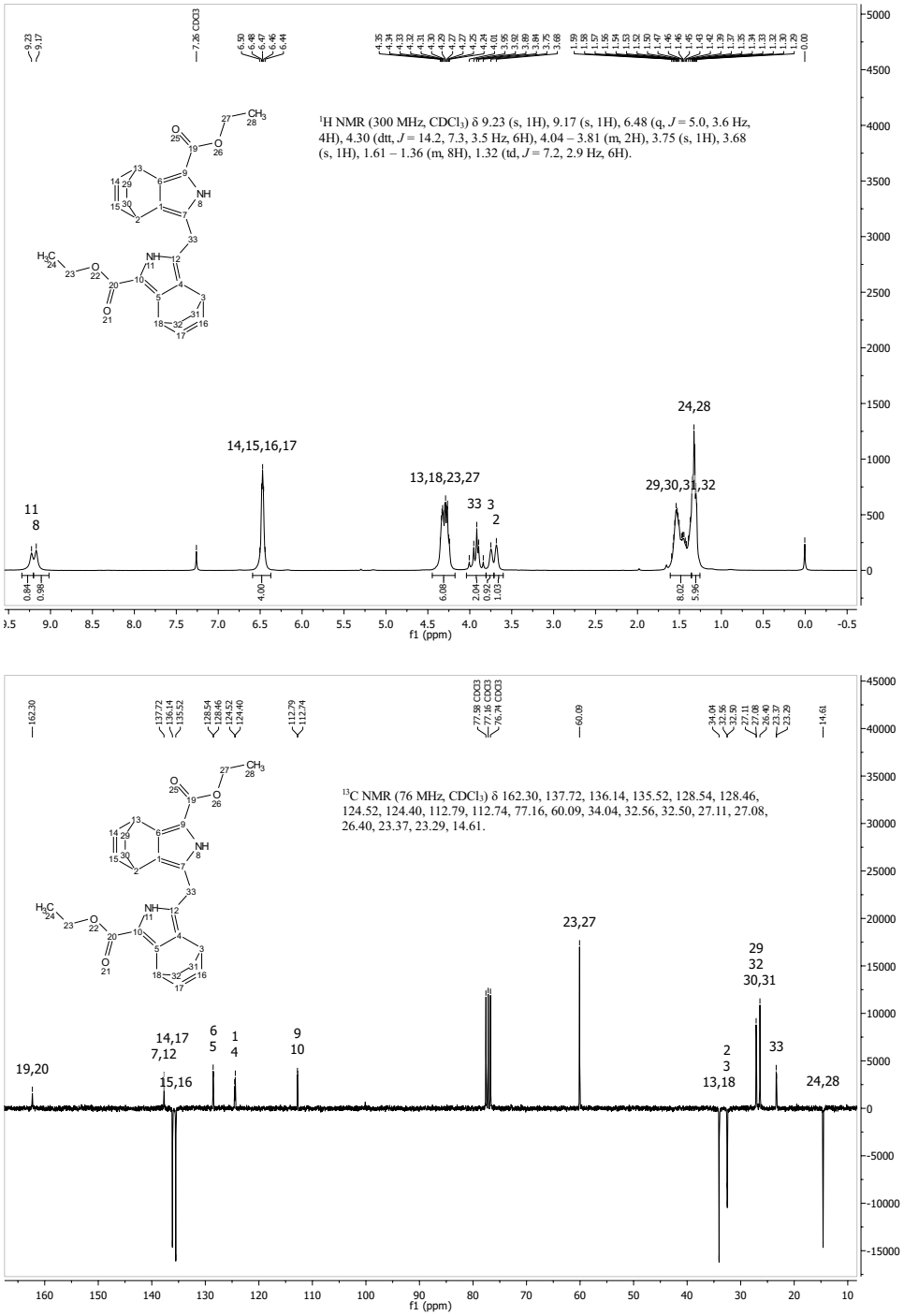

Figure 10.20: ^{1}H-NMR and ^{13}C-APT-NMR spectra of compound **17**

Compound 21

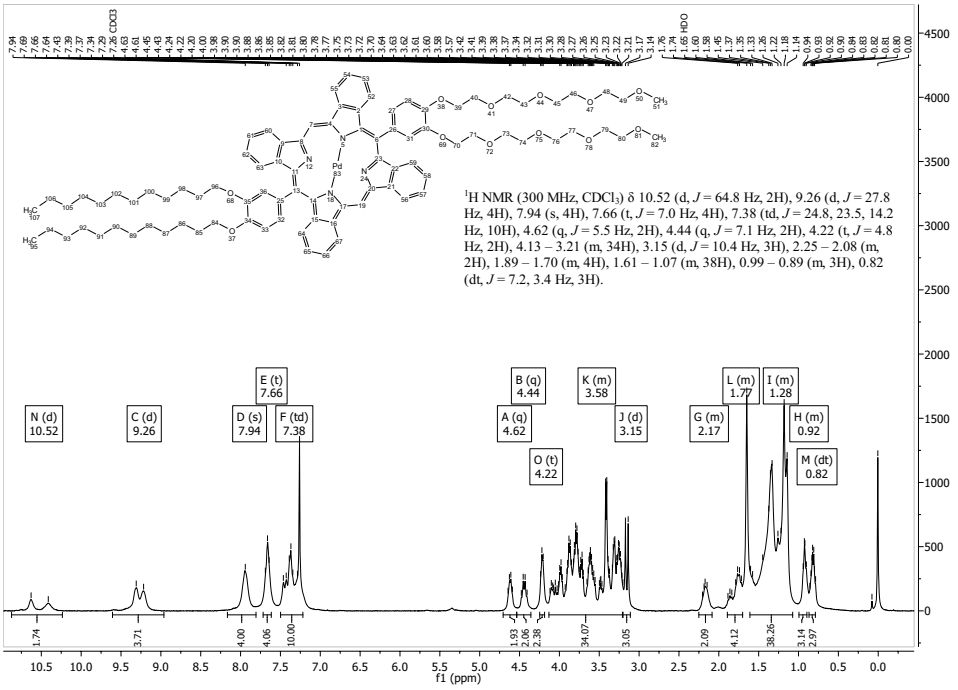

Figure 10.21: ^{1}H-NMR spectra of compound **30**

Compound 22

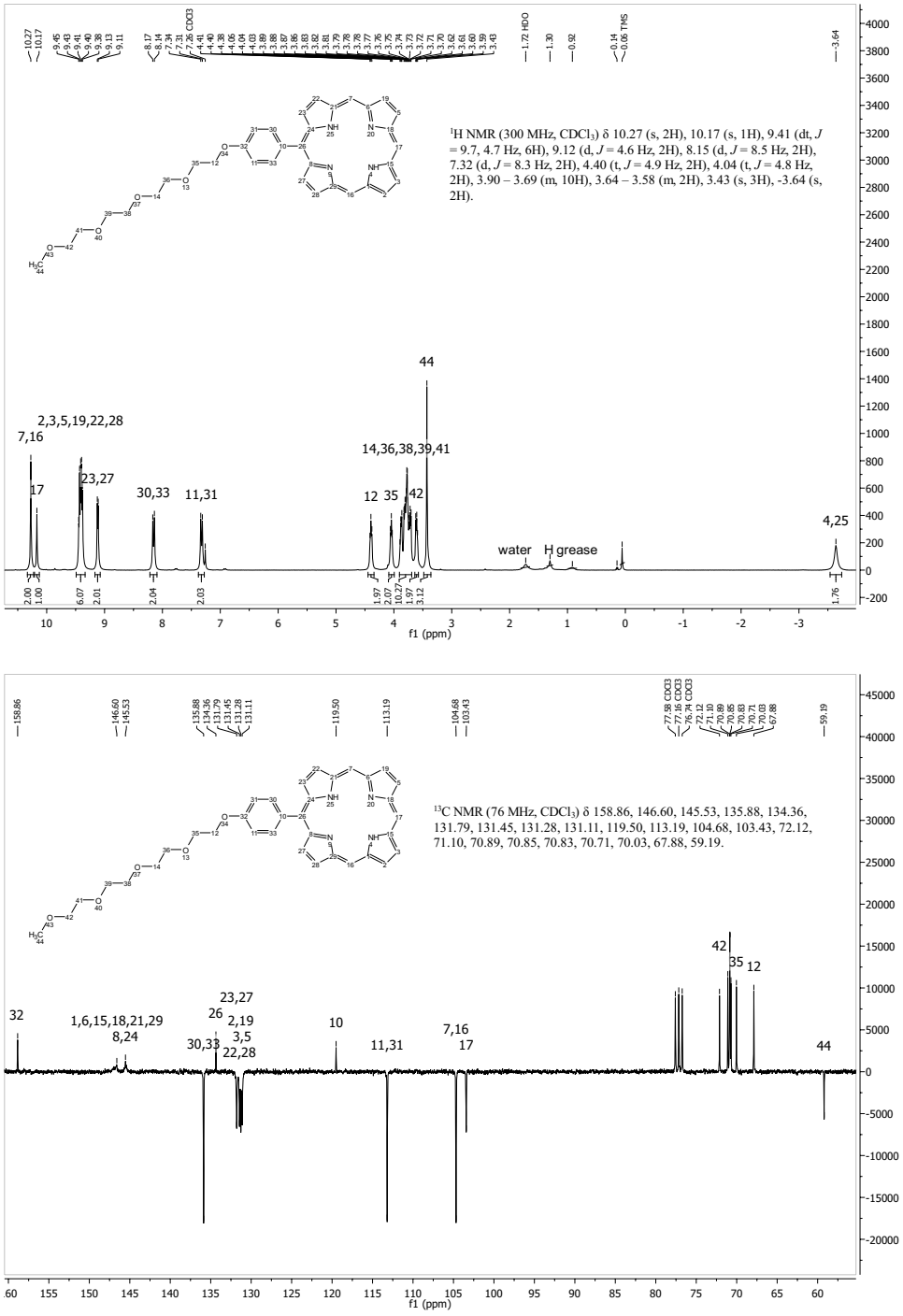

Figure 10.22: ^{1}H-NMR and ^{13}C-APT-NMR spectra of compound **22**

Compound 23

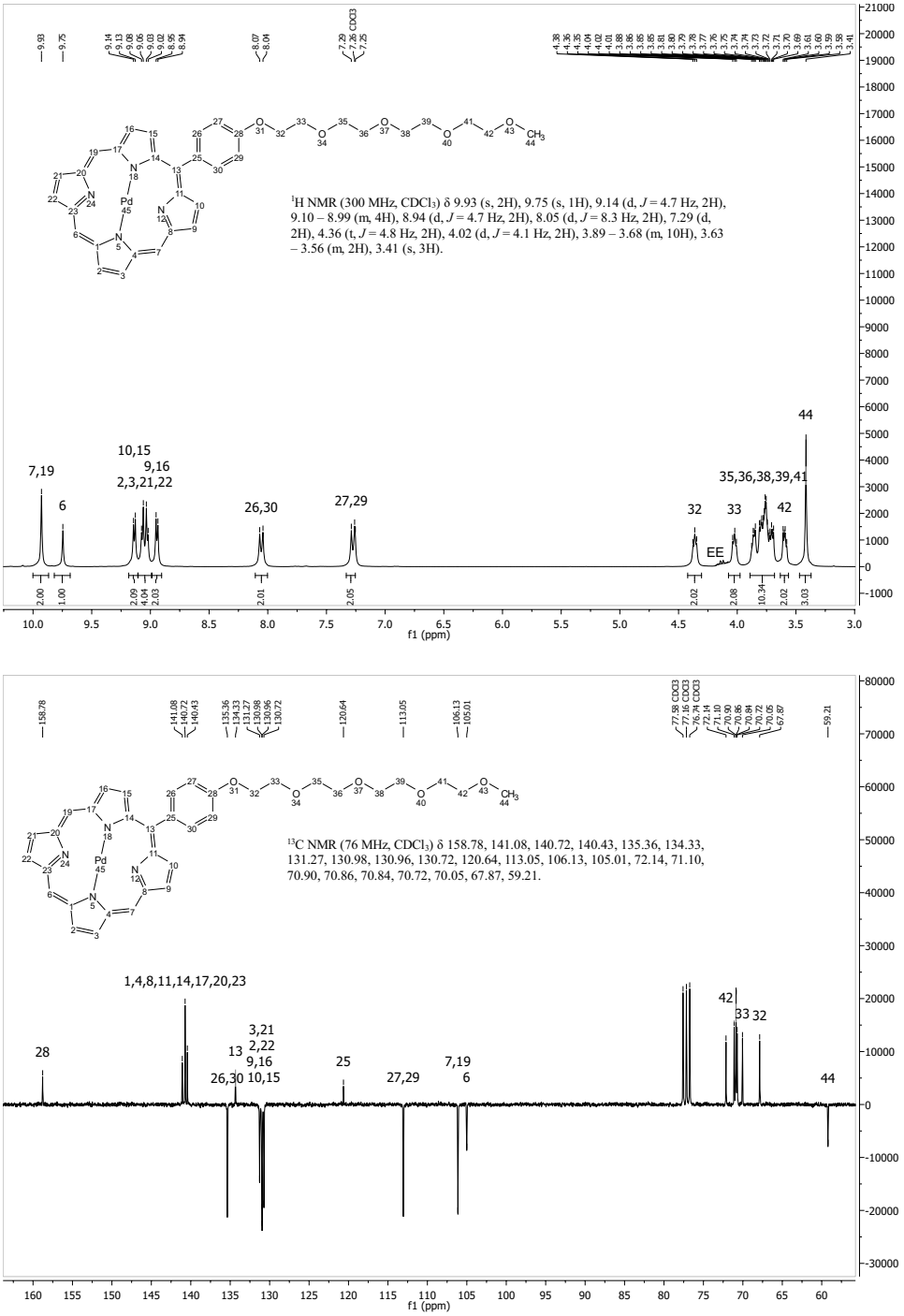

Figure 10.23: ^{1}H-NMR and ^{13}C-APT-NMR spectra of compound **23**

Compound 24

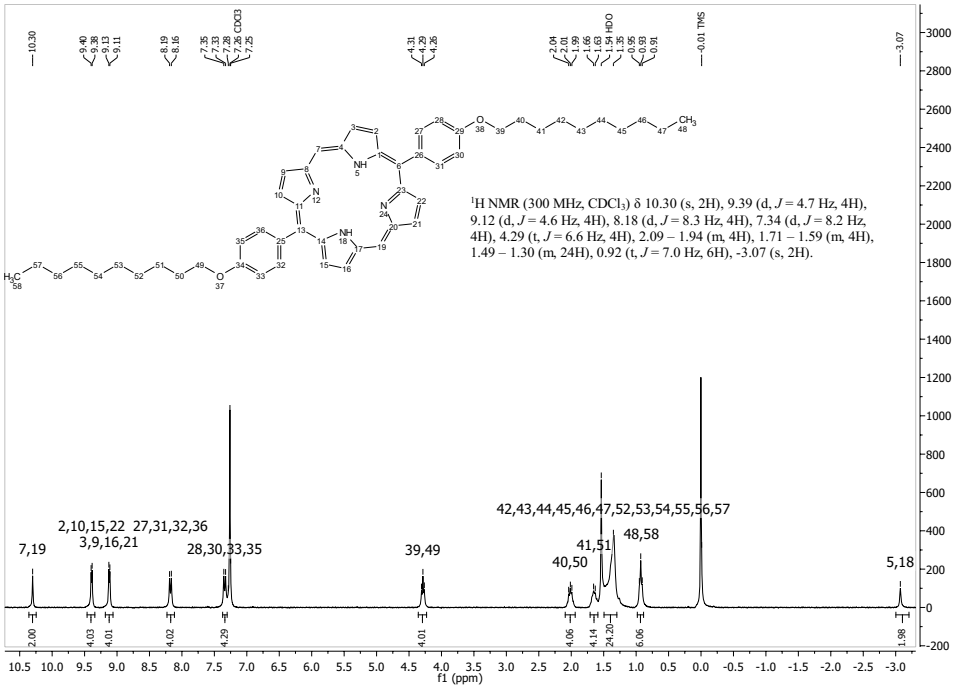

Figure 10.24: ^{1}H-NMR spectra of compound **24**

Compound 25

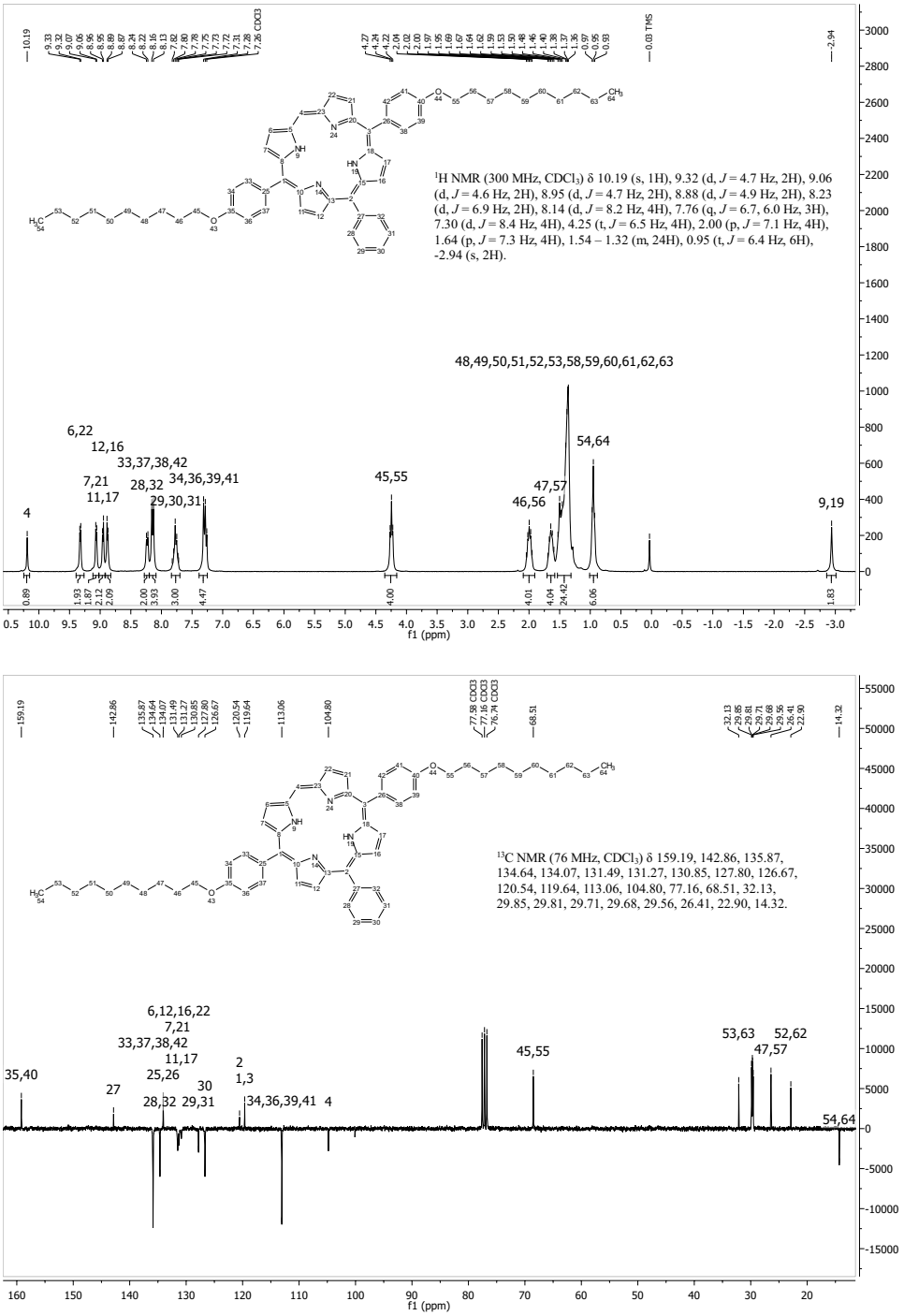

Figure 10.25: ^{1}H-NMR and ^{13}C-APT-NMR spectra of compound **25**

Compound 26

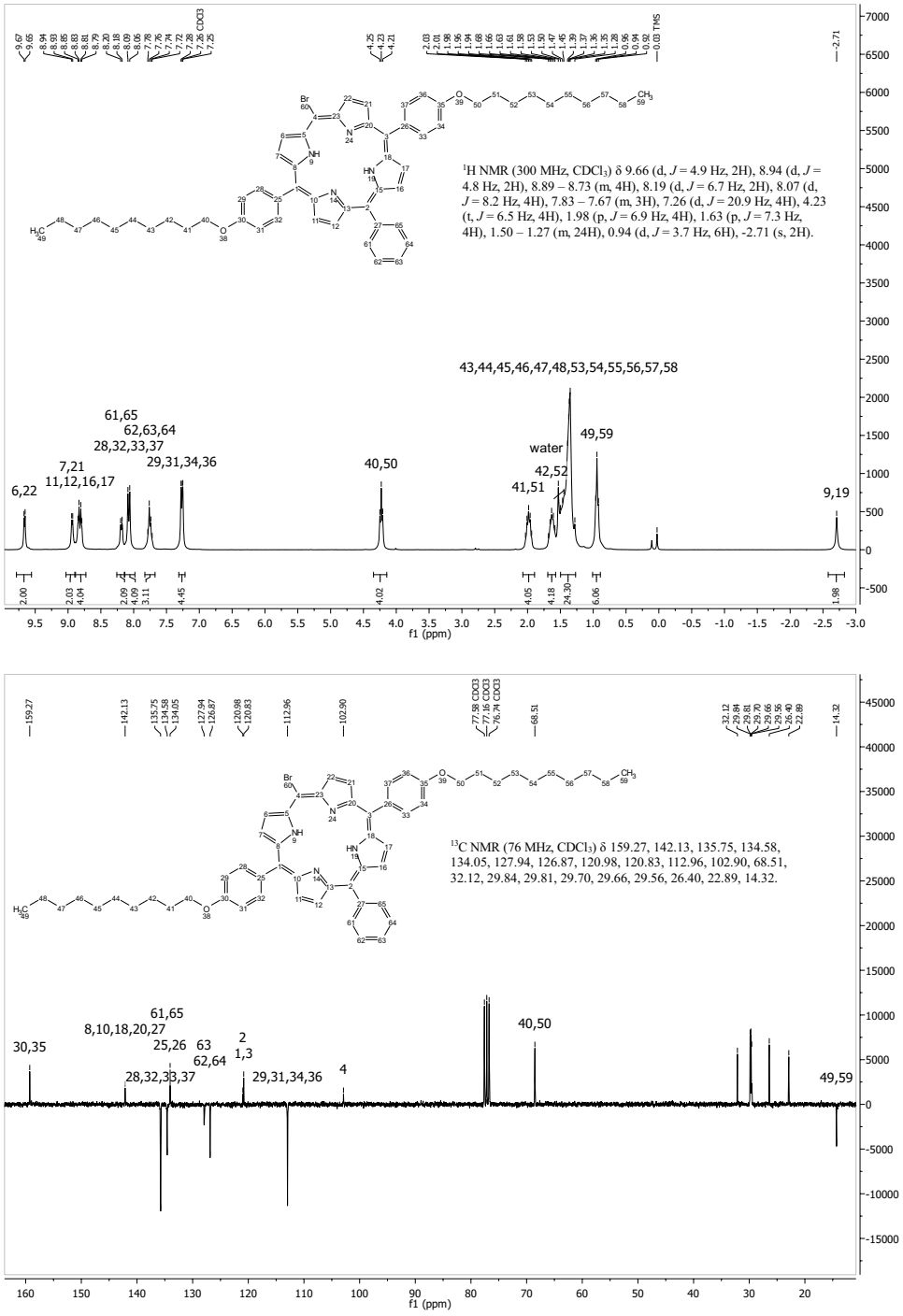

Figure 10.26: ^{1}H-NMR and ^{13}C-APT-NMR spectra of compound **26**

Compound 27

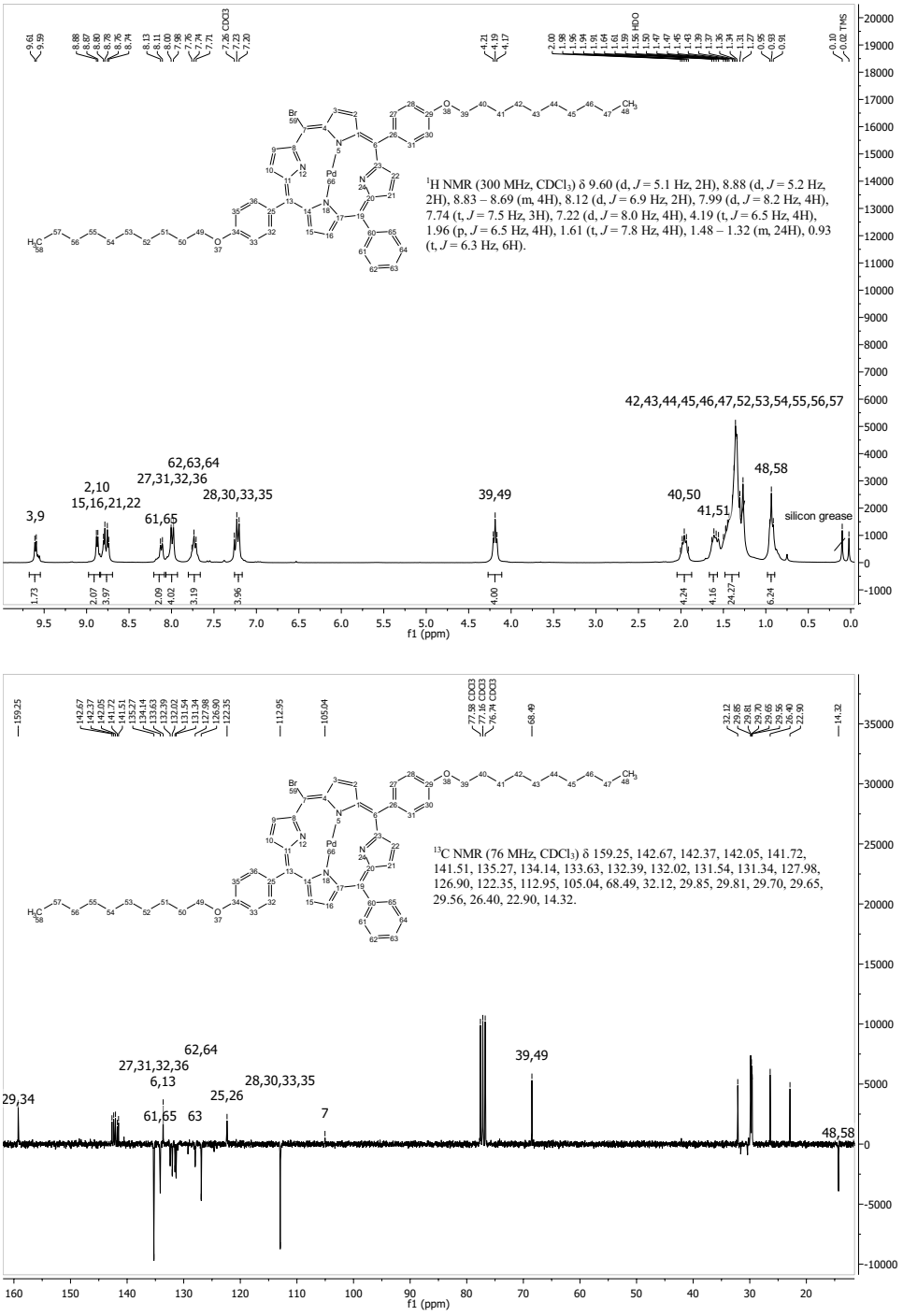

Figure 10.27: ^{1}H-NMR and ^{13}C-APT-NMR spectra of compound **27**

Compound 28

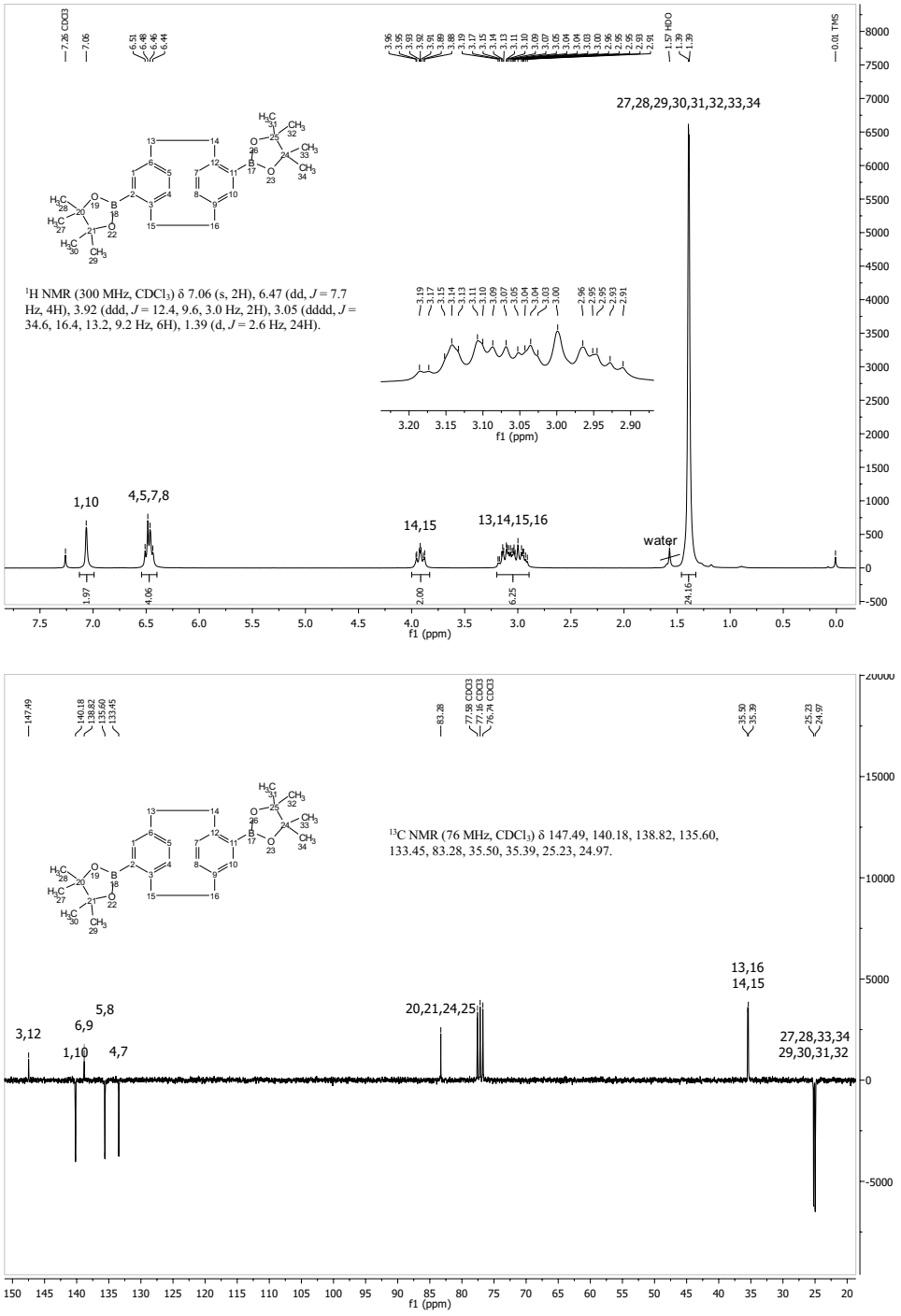

Figure 10.28: ^{1}H-NMR and ^{13}C-APT-NMR spectra of compound **28**

10.3 MS Data

Compound 5a

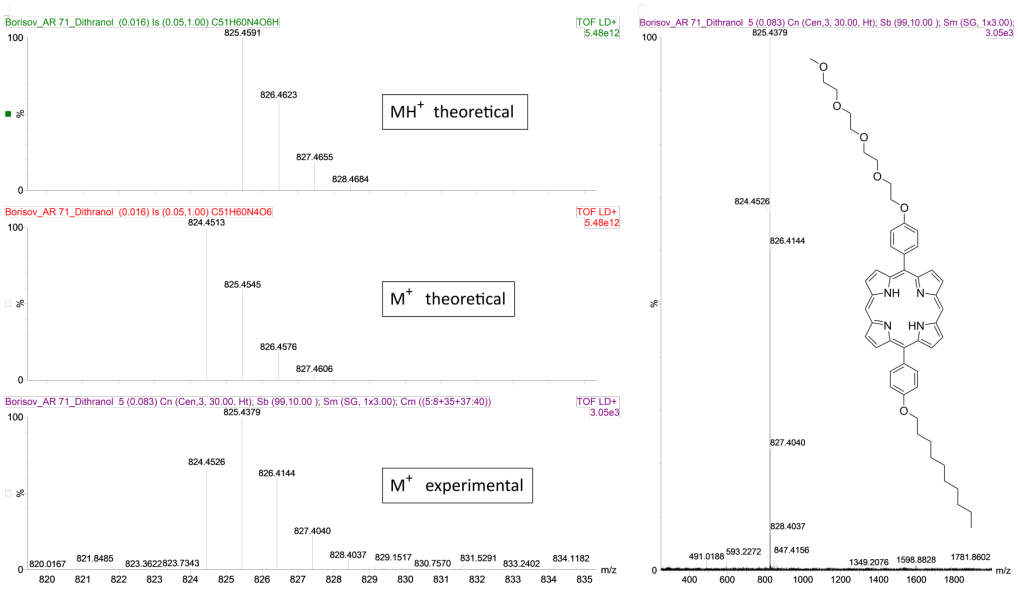

Figure 10.29: MALDI-TOF spectrum of MTMDP **5a** in a ditranol matrix, left: corresponding isotope pattern, right: full mass spectrum

Compound 6a

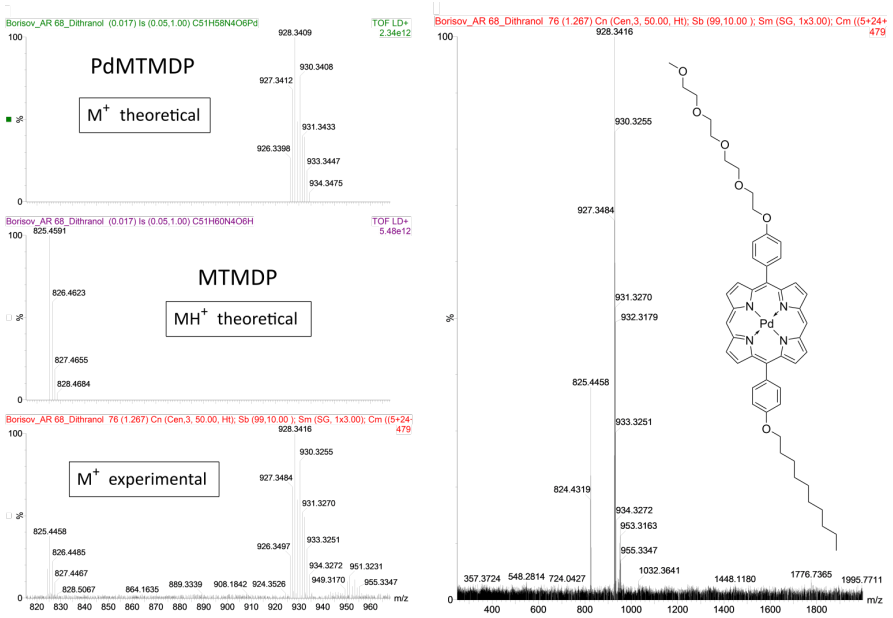

Figure 10.30: MALDI-TOF spectrum of PdMTMDP **6a** in a ditranol matrix, left: corresponding isotope pattern, right: full mass spectrum

Compound 5b

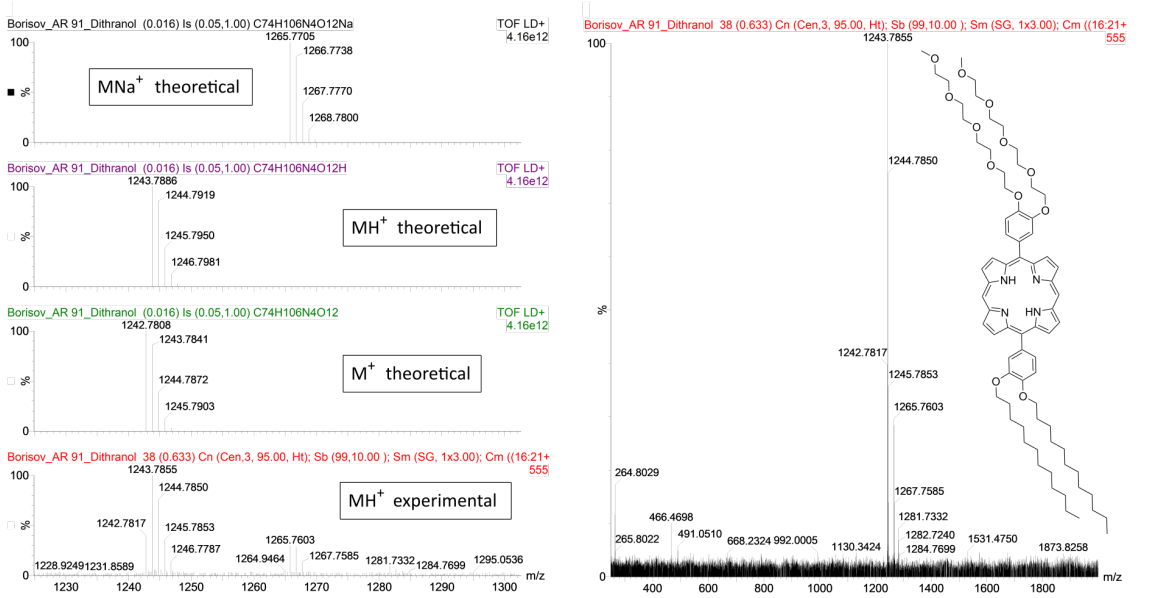

Figure 10.31: MALDI-TOF spectrum of DTDDP **5b** in a ditranol matrix, left: corresponding isotope pattern, right: full mass spectrum

Compound 6b

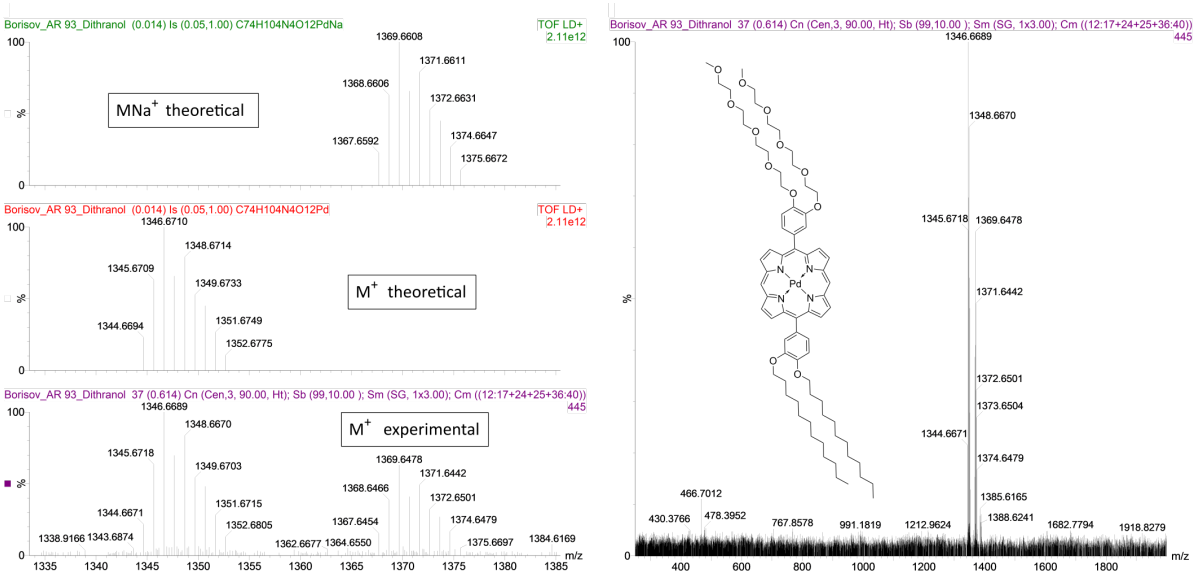

Figure 10.32: MALDI-TOF spectrum of PdDTDDP **6b** in a ditranol matrix, left: corresponding isotope pattern, right: full mass spectrum

Compound 5c

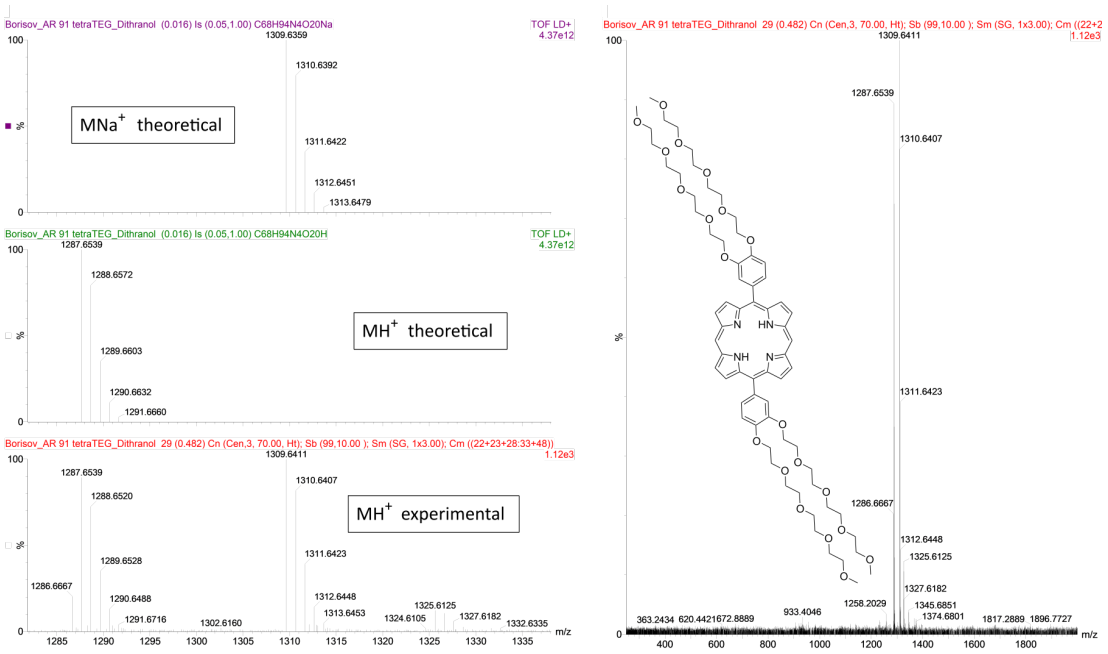

Figure 10.33: MALDI-TOF spectrum of TTP **5c** in a ditranol matrix, left: corresponding isotope pattern, right: full mass spectrum

Compound 6c

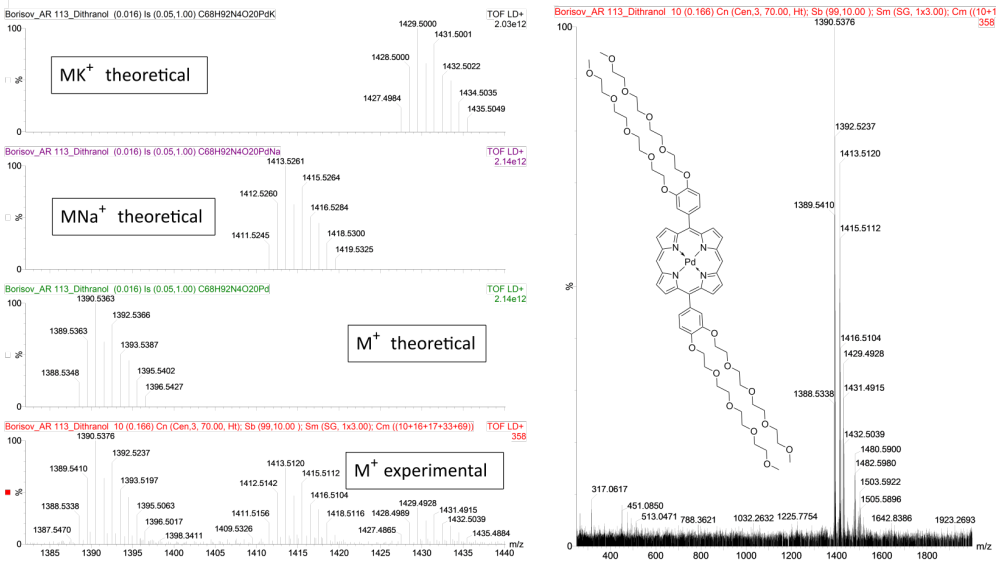

Figure 10.34: MALDI-TOF spectrum of PdTTP **6c** in a ditranol matrix, left: corresponding isotope pattern, right: full mass spectrum

Compound 19

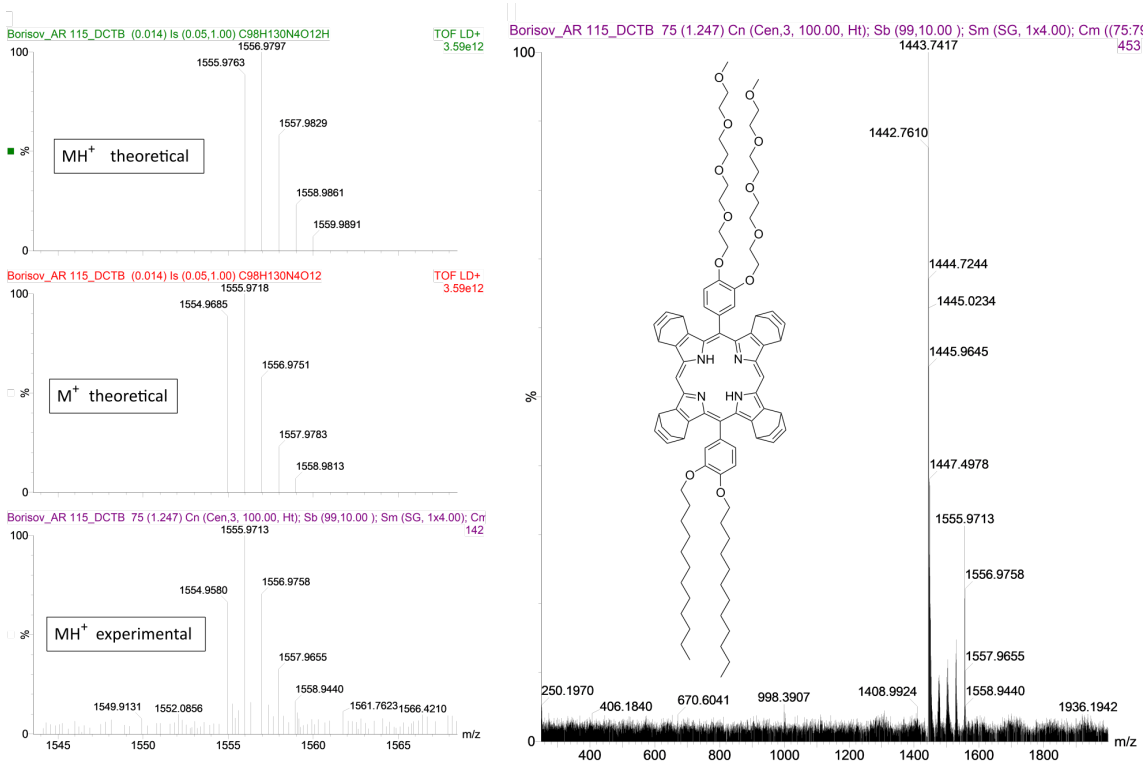

Figure 10.35: MALDI-TOF spectrum of DTDDTBCP **19** in a DCTB matrix, left: corresponding isotope pattern, right: full mass spectrum

Figure 10.36: MALDI-TOF spectrum of DTDDTBCP **19** in a DCTB matrix, experimental and theoretical isotope pattern of **19** and **19** with partly aromatized rings.

Compound 20

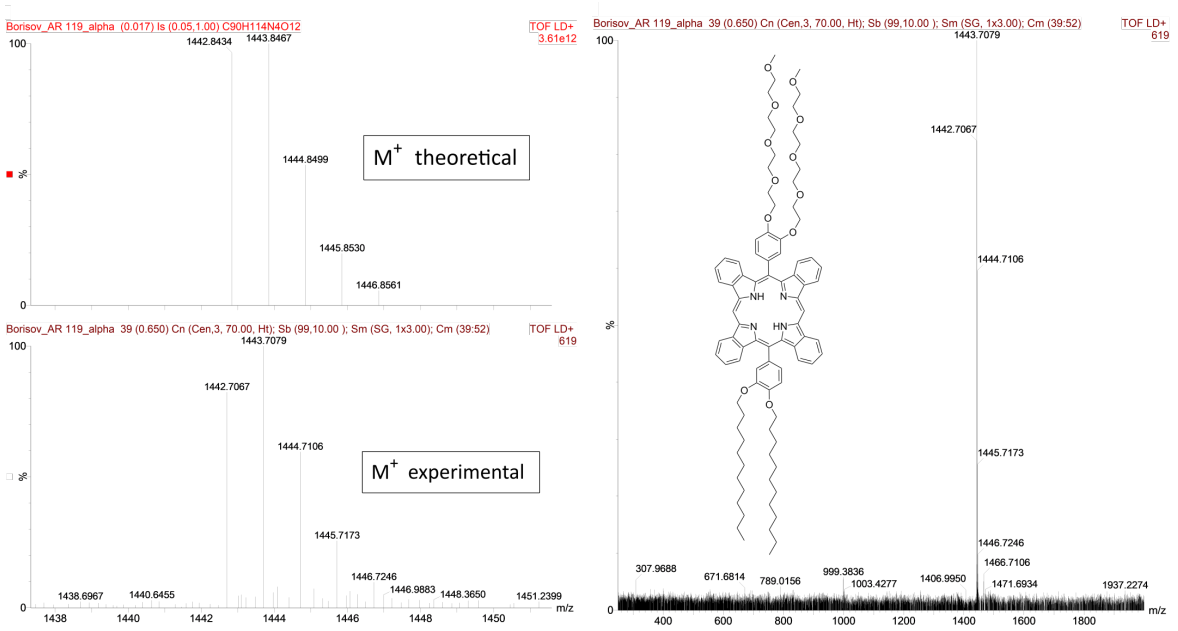

Figure 10.37: MALDI-TOF spectrum of DTDDTBP **20** in a alpha matrix, left: corresponding isotope pattern, right: full mass spectrum

Compound 21

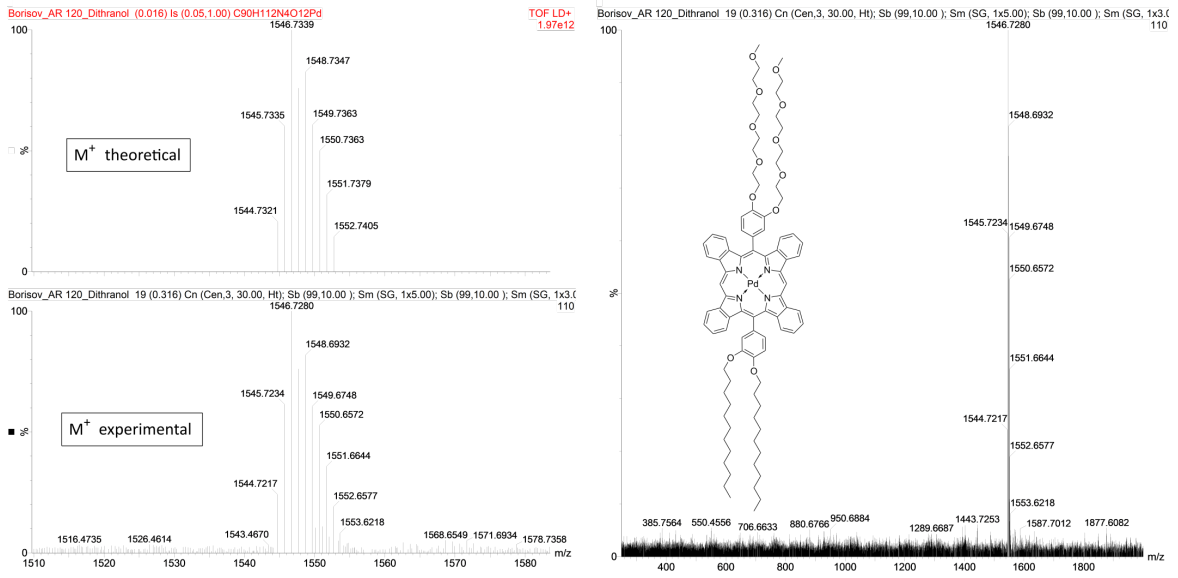

Figure 10.38: MALDI-TOF spectrum of PdDTDDTBP **21a** in a ditranol matrix, left: corresponding isotope pattern, right: full mass spectrum

Compound 22

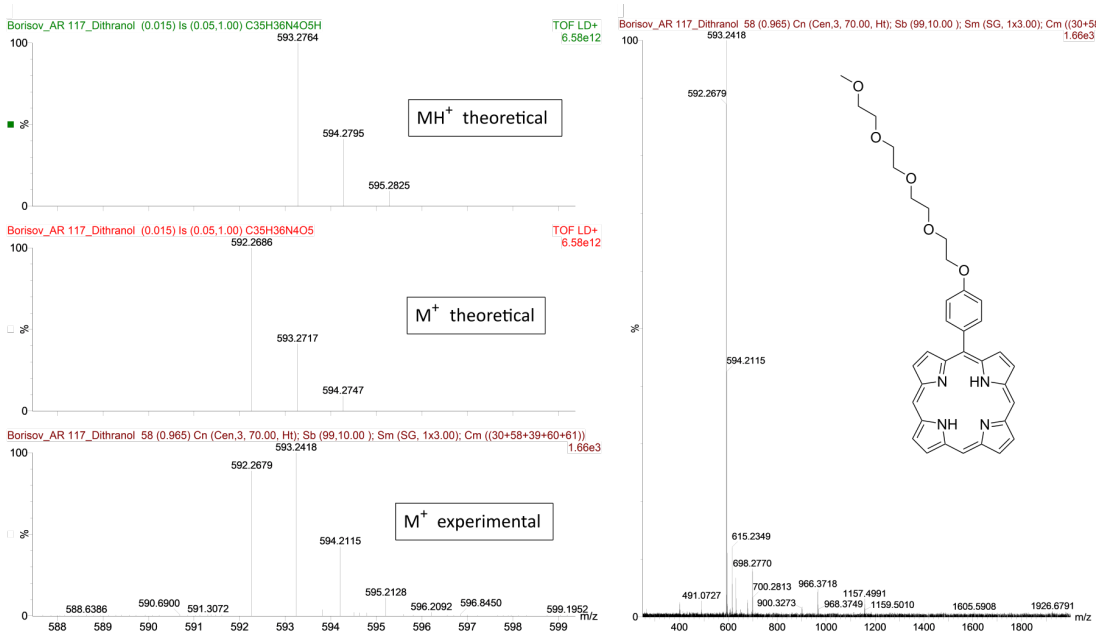

Figure 10.39: MALDI-TOF spectrum of MTP **22** in a ditranol matrix, left: corresponding isotope pattern, right: full mass spectrum

Compound 23

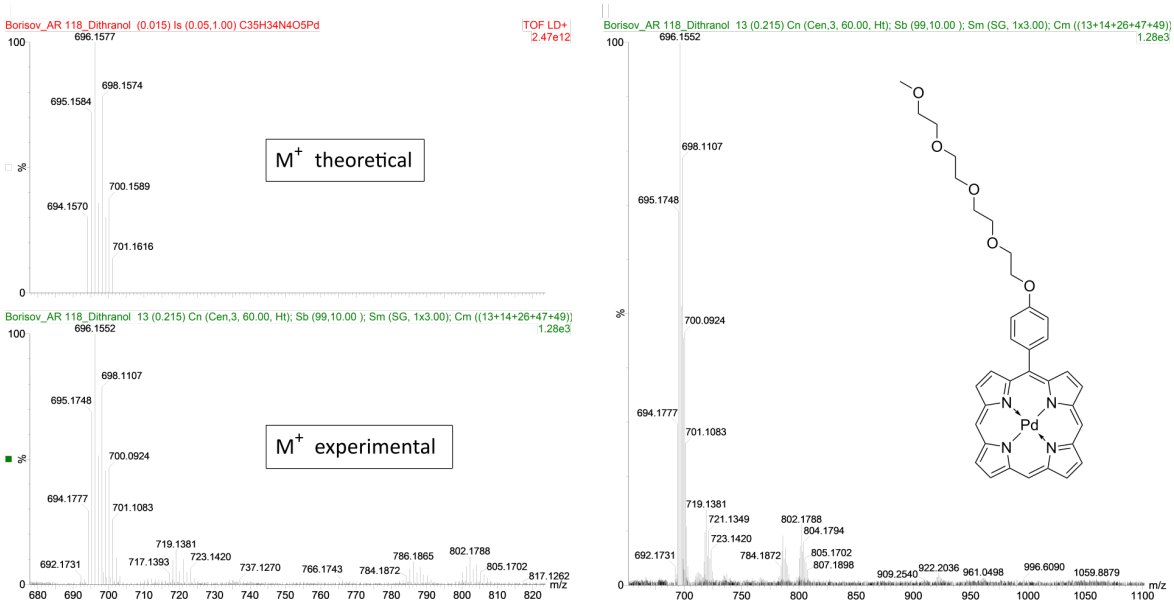

Figure 10.40: MALDI-TOF spectrum of PdMTP **23** in a ditranol matrix, left: corresponding isotope pattern, right: full mass spectrum